Role of Insulin receptor isoform A in breast Cancer

By
Liang Li, B.Sc., M.S.

A Thesis submitted to the University of Adelaide, South Australia in fulfilment of the requirements for the degree of Doctor of Philosophy

THE UNIVERSITY of ADELAIDE

School of Biological Sciences
The University of Adelaide
Adelaide, South Australia
September 2017

ABSTRACT

Insulin like growth factor II (IGF-II) binds to Insulin Receptor isoform A (IR-A) to sustain cell growth and proliferation. This autocrine loop exists in many human carcinomas and provides an additional proliferation and survival pathway to the type 1 insulin-like growth factor (IGF-1R) signalling pathway. In addition, activation of the IGF-II/IR-A autocrine loop provides a mechanism of resistance drugs target the type 1 insulin-like growth factor (IGF-1R). However, the mechanism of how IGF-II/IR-A differentiates itself from the IGF-II/IGF-1R pathway is still unclear. Additionally, a novel phosphorylation site Thr^{1148} (numbered in IR-A) of IR was found in response to insulin stimulation and its phosphorylation in the absence of any Tyr^{1146}, Tyr^{1150}, and Tyr^{1151} phosphorylation. We thus hypothesis that the The phosphorylation of Thr^{1148} inhibits the phosphorylation of Tyr^{1146}, Tyr^{1150}, and Tyr^{1151} of the activation loop, which is possibly due to steric hindrance and electrostatic repulsion of the phosphate group on Thr^{1148} preventing interaction of the activation loop with the tyrosine kinase.

The key areas of investigation included:

1. Investigate the role of Thr^{1148} phosphorylation in IR-A by overexpress the wild-type IR-A and its mutants Thr^{1148}Ala and Thr^{1148}Asp in R^- (Mouse fibroblast cells with IGF-1R KO).
2. Knock down the IR and IGF-1R separately in MDA-MB-231 and MCF-7 cells using inducible expressed miR30 shRNA and measure their characteristics (proliferation, migration, epithelial–mesenchymal transition) in response to insulin, IGF-I, and IGF-II stimulation separately.
3. Quantitative phosphoproteomics was conducted to compare the insulin/IR-A and IGF-II/IR-A signalling pathway with MDA MB 231 IGF-1RKD cell.

The key findings from this work included:

1. $Thr^{1148}Ala$ and $Thr^{1148}Asp$ inhibit the insulin sensitivity of IR-A, which indicate the Thr^{1148} phosphorylation inhibits the IR activation.
2. IRKD has no effect on proliferation of MCF-7 cells and the migration of MDA-MB-231 cells, but increases the proliferation of MDA-MB-231 cells.
3. IGF-1RKD inhibits the proliferation of both MCF-7 cells and MDA-MB-231 cells, but increases the migration of MDA-MB-231 cells.
4. IGF-1R increases the insulin sensitivity of MDA-MB-231 cells, shown by the Akt activation.
5. Insulin and IGF-II are confirmed to induce different signalling pathways confirmed by quantitative phosphoproteomics study. IGF-II is preferentially regulates the migration and stemness of MDA-MB-231 IGF-1RKD cells. Many markers are identified but verifications are still needed. Drug developed on the verified markers can be used to treat the patients who are resistant to anti-IGF-1R inhibitor.

STATEMENT OF ORIGINALITY

I certify that this work contains no material which has been accepted for the award of any other degree or diploma in my name, in any university or other tertiary institution and, to the best of my knowledge and belief, contains no material previously published or written by another person, except where due reference has been made in the text. In addition, I certify that no part of this work will, in the future, be used in a submission in my name, for any other degree or diploma in any university or other tertiary institution without the prior approval of the University of Adelaide and where applicable, any partner institution responsible for the joint-award of this degree.

I also give permission for the digital version of my thesis to be made available on the web, via the University's digital research repository, the Library Search and also through web search engines, unless permission has been granted by the University to restrict access for a period of time.

……..

Liang Li

PhD candidate,

School of Biological Sciences, University of Adelaide

September 2017

ACKNOWLEDGEMENTS

First and foremost, I want to thank my advisor Associate Professor Briony Forbes, for her tremendous guidance and encouragement throughout my entire Ph.D. training. I learnt tremendous skills from her, both in research and in life. I am grateful to work with her for so many years. I also would like to thank my co-supervisor Professor Peter Hoffmann, who provided me enormous help when I worked in his lab.

Thanks all the wonderful friends in Briony's lab and Peter's lab - Dr. Peter McCarhty, Dr. Harinda Rajapaksha, Dr. Cherlynn-Soh, Mrs. Carlie Sawtell, Miss Sheechee Ong, Miss Emily Crawley, Dr. YinYing Ho, and many others. Your company is a valuable memory to me.

Thanks the colleagues in Molecular Biological School of University of Adelaide and CNS of Flinders University. It's a pleasure to work in both lovely places.

I want to express my sincere thanks to the University of Adelaide and China Scholarship Council for providing me financial support.

Last but not least, I would like to thank my family: my grandmother, my parents, my parents in-law, my sister. You provide tremendous support, faith, love and understanding throughout all these years. To dearest wife Shuang Cui, no word can express how I thankful for you. We have been through so many tears and joys. I am grateful for your understanding, encouragement, and support. I am eager to have a family member after you finish your PhD study next year. My career and life are more meaningful because of the love and care that I have been privileged to receive from my whole family.

ABBREVIATIONS

Akt	Protein kinase B
CR	Cysteine-rich
DHB	2,5-Dihydroxybenzoic acid
dsRED	Red fluorescent protein
EMT	Epithelial to mesenchymal transition
ER	Oestrogen receptor
ESI	Electrospray ionization
FASP	Filter aided sample preparation
GH	Growth hormore
HCCA	α-Cyano-4-hydroxycinnamic acid
HER2	human epidermal growth factor receptor 2
HPLC	High performance liquid chromatography
ID	Insert domain
IGF	Insulin like growth factor
IGF-I	Insulin like growth factor I
IGF-II	Insulin like growth factor II
IGF-1R	IGF-I receptor
IGFBP	Insulin like growth factor binding protein
IR	Insulin receptor
IR-A	Insulin receptor isoform A
IR-B	Insulin receptor isoform B
IRES	Internal ribosome entry site
IRS	Insulin receptor substrate
JM	Juxtamembrane
MALDI-TOF	Matrix assisted laser desorption ionization time of flight
MAPK	Mitogen-activated protein kinases
MBR	Match between runs
MS/MS	Tandem mass spectrometry
mTOR	Mechanistic target of rapamycin
PI3K	Phosphoinositide 3 kinase
PR	Progesterone receptor
pTRE3G	Tet-On 3G promoter
Puro	Puromycin resistance gene
Q-TOF	Quadrupole time of flight
RISC	RNA induced silencing complex
RT	Retention time
RTK	Receptor tyrosine kinase
SDB-RPS	Styrenedivinylbenzene-reverse phase sulfonate
SILAC	Stable isotope labelling of amino acids
SMS	Somatostatin
Tet-On 3G	Tet-On 3G transactivator
TiO2	Titannium dioxide
TK	Tyrosine kinase
TM	Transmembrane

CHAPTER 1 INTRODUCTION 1
1.1 IGF SYSTEM OVERVIEW 2
1.1.1 Ligands 6
1.1.2 Receptors 8
Insulin receptor (IR) 8
IGF-1R 11
Hybrids 11
IGF-2R 12
1.1.3 IGFBPs 12
1.2 IGF SYSTEM IN NORMAL PHYSIOLOGY 13
1.3 STRUCTURAL BASIS OF RECEPTOR ACTIVATION 15
1.3.1 Ectodomain structure 15
1.3.2 Tyrosine kinase domain activation 16
1.4 IGF SIGNALLING PATHWAY ADAPTOR PROTEINS 20
1.5 DOWNSTREAM SIGNALLING PATHWAYS 22
1.5.1 MAPK pathway 22
1.5.2 PI3K/Akt pathway 22
1.5.3 IR signalling pathways 22
1.6 IGF SYSTEM IN CANCER 25
1.6.1 IGF-1R in cancer 25
1.6.2 IGF-II/IR-A autocrine loop in cancer 25
1.6.3 IGF system and epithelial to mesenchymal transition (EMT) 26
1.7 CURRENT CANCER TREATMENTS TARGETING THE IGF SYSTEM 26
1.7.1 Anti-ligand monoclonal antibodies 27
1.7.2 Anti-receptor monoclonal antibodies 27
1.7.3 Small molecule tyrosine kinase inhibitors 30
1.7.4 Other treatment strategies 32
1.8 SUMMARY, HYPOTHESIS AND AIMS 33
CHAPTER 2 MATERIALS 35
2.1 MATERIALS 36
2.2 PRIMERS 39
2.3 VECTORS 42
2.4 STRAIN 43
2.5 CELL LINES 43
2.7 BUFFERS 45
CHAPTER 3 METHODS 47
3.1 MOLECULAR BIOLOGY 48
3.1.1 Preparation of plasmid DNA 48
3.1.2 Large-scale plasmid purification 48
3.1.3 Analysis of DNA size, purity and concentration 48
3.1.4 Restriction enzyme digestion 48
3.1.5 Gel extraction of DNA fragments 49
3.1.6 Treating digestions with Antarctic Phosphatase 49
3.1.7 Ligating restricted DNA fragments into restricted vectors 49
3.1.8 Site-directed mutagenesis 50
3.1.9 Transformation 50
3.1.10 Generation of high Competency DH5α cells 51
3.1.11 Gibson Assembly of DNA fragments 51
3.1.12 Gateway LR cloning 51
3.1.13 Big Dye Sequencing reactions 51

3.1.14 RNA extraction ... 52
3.1.15 RNA quality check ... 52
3.1.16 cDNA synthesis ... 53
3.1.17 Semi-quantitative PCR ... 53
3.1.18 shRNA PCR ... 54
3.2 BIOCHEMISTRY ... 55
3.2.1 DC™ (detergent compatible) protein assay ... 55
3.2.2 EZQ™ Protein Quantitation ... 55
3.2.3 HEPES buffer cell lysis ... 55
3.2.4 SDS-PAGE and Western blotting ... 56
3.2.5 Flow cytometry ... 56
3.2.6 HPLC ... 57
3.3 CELL CULTURE ... 57
3.3.1 Maintenance of various cell lines ... 57
3.3.2 Transfection ... 58
3.3.3 Lentivirus production ... 58
3.3.4 Lentiviral infection and titration ... 58
3.3.5 Kill curve ... 59
3.3.6 Stable cell line selection ... 59
3.3.7 Inducible shRNA expression ... 59
3.3.8 Cell stimulation ... 60
3.3.9 Wound healing assay ... 60
3.3.10 Proliferation assay ... 60
3.3.11 Crystal Violet assay ... 60
3.4 QUANTITATIVE PHOSPHOPROTEOMICS ... 61
3.4.1 SILAC labeling ... 61
3.4.2 Determination of Isotope Incorporation Efficiency (should be > 95%) ... 61
3.4.3 Filter Aided Sample Preparation (FASP) Method ... 61
3.4.4 GdmCl buffer cell lysis ... 62
3.4.5 Acetone Precipitation ... 62
3.4.6 Trypsin/Lys-c digestion ... 63
3.4.7 TiO_2 enrichment ... 63
3.4.8 Desalting ... 63
3.4.9 MALDI-TOF ... 64
3.4.10 HPLC-MS/MS ... 64
3.4.11 Data analysis ... 65
3.5 STATISTICS ... 66

CHAPTER 4 ROLE OF INSULIN RECEPTOR THR^{1148} PHOSPHORYLATION ... 67
4.1 INTRODUCTION ... 68
4.2 STRATEGY ... 72
4.3 RESULTS ... 74
4.3.1 Vector verification by digestion and sequencing ... 74
4.3.2 Thr1148Ala and Thr1148Asp decreases the IR-A sensitivity to insulin ... 76
4.4 DISCUSSION ... 78

CHAPTER 5 ASSESSMENT OF THE ROLES OF IR-A AND IGF-1R IN BREAST CANCER CELLS ... 82
5.1 INTRODUCTION ... 83
5.2 RESULTS ... 87
5.2.1 IR and IGF-1R expression levels in breast cancer cells ... 87

5.2.2 Design and selection of shRNA sequences targeting the human IR and human IGF-1R 89
5.2.3 Cloning strategy for miR30 shRNA inducible knock down system construction 95
5.2.4 pENTR1a miR30 shRNA verification 96
5.2.5 pLVTPT miR30 shRNA verification 99
5.2.6 Virus infection optimization and stable cell line selection 100
5.2.7 shRNA selection 103
5.2.8 shRNA knock down time course 105
5.2.9 IR-A transduces insulin and IGF-II signals in MDA-MB-231 IGF-1R KD cells 107
5.2.10 Proliferation of MDA-MB-231 cell lines 111
5.2.11 Proliferation of MCF-7 cell lines 114
5.2.12 IGF-1R knock down enhanced the migration rate of MDA-MB-231 117
5.2.13 The E-cadherin levels in MDA-MB-231 cell lines 120
5.3 DISCUSSION 122

CHAPTER 6 QUANTITATIVE PHOSPHOPROTEOMICS COMPARISON OF INSULIN/IR-A AND IGF-II/IR-A SIGNALLING PATHWAY 126
6.1 INTRODUCTION 127
Quantitative phosphoproteomics 130
Methodology 130
6.2 RESULTS AND DISCUSSION 134
6.2.1 Phosphopeptide enrichment optimisation 134
6.2.1.1 Comparison of methods for concentration of protein and tryptic and Lys-C digestion: Acetone precipitation versus Filter-aided sample preparation (FASP) 136
6.2.1.2 Optimization of matrix used for MALDI-TOF spectrometry detection of phosphopeptides: HCCA versus DHB 140
6.2.1.3 Phosphopeptide enrichment 142
6.2.1.4 Optimisation of phosphopeptide elution from TiO_2 beads: MALDI-TOF mass spectrometry of β-casein and HPLC-MS/MS of MDA-MB-231 eluted with 0.83% and 2.5 % NH_4OH 145
6.2.1.5 DHB concentration optimization 147
6.2.1.6 Optimization of desalting methods 148
6.2.2 Quantitative phosphoproteomic analysis of the Insulin/IR-A and IGF-II/IR-A signalling pathways 150
6.2.2.1 Assessment of the Data Quality 153
6.2.2.2 Data analysis 164
6.3 CONCLUSION 172

CHAPTER 7 FINAL DISCUSSION 175

REFERENCES 184

APPENDIX 201

Chapter 1 Introduction

The insulin-like growth factor (IGF) system is a complex and tightly regulated network that controls growth, proliferation, survival and metabolism. Different components are expressed in varying degrees in all tissues, thereby leading to different outcomes. Substantial evidence has shown that deregulation of the IGF system is associated with diseases such as diabetes and cancer. IGFs play a role in the promotion of tumour growth and metastasis. The characteristic that the IGF system regulates the physiology at both a whole organism level and cellular level increases the difficulty of evaluating its functions in cancer. In this introduction, functions of the IGF system components, IGF signalling pathways, the roles of the IGF system in cancer, and IGF system related cancer treatments are discussed. The gaps in our understanding that form the basis of this study are highlighted.

1.1 IGF system overview

The IGF system comprises three homologous ligands (insulin, insulin-like growth factor I (IGF-I), and insulin-like growth factor II (IGF-II)), three transmembrane receptors (the insulin receptor (IR), the IGF-I receptor (IGF-1R), and the cation-independent mannose 6-phosphate receptor (M6P/IGF-2R)), and six high affinity IGF binding proteins that regulate the concentrations of the growth factors in serum (IGFBP-1 to -6) (Figure 1.1).

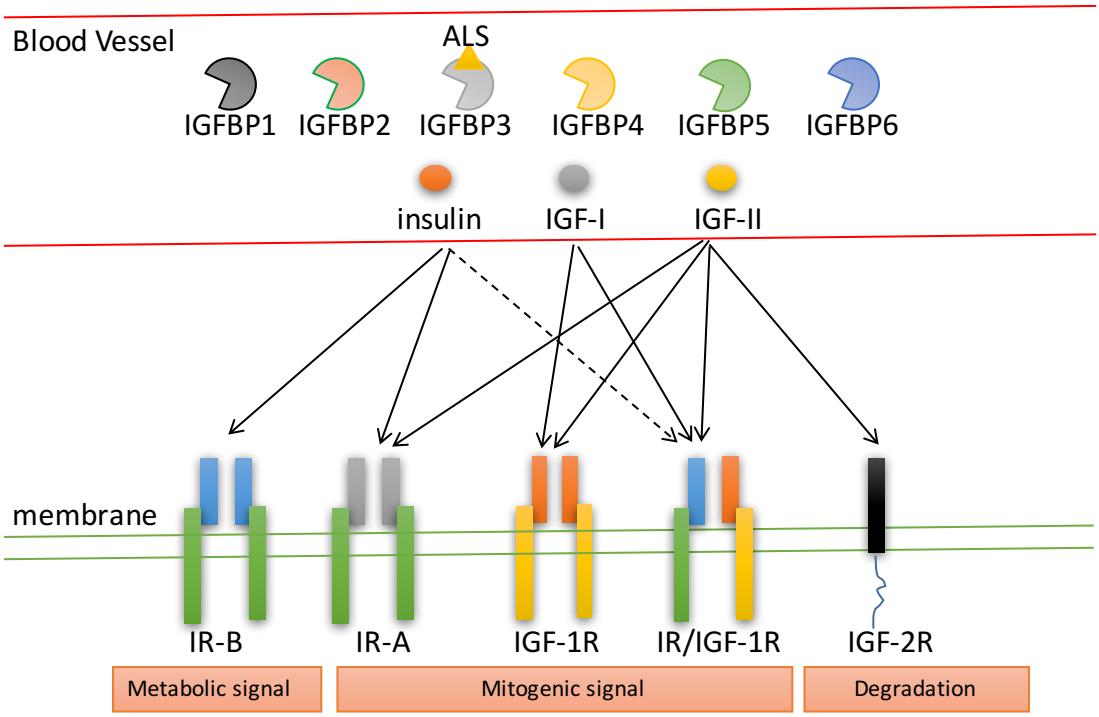

Figure 1.1: The IGF system. The IGF system includes the ligands (insulin, IGF-I, IGF-II; orange, grey and yellow circles), the receptors (IR-A grey/green, IR-B blue/green, IGF-1R orange/yellow, hybrids of IR/IGF-1R, IGF-2R black), the IGFBPs1-6 (coloured shapes) and acid labile subunit (ALS orange triangle). IGFs circulate in the serum mainly in an IGF: IGFBP-3:ALS complex. IGFBP proteolysis or binding to the ECM will lower the affinity for IGFs thereby releasing the IGFs from the complex. IGF-2R regulates the bioavailability of IGF-II.

The three ligands have different biological actions: insulin mainly regulates metabolic functions, whereas IGF-I and IGF-II mainly regulate mitogenic functions. Ligand signalling is mediated by interaction with the tyrosine kinase receptors, IR and IGF-1R. These two receptors are highly similar in sequence and structure, and thus can form IR/IGF-1R hybrid receptors. IR has two isoforms, IR-A (-exon11) and IR-B (+exon11) that arise by the alternative splicing of exon11. The isoforms are preferentially expressed in different growth stages and tissues, leading to their different biological functions. Because of the high structural similarity of the ligands and receptors, they share very similar downstream networks to form a very complex signalling system.

While there are variations in binding affinities reported by various groups (Table 1.1) the consensus shows that insulin can bind to both isoforms of insulin receptor (IR-A and IR-B) with high affinity to regulate metabolic and mitogenic signalling. IGF-I binds to the IGF-1R with a high affinity (Table 1.1). IGF-II can also bind to IGF-1R, but at 2-3 fold lower affinity (Pandini et al., 2002a). IGF-II also binds to the IR-A with high affinity (Table 1.1). IGF-II can also bind to the IGF-2R, but this receptor is not a classic signalling receptor. Upon IGF-II binding to the IGF-2R the complex is internalized, and IGF-II is targeted to lysosome degradation. As a result, the IGF-2R controls the level of IGF-II in the circulation. Almost all circulating IGFs are bound to IGFBPs either in binary complexes or ternary complexes with IGFBP-3 or IGFBP-3 and an acid-labile subunit (ALS), thereby regulating the bioavailability.

	IGF-I (nM)	IGF-II (nM)	Insulin (nM)	EC50/IC50	Reference
IGF-1R	0.2	0.6	>30.0	EC50	(Pandini et al., 2002b)
	0.8	4.4	>100.0	IC50	(Denley et al., 2004)
		0.5	>1000.0	EC50	(Benyoucef et al., 2007)
	0.019		3.8	EC50	(Slaaby et al., 2006)
IR-A	41.0		0.9	IC50	(Yamaguchi et al., 1993)
	9.0	2.2	0.2	IC50	(Benyoucef et al., 2007)
	>30.0	2.5	0.9	EC50	(Frasca et al., 1999)
	120.4	18.2	2.8	IC50	(Denley et al., 2004)
	34.4		2.7	EC50	(Pierre-Eugene et al., 2012)
IR-B	390.0		1.6	IC50	(Yamaguchi et al., 1993)
	>30.0	>20.0	1.0	EC50	(Frasca et al., 1999)
	90.0	10.0	0.5	IC50	(Benyoucef et al., 2007)
	366.0	68.0	1.4	IC50	(Denley et al., 2004)
	50.0		2.6	EC50	(Pierre-Eugene et al., 2012)
IR-A/IGF-1R	0.5	0.6	3.7	EC50	(Pandini et al., 2002b)
	3.0		130.0	EC50	(Pierre-Eugene et al., 2012)
	0.018		4.6	EC50	(Slaaby et al., 2006)
IR-B/IGF-1R	2.5	15	>100.0	EC50	(Pandini et al., 2002b)
	6.9		70.0	EC50	(Pierre-Eugene et al., 2012)
	0.017		5.1	EC50	(Slaaby et al., 2006)

Table 1.1: Binding affinities of ligands for receptors.

The deregulation of the IGF system has been detected in many diseases including neurodegeneration, Alzheimer' disease, cardiovascular disease, diabetes, and cancer. An elucidation of the intricate IGF signalling pathway is necessary for effective disease treatment. A more detailed description of the IGF system follows.

1.1.1 Ligands

Insulin is synthesized by beta cells in the pancreas as preproinsulin (Orci, 1986). It is then processed into proinsulin by the removal of the signal peptide. The amino-terminal B-chain and carboxyl-terminal A chain are connected by C-peptide in proinsulin. It is then processed into active insulin by releasing the C- peptide. The insulin contains two peptide chains, the A-chain of 21 amino acids and the B chain of 30 amino acids. The chains are linked by two inter-disulfide bonds (residues A7-B7 and A20-B19), and there is a third intrachain disulfide bond (A6-A11) (De Meyts, 2004). The insulin freely circulates in the blood and controls metabolism by regulating the blood glucose concentration (Beardsall et al., 2008). The C-peptide is also secreted into the blood and its circulating concentration is used to monitor type 1 and type 2 diabetes (Jones and Hattersley, 2013). C-peptide can bind to the surface receptors to activate PI3K/Akt (Phosphoinositide 3-kinase/ Protein kinase B) and MAPK (Mitogen-activated protein kinases) signalling pathways, thus regulates multiple cellular activities (Hills and Brunskill, 2008).

IGF-I is predominantly produced in the liver under the regulation of growth hormone (GH) and acts in a paracrine manner, but is also secreted locally by most tissues. It is a single chain peptide of 70 amino acids, which includes four domains: B, C, A and D. The A and B domains are structurally similar to the A and B domains of insulin, arising from a 50% sequence similarity (Figure 1.2). The C domain is equivalent to the C-peptide in the proinsulin, but no D domain exists in the insulin (Humbel, 1990; Pavelic et al., 2007). Even though IGF-I is expressed at low level during the embryonic period; it is necessary for postnatal growth and development.

IGF-II synthesis is also mainly produced in the liver, but not under the control of growth hormone. It is expressed during the foetal development stage (Pavelic et al., 2007). The adult expression of IGF-II normally takes place in the liver and epithelial cells. It is a single chain with 67 amino acids, which also contains four domains similar to IGF-I. The primary sequence of the B- and A- chains is also 50% similar to that of the B- and A- chains of insulin (Figure 1.2). The three disulfide bonds are also located in equivalent positions to insulin (Rinderknecht and Humbel, 1976). The *igf2* gene is imprinted, and only the paternal allele is expressed (Chao and D'Amore, 2008). It is crucial for placental development and foetal growth (Constancia et al., 2002).

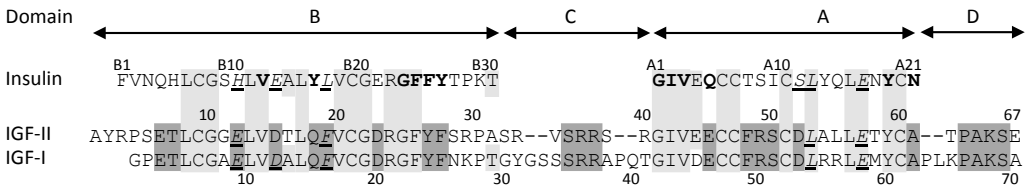

Figure 1.2: The amino acid sequences of Insulin, IGF-I, and IGF-II. Conservation across all three ligands is shown in light grey, whereas conservation between IGF-I and IGF-II is shown in dark grey. Insulin residues critical for IR binding and defined as site one residues are highlighted in bold type, and those defined as site two are underlined and in italics (Alvino et al., 2009).

The sequence similarities (Figure 1.2) between IGFs and insulin translate into their similar tertiary structures (Figure 1.3). They adopt a similar core structure especially in the regions confined by the disulfide bonds. There are three α-helices in the B-domain and two α-helices in the A-domain.

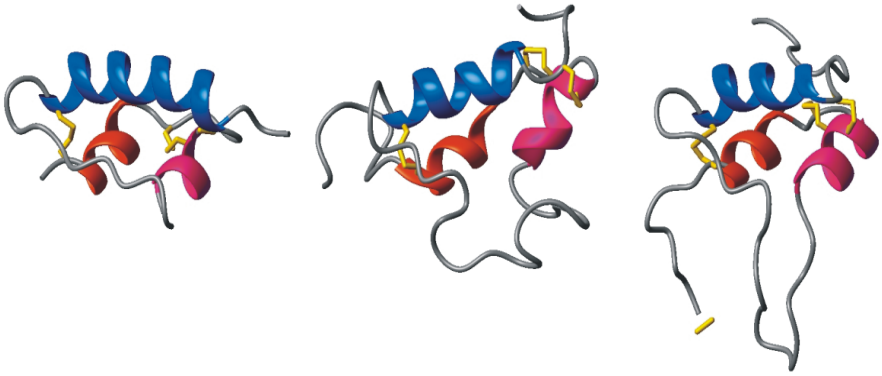

Figure 1.3: The tertiary structures of insulin, IGF-I, and IGF-II (From left to right). The blue ribbon indicates the α-helix in the B-chain, red and pink ribbons are α-helices in the A-chain and disulfide bonds are highlighted in yellow (Denley et al., 2005).

1.1.2 Receptors

Insulin receptor (IR)

Most of the RTKs dimerize or oligomerize upon ligand binding, thus leads to the activation of their kinase domains. Unlike most other RTKs, the IGF-1R and IR exist as preformed covalent dimers in the absence of the ligands (Heldin and Ostman, 1996).

IR is encoded by 22 exons with 21 introns. It comprises a α2β2-heterodimer, with the subunits covalently linked by three disulfide bridges (De Meyts and Whittaker, 2002) (Figure 1.4). The two α- subunits are entirely extracellular and comprise the leucine-rich domains L1 and L2, separated by a cysteine-rich (CR) domain, the fibronectin type III domains (FnIII-1, FnIII-2a/FnIII-2b, and FnIII-3), and an insert domain (ID) located between the FnIII-2a and 2b segments. The two β-subunits include a transmembrane segment (TM) and an intracellular domain that comprises the tyrosine activation domain (TK) flanked by the juxtamembrane (JM) and C-terminal tail (De Meyts, 2004; De Meyts and Whittaker, 2002). Alternative expression of the amino acids encoded by exon 11 (12 amino acids, residues 718-729) at the C-terminus of the receptor α-subunit results in the IR-A (-exon11) and IR-B (+exon11) (Moller et al., 1989).

IR isoforms are preferentially expressed in different tissues. The IR-A is mainly expressed in foetal tissues, adult brain and kidney (Frasca et al., 1999), whereas IR-B predominantly exists in adult liver, muscle and adipose tissues, and the classical insulin target tissues (Moller et al., 1989).

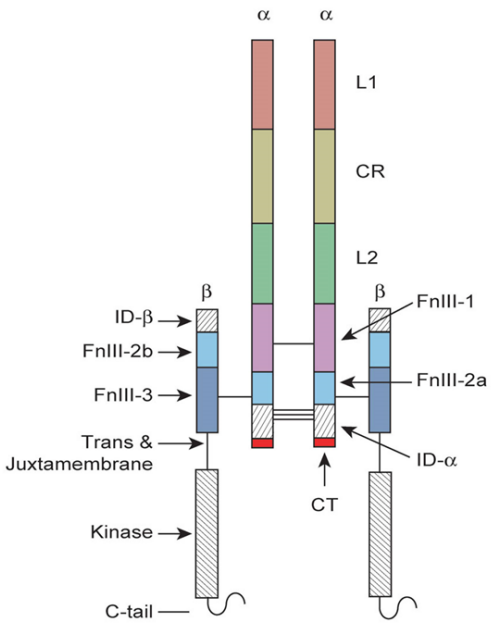

Figure 1.4: Schematic diagram of the insulin receptor homodimer. L1, L2: leucine-rich repeated domains; CR: cysteine-rich region; FnIII-1, FnIII-2a/FnIII-2b and FnIII-3: fibronectin type III domains; ID: the insert region of FnIII-2. CT: The C-terminal 16 residues of the α-chain (the so-called CT-peptide); C-tail: carboxyl-terminal tail. The two monomers are linked together by disulphide bonds (black lines). The α and β subunits are also linked together by disulphide bonds (black line) (Denley et al., 2005).

IGF-1R

The IGF-1R expression is ubiquitous. It has a similar sequence to the IR, with 41-84% sequence similarity depending on the region being compared (Adams et al., 2000). It has the same domain arrangement as the IR and a similar ectodomain tertiary structure. Both receptors belong to the receptor tyrosine kinase (RTK) family (Hubbard and Till, 2000).

Hybrids

IR isoforms and IGF-1R share high sequence and structural similarities, and thus they not only form homodimers described above but also form heterodimers. These heterodimers have different affinities to insulin and IGFs (Table 1.1). An IR-A/IGF-1R hybrid has a high affinity for IGF-I (EC50=0.3 nM) and IGF-II (EC50=0.6 nM) but binds to insulin with a much lower affinity (EC50=3.7 nM) (Pandini et al., 2002b). Insulin can also induce the phosphorylation of specific IGF-1R substrates when binding to IR-A/IGF-1R (Pandini et al., 2002b; Zhang et al., 2007). IR-B/IGF-1R only has high affinity for IGF-I (EC50=2.5 nM), much lower affinity to IGF-II (EC50=15 nM), but an insignificant affinity to insulin (EC50>100nM) (Pandini et al., 2002b). However, other studies show there is no significant difference in insulin binding affinity between IR-A/IGF-1R and IR-B/IGF-1R hybrids (Slaaby et al., 2006), with hybrid receptors having an affinity for insulin that is at least 50 fold poorer affinity than for IGF-I (Benyoucef et al., 2007; Slaaby et al., 2006). These controversial conclusions about the ligands binding affinities could be due to the contamination of IGF-binding proteins in the commercial radioimmunoassay grade bovine serum albumin used in binding assays (De Meyts and Whittaker, 2002; Slaaby et al., 2006). Slaaby *et al*. conducted three different binding assays, and all the assays showed the poor affinity of insulin for both types of hybrid receptor (Slaaby et al., 2006). Slaaby's data would be more reliable.

In cells expressing both IR and IGF-1R, the proportion of IR homodimer, IGF-1R homodimer and IR/IGF-1R heterodimer are randomly formed (Bailyes et al., 1997; Frattali et al., 1992b). If one receptor type is expressed at low abundance, it is mainly found within a heterodimer.

However, in some cancer tissues, some unknown factors affect the hybrids formation (Pandini et al., 1999).

In addition, formation of IR/IGF-1R hybrids will decrease insulin sensitivity due to their low affinity for insulin.

IGF-2R

IGF-2R is a monomeric membrane spanning glycoprotein, which contains one binding site for IGF-II and two binding sites for Mannose-6-Phosphate (M-6-P). However, IGF-2R has no intracellular signalling domain (Denley et al., 2005; Pavelic et al., 2007). Following binding of IGF-II, the IGF-2R: IGF-II is internalized, which leads to the lysosome degradation of IGF-II. As a result, the level of circulating IGF-II decreases (Denley et al., 2005; Pavelic et al., 2007).

1.1.3 IGFBPs

The IGFBPs-1 to -6 are proteins of about 30 kDa (Hwa et al., 1999). They share a similar three-domain structure, with N- and C- terminal domains linked by a less structured linker domain. In the serum, the IGFBPs bind to IGFs with high affinity (Firth and Baxter, 2002). About 80% of the circulating IGF-I is carried by IGFBP-3/acid-labile complex (Lewitt et al., 1994). This ternary complex cannot cross the vascular epithelial layer and act as an IGF reservoir within the circulation (Lewitt et al., 1994). The other IGFBPs also exist in the serum, but form binary complexes with IGFs. The smaller binary complex can cross the vascular epithelial layer so that they can deliver the IGFs to target tissues (Boes et al., 1992). The complex can be released by proteolysis of IGFBPs or binding of the IGFBPs to extracellular matrix (Firth and Baxter, 2002). Through these mechanisms, the IGFBPs play roles in the regulation of the levels of IGFs in the circulation.

1.2 IGF system in normal physiology

The IGF system regulates the biological activities at both cellular level and whole organism level (Pollak, 2008) (Figure 1.5). The GH-releasing hormone (GHRH) and somatostatin (SMS) control the release of growth hormone (GH) from the pituitary gland, which regulates the secretion of IGF-I. IGF-II is also mainly produced in the liver but is not under the control of GH. However, both IGFs can be regulated by IGFBPs. At the same time, insulin is secreted from the pancreas. Its expression can be inhibited by SMS. The blood brings them into the target tissues. Other cells (e.g. epithelial cells) can also secret IGFs by autocrine and paracrine mechanisms.

Under normal physiological conditions, ligands circulate the body with different concentrations: insulin at 0.1-1nM, IGF-I at about 20nM and IGF-II at about 90nM. With these ranges of ligand concentration, insulin can only bind to the insulin receptor, IGF-I can bind to IGF-1R or IR/IGF-1R hybrid, and IGF-II can bind to IR-A, IR-B, IGF-1R and IR/IGF-1R hybrids.

Knockout mice verify the physiological functions of the IGF system. Mice lacking the liver *igf-1* gene have an approximately 80% reduction in circulating total IGF-I levels (Svensson et al., 2008). The mice with *igf-1* knockout have 60% birth weight of normal mice, while the *igf-1r* knockout has 45% birth weight of normal mice (Liu et al., 1993). The phenotype of the *igf-1/igf-1r* double knockout appeared identical to that of the *igf-1r* knockout, which indicates the IGF-I was acting exclusively through the IGF-IR (Liu et al., 1993). The mice with *igf-2* knockout have 60% birth weight of the normal ones (Liu et al., 1993). The *igf-2*/*igf-1r* double knockout had more severe growth retardation than the *igf-1r* knockout alone, suggesting that IGF-II acts through another receptor in addition to the IGF-1R (Baker et al., 1993). Later studies find that the insulin receptor isoform A (IR-A) acts as a compensatory factor (Avnet et al., 2009; Frasca et al., 1999; Ulanet et al., 2010; Zhang et al., 2010).

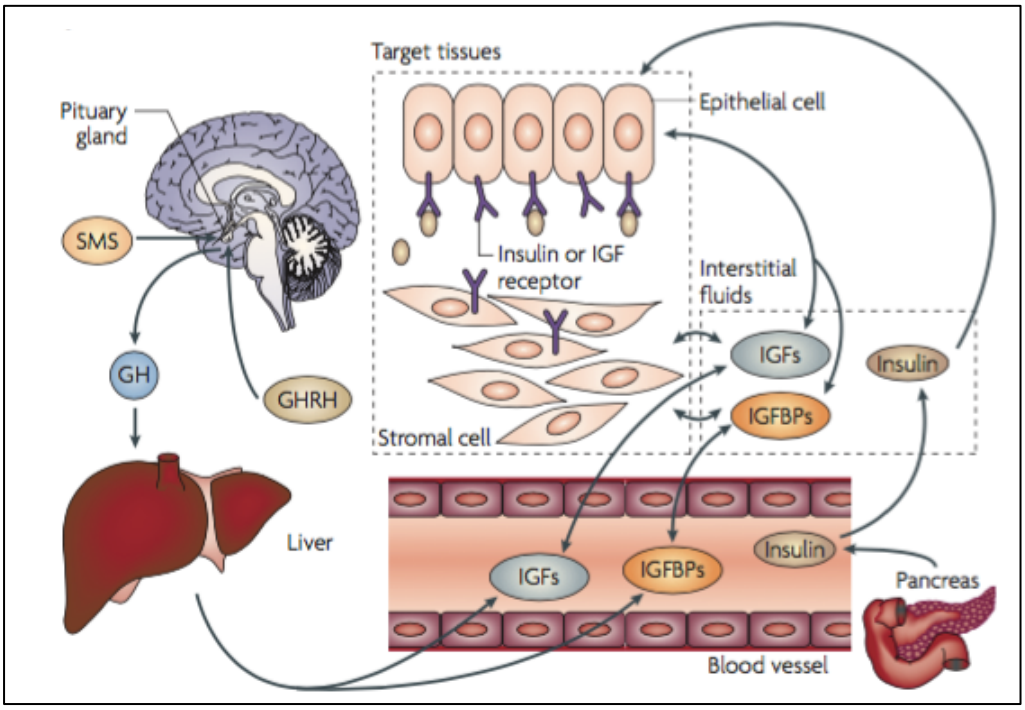

Figure 1.5: Key IGF system elements under normal physiological conditions. The principal source of IGF-I and IGF-II is the liver, while the only source of insulin is the pancreas. GHRH and SMS regulate the expression of GH in the pituitary and GH then controls IGF-I secretion. Blood vessels deliver the ligands to target tissues, which express IR and IGF-1R. SMS is released to inhibit insulin and glucagon secretion in the pancreas. IGFs: IGF-I, IGF-II; IGFBPs: IGF binding proteins; GH, growth hormone; GHRH, GH-releasing hormone; IRS, insulin receptor substrate; SMS, somatostatin (Pollak, 2008).

1.3 Structural basis of receptor activation

1.3.1 Ectodomain structure

The crystal structure of IR ectodomain was first reported by McKern et al (McKern et al., 2006) and Smith et al. refined it (Smith et al., 2010). The conformation of each ectodomain was an inverted "V" (Figure 1.6). The cross-linking studies and alanine-scanning mutagenesis showed that there are two insulin-binding sites: site1 formed by the L1 domain and the carboxyl-terminal segment of the other monomer; site2 involved the loops of the first and second fibronectin domains of the second monomer (Whittaker et al., 2008). Upon ligand binding, the ectodomain will undergo structural changes and transduce the signal into the membrane.

Uhles et al found that the 12 amino acids sequence encoded by exon 11 acts as a sorting signal rather than playing a structural role in the IR (Uhles et al., 2003). This motif is proposed to direct the different IR isoforms to different membrane domains. Thus IR-A and IR-B induce the various biological outcomes with different signalling cascade activations.

Figure 1.6: The IR ectodomain homodimer, showing the juxtaposition of domains between the monomers. One monomer is shown in tube representation, the other in atomic sphere representation. Individual domains are colored as follows: L1, brown; CR, yellow; L2, green; FnIII-1, magenta; FnIII-2, cyan; and FnIII-3, blue. The locations of potential N-linked glycosylation sites are shown in black (McKern et al., 2006).

1.3.2 Tyrosine kinase domain activation

The crystal structure of the unphosphorylated insulin receptor kinase domain shows the IR is *cis*-inhibited under basal conditions (Hubbard et al., 1994). The Tyr^{1150} of the activation loop is hydrogen-bonded to the catalytic loop, thus preventing the IR kinase activity (Hubbard et al., 1994). The juxtamembrane (JM) and α-C (α-helix at the N-terminal lobe of kinase domain) also inhibits auto phosphorylation (Cabail et al., 2015; Hubbard, 2013; Li et al., 2003). The binding of insulin triggers autophosphorylation of the IR in the activation domain and thus induces the signalling cascade (Hubbard, 2013). Hubbard et al suggested that the kinase domains from two monomers were within a trans auto phosphorylation range (Cabail et al., 2015; Hubbard, 2013; Li et al., 2003). However, the crystal structure of the phosphorylated IR-JMTK dimer (Figure 1.7) shows that the activation loops from different monomers are far away from each other, adopting a back-to-back position (Cabail et al.,

2015). If the two monomers in basal state formed a back-to-back position, the trans phosphorylation would be impossible. If the activation loops were face-to-face with each other ligand binding could induce trans phosphorylation and thus through charge repulsion promote the required rotation to allow the activation loop to move out of the catalytic site. As such, the crystal structure of the unphosphorylated IR-JMTK dimer will help us understand the auto phosphorylation process.

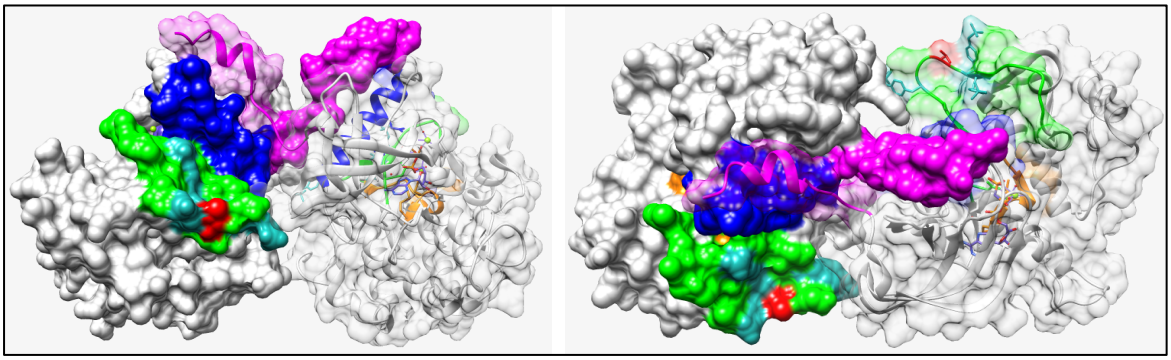

Figure 1.7: Crystal structure of phosphorylated IR-JMTK dimer viewed from the front (left) and top (right). One of the dimer is shown with molecular surface and another is shown with ribbon and molecular surface with 50% transparency. The juxamembrane (JM) region is coloured pink, the α-C (α-helix at the N-terminal lobe of kinase domain) is coloured blue, the activation loop is coloured green, the catalytic loop is coloured orange, the three tyrosines: $Tyr^{1146,1150,1151}$ are coloured cyan, and $Tyr^{1146,}$ is coloured red. Adapted from Cabail et al (Cabail et al., 2015).

A key step in the activation of the IR is the phosphorylation of the three tyrosines (1146, 1150, 1151) in the activation loop (Figure 1.8), which generates recruitment sites for the downstream signalling proteins that contain phosphotyrosine recognition domains such as src homology-2 (SH2) domains and the binding (PTB) domains (Pawson, 1995). After ligand binding, the Tyr^{1150} are phosphorylated first. The Phosphorylated Tyr^{1150} then forms a hydrogen bond with the side chain of Arg^{1152}. The subsequent phosphorylation of Tyr^{1151} allows the formation of hydrogen bonds with Arg^{1143} and Gly^{1154}. The formations of these hydrogen bonds stabilize the activation loop. The Phosphorylated Tyr^{1146} is free and exposed, suggesting it would be available to interact with downstream signalling proteins (Cabail et al., 2015; Hubbard, 1997, 2013).

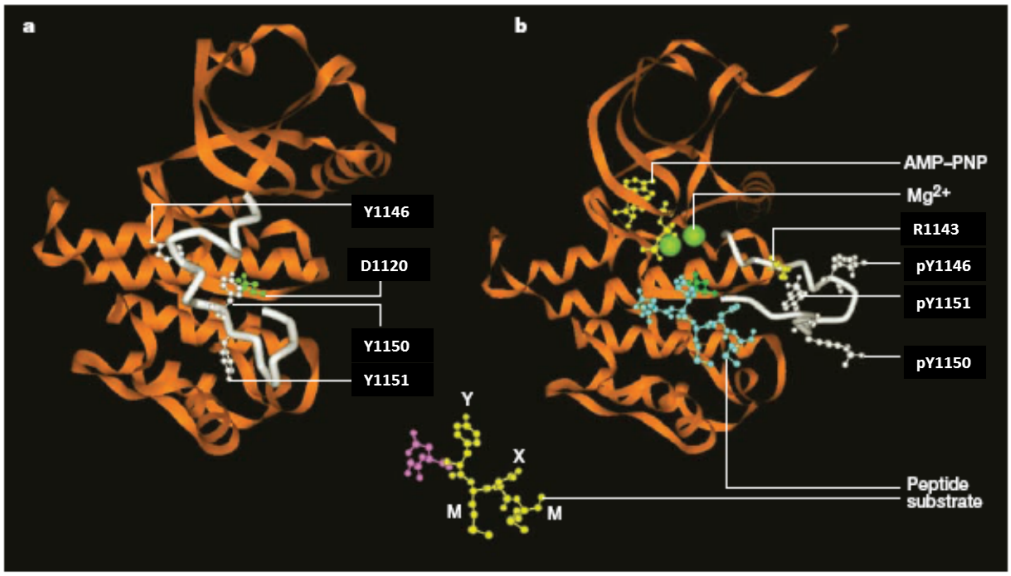

Figure 1.8: Structure of the tyrosine-kinase domain of the insulin receptor. (a): The inactive insulin receptor kinase. This figure illustrates the autoinhibition mechanism, whereby Tyr^{1150} is bound to the active site, hydrogen-bonded to a conserved Asp^{1120} residue (green) in the catalytic loop. Tyr^{1150} in effect competes with protein substrates before autophosphorylation. (b): The activated kinase with bound ATP analog (AMP–PNP), peptide substrate and magnesium (Mg^{2+}). Tyr^{1150} is one of the three tyrosines ($Tyr^{1146,1150,1151}$) that is autophosphorylated in the activation loop (shown in white) in response to insulin. In the

activated state (b), the activation loop moves out of the active site and the three tyrosine residues in the activation loop are phosphorylated. The Tyr^{1151} becomes hydrogen-bonded to a conserved Arg^{1143} residue at the beginning of the activation loop, which stabilizes the repositioned loop. The peptide substrate, with the Tyr-Met-Xaa-Met (YMXM) motif and AMP–PNP, adenylyl imidodiphosphate are also shown. Numbering corresponds to the IR-A. D: Asp, Y: Tyr, R: Arg, pY: Phosphoryalted Tyr. Adapted from Hubbard (Hubbard, 1997).

1.4 IGF signalling pathway adaptor proteins

The activation of the kinase domain and the following phosphorylation of different IR intracellular domain residues lead to the recruitment of adaptor proteins, kinases and phosphatases. The characterised interactions are highlighted in Table 1.2. The recruitment of these proteins in turn, promote or inhibit the activation of IR downstream signalling pathways.

Docking residue	Protein	Function
Tyr960	IRS-1	Known to be involved in both metabolic and mitogenic signalling (Abe et al., 1998; Hribal et al., 2000)
	IRS-2	Involved in both metabolic and mitogenic signalling (Sawka-Verhelle et al., 1996; Wu et al., 2008)
	IRS-3	IRS-3 is found in mouse only (Sesti, 2000; Xu et al., 1999)
	Shc	Activates Erk via Grb2, SOS & Ras complex (Farooq et al., 1999)
	Cbl	Regulates insulin-mediated glucose uptakes (Gupte and Mora, 2006)
	SOCS-3	Inhibits IR-mediated activation of StatB without modifying the kinase activity (Emanuelli et al., 2000)
Tyr1146, Tyr1150, Tyr1151	IRS-2	Involved in both metabolic and mitogenic signalling (Sawka-Verhelle et al., 1996)
	IRS-4	Expressed in human and mouse embryonic stages (Sesti, 2000)
	APS	Couple Cbl to IR. Enhances IR internalization but not degradation (Ahmed et al., 1999; Kishi et al., 2007)
	Grb7	Acts as an inhibitor for insulin signalling (Han et al., 2001; Kasus-Jacobi et al., 2000)
	Grb10	Acts as an inhibitor for insulin signalling (Stein et al., 2001)
	Grb14	Acts as an inhibitor for insulin signalling (Goenaga et al., 2009)
Thr1148	PKC-ε	Acts as an inhibitor for insulin signalling (Petersen et al., 2016)
Tyr1110	Grb2	Promote mitogenic responses (Hanke and Mann, 2009)
	PLCγ	Phosphorylates of T1336 on IR upon activation (Hanke and Mann, 2009)
Tyr1316	PP120	Regulates insulin-induced mitogenic action (Soni et al., 2000)
Thr1336	PKCδ	Involved in IR internalization, blocking the activation of PKCδ abrogate IR internalization (Braiman et al., 2001)

Table 1.2: Signalling molecules known to interact with the IR. The residues of the IR used as docking sites for signalling molecules are indicated. Also, comments regarding the biological activities of the signalling molecules are provided.

1.5 Downstream signalling pathways

Two main signalling pathways are activated upon insulin binding to the IR (Taniguchi et al., 2006): the mitogen-activated protein kinase (MAPK) pathway which mainly promotes proliferation; the PI3K/Akt pathway which mainly promotes metabolism (Figure 1.9).

1.5.1 MAPK pathway

The MAPK are a family of Ser/Thr protein kinases (Figure 1.9). When IR is activated, the Shc binds to phosphorylated Tyr^{960} and then forms the Shc-Grb2-Sos complex. The complex activates Ras, which then activates the following proteins: Raf, MEK1, Erk1/2 and p90rsk. p90rsk and Erk1/2 can phosphorylate or interact with a large number (>300) of cytosolic and nuclear substrates, including transcription factors (Yoon and Seger, 2006). Deregulation of the MAPK pathway affects the expression of genes involved in mitogenic outcomes and is reported in above 90% cancers.

1.5.2 PI3K/Akt pathway

The PI3K/Akt pathway (Figure 1.9) starts from the interaction of IRS with a p85 regulatory subunit of PI3K, following by the activation of catalytic subunit p110 of PI3K and the production of phospholipids: PIP3. PIP3 acts as a second messenger and activates PI3K-dependent kinase-1 (PDK1) and the serine/threonine kinase Akt. Akt has a range of substrates and thus is recognised as a central node in cell signalling. Akt can activate or inhibit glucose uptake, lipolysis, gluconeogenesis, lipogenesis and protein synthesis through the regulation of substrates. Akt also regulates proliferation, growth, and survival through regulation of substrates (such as FRHR and NFKB).

1.5.3 IR signalling pathways

In R^- mouse fibroblasts transfected with IR-A it has been shown that binding of insulin to the IR-A activates metabolic signalling, while IGF-II predominantly activates mitogenic effects in R^- mouse fibroblasts transfected with IR-A (Frasca et al., 1999). Jensen et al. also found that the S597 (an insulin mimetic peptide) only induces metabolic signaling when bound to

the IR-A (Jensen et al., 2007). This evidence demonstrates that different ligands can induce different signalling outcomes presumably by the recruitment of different adaptor proteins (Mlinar et al., 2007).

Several downstream proteins have been found to be differentially activated by insulin and IGF-II. With IGF-1R negative fibroblasts (R^-, derived from IGF-1R knockout mice) overexpressing the IR-A (R^-IR-A), Sacco et al. identified that IGF-II preferentially activated p70S6 kinase compared to insulin stimulation (Sacco et al., 2009). The same group (Morcavallo et al., 2011) performed a phosphotyrosine proteomic study and showed that while some signalling proteins were activated by both ligands, several proteins including IRS-2 and SPIN90, were phosphorylated upon IGF-II activation and not insulin activation. In addition, stimulation by these ligands induced different gene expression patterns (Pandini et al., 2003).

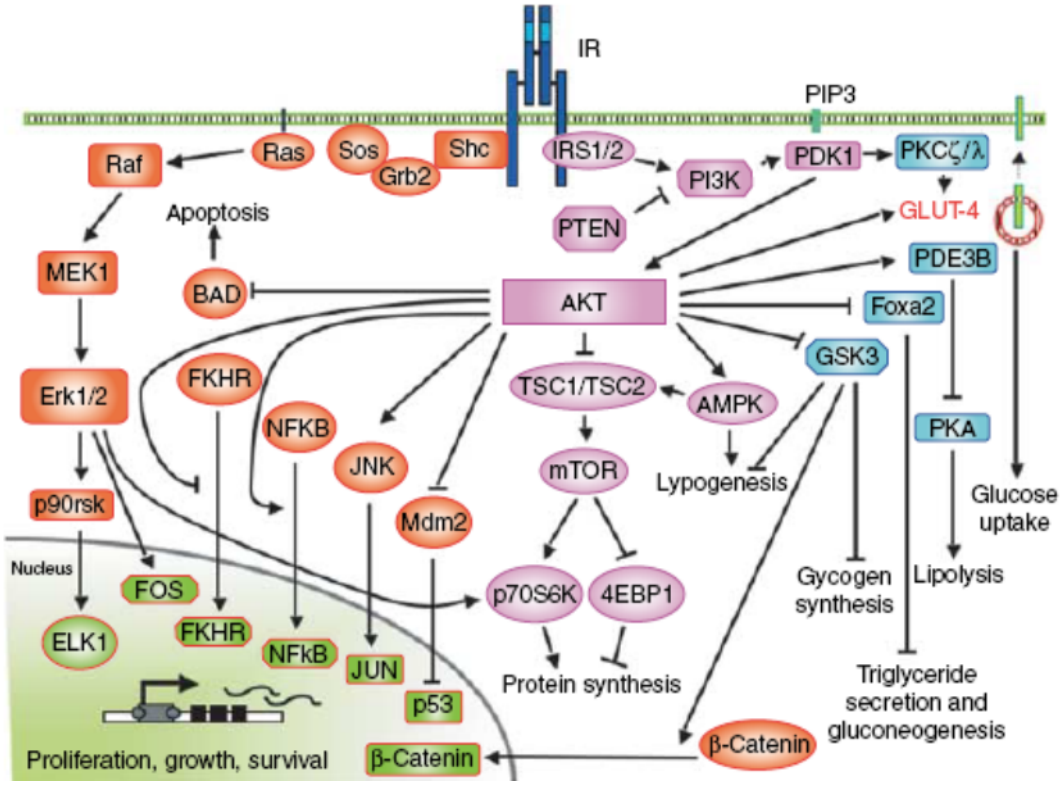

Figure 1.9: IR signalling pathways. After ligand binding, the activated IR phosphorylates several substrates, such as IRS1/2. IRS proteins interact with the regulatory subunit of PI3K leading to the activation of Akt. Akt interacts with a range of substrates to regulate metabolic and mitogenic biological activities. For example, Akt regulates protein translation and cell growth by inhibiting the Tubero sclerosis complex 1 and 2 (TSC1/TSC2) and thus activating mTOR. Insulin activation of the IR also triggers mitogenic signalling via the Ras/Raf/MEK/ERK pathway downstream of Shc/Grb2/Sos (figure from (Belfiore and Malaguarnera, 2011)).

1.6 IGF system in cancer

The dysregulation of the IGF system has been found in many cancer types, such as breast, prostate and colon cancers (Fair et al., 2007; Freier et al., 1999; Tennant et al., 1996). Epidemiological studies also show that the higher levels of IGFs and insulin are related to high risks of cancer (Fierz et al., 2010; Pisani, 2008). It is well known that the IGF system plays roles in the initial steps of malignant transformation and the later stages of tumor progression and metastasis (Saldana et al., 2013).

1.6.1 IGF-1R in cancer

IGF-1R sustains the cell survival and proliferation in many types of cancers. For example, Eliasz et al. (Eliasz et al., 2010) found that Notch-1 stimulates the survival of adenocarcinoma of the lung (ACL) cells in hypoxic microenvironment by the up-regulation of the IGF-1R pathway, as Notch-1 is a direct regulator of the IGF-1R promoter (Eliasz et al., 2010). The IGF-1R also promotes the survival of hepatocellular carcinoma (HCC) cells when treated with gefitinib, a cancer drug that inhibits the epidermal growth factor receptor (EGFR) pathway (Bodzin et al., 2012). The higher expression of IGF-1R can promote resistance to apoptotic effects in murine Lewis lung carcinoma cells (Li et al., 2012). Furthermore, antisense RNA targeting the IGF-1R reduces the tumour growth in many cancer models (Chernicky et al., 2002; Schillaci et al., 2006; Scotlandi et al., 2002).

1.6.2 IGF-II/IR-A autocrine loop in cancer

The IGF-II/IR-A signalling has been shown to provide an alternate mitogenic signalling pathway to the IGF-1R pathway in cancer cells that have developed resistance to anti-IGF-1R treatment (Avnet et al., 2009; Ulanet et al., 2010; Zhang et al., 2010). The IGF-II/IR-A signalling also stimulates cell migration (Sciacca et al., 2002). IR-A expression is increased in many types of cancer, such as breast and colon cancer (Brierley et al., 2010; Frasca et al., 1999). IGF-II expression is also increased in these types of cancers, especially in Triple

Negative Breast cancers (TNBC) (Fiore et al., 2010; Radhakrishnan et al., 2015; Toretsky and Helman, 1996).

1.6.3 IGF system and epithelial to mesenchymal transition (EMT)

Epithelial to mesenchymal transition (EMT) promotes tumor invasion, metastasis, and drug resistance. The features of EMT include decreased expression of E-cadherin and increased levels of mesenchymal markers such as vimentin, fibronectin, and N-cadherin (Zeisberg and Neilson, 2009).

The IGF-1R signalling can promote the epithelial to mesenchyme transition (EMT) in many cell types, such as ovarian carcinoma cells, human pancreatic carcinoma BxPC3 cells, childhood sarcomas and human chondrosarcoma cells (Burnier et al., 2011; Cheung et al., 2011; Irie et al., 2005; Jaquish et al., 2011). IGF-II also induces the degradation of E-cadherin and thus increases EMT transition (Morali et al., 2001). However, other studies have shown that IGF-II can also promote EMT features via the IR-A and not through activation of the IGF-1R (Vella et al., 2002; Zhao et al., 2012; Ziegler et al., 2014). The IGF-1R depletion actually promoted the more aggressive Wnt1-mediated murine mammary tumours, through the concomitant increased expression of IGF-II and IR-A (Rota et al., 2014). However, the EMT is a much more complicated process, besides under the regulation of IGF-1R and IR.

1.7 Current cancer treatments targeting the IGF system

There are several strategies to inhibit IGF action in cancer. One strategy is to decrease the bioavailability of ligands or receptors by monoclonal antibodies (Table 1.3). Another is to inhibit the receptor function by small molecule tyrosine kinase inhibitors (TKIs) (Table 1.4). Other strategies include the use of a modified IGFBP or siRNA treatment to decrease the functional proteins in IGF system; the use PI3K/Akt, mTOR or MAPK signalling pathway inhibitors to inhibit the IGF downstream signalling.

1.7.1 Anti-ligand monoclonal antibodies

Many monoclonal antibodies have been developed to target IGFs (Table 1.3). Two promising products are being tested in clinical trials, Xentuzumab and MEDI-573. Generally, antibody targeting the IGF induces a feedback to GH to produce more IGF and insulin as compensation, thus causing hyperinsulinemia, such as Xentuzumab (Boehringer Ingelheim) - the dual IGF-I/IGF-II monoclonal antibody (Mireuta et al., 2014). In tumor xenograft animal models, Xentuzumab can decrease tumor growth and even restore the sensitivity to the mutant-selective EGFR-TKI (WZ4002) (Martinez-Quetglas et al., 2016; Park et al., 2016a). However, its usage needs to be evaluated carefully, particularly the usage in children, because it inhibits the growth (Friedbichler et al., 2014).

MEDI-573 (AstraZeneca plc) – another dual IGF-I/IGF-II monoclonal antibody, significantly inhibits tumour growth in mice (Zhong et al., 2016). The elevated levels of insulin and growth hormone are not observed in its phase I trial, maybe the maximum usage is not reached yet (Haluska et al., 2014). Patients are currently being recruited for the Phase 2 clinical studies.

1.7.2 Anti-receptor monoclonal antibodies

Anti-IGF-1R monoclonal antibodies can be used to block ligand binding to the IGF-1R and to induce IGF-1R internalization and degradation as a means to inhibit IGF-1R signalling and biological action. Unfortunately, this strategy invariably leads to hyperglycemia and hyperinsulinemia, as there is increased secretion of more insulin and IGFs from a feedback effect (Gualberto and Pollak, 2009; Haluska et al., 2007).

Figitumumab failed to improve the overall survival of the patients in phase 3 clinical trials (Langer et al., 2014; Scagliotti et al., 2015). This failure resulted in discontinuation of its development. One possible reason for these failures is that cross talk exists between the IGF-1R pathway and the estrogen receptor and receptor tyrosine-protein kinase erbB-2 signalling pathways (Fox et al., 2011; Gee et al., 2005). Another main reason is the unregulated

expression of IGF-II and IR-A, which provides an alternative signalling pathway for IGF-II (Avnet et al., 2009; Baserga, 2013).

Monoclonal antibody	Stage of Development
IGF-I monoclonal antibodies	
Novartis patent anti-IGF-1/E	Preclinical
Roche patent anti-IGF-1	Preclinical
IGF-II monoclonal antibodies	
DX-2647	Preclinical
NIH patent anti-IGF-2	Preclinical
IGF-I and IGF-II monoclonal antibodies	
Xentuzumab (BI-836845)	Phase 2
MEDI-573	Phase 1
IGF-1R monoclonal antibodies	
Figitumumab	Phase 3 (Discontinued)
Ganitumab	Phase 3
Cixutumumab	Phase 2
Dalotuzumab	Phase 2
Teprotumumab	Phase 2
Robatumumab	Phase 2
Istiratumab	Phase 2
AVE1642	Phase 1
BIIB022	Phase 1
Biogen EI-04	Preclinical

Table 1.3: Antibodies that target the IGF system. Data are sourced from the Therapeutic Antibody Database (http://tabs.craic.com) (Oct 2016)

1.7.3 Small molecule tyrosine kinase inhibitors

Small molecule tyrosine kinase inhibitors (TKIs) compete for the ATP binding site in the catalytic domain of the IGF-1R and IR (Table 1.4). However, there is an overall lack of efficacy for TKIs used as sole agents to inhibit a range of cancer types due to the fact that the compensations of other signalling pathways (Bendell et al., 2015; Fassnacht et al., 2015). For example, Linsinib was ineffective in treating adrenocortical carcinoma and colorectal cancer in clinical trials, and any treatment with this drug was not recommended (Bendell et al., 2015; Fassnacht et al., 2015). The clinical trial of BMS- 754807 on patients with advanced or metastatic solid tumors was also terminated, due to the unreached expectations (ClinicalTrials.gov, https://clinicaltrials.gov/ct2/show/NCT00908024?term=BMS-+754807&rank=2). In addition, the compensation effect arose when receptors were inhibited in mice, leading to the increased IGFs and insulin levels in the serum (Dool et al., 2011).

Name	IGF-1R IC50 (Cell-free assay)	IR IC50 (Cell-free assay)	Stage of Development
OSI-906 (Linsitinib)	35nM	75nM	Phase 3
BMS-754807	1.8nM	1.7nM	Phase 2
Picropodophyllin (PPP)	1nM		Phase 1/2
KW-2450	7.39nM	5.64nM	Phase 1
GSK1838705A	2nM	1.6nM	Preclinical
GSK1904529A	27nM	25nM	Preclinical
BMS-536924	100nM	73nM	Preclinical
NVP-AEW541	150nM	140nM	Preclinical
NVP-ADW742	170nM		Preclinical
PQ401	<1μM		Preclinical
AG-1024	7μM	54μM	Preclinical
A-928605			Preclinical
Insm-18 (NDGA)			Preclinical
XL-228	2nM		Preclinical
ABDP			Preclinical

Table 1.4: A selection of small molecule inhibitors that target the IGF-1R and IR. Data are sourced from Selleckchem Database (Oct 2016) (http://www.selleckchem.com/IGF-1R.html?gclid=CIHr0pb0r8kCFQskvQodFacDOA) and AdooQ database (http://www.adooq.com/catalogsearch/result/?q=insulin+receptor).

1.7.4 Other treatment strategies

The modified IGFBPs are under development to regulate circulating IGF levels (Soh et al., 2015). Concern over the use of IGFBPs arises because IGFBPs are shown to have both IGF-dependent and independent actions (Yu and Rohan, 2000). The modified IGFBP-2 reported by Soh et al., took this into account by mutating or removing motifs responsible for IGF-independent actions while maintaining the ability to bind IGFs. This modified IGFBP was shown to inhibit breast tumour xenograft growth (Soh et al., 2015).

The use of RNAi as cancer treatments has been improved in many aspects, especially in decreasing off-target effects and optimising the delivery system (Sanderson et al., 2015). . However, there is still long way to go. Death of a patient in a phase 3 clinical trial of Revusiran from world-renowned gene therapy company Alnylam cast a shadow over gene therapy's future (http://www.genengnews.com/gen-news-highlights/after-18-deaths-in-phase-iii-alnylam-halts-revusiran-development/81253293).

It is well known that the PI3K/Akt, and MAPK signalling pathways are downstream of the IGF-1R. The inhibitors that target the molecules of the PI3K/Akt and MAPK signalling pathways are being developed (Pivonello et al., 2016). The combined inhibition of IGF-1R/IR and downstream signalling mediators is a promising approach (Herkert et al., 2016; Lamhamedi-Cherradi et al., 2016).

Several questions need to be addressed in the future: the crosstalk of the IGF system to other signalling pathways; the compensatory effects of increased levels of IGFs and insulin; the lack of biomarkers to select for sensitive and resistant patients; lack of optimisation of the dose and schedule; the lack of understanding of the role of IR-A/IGF-II signalling. A further understanding of the IGF system is necessary to enable the design of more effective treatment strategies.

1.8 Summary, Hypothesis and Aims

Dysregulation of the IGF system leads to cancer cell proliferation, survival, and migration. As discussed before, there are shared and different signalling pathways downstream of the IR-A, IR-B, and IGF-1R. Furthermore, the IGF-II/IR-A autocrine loop has been identified as an alternative signalling pathway causing resistance to the anti-IGF-1R therapies. It is therefore desirable to develop anticancer therapies that target the IGF-II/IR-A autocrine pathway specifically, without impairing the metabolic effects of the insulin receptor.

There have been many studies investigating the IGF-II/IR-A signalling pathway using various methods including standard immunoblotting (Frasca et al., 1999; Sciacca et al., 2002), microarray analysis (Pandini et al., 2003) and proteomics (Morcavallo et al., 2011). Overall these studies show that IGF-II is more potent in promoting mitogenic signals than insulin (Frasca et al., 1999; Sciacca et al., 2002). However, most studies so far have investigated IGF-II signalling via the IR-A using the R^-IR-A fibroblast cell line rather than in cancer cells in which the IGF-II:IR-A autocrine loop components are expressed. However, the markers identified to differentiate the Insulin/IR-A and IGF-II/IR-A signalling pathway in R^-IR-A cells are not always consistent with cancer cells. For example, the activation of the ephrin type-B receptor 4 (EphB4) through IR signalling is different between R^-IR-A and MCF-7, the EphB4 was activated by IGF-II in R^-IR-A cells while IGF-II was more effective to activate the EphB4 than insulin in MCF-7 cells (Morcavallo et al., 2011).

Based on the evidence listed above, I hypothesize that insulin and IGF-II induce both shared and different IR-A activation patterns (or phosphorylation patterns) and downstream signalling cascades to promote cancer cell proliferation and migration. The differences in signalling could in the future be potentially exploited as targets to inhibit tumour growth and metastasis.

The aims of this thesis were to:

1: Define the role of a previously undescribed phosphosite at residue Thr^{1148}, which is in the middle of the three phosphotyrosine sites in the activation loop, in insulin signalling. In this thesis, I used site-directed mutagenesis to help understand the role the Thr^{1148} phosphorylation in IR activation.

2: Identify a signature of kinase targets that is unique to IGF-II/IR-A autocrine signalling. To achieve this the following steps were taken:

i. Construct model breast cancer cell lines expressing only the IGF-1R or the IR through receptor knockdown (IGF-1RKD and IRKD).

ii. Analyse the biological activities of the model cell lines (proliferation assay, migration assay, EMT marker PCR) in response to insulin and IGF-II.

iii. Optimize an appropriate quantitative phosphoproteomics method.

iv. Identify the signature proteins that are differentially regulated between the Insulin/IR-A and IGF-II/IR-A signalling pathways in a breast cancer cell line predominantly expressing the IR-A using the optimized quantitative phosphoproteomics method.

Chapter 2 Materials

2.1 Materials

Materials	Sources
$^{13}C_6$-L-Arginine HCl	Silantes GmbH (#201204102)
$^{13}C_6$,$^{15}N_2$-L-Lysine HCl	Silantes GmbH (#211604302)
$^{13}C_6$,$^{15}N_4$-L-Arginine HCl	Silantes GmbH (#201604102)
2-log DNA ladder	New England Biolabs, USA
2% Bis	Bio-Rad, Hercules, CA, USA
4-(2-hydroxyethyl)-1-piperazineethanesulfonic acid, HEPES	Scharlau, Barcelona, Spain
4,4,5,5-D_4-L-Lysine 2HCl	Silantes GmbH (#211104113)
40% Polyacrylamide	Bio-Rad, Hercules, CA, USA
Acetic acid, glacial	VWR International, Radnor, PA, USA
Acetonitrile	Merck, Kenilworth, NJ, USA
ACTRAPID (Insulin)	Novo Nordisk Australia
Agarose	Sigma, St. Louis, MO, USA
Ammonium bicarbonate	BDH (Poole, UK)
Ammonium persulphate, APS	Sigma, St. Louis, MO, USA
Anti-rabbit HRP, 1:3000 dilution	Jackson ImmunoResearch, USA
Applied Biosystems Fast SYBR® Green Mastermix	Life Technologies, Carlsbad, CA, USA
Boric acid	Sigma, St. Louis, MO, USA
Bovine serum albumin, BSA	Sigma, St. Louis, MO, USA
Calcium chloride, CaCl2	Ajax chemicals Ltd., Sydney, Australia
Charcoal Stripped Fetal Bovine Serum	Thermo Fisher Scientific (#12676011)
CHCA	Bruker Daltonics
Chloroform	Sigma, St. Louis, MO, USA
cOmplete ULTRA Tablets, Mini, EDTA-free, EASYpack	Roche
Coomassie G-250	Sigma, St. Louis, MO, USA
Crystal violet	Sigma-Aldrich
DC™ Protein Assay Kit II	Bio-Rad (#5000112)
DHB	Bruker Daltonics
Dialyzed fetal bovine serum, US origin	Thermo Fisher Scientific
Diethylpyrocarbonate (DEPC)	Life Technologies, Carlsbad, CA, USA
DMEM, high glucose, HEPES	Thermo Fisher Scientific (#12430-062)
DMSO for molecular biology	Sigma-Aldrich (Castle Hill, Australia)
dNTPs	New England Biolabs, USA

DTT	Sigma-Aldrich (Castle Hill, Australia)
DMEM - SILAC	Sigma-Aldrich (#D9443)
EDTA	Sigma, St. Louis, MO, USA
Empore™ SPE Disks	3M™
Ethanol	Sigma, St. Louis, MO, USA
Fetal Bovine Serum	Thermo Fisher Scientific (#10099141)
Formaldehyde solution, 37 wt. % in H2O	Sigma-Aldrich (Castle Hill, Australia)
Formic acid (FA, p.a., >98% purity)	Fluka Chemie (Neu-Ulm, Germany)
Gateway® LR Clonase® Enzyme mix	Thermo Fisher Scientific (#11791019)
GelRed	Biotium Inc., Hayward, CA, USA
Geneticin® Selective Antibiotic (G418 Sulfate) (50 mg/mL)	Thermo Fisher Scientific (#10131027)
GlutaMAX™ Supplement	Thermo Fisher Scientific (#35050061)
Glycine	VWR International, Radnor, PA, USA
Guanidine hydrochloride (GdmCl)	Sigma-Aldrich (#G3272)
HF Phusion® Polymerase and buffer	New England Biolabs, USA
High Capacity RNA to cDNA kit	Life Technologies, Carlsbad, CA, USA
Human gamma globulin	Sigma-Aldrich (Castle Hill, Australia)
Hydrochloric acid, HCl	Sigma, St. Louis, MO, USA
IGF-I	Gropep, Australia
IGF-II	Gropep, Australia
Iodoacetamide, IAA	Sigma-Aldrich (Castle Hill, Australia)
Isopropanol	Sigma, St. Louis, MO, USA
Lipofectamine® LTX with Plus™ Reagent	ThermoFisher
L-Arginine	Sigma-Aldrich (#A5006)
L-Leucine	Sigma-Aldrich (#L8912)
L-Lysine	Sigma-Aldrich (#L5501)
LR3 IGF-I	GroPep
lysyl endopeptidase, biochemistry grade	WAKO (#12502543)
Methanol	RCI Labscan, Thailand
Microcon YM-30	Millipore, Billerica, MA
Normal rat serum	Forbes Lab
Normal mouse IgG1	Santa Cruz Biotechnology (#SC-3877)
Penicillin-Streptomycin (10,000 U/mL)	Thermo Fisher Scientific (#15140122)
Phosphoric acid	Sigma, St. Louis, MO, USA

PhosSTOP™	Roche
Polybrene	Sigma-Aldrich
Protein Standard I	Bruker Daltonics, Billerica, MA, USA
Puromycin dihydrochloride	Sigma-Aldrich
QIAGEN Plasmid Midi Kit	QIAGEN
Sodium chloride, NaCl	Sigma, St. Louis, MO, USA
Sodium dodecyl sulphate, SDS	Bio-Rad, Hercules, CA, USA
Sodium phosphate	Ajax chemicals Ltd., Sydney, Australia
Stage Tips C8 material 200uL tip 96pcs	Thermo Fisher Scientific (#SP321)
Streptavidin HRP	R&D Systems, Minneapolis, MN, USA
Sulphuric acid	Ajax chemicals Ltd., Sydney, Australia
Sulphuric acid, H2SO4	Sigma, St. Louis, MO, USA
Supported nitrocellulose membrane	GE Healthcare Life Sciences, Parramatta, NSW, Australia
Syringe filter (0.22, 0.45 µm)	Sartorius AG, Gottingen, Germany
Tetramethylethylenediamine, TEMED	Sigma, St. Louis, MO, USA
Titansphere PHOS-TiO, 10um, 500mg	GL Sciences (#5010-21315)
TRI-reagent	Sigma, St. Louis, MO, USA
Trifluoroacetic acid, TFA	Merck, Kenilworth, NJ, USA
Tris	Sigma, St. Louis, MO, USA
Trypsin	Promega (Madison, WI, USA)
Trypsin-EDTA (0.5%), no phenol red	Thermo Fisher Scientific (#15400054)
Tween-20	Sigma, St. Louis, MO, USA
Western Lightning Plus	Perkin-Elmer, Turku, Finland
X-ray film (Curix ortho HT-G 100 NIF Ecopac)	Agfa, Belgium
ZipTip Pipette Tips	Merck Millipore

Table 2.1: Materials used in this thesis.

2.2 Primers

All the primers used in this thesis for PCR, site- directed mutagenesis, sequencing and shRNA are shown in Table 2.2.

Name	Sequence	Usage
IR primer	Forward: CTGGGAGAGGCAGGCATATGACAGT GAGCTGTTCG Reverse: CCTGGTTGCAAGCCTGCAGATCGAT GCGATAGCCC	PCR, IR-A size: 473bp, IR-B size: 509bp
IGF-1R	Forward: ACT TCT GCG CCA ACA TCC TCA Reverse: CCC TTT AGT CCC CGT CAC TTC C	PCR, size: 572bp
GAPDH	Forward: TGG TAT CGT GGA AGG ACT CAT GAC Reverse: ATGCCAGTGAGCTTCCCGTTCAGC	PCR, size: 189bp
E-cadherin	Forward: CACGGTAACCGATCAGAATG Reverse: ACCTCCATCACAGAGGTTCC	PCR, size: 102bp
T-A	Forward: GACATCTACGAGGCCGACTACTACA GAAAG Reverse: CTTTCTGTAGTAGTCGGCCTCGTAG ATGTC	Site directed mutagenesis, mutation of IR Threonine 1148 to Alanine
T-D	Forward: CTTTCTGTAGTAGTCGTCCTCGTAGA TGTC Reverse: GACATCTACGAGGACGACTACTACA GAAAG	Site directed mutagenesis, mutation of IR Threonine 1148 to Aspartic acid
Forward primer-T7	CGAAATTAATACGACTCACTATAGG G	Sequencing

shGL3	TGCTGTTGACAGTGAGCGCCCGCCT GAAGTCTCTGATTAATAGTGAAGCC ACAGATGTATTAATCAGAGACTTCA GGCGGTTGCCTACTGCCTCGGA	shRNA negative control
shIR1	TGCTGTTGACAGTGAGCGACGCATG TAAATTTTTATCAAATAGTGAAGCC ACAGATGTATTTGATAAAAATTTAC ATGCGCTGCCTACTGCCTCGGA	shRNA targeting site 6578-6599bp of IR
shIR2	TGCTGTTGACAGTGAGCGCCCAGGA GAATTTCAAGTTTTATAGTGAAGCC ACAGATGTATAAAACTTGAAATTCT CCTGGATGCCTACTGCCTCGGA	shRNA targeting site 4707-4728bp of IR
shIR3	TGCTGTTGACAGTGAGCGCCGGGAA AATACAGCATGTAAATAGTGAAGCC ACAGATGTATTTACATGCTGTATTTT CCCGATGCCTACTGCCTCGGA	shRNA targeting site 6271-6292 of IR
shIR4	TGCTGTTGACAGTGAGCGAGCCCAT GATTTTACTGTCAAATAGTGAAGCC ACAGATGTATTTGACAGTAAAATCA TGGGCGTGCCTACTGCCTCGGA	shRNA targeting site 3610-3631bp of IR
shIGF-1R1	TGCTGTTGACAGTGAGCGCCATGGC CAATTTGTTACATAATAGTGAAGCC ACAGATGTATTATGTAACAAATTGG CCATGTTGCCTACTGCCTCGGA	shRNA targeting site 10955-10976bp of IGF-1R
shIGF-1R2	TGCTGTTGACAGTGAGCGCGCCGAA GATTTCACAGTCAAATAGTGAAGCC ACAGATGTATTTGACTGTGAAATCT TCGGCTTGCCTACTGCCTCGGA	shRNA targeting site 3479-3500bp of IGF-1R
shIGF-1R3	TGCTGTTGACAGTGAGCGACGGAGT CACATTTCAATGGTATAGTGAAGCC ACAGATGTATACCATTGAAATGTGA CTCCGCTGCCTACTGCCTCGGA	shRNA targeting site 8590-8611bp of IGF-1R
shIGF-1R4	TGCTGTTGACAGTGAGCGCCAAGGG CAATTTGCTCATTAATAGTGAAGCC ACAGATGTATTAATGAGCAAATTGC CCTTGATGCCTACTGCCTCGGA	shRNA targeting site 10479-10500bp of IGF-1R
M30c Iso Forward	Forward: CTTGCTGGGATTACTTCTTCAGGTTA ACCCAACAGAAGGCTCGAGAAGGT ATATTGCTGTTGACAGTGAGCG Reverse: AACAAGATAATTGCTCCTAAAGTAG CCCCTTGAATTCGATTCCGAGGCAG TAGGCA	Amplification of the shRNA PCR product used for Gibson assembly
pENTR sequencing primer	GTGTCTCAAAATCTCTGATGTTAC	shRNA vector Sequencing

Tabel 2.2: Primer list. The shRNA targets are mapped using numbering from the IGF-1R (NCBI reference number: NM00875.3) and IR (NCBI reference number: NM_000208.2) sequences.

2.3 Vectors

Name	Source	Usage
pMK-RQ_IR-A fragment	Synthesized at GENEART	Synthesize the IR-A fragment
pMK-RQ_InsR_3×myc	Synthesized at GENEART	Synthesize IR fragment with myc tag at the C-terminal
pcDNA3.1 (IR-B)	Synthesized at GENEART	Synthesize the IR-B cDNA
pBluescript(KS+)	Addgene	Used for Site-directed mutagenesis
pcDNA3.1 (IR-Amyc)	Generated in this thesis	Used for cell transfection and protein overexpression
pcDNA3.1 (T1148A IR-Amyc)	Generated in this thesis	Used for cell transfection and protein overexpression
pcDNA3.1 (T1148D IR-Amyc)	Generated in this thesis	Used for cell transfection and protein overexpression
pLV-TRE3G-IRES- Puro	Whitelaw Lab	Lentivector backbone
pENTR1a-dsRed-m30c	Whitelaw Lab	Used for Gibson assembly and sequencing
pCMV-dvrp8.2	Addgene	2nd generation lentiviral packaging plasmid
pRSV-Rev	Addgene	3rd generation lentiviral packaging plasmid
pMD2.G (VSV-G)	Addgene	VSV-G envelope expressing plasmid
pLV-TRE3G-IRES- Puro-shGL3	Whitelaw Lab	Lentivector expressing shRNA negative control

Table 2.3: Vectors used in this thesis.

2.4 Strain

Strain	Genotyoe
DH5α	F– Φ80*lac*ZΔM15 Δ(*lac*ZYA-*arg*F) U169 *rec*A1 *end*A1 *hsd*R17 (rK–, mK+) *pho*A *sup*E44 λ– *thi*-1 *gyr*A96 *rel*A
DB3.1	F– *gyr*A462 *end*A1 Δ(sr1-*rec*A) *mc*rB *mrr hsd*S20(rB–, mB–) *sup*E44 *ara*-14 *gal*K2 *lac*Y1 *pro*A2 *rps*L20(SmR) *xyl*-5 λ– *leu mtl*1

Table 2.4: The *E. coli* strains used in this thesis.

2.5 Cell lines

Cell line	Characteristics	Source
R^-	Mouse fibroblast cells with IGF-1R KO	A gift from Professor R. Baserga (Philadelphia, USA)
R^- IR-Amyc	R^- cells overexpressing IR-A-myc	Generated in this thesis
R^- T1148A IR-Amyc	R^- cells overexpressing IR-A-myc with Threonine 1148 replaced by Alanine	Generated in this thesis
R^- T1148D IR-Amyc	R^- cells overexpressing IR-A-myc with Threonine 1148 replaced by Aspartic acid	Generated in this thesis
293T	Highly transfectable derivative of human embryonic kidney 293 cells	American Type Culture Collection (Manassas, VA)
MDA-MB-231	Negative for estrogen receptors, progesterone receptors, and HER2; Metastatic Breast Cancer	American Type Culture Collection (Manassas, VA)
MCF-7	Postive for estrogen receptors, progesterone receptors, and HER2; Non-metastatic Breast Cancer	American Type Culture Collection (Manassas, VA)

Table 2.5: Cell lines used in this thesis.

Name	Target	Host	Catalog (Company)	Dilution/Working concentration
Phospho-IR/IGF1R (Tyr1158, Tyr1162, Tyr1163) Antibody	Activation loop of IR/IGF-1R	Rabbit	#44-806G (Invitrogen)	1:500
Anti-Insulin Receptor beta antibody [C18C4]	IR-beta subunit	Mouse	ab69508 (abcam)	1:1000
IGF-I Receptor β Antibody	IGF-1R beta subunit	Rabbit	#3027(Cell signaling)	1:1000
24-60 monoclonal antibody	IGF-1R alpha subunit	Mouse	GroPep	0.04 mg/ml
83-7 monoclonal antibody	IR-alpha subunit	Mouse	GroPep	0.04 mg/ml
beta-Tubulin antibody	TUBA4A	Mouse	#32-2600 (Life technologies)	1:1000
Phospho-Akt (Thr308) Antibody	Phospho-Akt (Thr308)	Mouse	#9275 (Cell signaling)	1:1000
Pathscan Multiplex Western Cocktail	pAKT, pS6, p44/42 (Erk), phospho p90RSK and eIF4E	Rabbit	#5301 (Cell signaling)	1:200
IgG1 negative control	IgG1	Mouse	MABC002 (Chemicon)	0.04 mg/ml
IgG antibody, FITC conjugated	IgG	Mouse	AB7138F (Chemicon)	1:100
IRDye® 680LT Donkey anti-Mouse IgG (H + L)	Secondary antibody		P/N 925-68022 (LI-COR)	1:50,000
IRDye® 800CW Donkey anti-Rabbit IgG (H + L)	Secondary antibody		P/N 925-32213 (LI-COR)	1:50,000

Table 2.6: Antibodies used in this thesis.

2.7 Buffers

4× SDS protein loading dye: 40% Glycerol; 240 mM Tris/HCl pH 6.8; 8% SDS, 0.04% bromophenol blue; 5% beta-mercaptoethanol (added fresh).

6× DNA loading dye: 0.25% w/v bromophenol blue; 0.25% w/v xylene cyanol FF; 30% v/v glycerol.

1X TBE: 89 mM Tris; 89 mM boric acid; 2 mM EDTA; pH 8.3.

1X Sodium Borate (SB) Buffer: 0.8 g of NaOH; 2.35 g of boric acid in 1L deionized water.

LB medium: 10 g of tryptone; 5 g of yeast extract; 10 of g NaCl in 1L deionized water, pH 7.0 , autoclaved.

HEPES lysis buffer: 20 mM HEPES; 150 mM NaCl; 1.5 mM $MgCl_2$; 10% Glycerol; 1% Triton X-100; 1 mM EGTA; pH7.5. 100mM NaF, 2mM Na_3VO_4, 1% Protease Inhibitor Cocktail (Sigma-Aldrich) and 1% PhosSTOP (Roche) were added fresh.

Coomassie Blue Stain: 10% (v/v) acetic acid; 0.006% (w/v) Coomassie Blue dye in MQH_2O.

Isopropanol Fixing Solution: 10% (v/v) acetic acid; 25% (v/v) isopropanol in MQH_2O.

GdmCl lysis buffer: 6 M GdmCl; 100 mM Tris pH 8.5; 10 mM TCEP; 40 mM CAA, 1% PhosSTOP (Roche).

1× Phosphate buffered saline (PBS): 137 mM NaCl, 10 mM Phosphate, 2.7 mM KCl, and pH of 7.4

Disruption Buffer: 200 mg/l EDTA in PBS and was filtered (0.22 µm).

Staining buffer: PBS containing 1% BSA and 0.01% sodium azide.

RIPA buffer: 50 mM TRIS, 150 mM NaCl, 0.1% SDS, 0.5% sodiumdesoxycholate, 1% triton X-100.

GTS Running buffer: 25 mM Tris, 192 mM glycine, 0.1% SDS

Transfer Buffer: 25 mM Tris, 190 mM glycine, 20% methanol

Chapter 3 Methods

3.1 Molecular Biology

3.1.1 Preparation of plasmid DNA

Routine preparation of plasmid DNA was performed using the QIAprep Spin Plasmid Miniprep Kit (Qiagen), according to the manufacturer's instructions. DNA was eluted using 40 µL H_2O and stored at –20°C.

3.1.2 Large-scale plasmid purification

When larger amounts of plasmid DNA were required, the QIAGEN Plasmid Midi Kit was used, according to the manufacturer's instructions. Plasmid DNA was eluted with 400 µL TE buffer.

3.1.3 Analysis of DNA size, purity and concentration

DNA samples were assessed for size, purity and concentration using agarose gel electrophoresis. Agarose was mixed with 1X TBE or 1X SB (DNA size<1kb) and melted in a microwave oven and then cast into minigels ranging from 1% – 2.5% agarose. Prior to loading into the wells, DNA samples were mixed with 6x DNA loading dye in 1X TBE or 1X SB buffer. Gels were visualized using a UV transilluminator coupled to a CCD camera (ChemiDoc, Biorad) or ChemiDoc Imaging System. Comparison of DNA bands with DNA molecular markers (New England Biolabs) allowed estimation of DNA size and concentration. Accurate measurement of DNA concentration was performed using a NanoDrop 2000 spectrophotometer (Thermo Scientific).

3.1.4 Restriction enzyme digestion

Restriction digests of DNA were performed using restriction enzymes from New England Bio- labs according to the manufacturer's instructions. Reaction volumes ranged from 5–50 µl, reaction times ranged from 1 hour to overnight and reaction conditions and incubation temperatures were used as specified by the manufacturer.

3.1.5 Gel extraction of DNA fragments

Digested DNA fragments or plasmids required for cloning were run on a large-well agarose gel at 90 V. The gel was then immersed in GelRed DNA stain (Biotium) for 20 minutes and DNA bands were visualized using a Safe Imager bright light transilluminator (Invitrogen). Bands were excised from gels using a clean scalpel blade, and DNA was purified using the QIAquick Gel Extraction Kit (Qiagen) according to the manufacturers instructions, with a 30 µl elution volume. 1 µl of the gel extraction was checked for purity and concentration on an agarose gel or NanoDrop spectrophotometer.

3.1.6 Treating digestions with Antarctic Phosphatase

Linearized vectors with compatible ends were treated with Antarctic Phosphatase (New England Biolabs), which catalyzes the removal of 5' phosphate groups from DNA thereby preventing self religation. Treatment with Antarctic Phosphatase thus reduced the background number of colonies on transformation plates resulting from religated, singly-cut vector without the desired insert. 5 units of Antarctic Phosphatase were added to restriction digests made up to 1x Antarctic Phosphatase buffer (New England Biolabs) and reactions were incubated for 15 minutes at 37°C and then heat inactivated at 65°C for 5 minutes.

3.1.7 Ligating restricted DNA fragments into restricted vectors

Ligations were performed in 10 µl reaction volumes, containing 0.5–2 units of T4 DNA ligase, 1x ligase buffer (New England Biolabs) and an approximate 3:1 molar ratio of insert to vector DNA, with the concentration of vector DNA in the range 10–100 ng. A control reaction containing vector but lacking insert DNA was prepared identically to determine the number of background colonies resulting from the vector DNA alone. Following incubation for 1 hour at room temperature, 5 µl of the ligation reaction was transformed into competent cells.

3.1.8 Site-directed mutagenesis

PCR set-up: 0.5 µl of Phusion High-Fidelity DNA Polymerase, 10 µl of 5× buffer, 1 µl of 10 mM dNTP, 1.25 µl of 100 ng/µl forward primer, 1.25 µl of 100 ng/µl reverse primer, 50 ng of plasmid in 50 µl reaction.

Cycling parameters:

Segment	Temperature	Time	Cycle number
Initial denaturation	98°C	1 minute	1
Denaturation	98°C	30 seconds	18
Annealing	55°C	1 minute	
Extension	72°C	2.5 minutes	

Table3.1: Site-directed mutagenesis PCR cycling parameters.

300 units of DpnI (New England Biolabs) were added into 20 µl of PCR products to digest the methylated, non-mutated DNA template and 5 µl of the digested products were used for transformation.

3.1.9 Transformation

Competent cells were thawed on ice (approximately 20-30 minutes). DNA (usually 100 pg to 100 ng) was mixed into 20-50 µl of competent cells in a microcentrifuge tube. The competent cell/DNA mixture was left on ice for 20-30 minutes. The competent cell/DNA mixture was heat shocked for 45 seconds at 42°C. The tube was chilled again on ice for 2 min. LB or SOC media (500-900 µl, without antibiotic) was added and cultured in 37°C shaking incubator for 45 minutes. Some or all of the transformation was plated onto a 10 cm LB agar plate containing the appropriate antibiotic (Ampicillin concentration at 100 µg/ml, Kanamycin concentration at 25 µg/ml) and incubated at 37°C overnight.

3.1.10 Generation of high Competency DH5α cells

High competency cells were needed for transformation with Gibson Assembly products. The method is based on the original Inoue method (Inoue et al., 1990). Transformation buffer contains: 10 mM of PIPES (1,4-Piperazinediethanesulfonic acid), 15 mM of $CaCl_2$-$2H_2O$, 250 mM of KCl and 55 mM of $MnCl_2$ at pH 6.7-6.8. It was filtered (0.22 μm) and kept at 4°C. Cells were incubated on shaker (150-250 rpm) at 18°C to culture density between 0.4-0.6 O.D. (600 nm) and then centrifuged down at 3,000 rpm and chilled on ice. Cells were then washed by 1/3 volume of ice-cold transformation buffer and chilled on ice for 10 minutes before another spin down. Cells were re-suspended with 1/12.5 volume of ice-cold transformation buffer with 7% DMSO. Cells were diluted into 100 μl aliquots, frozen with dry ice and stored in -80°C.

3.1.11 Gibson Assembly of DNA fragments

Gibson assembly was performed with Gibson Assembly Master Mix (New England Biolabs), according to the manufacture's instructions. Briefly, 25 ng of vector with the molar ratio of vector to DNA fragment 1: 5 and 2.5 μl of Gibson Assembly Master Mix were used in 5 μl volume. The reaction was incubated for 1 hour at 50°C and all 5 μl for transformation.

3.1.12 Gateway LR cloning

Gateway LR Clonase Enzyme mix (ThermoFisher) was used to construct the lentivector with shRNA fragment. Reaction set-up: 150 ng of entry vector, 150 ng of destination vector, 2 μl of 5×LR buffer, 1 μl of LR Clonase Enzyme mix in 10 μl of total reaction. The reaction was conducted at 25°C overnight and terminated by mixing with 1 μl of proteinase K solution for 10minutes at 37°C.

3.1.13 Big Dye Sequencing reactions

DNA sequencing was performed using BigDye Terminator Version 3.1 (Applied Biosystems) according to the directions provided by the Australian Genomics Research Facility (AGRF)

sequencing service (http://www.agrf.org.au/index.php?id=72). Briefly, sequencing reactions contained 2µl BigDye v3.1 Ready Mix, 6 µl of 5x BigDye buffer, 250-500 ng of template and 3 pmoles of primer in a total volume of 20 µl. Sequencing reactions were incubated in thin-walled 0.2 ml PCR tubes at 96°C for 2 minutes, then 25 cycles of 96°C for 20 seconds, 50°C for 10 seconds and 60°C for 4 minute. Sequencing reactions were then precipitated by adding 80 µl of 75% isopropanol and transferred to a 1.5 ml Eppendorf tube. Sequencing products were incubated at room temperature for 15 minutes and then collected by centrifugation at maximum speed at room temperature for 20 minutes. The pellet was then washed with 150 µl of 75% isopropanol, centrifuged for a further 5 minutes with the tubes in the same orientation, and the supernatant was removed. Samples were then dried. The resultant chromatograph and sequence files were viewed using ApE Plasmid Editor.

3.1.14 RNA extraction

RNA extraction was processed with TRI Reagent® (Sigma). 0.5 ml of TRI Reagent® (Sigma) was used for one well of 6-well plates. The other reagents were used with ratio according to the manufacturer's instructions. Finally, RNA was dissolved in 30 µl of diethylpyrocarbonate (DEPC) treated water (DEPC treated water was prepared previously by making up 0.1% DEPC in MQ water and autoclaving). The isolated RNA was stored in -80°C until required.

3.1.15 RNA quality check

Upon extraction, RNA concentration was determined using a NanoDrop 2000 UV-Vis spectrophotometer (Thermo Scientific). Concentration of the RNA was determined at 260 nm while the ratios of absorbance at 260 nm/280 nm of 2.0 was considered pure. Besides a check by spectrophotometry, the quality of the extracted RNA (2 µg) was also checked using gel electrophoresis to detect the 18s and 28s ribosomal RNA.

3.1.16 cDNA synthesis

2 µg of RNA was reverse transcribed to cDNA using the High-Capacity RNA-to-cDNA™ kit (Life Technologies) according to manufacturer's instructions. Briefly, the reaction mix was prepared as outlined in Table 3.2. The cDNA was synthesised in a Peltier Thermal Cycler 200 (MJ Research, CA, USA) using the cycling parameters: 37°C for 60 minutes followed by 95°C for 5 minutes. When the transcription reaction is completed the cDNA was stored at -20°C.

Component	**Volume (µL)**
2X RT buffer	10
20X Enzyme Mix	1
2 µg RNA	X
DEPC treated water	9-X
Total volume	20

Table 3.2: Volume of components needed for the reverse transcription reaction mix, x is the volume needed for 2 µg of RNA.

3.1.17 Semi-quantitative PCR

Taq DNA Polymerase (New England Biolabs) was used to conduct the semi-quantitative PCR according to manufacture's instructions. Briefly, 100 ng of cDNA was used in a 25 µl reaction; the reaction mix was prepared as outlined in the Table 3.3:

Component	**Component volume (µl)**
10X reaction buffer	2.5
50mM $MgSO_4$	0.5
10mM dNTPs	0.5
10µM forward primer	0.5
10µM reverse primer	0.5
cDNA Template (100 ng/µl)	1

DEPC water	19
Taq polymerase	0.5
Total volume	25

Table 3.3: Volume of components needed for the PCR reaction mix.

The PCR was performed in a Peltier Thermal Cycler 200 (MJ Research, CA, USA) using the cycling parameters in Table 3.4:

Segment	**Temperature**	**Time**	**Cycle number**
Initial denaturation	98°C	3 minutes	1
Denaturation	98°C	30 seconds	30 (except IR PCR using 40)
Annealing	55°C	30 seconds	
Extension	72°C	1 minutes	
Final extension	72°C	10 minutes	1

Table 3.4: PCR parameters.

3.1.18 shRNA PCR

Phusion High-Fidelity DNA Polymerase (New England Biolabs) was used to conduct the PCR according to manufacture's instructions. Briefly, 1 μM of 97-mer shRNA template was used in a 50 μl reaction; the reaction mix was prepared as outlined in the Table 3.5:

Component	**Component volume (μl)**
5X Phusion GC buffer	10
10mM dNTPs	1
10μM forward primer	1
10μM reverse primer	1
1 μM Template	1
Milli-Q water	35.5
Polymerase	0.5
Total volume	50

Table 3.5: Volume of components needed for the PCR reaction mix.

The PCR was performed in a Peltier Thermal Cycler 200 (MJ Research, CA, USA) using the cycling parameters in Table 3.6:

Segment	Temperature	Time	Cycle number
Initial denaturation	98°C	30 seconds	1
Denaturation	98°C	10 seconds	35
Annealing	54°C	30 seconds	
Extension	72°C	6 seconds	
Final extension	72°C	10 minutes	1

Table 3.6: PCR parameters.

3.2 Biochemistry

3.2.1 DC™ (detergent compatible) protein assay

The DC™ (detergent compatible) protein assay (Bio-rad) is a colorimetric assay for protein concentration following detergent solubilisation. The reaction is similar to the well-documented Lowry assay with modifications. Protein concentrations were measured with this kit, according to manufacture's microassy instructions. The measurement was performed with 2030 Multilabel Reader (Perkin Elmer).

3.2.2 EZQ™ Protein Quantitation

EZQ™ Protein Quantitation kit (Molecular Probes) was used for the protein samples for proteomic assays according to manufacturer's instructions. The measurement was performed with Gel Doc EZ Imager (Bio-rad) using the set-up of SYPRO Ruby (excitation wavelength peak at 302 nm). The quantitation was performed with Image Quant.

3.2.3 HEPES buffer cell lysis

Cells in a 6-well plate were washed with PBS and then lysed with 300 µl of HEPES buffer followed by an incubation for 30 minutes at 4°C with shaking and centrifugation for 15 minutes with 12,000×g at 4°C. The supernatant was transferred into a new tube in 100 µl

/tube aliquots. Protein concentration was determined as described in section 3.2.2. Remaining samples were stored at −80 °C.

3.2.4 SDS-PAGE and Western blotting

Proteins (30 μg) were loaded onto 7.5% polyacrylamide gels (Invitrogen, Carlsbad, CA, USA) after boiling in 4×SDS sample buffer containing 10% β-mercaptoethanol for 5 minutes at 95°C. Electrophoresis was performed between100-120 V using GTS running buffer, following by transfer to a 0.2 μm PVDF membrane (GE Healthcare) at 170 mA for 2 hours using the transfer buffer. After transfer, the membrane was blocked in TBS Tween-20 (TBST) solution (10 mM Tris-HCl, pH 7.5, 150 mM NaCl, 0.05% Tween-20) containing 3% BSA (#A6003, Sigma-Aldrich) for 1 h at room temperature with agitation. Membranes were incubated with specific antibodies (Table 2.7) using the concentrations and conditions recommended by the supplier in TBST containing 3% BSA (#A6003, Sigma-Aldrich) overnight at 4°C with agitation. After washing thrice with TBST for 10 minutes each, the blot was incubated with IRDye secondary antibody at 1/5000 dilution in 3% BSA-TBST for 1 hour at room temperature with agitation. Following three washes with TBST for 10 minutes each, the blot was visualized using Odyssey CLx (LI-COR) Imaging system. The intensity of the signal was quantified using Image Studio™ Lite software (LI-COR). Tubulin was used as a loading control. Three biological replicates were conducted.

3.2.5 Flow cytometry

Cells were disrupted with disruption buffer and suspended to 5×10^6 cells/ml in staining buffer (PBS containing 1% BSA and 0.01% sodium azide). Fc receptors were blocked with purified human gamma globulin (50 μg per 10^6 of cells) at room temperature for 20 minutes. The blocked cell suspension (50 μl) was aliquoted to a round bottom tube, followed by centrifugation and re-suspension with 100 μl of IgG1 or antibodies (final concentration at 0.04 mg/ml) at 4 °C for 40-60 minutes. The cells were then washed twice with staining buffer, followed by incubation with 100 μl of FITC-conjugated anti-IgG detection antibody diluted in

staining buffer containing 10% normal rat serum on ice in the dark for 30 minutes. The labeled cells were washed three times with staining buffer followed by fixtation with 3.7% formaldehyde in PBS in dark on ice for 20 minutes. Cells were then re-suspended with 500 µl of 1% formaldehyde in PBS and then detected on a BD Accuri™ C6 (BD Australia). A total of 10,000 events were recorded. Only viable cells were gated. The data was analysed with the BD Accuri™ C6. Three biological replicates were conducted.

3.2.6 HPLC

An Agilent 1100 capillary HPLC (LC) system was used for ligand concentration measurement. The system was operated using binary gradients of solvent A (0.1% TFA in ultrapure water) and solvent B (0.01% TFA, 80% ACN, 20% ultrapure water). A C4, 4.6×150 mm, 10micron column (Vydac, USA) was used for separation. About 2 µg of ligands in 110 µl of 0.1%TFA were loaded separately. Analysis was performed using a 25-55% ACN gradient over 30 minutes in the presence of 0.1% TFA at a flow rate of 0.5 ml/min. Ligand amount was calculated using the absorbance area at 215 nm, comparing to LR3 IGF-I standard.

3.3 Cell culture

3.3.1 Maintenance of various cell lines

MCF-7 and MDA-MB-231 cells were cultured routinely in Dulbecco modified Eagle medium (DMEM), supplemented with 10% fetal calf serum (FCS), 1% Penicillin-Streptomycin, 1% GlutaMAX™ Supplement.

R^- cells and the cells lines based on R^- cells were cultured in the same medium as above with extra supplement of 0.5% G418.

3.3.2 Transfection

Before transfection, plasmids based on pcDNA3.1 backbone was linearized with P*vuI* (NEB) and purified with gel extraction. This linearized plasmid will decrease the likelihood of the vector integrating into the genome in a way that disrupts the gene of interest or other elements required for expression in mammalian cells. Transfection was processed with Lipofectamine® LTX with Plus™ Reagent (ThermoFisher), according to the manufacture's instructions in a 24-well format. Briefly, cells were seeded 2 days before transfection with density of 1×10^4 cells/cm^2, whereby the cells reach 70-80% confluence on the day of transfection. Medium was changed to antibiotic and serum free DMEM medium the night before transfection. DNA, PLUS reagent and LTX reagent were diluted with 100 µl of antibiotic and serum free DMEM medium in order with the amounts of 500 ng, 0.5 µl, 1.5 µl separately and incubated for 30 minutes. The mixture was added dropwise onto the cells. Medium was changed to DMEM medium containing antibiotic and serum 4 hours after the transfection and cultured to grow at 37°C.

3.3.3 Lentivirus production

To produce retroviral supernatants, 293T packaging cells were transfected with 12.5 µg of specific or control lentivector, 3.75 µg of pMD2.G (VSV-G), 7.5 µg of pCMV-dvrp8.2 and 6.25 µg of pRSV-Rev in 100-mm tissue culture dishes according to the transfection method described above. The medium was replaced 16 hours later, and virus-containing supernatants were harvested at 48 hours post-transfection. Supernatants were filtered through a 0.45 µm Minisart syringe filter and stored at -80°C.

3.3.4 Lentiviral infection and titration

Overnight incubation method: Cells were plated in a 60-mm tissue culture dish until 40% confluence. Cell medium was replaced with antibiotic free DMEM, followed by infection with viral supernatants with 8 µg/ml of polybrene. The supernatant was renewed by cell growth medium the following day.

Spin method: Cells were plated in a 60-mm tissue culture dish until 40% confluence. Cell medium was replaced with antibiotic free DMEM, followed by infection with viral supernatants with 8 μg/ml of polybrene. The plates were centrifueged at 33°C for 2 hours at 2250 rpm. The supernatant was replaced by cell growth medium.

In the next 24 or 48 hours, cells were used for stable cell line selection or infection efficiency detection by adding 1 μg/ml of Doxycycline to induce the expression of dsRed fluorescent protein. About 48hours later, cells were detected under normal light and under a cy3 filter (575-625 nm) using Olympus IX70 Fluorescence Microscope.

3.3.5 Kill curve

Cells were seeded at density of 2×10^4 cells/cm^2 for overnight culture. G418 was added at various concentrations of 0, 50, 100, 200, 400, 600, 800, and 1,000 μg/ml and changed every other day. The optimum dose was determined at which all cells were dead after 7 days. Kill curve of puromycin dihydrochloride was measured using the method above but with the concentrations of 0, 0.25, 0.5, 0.75, 1.0, 1.5, 2, 3, 5 μg/ml.

3.3.6 Stable cell line selection

Twenty-four hours after transfection cells were seeded into a 6-well plate at a ratio of 1 in 10 dilution. Optimized concentration of antibiotic were added into the medium the next day after subculture. Medium containing antibiotic was changed every other day. The cells were expanded if they reached confluence and used for an experiment or stored at -80°C.

3.3.7 Inducible shRNA expression

shRNA expression in cell lines was induced with 1 μg/ml Doxycyline. Time course of knock down effect was processed at 24 hours, 48 hours, 72 hours, 96 hours and 120 hours. Induction for 96 hours before assay was selected unless otherwise indicated.

3.3.8 Cell stimulation

Cells were seeded into plates and allowed to attach for 24 or 40 hours. They were washed with PBS and then starved by replacing with serum free DMEM medium supplemented with 1%BSA overnight. Cells were subsequently incubated with various concentrations of ligands diluted in DMEM supplemented with 1%BSA for 10minutes at 37°C.

3.3.9 Wound healing assay

Cells were plated into 24-well cell culture plates in DMEM containing 10% FBS and were grown to confluence. Cells were washed with serum-free medium and serum starved for 16 h. A scratch was made across the cell layer with a 200µl sterile pipette tip. After washing with serum-free medium twice, plates were photographed immediately after scratching. Cells were treated with ligands diluted in serum-free DMEM containing 1% BSA. Plates were photographed after 24 h at the identical location of initial image.

3.3.10 Proliferation assay

Cells were cultured in T75 flask and Doxycycline treated for 3 days to induce knock down of IR or IGF-1R. Then cells were seeded into 48 well plate at a density of 4,000 cells per well, allowed to attach for 24 hours and starved in growth factor–depleted medium comprising DMEM supplemented with 2% charcoal-treated calf serum and 1 µg/ml Doxycyline for 4 hours. Cells were incubated subsequently in various concentrations of ligands diluted in DMEM supplemented with 2% charcoal-treated calf serum and 1 µg/ml Doxycyline for 4 days. Doxycyline was replenished everyday and ligands every other day. Cell growth was determined by measuring the amount of DNA in each well using crystal violet.

3.3.11 Crystal Violet assay

At the end of the incubation time, cells were washed with 500 µl of PBS, fixed and stained for 10 min with 200µl of 4% paraformaldehyde and 1% crystal violet dye in PBS. Excess crystal violet dye was removed and plates were extensively washed with water to remove traces of

unbound crystal violet dye. After air-drying, the bound dye was dissolved in 200 µl of 1% SDS. Optical density was read at 540 nm using a plate reader.

3.4 Quantitative Phosphoproteomics

3.4.1 SILAC labeling

Cells were cultured in DMEM deficient in L- arginine, L-lysine, L-leucine and supplemented with 10% dialyzed fetal bovine serum, penicillin/streptomycin, GlutaMAX and L-leucine and either L-arginine (Arg-0) and L-lysine (Lys-0), $^{13}C_6$-L-Arginine HCl (Arg-6) and 4,4,5,5-D_4-L-Lysine 2HCl (Lys-4), or $^{13}C_6$,$^{15}N_4$-L-Arginine HCl (Arg-10) and L-lysine $^{13}C_6$,$^{15}N_2$-L-Lysine HCl (Lys-8) for at least 3 passages with 1 in 10 dilutions. Concentration of Arg, Lys and Leu were at 84 µg/ml, 146 µg/ml and 105 µg/ml respectively, the same as found in DMEM medium. After 3 passages of growth time, the cells were used for incorporation efficiency determination and storage.

3.4.2 Determination of Isotope Incorporation Efficiency (should be > 95%)

Cells from each sample (light, medium and heavy) in 6-well plate were lysed with 300 µl of RIPA buffer and processed with the Filter Aided Sample Preparation method (FASP) and 1 µl was used for HPLC-MS/MS analysis.

3.4.3 Filter Aided Sample Preparation (FASP) Method

1. Proteins in lysis buffer was made up to ~200uL with freshly made 7M urea / 100mM ammonium bicarbonate. 10uL of 1M DTT was added to final concentration of 50 mM and incubated at 20^o C with slow agitation for 1 hour. The reduced samples were loaded into the Microcon YM-30 devices (Millipore, Billerica, MA) and centrifuged at 14, 000 x g for 10 min. Residual DTT was removed by adding 100uL of 7M urea / 100mM ammonium bicarbonate and centrifugation for 10 minutes at 14, 000 x g. Alkylation was carried out with the addition of 100uL of 55 mM IAA in 7M urea /100mM ammonium bicarbonate to the spin columns. They were centrifuged for just a few seconds to ensure the liquid was in close contact with the proteins retained by the filter and incubated in the dark for 20 minutes at 20^o C with gentle agitation. Samples

were centrifuged at 14,000 x g for 10 minutes to remove IAA. The columns were then rinsed twice with the addition of 100uL of 7M urea / 100mM ammonium bicarbonate and centrifuged for 10 minutes at 14,000 x g. The columns were then rinsed twice with the addition of 100uL of 50mM ammonium bicarbonate and centrifuged for 10 minutes at 14,000 x g. Final equilibration was carried out with the addition of 100uL 5mM ammonium bicarbonate and centrifugation at 14,000 x g for 15 mins. The proteins were digested overnight at 30 °C with trypsin (Promega) (1 µg of trypsin: 100 µg of protein). The peptides were collected from the filter by centrifugation followed by additional elution with water. The peptide-containing filtrate was dried until a few microliters liquid remained and reconstituted in 1% formic acid/2%ACN to concentrations between 100 ng/µl to 1 µg/µl.

3.4.4 GdmCl buffer cell lysis

Cells in 100-mm petri dish were solubilized in 1 ml of GdmCl lysis buffer (6 M GdmCl, 100 mM Tris pH 8.5, 10 mM TCEP, 40 mM CAA), and heated for 5 minutes at 95 °C. Cell lysates were cooled on ice for 15 minutes, sonicated (Branson probe sonifier output 3-4, 50% duty cycle, 3× 30 s), and heated again (95 °C for 5 minutes), followed by centrifugation for 30 minutes at 3,500 g (4 °C), and an aliquot removed to a clean tube, diluted 50% with milliQ H_2O, and precipitated with acetone.

3.4.5 Acetone Precipitation

NaCl was added to the protein sample to a final concentration of 100 mM and then mixed with 6 times volume of pre-chilled acetone at -20°C. Protein was precipitated overnight and collected by centrifuging for 15 minutes at 20,000 g (-9 °C). Pellets were washed twice with –20 °C 80% acetone and air dried upside down for ~10 minutes at RT or until no residual acetone odor remained. Pellets were resuspended in 1 ml of TFE (2,2,2-trifluoroethanol) digestion buffer (10% TFE, 100 mM ammonium bicarbonate) with sonication (Bioruptor, 4 °C for 5 minutes, or until a homogenous suspension was formed). Protein concentration was determined (EZQ assay) and samples diluted to equal concentration in 500 µl of TFE digestion buffer. Remaining samples were stored at –80 °C.

3.4.6 Trypsin/Lys-c digestion

Briefly, the samples were digested in TFE buffer with 1:100 (enzyme:protein) LysC for 2 hours, followed by digestion with 1:100 (enzyme:protein) trypsin overnight with rapid agitation (1,000 r.p.m.) at 37 °C.

3.4.7 TiO_2 enrichment

TiO_2 beads were weighed out at a ratio of 10:1 (w:w) beads to protein. Beads were resuspended in Loading buffer 1 (80% ACN, 6% TFA) at a concentration of 100µl of Loading buffer 1 per sample. TiO_2 bead suspension incubated in Bioruptor at 4°C for 1 min to disaggregate the beads.

The digested peptides were incubated with 4 volumes of DHB buffer [200 mg/mL DHB, 80% (v/v) ACN, 6% (v/v) TFA] for 5 minutes at room temperature in a ThermoMixer at 1,000 rpm, followed by incubation with TiO_2 beads for another 5 minutes at 40°C in a ThermoMixer at 1,000 rpm. The sample was then washed once with 200 µl of DHB buffer and transferred into a new tube, followed by three washes with wash buffer [60% ACN (v/v), 1% TFA (v/v)] to remove the DHB and non-specific binding peptides. The beads were dried and eluted with 60µl of elution buffer (15% NH_4OH, 40% ACN). The sample was concentrated in the speedyVac for 5-10 min at 45 °C, or until about 30 µl remained, and was then acidified with 10% TFA immediately.

3.4.8 Desalting

Stagetips were prepared beforehand by pressing 2 layers of disk (C18 or SDB-RPS) into 200µl sterile pipette tip according to the protocols described in Rappsilber et al paper (Rappsilber et al., 2007).

Samples were then desalted with C18 (or SDB-RPS) stagetips (where from???) before loading onto the HPLC. C18 stagetips were activated and equilibrated with 50 µl of ACN, 50 µl of 30%MeOH, 0.2% TFA and 50 µl of 0.2% TFA sequentially. Samples were loaded onto

the stagetips, which were then washed twice with 0.2% TFA, followed by elution with 30 µl of elution buffer (80% ACN, 0.1%TFA). The elute was concentrated in the speedyVac and re-suspended with 25 µl of MS loading buffer (2% ACN, 0.1% TFA).

Ziptip: Desalting was achieved using a Ziptip containing 0.6 µl C18 resin (Merck Millipore ZTC18S096) according to manufacture's protocol. Briefly, the Ziptip was equilibrated 3 times with 100% Acetonitrile, 3 times with 0.1% formic acid and the sample was loaded by pipetting the protein digest up and down 10 times through the Ziptip. The sample was washed 6 times with 0.1% formic acid and eluted by pipetting up and down 10 times with 4 μl 60% acetonitrile/0.1% formic acid. The volume was increased to 25 µl with MS loading buffer (2% ACN, 0.1% TFA).

3.4.9 MALDI-TOF

Briefly, the sample (0.5 µl), was mixed in a 1:1 ratio with DHB matrix solution (10 mg/ml 2,5-DHB dissolved in 50%ACN/0.05% TFA/0.05% PA) or α- Cyano- 4- hydroxycinnamic acid (HCCA) matrix (10 mg/ml HCCA dissolved in 30%ACN/0.1% TFA) and spotted onto the steel MALDI target and dried. MALDI TOF mass spectra were acquired using a Bruker ultraflex III MALDI-TOF/TOF mass spectrometer (Bruker Daltonics) operating in reflectron positive ion mode. FlexControl (version 3.1, Bruker Daltonics) software was used to control the analysis.

3.4.10 HPLC-MS/MS

Nano-LC-ESI-MS/MS was performed on an Ultimate 3000 RSLC system (Thermo-Fisher Scientific) coupled to a LTQ XL Orbitrap ETD MS instrument (Thermo-Fisher Scientific). 10 µl of digested peptides were pre-concentrated on a trapping column (Thermo Fisher Scientific) (Acclaim PepMap100, C18, pore size 100 Å, particle size 3 µm, 75 µm ID × 2 cm length) at a flow rate of 1 µl/min for 10 min in 2% (v/v) ACN/0.1 (v/v) FA and then separated on ananalytical column (Thermo Fisher Scientific, Bremen, Germany) (Acclaim PepMap RSLC, C18, pore size 100 Å, particle size 2 µm, 75 µm inner diameter (ID) × 15 cm length) at a flow

rate of 300 nl/min using the following buffer system: (A) 2% ACN, 0.1% FA in water; (B) 80% ACN, 0.1% FA in water. A two-steps gradient was applied from 5% to 40% B over 50 minutes and to 90% B over 20 minutes, followed by 10 minutes wash in 90% B before equilibration with 5% B for 19.5 minutes.

MS full scans were acquired in the Orbitrap analyser in the mass range of 300–1700 Da at a resolution of 60,000. The nine most intense precursor ions with charge states ≥2 with minimum signal intensity of 500 were selected for isolation and were subjected to CID fragmentation using a dynamic exclusion of 180 seconds. All unassigned charge states and a charge state of one were rejected. CID was set to use an activation of 0.25, activation time of 15 ms and normalised collision energy of 35%.

3.4.11 Data analysis

Raw mass spectrometry data was analyzed with MaxQuant, using default parameters with minor changes. Trypsin/p and Lys-C were used for digestion and up to two maximum missed cleavages was allowed. Default, R6K4 and R10K8 were selected for multiplicity parameter. Oxidized methionine (M), acetylation (protein N-term) and phospho (STY) were selected as variable modifications, and carbamidomethyl (C) as fixed modifications with maximum number of modifications and labeled peptides was set to three. The minimum required peptide length was 6 amino acids and maximum 25. Mass tolerances for precursor ions and fragment ions were set to 20 ppm and 0.5 Da, respectively.

Unique and razor peptides were selected for quantification. Database searching was performed using the Andromeda search engine integrated into MaxQuant against the human SwissProt database (downloaded on September 2015), with a false-discovery rater (FDR) < 0.01 at the level of proteins, peptides and modifications. Match between runs (MBR) was enabled with a matching time window of 0.7 min to match the biological and technical replicates.

Proteomics Quality Control (PTXQC) is used to evaluate the data from Maxquant output (Bielow et al., 2016).

Network analysis, Pathway analysis and Gene Ontology analysis were performed with InnateDB and NetworkAnalyst (Breuer et al., 2013; Xia et al., 2014; Xia et al., 2015). The Gene Ontology Biological Processes (GOBP) and pathways that were significantly enriched with a P-value of less than 0.05 were used in the analysis.

3.5 Statistics

Data are presented as mean ± SD of at least three independent experiments unless stated otherwise. Significance of differences in knock down verification experiments were calculated by t-test. Over-representation Analysis (ORA), the Hypergeometric algorithm and the Benjamini & Hochberg correction method were selected in InnateDB for network analysis. Proliferation and migration assays were evaluated by 2-way ANOVA. P-values below 0.05 were considered statistically significant.

Chapter 4 Role of insulin receptor Thr^{1148} phosphorylation

4.1 Introduction

The insulin receptor (IR) is a receptor tyrosine kinase that mediates the actions of insulin. IR transduces signals through autophosphorylation and phosphorylation of other intracellular signalling molecules. More than 26 phosphorylation sites (including tyrosine, serine and threonine sites) are phosphorylated within the IR intracellular domain upon insulin stimulation (http://www.phosphosite.org/proteinAction.action?id=608&showAllSites=true) (Figure 4.1). At present, seven tyrosine residues have been identified as targets for autophosphorylation (Youngren, 2007): two tyrosine residues - Tyr^{953} and Tyr^{960} in the juxtamembrane region; three tyrosine residues- Tyr^{1146}, Tyr^{1150} and Tyr^{1151} in the kinase domain; and two tyrosine sites- Tyr^{1316} and Tyr^{1322} located close to the C terminus. Additionally, Ser/Thr phosphorylation can activate or inhibit IR signalling. For example, the phosphorylation of Ser^{1275} and Ser^{1309} activates the IR (Tennagels et al., 2001), while the phosphorylation of $Ser^{1293/1294}$ and Thr^{1336} inhibits IR signalling (Lewis et al., 1990a; Lewis et al., 1990b).

As the IR can transduce different biological signals in response to insulin, IGF-II or insulin analogues, the Forbes lab aims to map the phosphorylation profile of the insulin receptor intracellular domain by combining insulin receptor pull down and mass spectrometry of beta subunit tryptic phosphopeptides. Preliminary data generated by Dr Peter McCarthy in 2013 identified phosphorylation of Thr^{1148}, which is located in the activation loop. At the time, there was no publically available data reporting detection by mass spectrometry of Thr^{1148} phosphorylation, and the significance of Thr^{1148} phosphorylation with respect to IR tyrosine kinase activation was unknown. In fact only a single publication had investigated the influence of Tyr^{1146}, Tyr^{1150} and Tyr^{1151} on the ability of protein kinase CK2 to phosphorylate Thr^{1148} *in vitro* using synthetic peptides (Marin et al., 1996). Under those conditions Thr^{1148} was only phosphorylated efficiently by CK2 if all three Tyr were also phosphorylated. In

contrast, in our preliminary study Thr^{1148} phosphorylation was only detected on peptides *lacking* phosphorylation of neighbouring Tyr^{1146}, Tyr^{1150} and Tyr^{1151} residues (Figure 4.2).

We speculated that there are two possible reasons to explain why we did only detect tryptic peptides with phosphorylated Thr^{1148} in the absence of any Tyr^{1146}, Tyr^{1150} and Tyr^{1151} phosphorylation: 1. Phosphorylation of Thr^{1148} and any of Tyr^{1146}, Tyr^{1150} and Tyr^{1151} can occur simultaneously, but the phosphorylated peptide was not detected by mass spectrometry under the conditions of the experiment due to both its multiple negative charges and/or low abundance; or 2. The phosphorylation of Thr^{1148} inhibits the phosphorylation of Tyr^{1146}, Tyr^{1150} and Tyr^{1151} of the activation loop, which is possibly due to steric hindrance and electrostatic repulsion of the phosphate group on Thr^{1148} preventing interaction of the activation loop with the tyrosine kinase.

Therefore, the aim of this chapter was to elucidate which of these two possibilities is true.

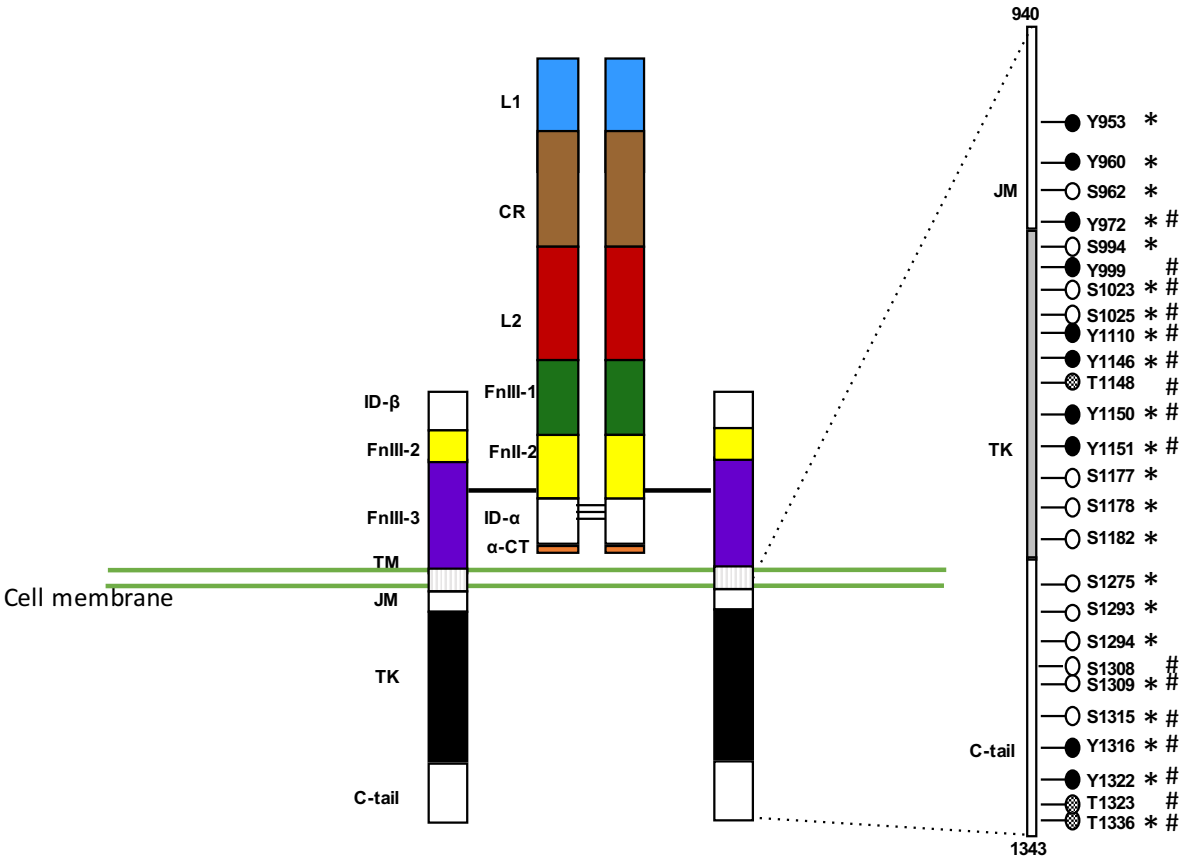

Figure 4.1: Schematic representation of the IR-A domain structure and intracellular phosphorylation. Domain structure: L1 (Blue) and L2 (Red), large domains 1 and 2 (Leucine-rich repeats); CR (Brown), cysteine rich domain; FnIII-1 (Green), FnIII-2 (Yellow), FnIII-3 (Purple), fibronectin type III domains; ID (White), insert domain; α-CT (Orange), carboxy-terminal α-chain; TM (White), transmembrane domain; JM (White), Juxtamembrane domain; TK (Black), tyrosine-kinase domain; C-tail (White), carboxy-terminal tail. Currently known tyrosine (solid), serine (open) and threonine (hatched) phosphorylation sites identified by a variety of techniques (IR-A numbering). * = Sites were determined using site-specific methods; # = Sites were determined using mass spectrometry. T: Thr, S: Ser, Y: Tyr. Phosphosite information was derived from the PhosphoSitePlusDatabase (http://www.phosphosite.org/proteinAction.action?id=608&showAllSites=true).

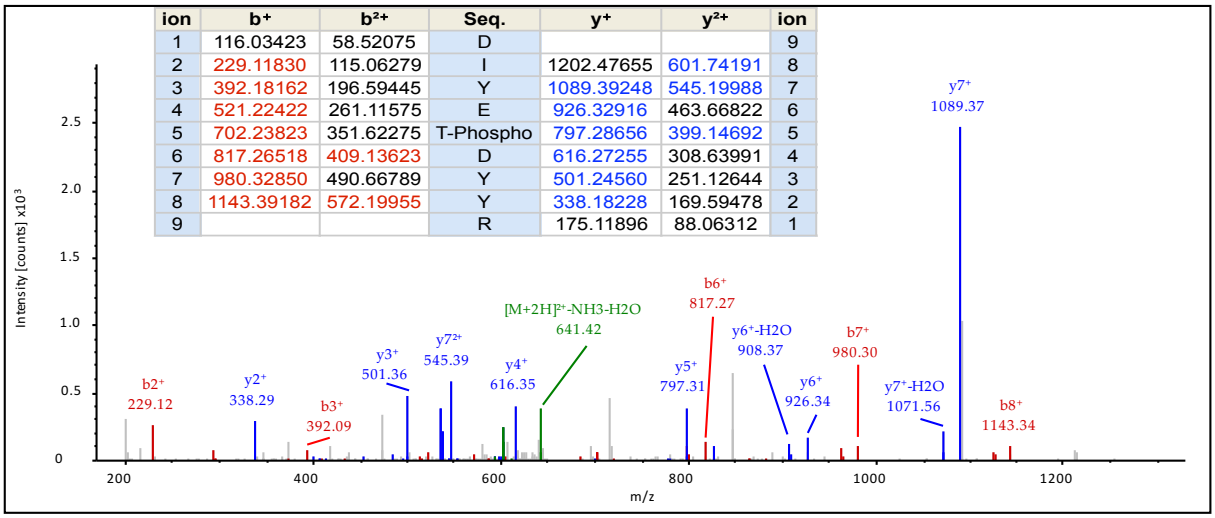

Figure 4.2: Tryptic peptide containing the activation loop detected by MS/MS. R$^-$IR-A cells (IR-A overexpressing mouse fibroblast cells derived from IGF-1R knock out mice) were stimulated with 10 nM insulin for 10 minutes and the IR was enriched, digested and detected with HPLC-MS/MS. This data shows the phosphorylation of Thr^{1148} accompanied by the unphosphorylated Tyr^{1146}, Tyr ^{1150} and Tyr ^{1151}. Figure and data were generated by Dr Peter McCarthy.

4.2 Strategy

Site-directed mutagenesis is a commonly used way to elucidate the role of phosphorylation in the biological activity of a protein of interest. Mutation of Thr^{1148} in IR-A to Ala (A) or Asp (D) was performed to mimic the unphosphorylated or phosphorylated state of this residue respectively. Secondly, a myc-tag was also added to the C-terminus of the IR in order to facilitate immunoprecipitation. Figure 4.3 shows the exact molecular cloning steps. The construction of pcDNA3.1 (IR-Amyc) was achieved using an existing pcDNA3.1 (IR-B) clone. Two synthetic cDNA fragments were purchased from GeneArt: one fragment enabled the introduction of the IR-A sequence (ie a fragment encompassing the exon 10/exon 12 boundary and lacking exon 11); and the other allowed the introduction of the sequence encoding a myc-tag at the C-terminus of IR. The IR-A fragment (without exon11) was flanked by *BamHI* and *EcoRV* enzyme digestion sites that were used to replace the equivalent IR-B fragment (Figure 4.3). The myc-tag was ligated to the 3' end of IR-B cDNA with *StuI* and *XbaI* enzyme digestion sites. By ligation of these fragments into the pcDNA3.1 (IR-B) plasmid; the pcDNA3.1 (IR-Amyc) was generated.

In order to conduct site-directed mutagenesis, the fragment encoding Thr^{1148} was ligated into the pBlueScript (SK+) vector with *EcoRI* and *NotI* enzyme digestion sites. The use of this strategy avoided unwanted introduction of errors to the large IR coding sequence and allowed for easy sequencing of the mutagenesis site. The site-directed mutagenesis was conducted using the primers in Table 2.2, and following sequencing, the correct fragments were ligated back into pcDNA3.1 (IR-Amyc) (Figure 4.3).

The vectors pcDNA3.1 (IR-Amyc), pcDNA3.1 (T1148A IR-Amyc) and pcDNA3.1 (T1148D IR-Amyc) were used to transiently transfect the R^- (mouse fibroblast cells derived from IGF-1R knock out mice) cells separately. Cells were then stimulated with insulin and the IR activation levels were measured.

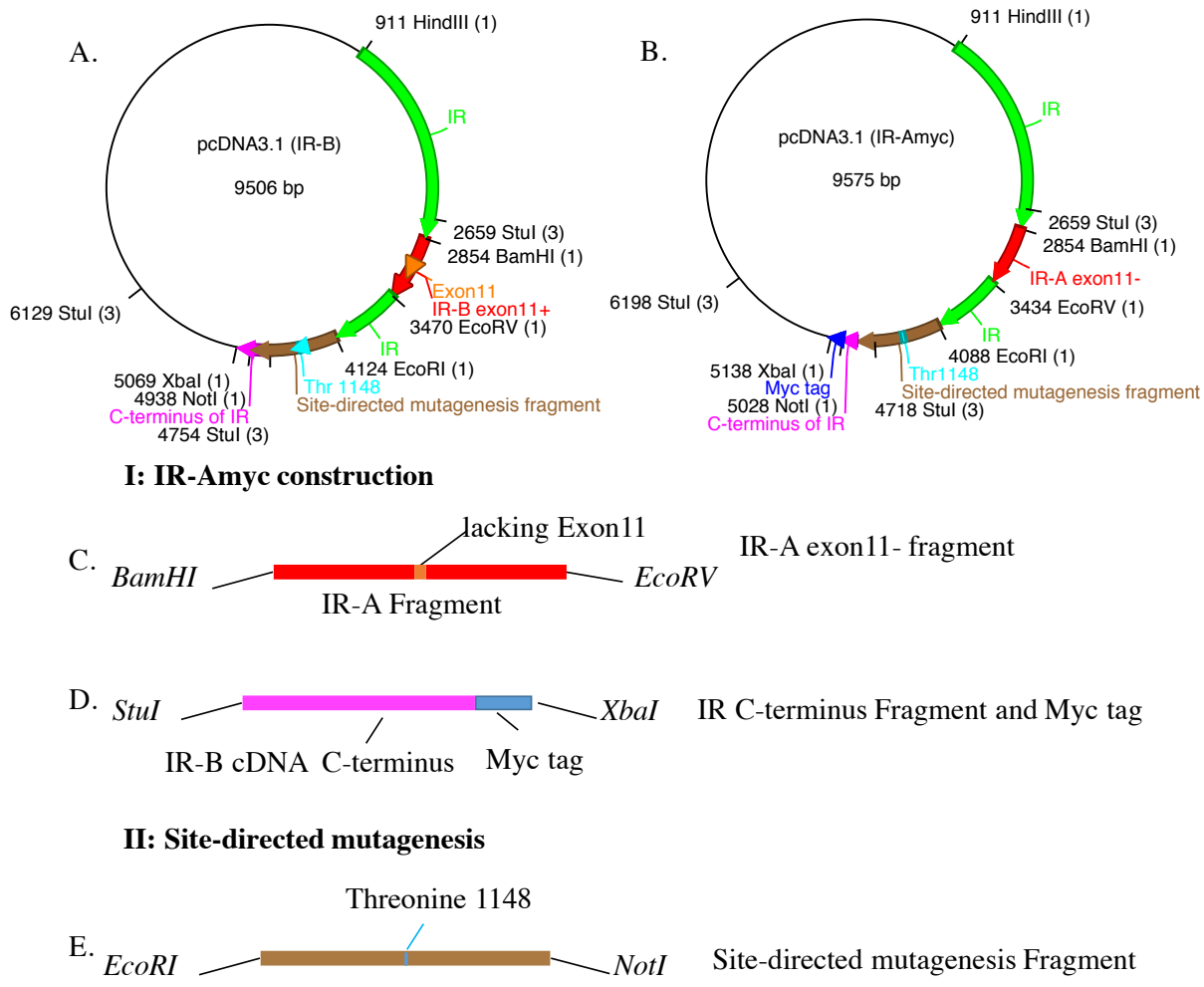

Figure 4.3: Vector maps of the starting vector pcDNA3.1 (IR-B) (A) and final constructs pcDNA3.1 (IR-Amyc), pcDNA3.1 (T1148A IR-Amyc) or pcDNA3.1 (T1148D IR-Amyc) construction (B). Schematic diagrams of the fragments used to generate I. the wild type IR-Amyc vector and II. The mutant IR-A myc vectors are shown. The wild type IR-Amyc vector was constructed using enzyme digestion and ligation into the starting vector pcDNA3.1 (IR-B) of two cDNA fragments synthesized by GeneArt: one fragment was the IR-A exon11- fragment (C, red) and the other fragment was the sequence encoding the myc-tag (blue) at the C-terminus of IR (purple) (D). The fragment without exon11 (red) was used to replace the equivalent IR-B fragment flanked by *BamHI* and *EcoRV* enzyme digestion sites. The myc-tag (blue) incorporated into a C-terminal fragment flanked by the *StuI* and *XbaI* enzyme digestion sites (pink) was ligated to the C-terminal end of the IR. At the same time, fragments

generated in site-directed mutagenesis reactions to introduce the IR T1148A and T11148D mutations (brown) were ligated into pBlueScript (SK+) vector with *EcoRI* and *NotI* enzyme digestion sites. These fragments were subsequently used to replace the equivalent fragment in the wild type IR-Amyc construct.

4.3 Results

4.3.1 Vector verification by digestion and sequencing

pcDNA3.1 (IR-Amyc), pcDNA3.1 (T1148A IR-Amyc) and pcDNA3.1 (T1148D IR-Amyc) were verified by enzyme digestion and sequencing (Figure 4.4). pcDNA3.1 (IR-Amyc) was digested with either *BamHI*/*NotI* or *HindIII*/*XbaI* separately. The length of the linear pcDNA3.1 (IR-Amyc) construct is 9575bp. The digestion with *BamHI*/*NotI* resulted in two fragments: 7401bp and 2174bp. The length of the linear pcDNA3.1 (IR-B) is 9506bp. The digestion with *BamHI*/*NotI* resulted in two fragments: 7422bp and 2084bp.The presence of the fragment with the size of 2174bp verified the deletion of exon11, which indicated the correct construction of IR-A cDNA. The digestion with *HindIII*/*XbaI* also resulted in two fragments: 5348 bp and 4227 bp (Figure 4.4). The fragment with the size of 4227bp (it would be 4122bp without myc-tag) verified the addition of myc-tag at the C-terminal of IR-A. The introduction of the alanine and aspartic acid mutations in the pcDNA3.1 (T1148A IR-Amyc) and pcDNA3.1 (T1148D IR-Amyc) constructs were verified by sequencing (Figure 4.4).

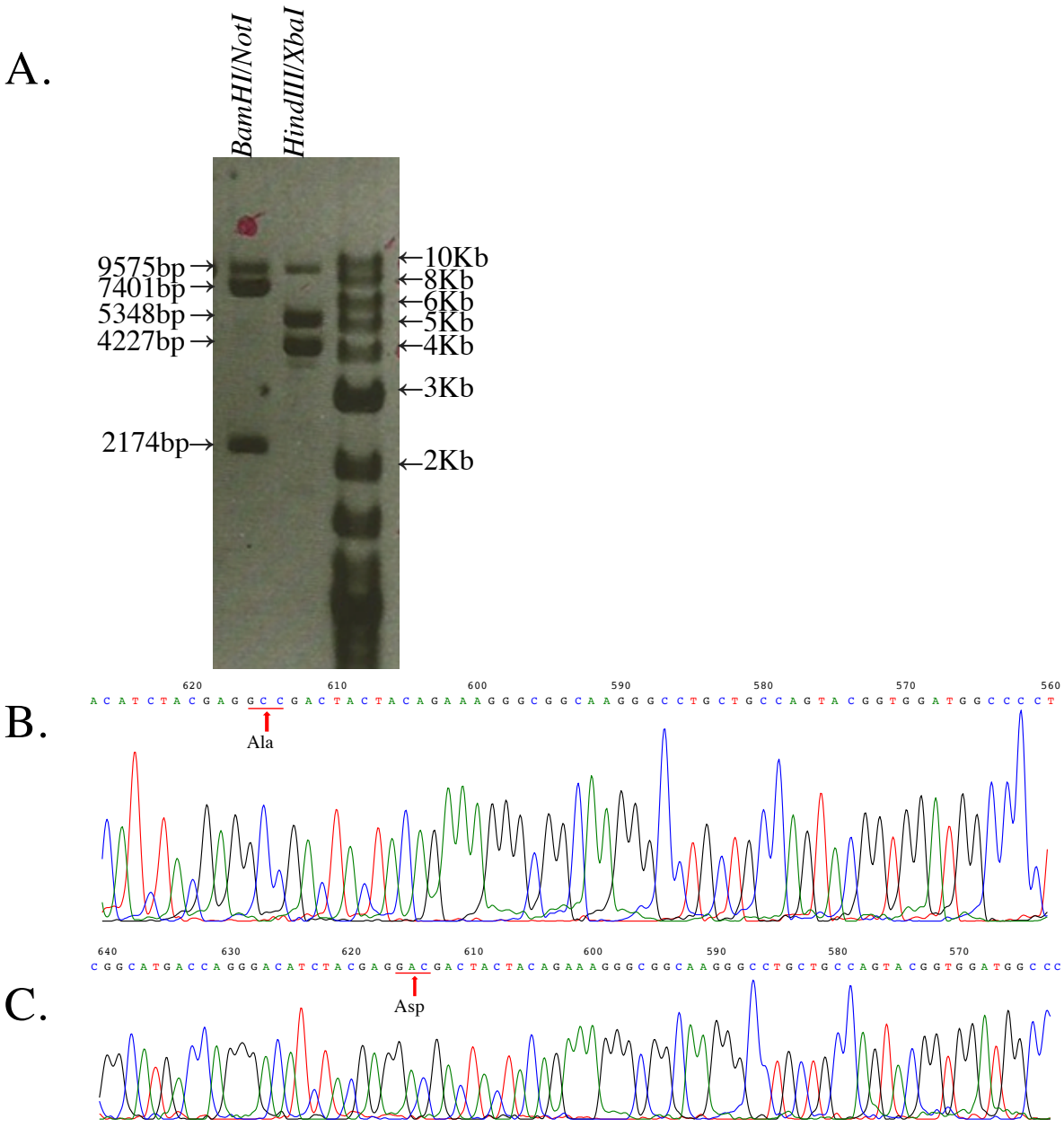

Figure 4.4: pcDNA3.1 (IR-Amyc), pcDNA3.1 (T1148A IR-Amyc) and pcDNA3.1 (T1148D IR-Amyc) verification. pcDNA3.1 (IR-Amyc) (A.) was digested with either *BamHI/NotI* or *HindIII/XbaI* separately according to the method described in section 3.1.4 to demonstrate correct incorporation of the IR-A exon 11- fragment and the IR C-terminus fragment and Myc tag. pcDNA3.1 (T1148A IR-Amyc) (B.) and pcDNA3.1 (T1148D IR-Amyc) (C.) were verified by sequencing according to the method described in section 3.1.13.

4.3.2 Thr1148Ala and Thr1148Asp decreases the IR-A sensitivity to insulin

To investigate the role of Thr^{1148} phosphorylation in IR activation, I generated recombinant wild-type (WT) and mutant- Thr^{1148}Ala and Thr^{1148}Asp expression constructs and transiently transfected them into R^- cells. The cells were serum starved, and then stimulated with 100 nM of insulin for 10 minutes. Untransfected R^- cells were used as the background control. Cell lysates were analysed by immunoblotting. Phospho-IR/IGF1R (Tyr^{1158}, Tyr^{1162}, Tyr^{1163}) antibody and Anti-Insulin Receptor beta antibody were used to measure IR activation and total IR expression, respectively (Figure 4.5).

From Figure 4.5A, it is evident that the IR-A and its mutants were overexpressed to varying extents (Figure 4.5A upper panel). To assess the extent of activation the level of of Tyr^{1146}, Tyr^{1150}, and Tyr^{1151} phosphorylation was normalised to the overall amounts of transiently expressed receptor. With wild-type IR-A, insulin stimulated Tyr^{1146}, Tyr^{1150}, and Tyr^{1151} phosphorylation more than 14-fold above basal. The basal levels of Tyr^{1146}, Tyr^{1150}, Tyr^{1151} phosphorylation of the Thr^{1148}Ala mutant receptor appeared higher than the basal wild type receptor Tyr^{1146}, Tyr^{1150}, Tyr^{1151} phosphorylation. However, when normalized against the total receptor levels this was not statistically significant. Insulin stimulated a 3.7 fold higher level of Tyr^{1146}, Tyr^{1150}, Tyr^{1151} phosphorlyation on the Thr^{1148}Ala mutant receptor above basal. Similar to the Thr^{1148}Ala mutant, the basal level of phosphorylated Tyr^{1146}, Tyr^{1150} and Tyr^{1151} on the Thr^{1148}Asp mutant appeared higher than wild type receptor but this was not statistically significant. Insulin stimulated a 3 fold higher level of Tyr^{1146}, Tyr^{1150}, Tyr^{1151} phosphorlyation on the Thr^{1148}Asp mutant receptor above basal. The fold change above basal for both mutants (3.7 and 3 fold, respectively) was significantly lower than for wild type (~14 fold). Therefore, both Thr^{1148}Ala and Thr^{1148}Asp were found to be significantly less responsive to insulin than the wild type IR-A.

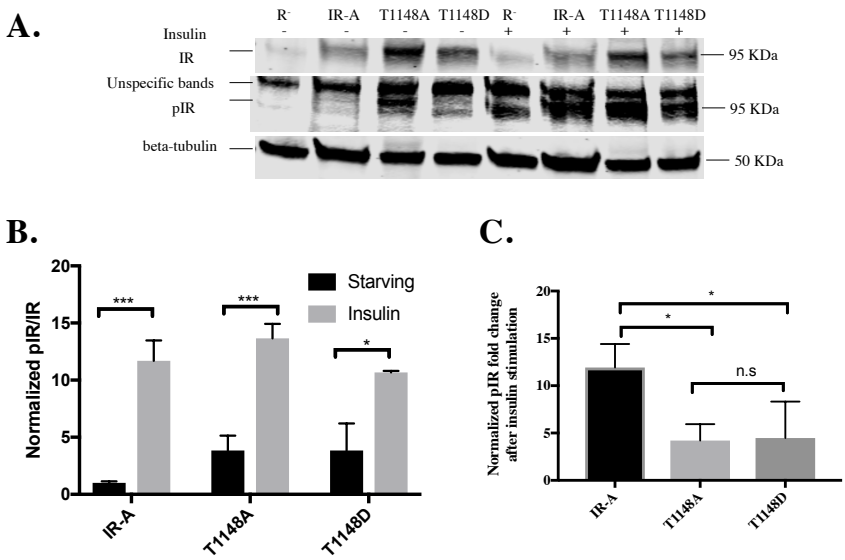

Figure 4.5: The activation of wild type IR and IR with Thr^{1148} mutations in response to insulin. The R$^-$ cells were transiently transfected with pcDNA3.1 (IR-Amyc), pcDNA3.1 (T1148A IR-Amyc) or pcDNA3.1 (T1148D IR-Amyc) according to the methods described in section 3.3.8. The cells were stimulated with 100 nM insulin for 10 minutes according to the methods described in section 3.3.8. (A). The western blots were conducted according to the methods described in section 3.2.4. Phospho-IR/IGF1R (Tyr1158, Tyr1162, Tyr1163) Antibody (Invitrogen #44-806G), Anti-Insulin Receptor beta antibody (Abcam#65098) and beta-tubulin antibody (Life technologies #32-2600) were used according to the concentrations described in the Table 2.6. Tubulin was used as a loading control. Raw blot is shown in appendix 13. (B) Levels of phosphorylated IR relative to the total IR. Intensities of phosphorylated IR were normalized to intensities of total IR. (C) Fold change of phosphorylated IR with insulin stimulation comparing to starving condition. The bars show the S.E.M. of 3 biological replicates. Statistical significance was determined by one-way ANOVA (*, $P \leq 0.05$; ***, $P \leq 0.001$).

4.4 Discussion

Our initial mass spectrometry experiment detected a peptide that was phosphorylated on Thr^{1148} without phosphorylation of Tyr^{1146}, Tyr^{1150}, and Tyr^{1151}. This observation led us to hypothesise that the phosphorylation of Thr^{1148} has an inhibitory effect on the IR activation due to the introduction of a larger negatively charged modification at this residue. In order to verify this hypothesis, constructs encoding recombinant wild type IR and IR with Thr^{1148} mutated to Ala or Asp were generated and IR were overexpressed in R^- cells.

The Thr^{1148}Ala and Thr^{1148}Asp mutants were introduced to either prevent phosphorylation or mimic a constitutively phosphorylated state at that residue, respectively. We already knew from our preliminary experiments that the IR-A cells express the kinase responsible for Thr^{1148} phosphorylation. If the hypothesis was correct that Thr^{1148} phosphorylation would inhibit IR Tyr^{1146}, Tyr^{1150}, and Tyr^{1151} phosphorylation then it was expected that insulin stimulation of cells expressing the Thr^{1148}Ala mutant would lead to increased levels of IR Tyr^{1146}, Tyr^{1150}, and Tyr^{1151} phosphorylation. In contrast, the Thr1148Asp would mimic phosphorylation at this residue and there would be lower levels of insulin stimulated Tyr^{1146}, Tyr^{1150}, and Tyr^{1151} phosphorylation.

There were substantial differences in the expression of each of the constructs used here which makes interpretation of the relative phosphorylation difficult. In the future it would be good to alter the experimental conditions so that similar levels of expression were achieved to assist in the interpretation of these results. However, having performed replicate experiments with transient expression we found that while it appeared that both mutants had a higher level of phosphorylation in the basal state this was not statistically significantly. This is consistent with the recent report by Petersen et al (Petersen et al., 2016) who saw no increase in basal phosphorylation with a GFP Thr^{1160}Glu mutant (equivalent to Thr^{1148} in IR-A) expressed in HeLa cells or when the Thr^{1150}Ala mutant was knocked into the mouse IR gene (the mouse IR-B residue equivalent to Thr^{1148} in IR-A). In hepatocytes of mice infused with glucose the

basal phosphorylation of the IR did not change. It is important to note there are several differences between that report and the current study, including the incorporation of the large GFP tag at the C-terminus and the use of and a different method of detection. For the GFP tagged Thr^{1160}Glu mutant, an antibody directed to the beta subunit was used for immunoprecipitation followed by detection of receptor phosphorylation with an anti-phospho Tyr antibody, whereas in this study the antibody specific for Tyr^{1146}, Tyr^{1150}, and Tyr^{1151} phosphorylation was used. It is possible that global Tyr phosphorylation was not altered but specific phosphorylation at the activation loop was affected (albeit not significantly here).

Next, phosphorylation of the mutants in response to insulin was measured. Thr^{1148}Ala and Thr^{1148}Asp mutants both were phosphorylated in response to insulin (as detected by Phospho-IR/IGF1R Tyr^{1158}, Tyr^{1162}, Tyr^{1163} antibody). There was a 3.7 fold and 3 fold induction of Thr^{1148}Ala and Thr^{1148}Asp mutants, respectively. The inhibitory effect of the negative charge of Asp on Tyr^{1146}, Tyr^{1150}, Tyr^{1151} phosphorylation is consistent with the recent report by Petersen et al (Petersen et al., 2016) who did not see an increased basal phosphorylation with the introduction of a negative charge with a GFP tagged Thr^{1160}Glu mutant. They also saw a marked reduction in Tyr^{1158}, Tyr^{1162}, Tyr^{1163} phosphorylation to almost undetectable levels. This more dramatic effect may be due to the fact that Glu is sometimes a better mimic of phosphorylated Thr than Asp, as the Glu has a longer side chain than Asp. It could alternatively be that these mutants were analysed in different IR isoform backgrounds. Petersen et al. (Petersen et al., 2016) introduced mutants into the IR-B whereas this study used IR-A.

Interestingly, since our phosphoproteomic study there have been many reports of Thr^{1148} phosphorylation in the PhosphotitePlus database (http://www.phosphosite.org/proteinAction.action?id=608&showAllSites=true). Two studies have reported detection of peptides with phosphorylation of Thr^{1148} and either Tyr^{1151}, Tyr^{1146} or Tyr^{1150} phosphorylation (ie one pThr and one pTyr). In one study using samples from

Cholangiocarcinoma patients, pThr^{1148} was detected on a peptide also containing phosphorylated Tyr^{1150} and Tyr^{1151} (Gu et al., 2011). Another study was conducted on insulin stimulated 3T3 cells. Here it was shown that pThr^{1148} was present on a peptide also containing phosphorylated Tyr^{1146} and Tyr^{1151} (Humphrey et al., 2013). Furthermore, Petersen et al. also reported detection of peptides containing phospho Thr^{1148} and either phosphorylated Tyr^{1150} or Tyr^{1146}, as well as a peptide with phospho Thr^{1148} and both phospho Tyr^{1146} and phospho Tyr^{1150} (Petersen et al., 2016). This result seems contradictory to their implication that phosphorylation of Thr^{1148} inhibits Tyr^{1151}, Tyr^{1146} or Tyr^{1150} phosphorylation.

The inhibition of Tyr^{1146}, Tyr^{1150}, Tyr^{1151} phosphorylation by the Thr^{1148}Ala mutation was not expected. This suggests that the absence of phosphorylation of the Thr^{1148}Ala residue does not relieve any inhibition by a negatively charged phosphate group, as we would have expected an increase in Tyr^{1146}, Tyr^{1150}, Tyr^{1151} phosphorylation if that were the case. On the contrary it suggests either that an alanine at this position might alter the local structure and thereby influence the accessibility of the three Tyr to the kinase for autophosphorylation or that phosphorylation of Thr^{1148} has in fact a positive influence on kinase activity and its absence lead to a poorer response to insulin. Alternatively, phosphatases (T-Cell Protein Tyrosine Phosphatase) and adaptor proteins (Growth factor receptor-bound protein 7,10,14) are known to dephosphorylate the phopshoryaltated Tyr^{1146}, Tyr^{1150}, Tyr^{1151} (Goenaga et al., 2009; Goldstein et al., 2000; Han et al., 2001; Stein et al., 2001; Walchli et al., 2000). The Thr^{1148}Ala mutation might also facilitates the interactions of phosphorylated of Tyr^{1146}, Tyr^{1150}, Tyr^{1151} to these molecules.

Also, the lower phosphorylation of Tyr^{1146}, Tyr^{1150}, Tyr^{1151} in the IR-A Thr^{1148}Ala mutant is not consistent with the report of Petersen et al (Petersen et al., 2016) who saw higher phosphorylation of Tyr^{1158}, Tyr^{1162}, Tyr^{1163} in the IR-B Thr^{1160}Ala mutant. The experiment designs in the Petersen et al study and this study have huge differences: this study used the R- mouse fibroblasts transfected with IR-A as model and phosphorylation of Tyr^{1146}, Tyr^{1150},

Tyr^{1151} in the IR-A to indicate the IR activation; While Petersen et al used the High fat diet-induced hepatic insulin resistance mice as study model and the phosphorylation of Tyr^{1162} of IR-B in the liver to indicate the IR activation. The differences of study models (cell line vs mice), the cell types (fibroblast vs liver cells), the IR isoforms (IR-A vs IR-B), IR expression levels (overexpressed vs normal) could all affect the outcomes. In addition, using phosphorylation of Tyr^{1162} of IR-B and phosphorylation of Tyr^{1146}, Tyr^{1150}, Tyr^{1151} in the IR-A as IR activation marker might reflect different IR activation stages. As explained previously, the IR activation has intermediate stages, the Tyr^{1162} are phosphorylated first, followed by the phosphorylation of other two sites (Cabail et al., 2015; Hubbard et al., 1994). The Thr^{1148}Ala mutant could increase the phosphorylation of Tyr^{1162} of IR-B as shown by Peterson et al, but the changed structure inhibited the phosphorylation of the whole three Tyr as shown in this study.

Finally, *in vitro* studies by Petersen et al and Marin et al provide evidence that phospholipase C epsilon (PKCε) and protein kinase CK2 can act as kinases at Thr^{1148}, although neither study gives direct evidence of either kinase being responsible *in vivo*.

In summary, IR activation in response to insulin is inhibited by mutation of Thr^{1148} to Asp and Ala in this study. The Thr^{1148}Asp might inhibit the IR activation by the electrostatic repulsion of the negative charge group. Alternatively, the lack of response to insulin by both Thr^{1148}Ala and Thr^{1148}Asp may be due to the conformational change introduced in the activation loop. This may indirectly either alter the IR kinase activity or the access of downstream,kinases to the residues (Tyr^{1158}, Tyr^{1162}, Tyr^{1163}).

Chapter 5 Assessment of the roles of IR-A and IGF-1R in breast cancer cells

5.1 Introduction

Breast cancer is a group of heterogeneous diseases that display enormous variations in their molecular and clinical behaviour. Based on the expression status of the oestrogen receptor (ER), progesterone receptor (PR) and human epidermal growth factor receptor 2 (HER2), breast cancers are categorized into 2 types: Triple-positive breast cancer (ER+, PR+ and HER2+) and Triple-negative breast cancer (ER-, PR- and HER2-). Even though more intricate classifications are under investigation (Dawson et al., 2013) the current classification remains the fundamental basis for prognostic and clinical evaluation. Hormone positive breast cancers account for about 75-80% of all cases and are sensitive to hormone-based therapies which target the hormone receptors (Dawson et al., 2013). Triple-negative breast cancers are sensitive to chemotherapy, which kills cancer cells by stopping them from dividing or by inducing apoptosis, but have a poorer prognosis and are aggressive with a high rate of recurrence.

The IGF system is dysregulated in many types of cancers, including breast cancer (Malaguarnera and Belfiore, 2011; Park et al., 2016b; Pollak, 2008, 2012; Zhang et al., 2010). The IGF system can promote survival, proliferation and metastasis in breast cancer (Malaguarnera and Belfiore, 2011; Park et al., 2016b; Zhang et al., 2010). Within this complex system, the IGF-1R has attracted most of the research attention due to its prevalent overexpression in cancer, acting as the primary receptor for IGFs. Many different approaches have been developed to block IGF-1R signalling, including tyrosine kinase inhibitors and monoclonal antibodies that inhibit IGF binding or down regulate the receptor. However, clinical studies have shown that patients become resistant to these approaches (Baserga, 2013; Beckwith and Yee, 2015; Langer et al., 2014; Scagliotti et al., 2015). The mechanisms underlying the resistance are diverse, but can involve signalling via the IR-A stimulated by IGF-II (Frasca et al., 1999; Sciacca et al., 2002).

Overexpression of IGF-II and the IR-A has been shown to play a role in cancer growth and survival. The IR-A apparently provides an alternative pathway through which IGF-II can act (Avnet et al., 2009; Baserga, 2013; Frasca et al., 1999; Sciacca et al., 2002). The relative roles of the IR-A and IGF-1R in regulating growth, survival and migration are still not well understood in cancer cells co-expressing both receptors.

IR-A/IGF-1R hybrids are also widely distributed in mammalian cells, and the signalling via hybrids results in similar outcomes as promoted via the IGF-1R in response to IGF-I and IGF-II signals (Bailyes et al., 1997; Pandini et al., 1999; Slaaby, 2015).

In order to study the specific roles of IR-A in cancer cells, it is necessary to eliminate the effects of the IGF-1R and the hybrids. This chapter aimed to address this knowledge gap of the relative roles played by the IR-A and IGF-1R by specifically knocking down either the IR or IGF-1R in the two breast cancer cell lines, MCF-7 (ER^+, PR^+ and $HER2^-$) and MDA-MB-231 (ER^-, PR^- and $HER2^-$) cells. Both cell lines express IR-A, IGF-1R and IR-A/IGF-1R hybrids. However, there is controversy about the relative levels of IR and IGF-1R in MDA-MB-231 and MCF-7 (Davison et al., 2011; Mancini et al., 2014; Zhang et al., 2007). Therefore, it was important to initially characterise the IR and IGF-1R expression in MDA-MB-231 and MCF-7.

In order to avoid phenotypic changes in either cell line when knocking down the receptors, a modified inducible knock down system based on the miR30 shRNA system was chosen. This system was developed in the laboratory of Whitelaw et al (Bersten et al., 2015; Dow et al., 2012). The shRNA sequences were embedded in the miR30 shRNA, which is an endogenously expressed small microRNA (Figure 5.1) (Zeng et al., 2002). The 22mer length anti-sense/target sequence is linked by a miR30 loop structure into the miR30 context sequence. In cells, the transcribed sequence is directly processed by Drosha and Dicer to yield the mature small RNAs that enter the RNA-induced silencing complex (RISC) (Cullen, 2004).

In RISC, the guide strand binds to the targeted mRNA and causes its degradation (Cullen, 2004; Dickins et al., 2005; Dow et al., 2012).

The expression of the miR30-based shRNAs is regulated by a RNA Pol II promoter (pTRE3G) in this modified system (Dickins et al., 2005; Stegmeier et al., 2005) (Figure 5.1). The TRE3G promoter drives the expression of a single transcript encoding dsRED (a fluorescent indicator of expression) and the shRNA. Also included on the vector is the cDNA sequence encoding the Tet-On3G transactivator and the puromycin resistance protein, with an intervening IRES, with expression constitutively driven by the phosphoglycerate kinase-1 promoter (pPGK). In the presence of doxycycline (Dox), a complex is formed between Dox and the Tet-On3G protein, leading to a structural change in the Tet-On3G that allows it to bind to the TRE3G promoter, thereby promoting the expression of dsRED and the miR30 shRNA (Bersten et al., 2015; Dow et al., 2012; Stegmeier et al., 2005). Thus inducible gene silencing is achieved.

In this chapter, I will: i. Construct model breast cancer cell lines expressing only the IGF-1R or the IR through receptor knockdown (IGF-1RKD and IRKD). ii. Analyse the signalling response to insulin and IGF-II and resultant biological activities of the model cell lines (proliferation assay, migration assay, EMT marker PCR).

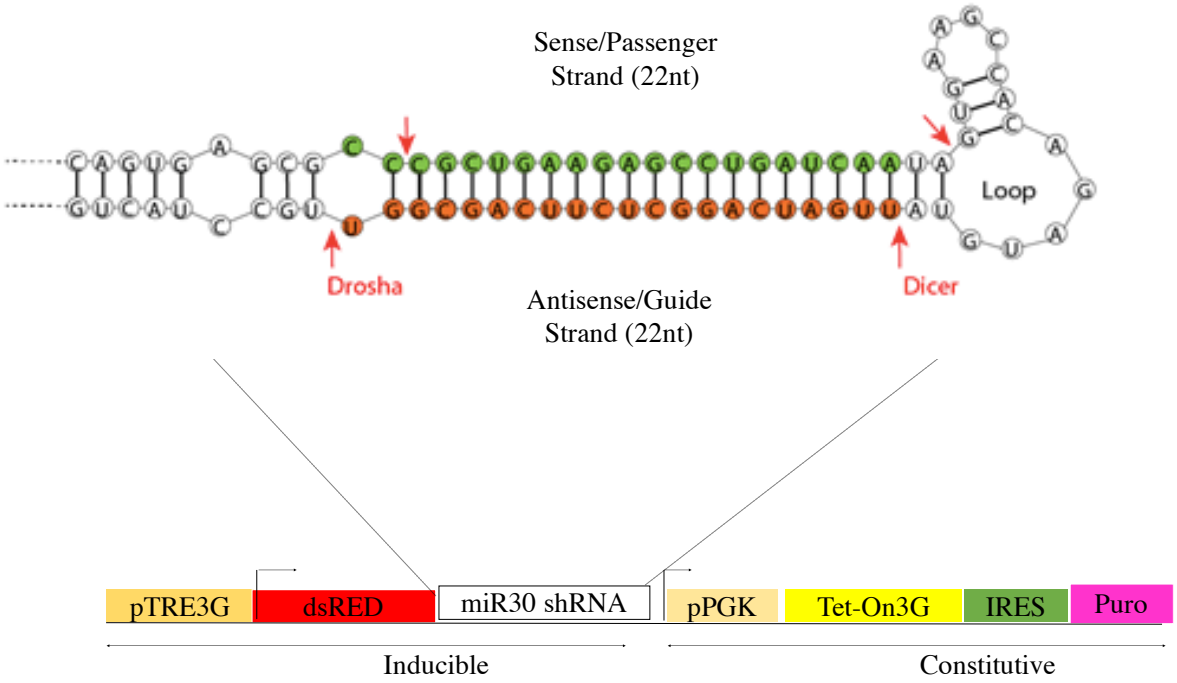

Figure 5.1: Structure of miR30 shRNA cassette (above) and inducible miR30 shRNA system (below). The miR30 shRNA cassette includes: sense/anti-sense strand 22mer (green/orange) and common miR30 context regions (black). After maturation, the guide strand (antisense strand, orange) will target the mRNA sequence and induce its degradation. This miR30 shRNA cassette figure was edited from transomic technologies (http://www.transomic.com/Products/RNAi/shRNA.aspx#620f0f4d-5b24-4f1b-a843-3084b2319e6b, 6689108). The inducible miR30 shRNA system includes: the pTRE3G, Tet-On 3G promoter; dsRED, red fluorescent protein; pPGK, PGK promoter; Tet-On3G, Tet-On 3G transactivator, IRES, internal ribosome entry site; Puro, puromycin resistance gene.

5.2.1 IR and IGF-1R expression levels in breast cancer cells

In order to characterise the MDA-MB-231 and MCF-7 cell lines, the mRNA levels of IR and IGF-1R were measured. Briefly, cells were cultured in DMEM medium supplemented with 10% FBS and Penicillin-Streptomycin (100 U/mL). RNA was extracted and 100ng of template was used for PCR in a volume of 50 µl. 5 µl of PCR product was loaded onto a 2% SB agarose gel and stained with GelRed. The PCR indicated that MCF-7 cells express much higher levels of IGF-1R mRNA than MDA-MB-231 cells (normalised to a GAPDH control). The MCF-7 cells expressed slightly higher levels of total IR mRNA than the MDA-MB-231 cells (Figure 5.2-A, B). In addition, the ratio of IR-A/B isoforms was similar to a previous report (Zhang et al., 2007) showing that MCF-7 cells expressed equal mRNA levels of IR-A and IR-B, whereas MDA-MB-231 cells predominantly expressed IR-A.

The IGF-1R and IR cell surface protein expression was measured with flow cytometry according to the methods described in section 3.2.5. MCF-7 cells expressed higher levels of IGF-1R on the cell surface than MDA-MB-231 cells (Figure 5.2-C, D). This is expected and correlated with the PCR result (Figure 5.2-A). MCF-7 cells also expressed significantly higher IR surface levels than MDA-MB-231 cells (Figure 5.2-C, D). This was subtly different to what we saw with the mRNA levels (Figure 5.2-B). The post-translational processing and receptor internalization rates might account for the differences between the PCR and cell surface expression results. In summary, differences in receptor expression were confirmed here and these results provided a sound basis for studies of the roles of the IGF-1R and IR-A in promoting cell growth, survival and migration in these cell lines.

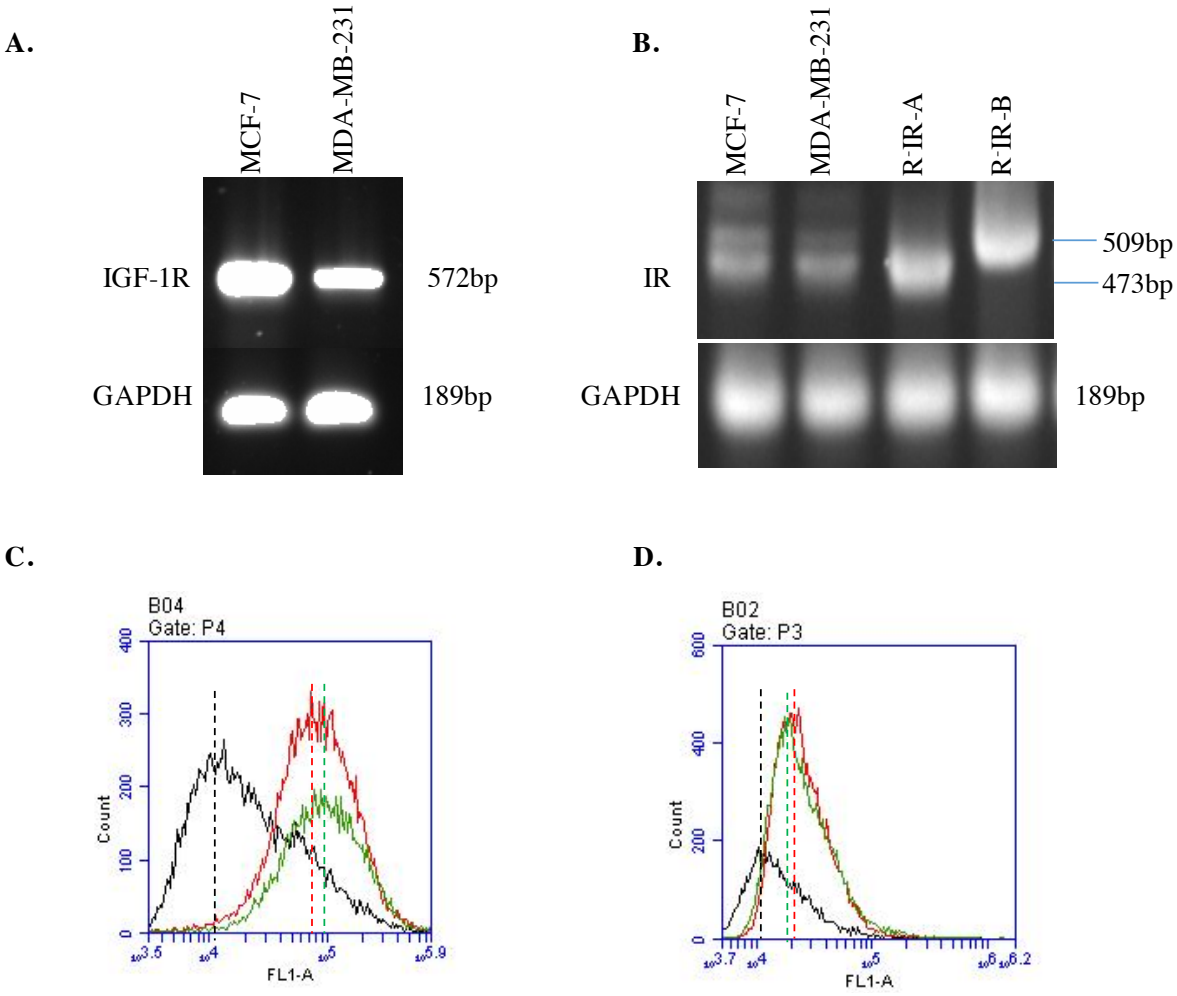

Figure 5.2: IR and IGF-1R expression levels in MDA-MB-231 and MCF-7 cells. (A) The amplification of IGF-1R and GAPDH resulted in 572bp and 189bp products respectively. (B) PCR primers that flank exon11 were used to distinguish between IR-A (473bp) and IR-B (509bp). IGF-1R depleted mouse 3T3-like cells with human IR-A (R^-IR-A) or IR-B (R^-IR-B) isoform overexpression were used as controls. MCF-7 (C) and MDA-MB-231 (D) cell surface receptor levels were assessed by flow cytometry using specific antibodies as described in section 3.2.5. Curves indicate IgG1 isotope control (black), IR (red) and IGF-1R (green) staining, and their respective geometric medians are shown as dotted lines.

5.2.2 Design and selection of shRNA sequences targeting the human IR and human IGF-1R

To assess the relative roles of the IR and IGF-1R in the MCF-7 and MDA-MB-231 cell lines each receptor was knocked down individually, resulting in cell lines listed in Table 5.1. For this purpose, a set of shRNAs were designed to be used in a modified inducible knock down system based on the miR30 shRNA system.

	MDA-MB-231	**MCF-7**
IGF-1R shRNA	shIGF-1R1	shIGF-1R1
	shIGF-1R2	shIGF-1R2
	shIGF-1R3	shIGF-1R3
	shIGF-1R4	shIGF-1R4
IR shRNA	shIR1	shIR1
	shIR2	shIR2
	shIR3	shIR3
	shIR4	shIR4
shRNA negative control	shGL3	shGL3

Table 5.1: Stable cell lines generated in this study.

In theory, any shRNA sequence can be inserted into the miR30 context to induce targeted mRNA degradation. However, not all shRNA sequences have high knock down efficiency due to the preferences of RISC loading and the multistep miRNA maturation steps (Fellmann et al., 2011). Studies with siRNA datasets show low GC content/high AU content at the 5' end of the guide sequence is preferred by the RISC and required for efficient target mRNA

binding (Reynolds et al., 2004; Tomari and Zamore, 2005). By analysing the dataset of around 20,000 shRNAs, Fellmann et al (Fellmann et al., 2011) uncovered a set of parameters for effective shRNA design including: A/U at position 1, no A at position 20, A/U at position 13 or U at position 14, and G at position 20 and 21. The shRNA with these parameters are strongly preferred by Drosha/DGCR8 cleavage, which promotes the transition from pre- to mature miRNAs (A/U in position 1 is also preferred for Dicer/TRBP cleavage and likely AGO2 loading (Fellmann et al., 2011). In summary, shRNA selection and design needs to be conducted according to the following parameters (Figure 5.3-A) for desirable knock down efficiency: A/U at position 1, 40-80% A/U content, >50% A/U content at positions 1-14, (A/U%1-14)/ (A/U%15-21) >1, no A at position 20, A/U at position 13 or U at position 14, no 'AAAAA' or 'TTTTT' or 'CCCC' or 'GGGG'. Only the sequences that passed all the criteria were selected for cloning and screening in the current study.

A mismatch at the 22nd base of the shRNA enables more efficient processing by the RNAi machinery by mimicking the structure of the endogenous miR30 (Figure 5.3-B). First, the reverse complement of the 21-mer guide strand (grey) is used to generate the 21-mer sense strand (or 21-mer target site; green); one nucleotide needs to be included at the 5' end (orange) according to the nucleotide at the 5' end of the 21-mer target site in the mRNA transcript (grey); if the 5' end nucleotide in the mRNA is an A or U, the first base of the 22-mer sense strand becomes a C, and if the 5' end nucleotide in the mRNA is a C or G, the first base of the 22-mer sense strand becomes an A. The final 22-mer sense strand is then inserted into a 97-mer cloning template (Figure 5.3-C).

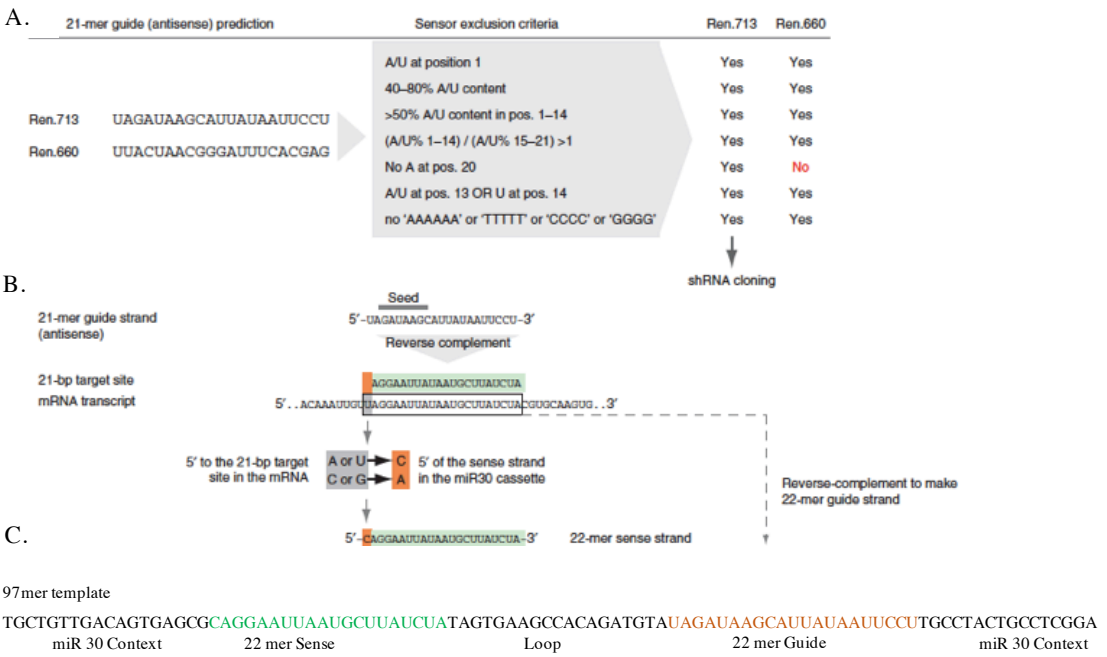

Figure 5.3: shRNA sequence design parameters. (A) Example of predicted shRNA guide strands screened against a series of Sensor exclusion criteria (grey box). The example shows two potential 21-mer predictions targeting the Renilla luciferase cDNA. Each shRNA is given a numerical designation (e.g., Ren.713) that reflects the first nucleotide position of the target sequence in the mRNA transcript. Sequences that pass all criteria are selected for cloning and testing in vitro. (B) Process of transforming the 21-mer guide strand predictions into miR30-based cloning templates. (C) The final 22-mer sense strand is then inserted into a 97-mer PCR cloning template (Dow et al., 2012).

The *Homo sapiens* insulin-like growth factor 1 receptor (hIGF-1R) mRNA (gi|119220593) (Figure 5.4) and *Homo sapiens* insulin receptor (hIR) transcript variant 1 mRNA (>gil119395735) (Figure 5.5) sequences were used as templates for *in silico* shRNA design. The methods for shRNA sequence selection were according to the parameters described above. The more parameters the sequence passed, the higher the score was. The four candidate sequences with the highest scores for each gene were selected and named as shIGF-1R1-R4 or shIR1-R4 according to their rankings from highest to lowest score. The shIGF-1R1, shIGF-1R3, shIR1, shIR2 and shIR3 were located in the three prime untranslated regions (3'-UTR) of the hIGF-1R and hIR sequences respectively, whereas shIGF-1R2, shIGF-1R4 and shIR4 were located in the coding sequence regions (CDS).

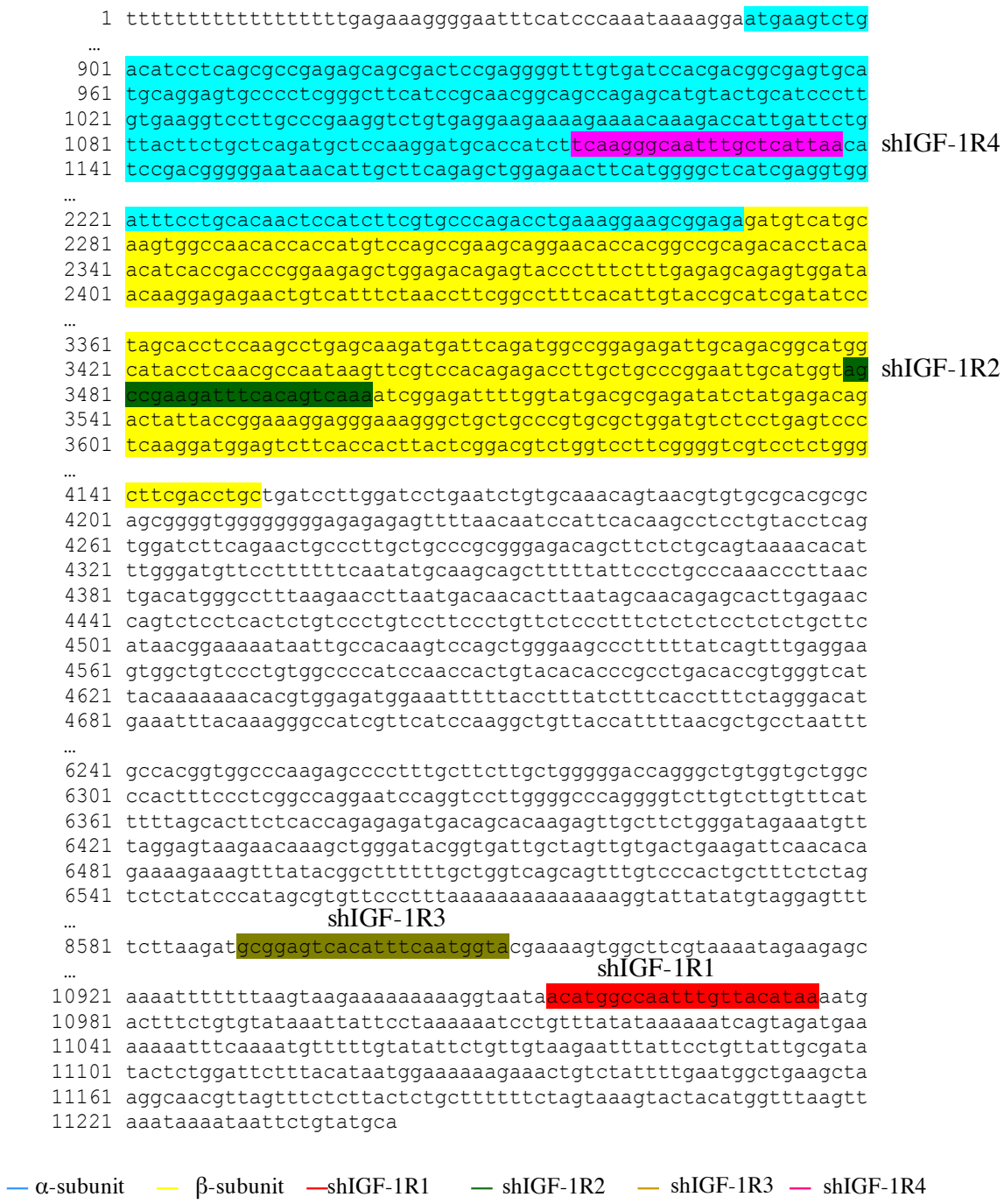

Figure 5.4: Homo sapiens insulin-like growth factor 1 receptor (hIGF-1R) mRNA sequence (gil119220593) is truncated (see numbering) to allow all shRNAs to be mapped onto the IGF-1R mRNA sequence. The sequence encodes two subunits: α-subunit (blue) and β-subunit (yellow). The shRNA candidate targeting sequences are marked in different colours. The entire 97 mer shRNA sequences are listed in Table 2.2.

Figure 5.5: Homo sapiens insulin receptor (hIR), transcript variant 1, mRNA (>gi|119395735 is truncated (see numbering) to allow all shRNAs to be mapped onto the IR mRNA sequence. The sequence encodes two subunits: α-subunit (blue) and β-subunit (yellow). shRNA candidate targeting sequences are marked in different colours. The entire 97 mer shRNA sequences are listed in Table 2.2.

5.2.3 Cloning strategy for miR30 shRNA inducible knock down system construction

Having designed the shRNA sequences these were then cloned into the miR30 inducible knock down vector. The miR30 shRNA inducible knock down system construction included the following steps: 1. Amplification of the 97-mer template containing shRNA by PCR, and 2. Ligation of the amplified shRNA template into pENTR1a vector by Gibson assembly. The resultant vector constructs were used for sequencing, 3. Insertion of the sequence-verified shRNA fragment into the lentivector pLVTPT by Gateway cloning (Figure 5.6).

pENTR1a and lentivector pLVTPT were gifts from the Whitelaw lab, University of Adelaide (Plasmid map see Appendix 1). The 97-mer template containing shRNA were first amplified using the M30c Iso primer pair (Table 2.2) according to the method described in section 3.1.18. The PCR introduces *XhoI* and *EcoRV* restriction enzyme sites and a short overhang sequence complementary to the pENTR1a vector. The pENTR1a vector and shRNA PCR products were digested and gel purified according to the method described in sections 3.1.4 and 3.1.5. The two purified fragments were joined together using Gibson assembly according to the method described in the section 3.1.11 and the sequences were verified by sequencing according to the method described in the section 3.1.13. Both pENTR1a and pLVTPT lentivectors were previously modified with Gateway cloning cassettes (AttL1 and AttL2 or AttR1 and AttR2 sequences, respectively), thus enabling the dsRed and shRNA fragments in pENTR1a to be introduced via the AttR1 and AttR2 cassette in the pLVTPT lentivector (Figure 5.6). Gateway cloning was conducted according to the method described in section 3.1.12. The shRNA containing lentivector pLVTPT miR30 shRNA was then used to produce lentivirus according to the method described in section 3.3.3.

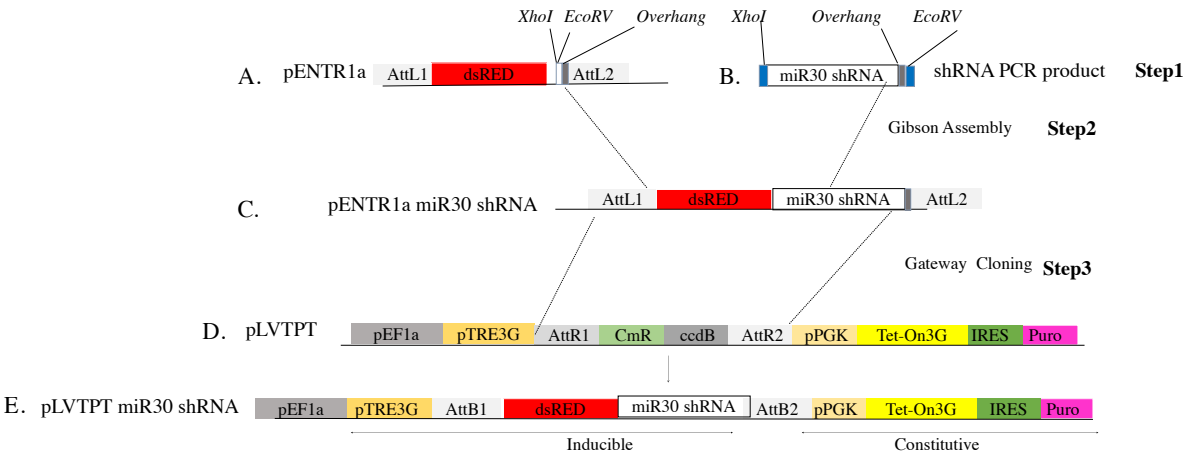

Figure 5.6: miR30 shRNA inducible knock down system construction. This flow chart includes several main steps: Step 1. Preparation of fragments to be introduced into the final pLVTPT miR30 shRNA vector. This involved (A) digestion of the pENTR1a vector with *XhoI* and *EcoRV* and (B) amplification of the 97-mer template containing shRNA by PCR; Step 2. Ligation of the amplified shRNA template into pENTR1a vector by Gibson assembly, which results the pENTR1a miR30 shRNA (C). This product is used for sequencing. Step 3. Insertion of the sequencing verified shRNA fragment into the pLVTPT lentivector (D) by Gateway cloning, resulting in the pLVTPT miR30 shRNA vector (E). Schematic diagrams of the DNA fragments used indicate the following components: dsRED (red), red fluorescent protein; pTRE3G (orange), Tet-On 3G promoter; pPGK (dark yellow), PGK promoter; Tet-On3G (yellow), Tet-On 3G transactivator; IRES (green), internal ribosome entry site; Puro (pink), puromycin resistance gene; AttL1, AttL2, AttR1, AttR2, AttB1, AttB2, Gateway cloning recombination sites; CmR, chloramphenicol resistance protein; ccdB, Toxin CcdB.

5.2.4 pENTR1a miR30 shRNA verification

The Ligation of pENTR1a miR30 shRNA was conducted according to the method described in section 3.1.11 using Gibson Assembly. After the insertion of each shRNA into the pENTR1a vector, *EcoRI* restriction digestion was used to screen for successful ligation. The *EcoRI* digestion cut the pENTR1a into two fragments of 2385bp and 872bp (Appendix 1),

whereas it cut the pENTR1a miR30 shRNA vector into two fragments of 2385bp and 969bp (Appendix 2), due to the insertion of the 97 mer shRNA fragment.

All eight of the shRNA sequences that target the hIR and the hIGF-1R were mixed at equal concentrations with the pENTR1a vector backbone in one ligation reaction. When the fragments were mixed equally, theoretically each has an equal chance to ligate with the vector. Thirteen out of the 16 colonies picked after ligation contained miR30 shRNA fragments (81% efficiency). These constructs were sequenced before the shRNA inserts were cloned into the pLVTPT lentivector. The 13 ligated vectors contained all 8 different miR30 shRNA fragments (shIR 1-4 and shIGF-1R 1-4) (Figure 5.7).

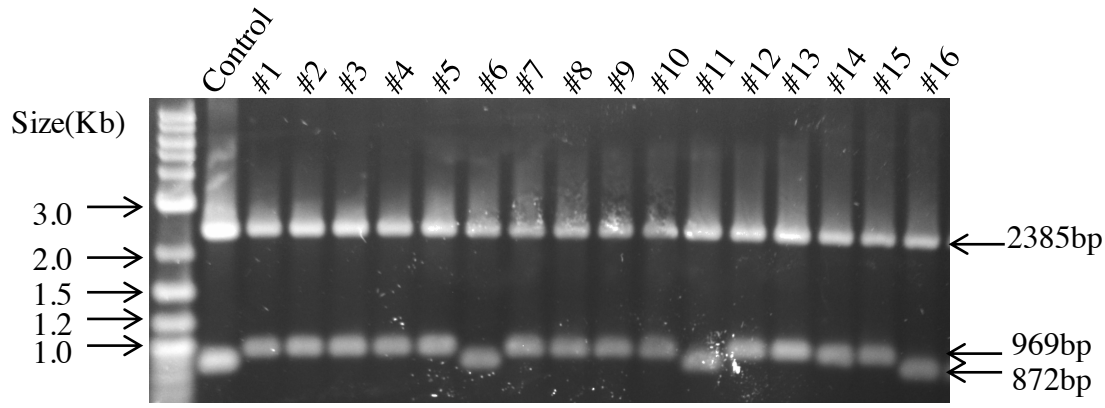

Figure 5.7: pENTR1a shRNA verification. pENTR1a shRNA ligation products (number 1-16) were digested with EcoRI using the original pENTR1a vector as a control. Digestion products were separated by electrophoresis on a 2% TBE agarose gel and visualized using GelRed staining. The bands on the left are 2-log DNA ladder.

5.2.5 pLVTPT miR30 shRNA verification

The Gateway LR cloning was used to construct the pLVTPT miR 30 shRNA according to the methods described in section 3.1.12. Individual pENTR miR30 shRNA vector was combined with the pLVTPT vector in a total of eight reactions. The shRNA fragment flanked by AttL1 and AttL2 in pENTR1a miR30 shRNA vector was introduced into the complementary region in the pLVTPT flanked by AttR1 and AttR2. pLVTPT miR30 shRNA vectors were used to transform the *E. coli* strain *DH5α* and were selected on kanamycin plates. Successful cloning of the shRNA sequences into the pLVTPT vector was detected by *EcoRV* digestion, which was expected to yield 3 fragments (7962bp, 1183bp and 1378bp, Appendix 4), while the digest of the empty pLVTPT vector yielded 7962bp, 1713bp and 1378bp fragments (Appendix 3). The clones contained the expected fragements indicating successful introduction of the shRNA sequences into the pLVTPT vector (Figure 5.8).

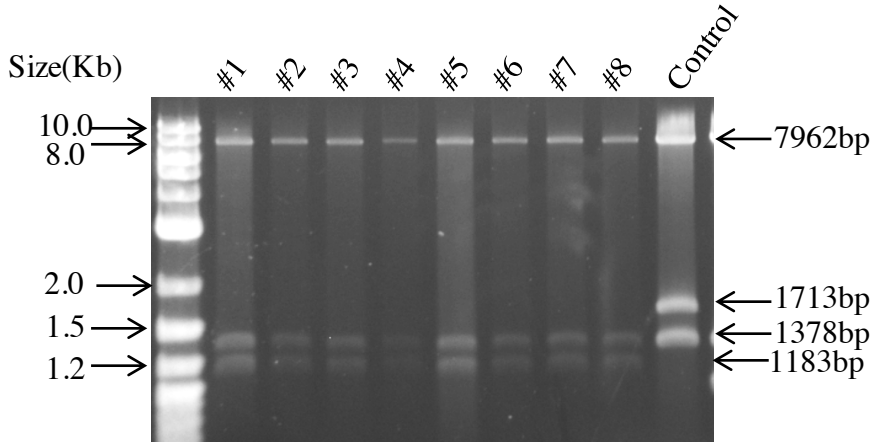

Figure 5.8: pLVTPT miR30 shRNA verification. pLVTPT miR30 shRNA vectors targeting IR (#1-4) or IGF-1R mRNA (#5-#8) were digested with EcoRV and using pLVTPT as a control. Digestion products were separated by electrophoresis on 1% TBE agarose gels and visualized using GelRed staining.

5.2.6 Virus infection optimization and stable cell line selection

Having successfully constructed four shRNA pLVTPT vectors to target the IR and four targeting the IGF-1R the next step was to produce lentivirus and infect the MCF-7 and MDA-MB-231 cells. An additional vector (shGL3) was constructed in the Whitelaw lab (The University of Adelaide) to target the Luciferase gene and was used as shRNA negative control. A total of 18 stable cell lines were generated (Table 5.1).

The lentivirus was produced by transient transfection of the lentivector pLVTPT miR30 shRNA and virus packaging vectors in human embryonic kidney (HEK) 293T cells according to the protocol described in section 3.3.3. Virus-containing supernatants were used for the infection of MDA-MB-231 and MCF-7 cells.

In order to facilitate the establishment of the stable cell lines through miR30 RNA genomic integration, the lentivirus infection conditions were first optimized with the following parameters: cell density, virus:medium ratio, virus cell contact time and condition. MDA-MB-231 cells were used initially to determine optimal viral infection conditions and then these were applied to MCF-7 cells. The Doxycycline (Dox) was added the next day to induce the reporter protein (dsReD) expression (Figure 5.9-A). The dsRed was confirmed using the fluorescence microscope (Cy3 filter, 575-625nm) to detect dsRed expression. In the absence of Dox, dsRed was undetectable as expected as under these conditions the Tet-On-3G cannot bind the TRE3G promoter. In the presence of Dox, the dsRed was robustly expressed. By overlaying the images of cells taken under the light microscope and the fluorescence microscope, the infection efficiency could be calculated. Ideally above 80% infection efficiency would be reached.

Firstly, the ratio of virus: medium (volume:volume) was optimized using the ratios of 1:1,1:3 and 1:9. A ratio of 1:1 led to the highest infection rate with 20% of cells being infected (Figure 5.9-B). This condition was used for further refinement. There are basically two ways to increase the infection rate: prolong the virus-cell contact time (overnight virus-cell

incubation, from now on referred to as the "overnight incubation method") and improve virus-cell contact (increase virus-cell contact by centrifuge, from now on referred to as the "spin method"). When comparing the two methods (described in section 3.3.4) the overnight incubation method generally resulted in a higher infection rate than the spin method (Figure 5.9-C). The effect of cell seeding density on virus infection rate was also optimized using cells seeded at 10,000, 20,000, 50,000 cells per well. Low cell seeding density improved the infection rate to an approximately 40% (overnight incubation method, virus: medium ratio of 1:1). Below this seeding density the cells did not grow well and therefore lower densities were not tested. Stable cell lines were selected according to the method described in section 3.3.6.

Interestingly, using the same conditions on MCF-7 cells only a 26.2% infection rate was achieved, compared to the 40% infection rate with MDA-MB-231 cells. Even though the infection rate was not as high as expected, stable cell lines were also successfully selected according to the method described in section 3.3.6. Obviously, it was sufficient to select the stable cell lines using the optimised method.

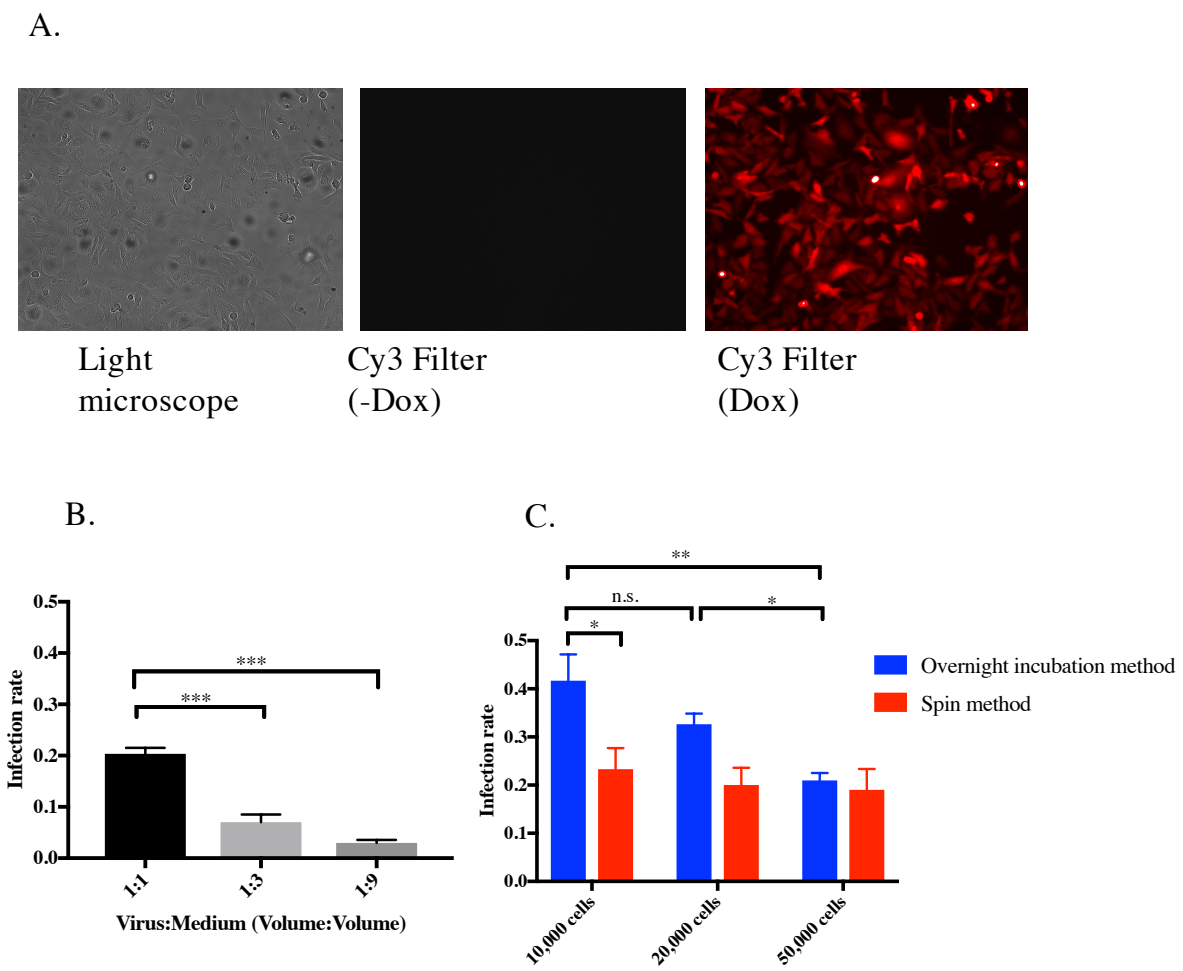

Figure 5.9: Virus infection optimization. MDA-MB-231 cells were seeded into 6-well plates and infected with lentivirus produced in 293T cells. Two days after infection, 1 µg/ml of Dox was added into medium and dsRED fluorescence was detected 24 hours later. Fluorescent cell to total cell ratio was calculated to provide an indication of infection rate. (A) Cells were detected under the light microscope or with the Cy3 filter (575-625nm) with or without Dox induction. Factors affecting the infection rate were optimized: (B) ratio of virus to medium (volume:volume), and (C) infection method and cell density. No significant differences were found between cell densities with spin method. The bars show the S.E.M. of 5 technical replicates. Statistical significance was determined by one-way ANOVA in Figure 5.9-B and two-way ANOVA in Figure 5.9-C (* represents $P<0.05$ and *** represents $P<0.001$).

5.2.7 shRNA selection

Following the selection of the cell lines, the knock down efficiency of each shRNA was measured. Initially the knockdown efficiency of shRNAs was measured in the MDA-MB-231 cell lines. shRNA expression was induced by adding Dox (1 μg/ml) into the culture medium for four days. Cells were then lysed and the receptor levels were measured with Western-blotting according to the methods described in section 3.2.4.

Even though all four shRNAs targeting the IGF-1R passed the selection parameters described above(Dow et al., 2012), significant differences in knock down efficiency were seen between individual shRNAs. The shIGF-1R2 induced knock down by 91%, shIGF-1R4 by 46%, while shIGF-1R1 and shIGF-1R3 did not induce knock down. Interestingly, shIGF-1R2 and shIGF-1R4 targeted the CDS region, while shIGF-1R1 and shIGF-1R3 targeted the 3'-UTR region. The possible explanation of these differences is that the disruption of CDS region would directly decrease the protein translation. Importantly, the IR level was not significantly affected by IGF-1R knock down (Figure 5.10-A, C). The raw data of Figure 5.11-A, C are shown in Appendix 14.

Similarly, differences in knock down efficiency were seen between the shRNAs targeting the IR. The shIR4 induced knock down by 93%, shIR-3 by 80%, shIR-1 by 50% and shIR-2 by 20%. The IGF-1R levels in each cell line was not significantly affected by IR knock down (Figure 5.10-B, D). The results were consistent with the shRNAs targeting the IGF-1R, the most efficient shRNA targeting the IR (shIR4) also targeted the CDS region. The shIR1, shIR2 and shIR3 targeted the 3'-UTR, but they were effective to varying degrees at reducing IR expression. From these results, it can be concluded that shRNAs designed to target CDS regions are possibly more reliable than those targeting the 3'UTR. As shIR4 and shIGF-1R2 were verified to induce desirable knock down effect of the receptors, these two cell lines were thus used for the following experiments and are referred to as IRKD and IGF-1RKD from now on.

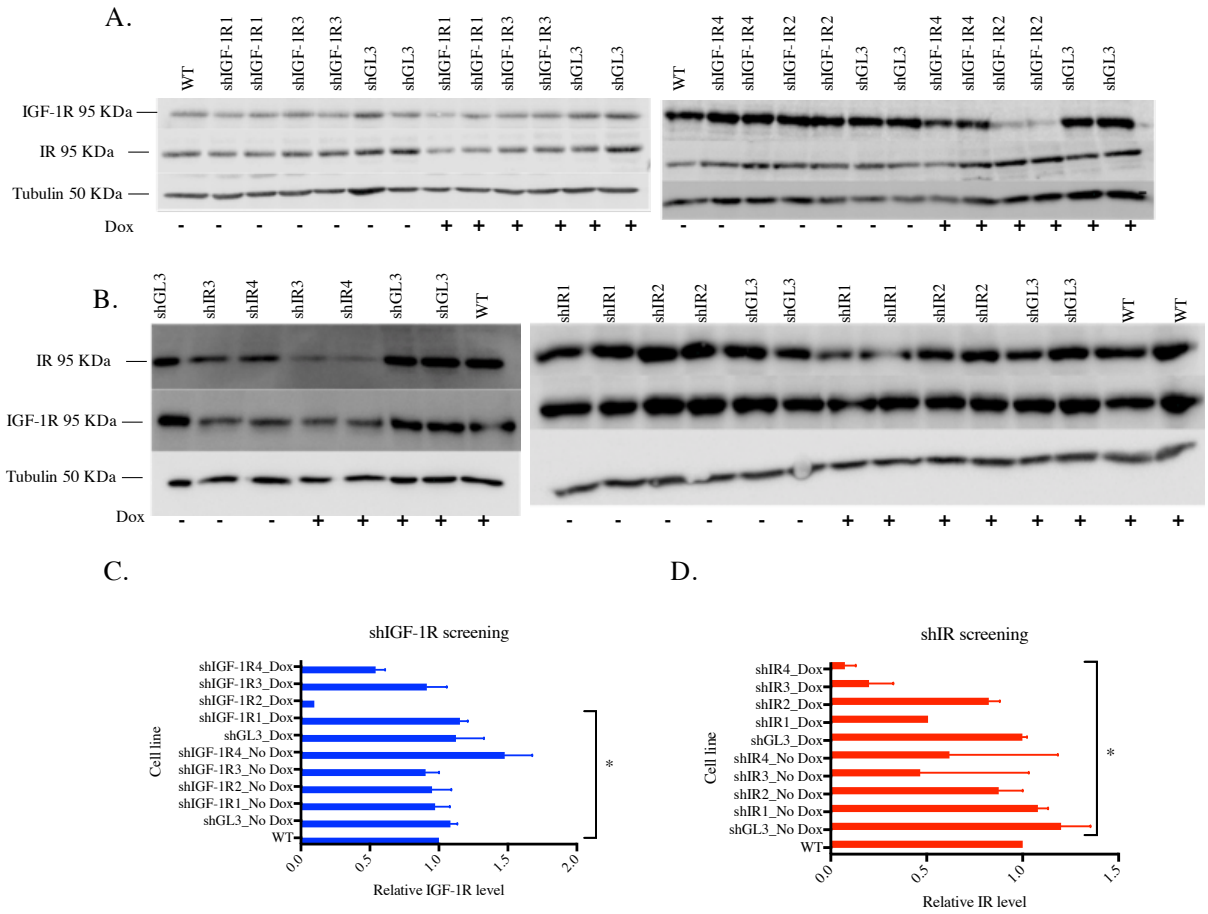

Figure 5.10: shIGF-1R (A and C) and shIR (B and D) screening in MDA-MB-231 cell lines. Four different shRNA that target different areas of IGF-1R or IR mRNA were designed and the shRNA that targets the luciferase gene (pGL3) was used as a negative control. The expression of each shRNA was induced in duplicate by adding Doxycycline (1 μg/ml) into the medium (+) of two replicate wells. After four days, cells were lysed and receptor levels were measured by immunoblot with Anti-Insulin Receptor beta antibody [C18C4] (Abcam #ab69508) and IGF-I Receptor β Antibody (Cell signalling #3027) according to the methods described in section 3.2.4. Quantitation of shIGF-1R (C) and shIR (D) knockdown immunoblots showed the differences in efficiency of knockdown of the different shRNAs. The bars show the S.E.M. of 3 biological replicates, each with technical duplicates. Statistical significance was determined by one-way ANOVA (* represents $P<0.05$). The raw data of Figure 5.10-A, C are shown in Appendix 14.

5.2.8 shRNA knock down time course

In order to further understand the knock down kinetics and to select the optimal conditions for the knock down a time course was conducted with shIGF-1R2 in both MDA-MB-231 (Figure 5.11-A, B) and MCF-7 (Figure 5.11-C, D) cells. The raw data of Figure 5.11-A, C are shown in Appendix 15.

The knock down effect started as early as 24 hours with Dox induction and the knock down effects increased with longer Dox induction time. The maximum knock down by shIGF-1R2 was reached in MDA-MB -231 (91%) and MCF-7 (72%) cells after 96 hours of Dox induction. So the 96 hours Dox induction time was selected for the following experimental design.

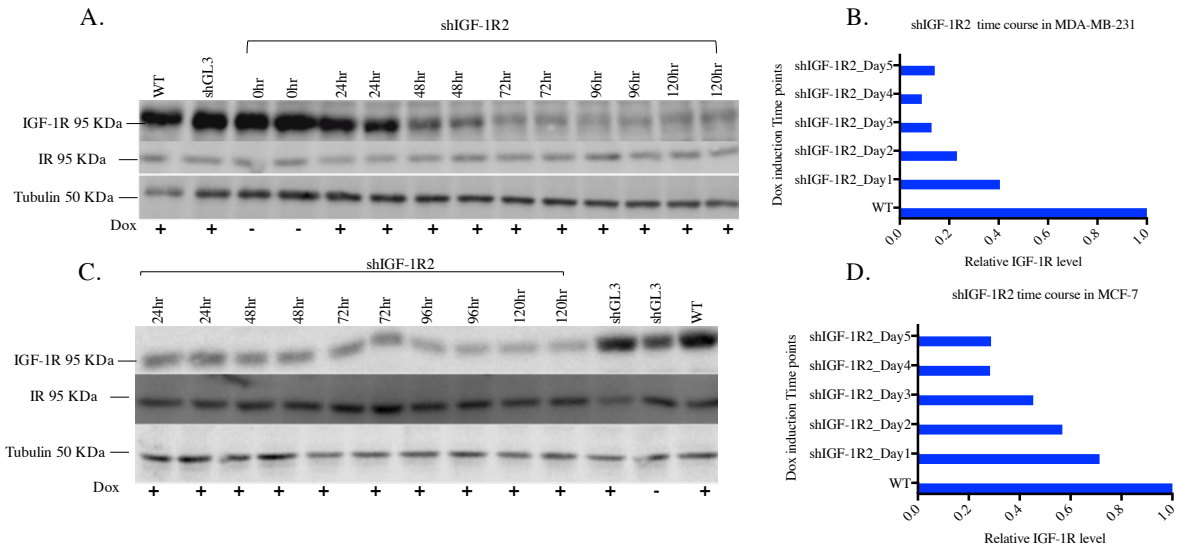

Figure 5.11: shIGF-1R2 time course in MDA-MB-231 (A and B) and MCF-7 (C and D) cells. The expression of shRNA was induced in duplicate by adding Doxycycline (1 μg/ml) into medium of two replicate wells. Samples were taken each day for 5 days. Cells were lysed and receptor levels were measured according to the methods described in section 3.2.4. Biological duplicates were conducted. Bars represent the average of biological duplicates. The raw data of Figure 5.11-A, C are shown in Appendix 15.

5.2.9 IR-A transduces insulin and IGF-II signals in MDA-MB-231 IGF-1R KD cells

Cell lines were then subjected to a series of assays to measure the *in vitro* response to insulin and IGFs with the aim to understand the relative contribution of the IR-A and IGF-1R to biological responses to these ligands. Initially a small scale experiment using just the MDA-MB-231 wild-type, shGL3 and shIGF-1R2 (shIGF-1R) cell lines was conducted to see if we could detect any difference between the response to insulin and IGF-II in cells expressing only the IR-A (ie in the MDA-MB-231 shIGF-1R cell line).

Phosphorylation of proteins from Akt and MAPK signalling pathways were detected in MDA-MB-231 wild-type, shRNA negative control- shGL3 and shIGF-1R with/without Dox induced knock down (Figure 5.12). The cells were seeded and incubated with/without Dox in medium for 3 days before overnight starvation, then cells were stimulated with 10 nM insulin or 100 nM IGF-II for 10 minutes and lysed immediately. The concentrations of 10 nM insulin and 100 nM IGF-II were chosen to take into account the difference in IR-A binding affinities (see Table 1.1). Western blotting was conducted according to the method described in section 3.2.4.

All MDA-MB-231 cell lines responded to insulin and IGF-II stimulation with an increase in Akt phosphorylation (pSer473 and pThr308, Figure 5.12-B,C). The Akt responses of the wild type and GL-3 control cell lines were similar. In both cell lines there was a greater response to 100 nM IGF-II than 10 nM insulin. There was also a greater response to 100 nM IGF-II than 10 nM insulin in the MDA-MB-231 shIGF-1R cells without Dox. As these cells express both the IR-A and the IGF-1R it is possible that this response reflects predominantly IGF-1R signalling or hybrid receptor signalling.

Interestingly, upon IGF-1RKD the Akt phosphorylation response to insulin was markedly increased and reached the same level as seen with 100nM IGF-II stimulation. In this cell line the predominant receptor expressed is the IR-A and there are no hybrid receptors. No increase in IGF-II response was detected with Dox induction of IGF-1R KD. This could be due maximum activation having been reached, although this is yet to be determined with dose

response study. Importantly, this result demonstrates that these MDA-MB-231 IGF-1RKD cells respond to both insulin and IGF-II via the IR-A.

In MDA-MB-231 wild-type, GL-3 and IGF-1RKD cell lines the phosphorylation levels of 90RSK (pSer380), 44/42 MAPK (pThr202/pTyr204) and S6 (pSer235/236) did not increase as compared to the non-stimulated state, regardless of whether it was in response to insulin or IGF-II (Figure 5.12-D, E, F). These findings suggest that in these cells lines the MAPK signalling pathway is not activated above basal by insulin and IGF-II. The raw data of Figure 5.12-A is shown in Appendix 16.

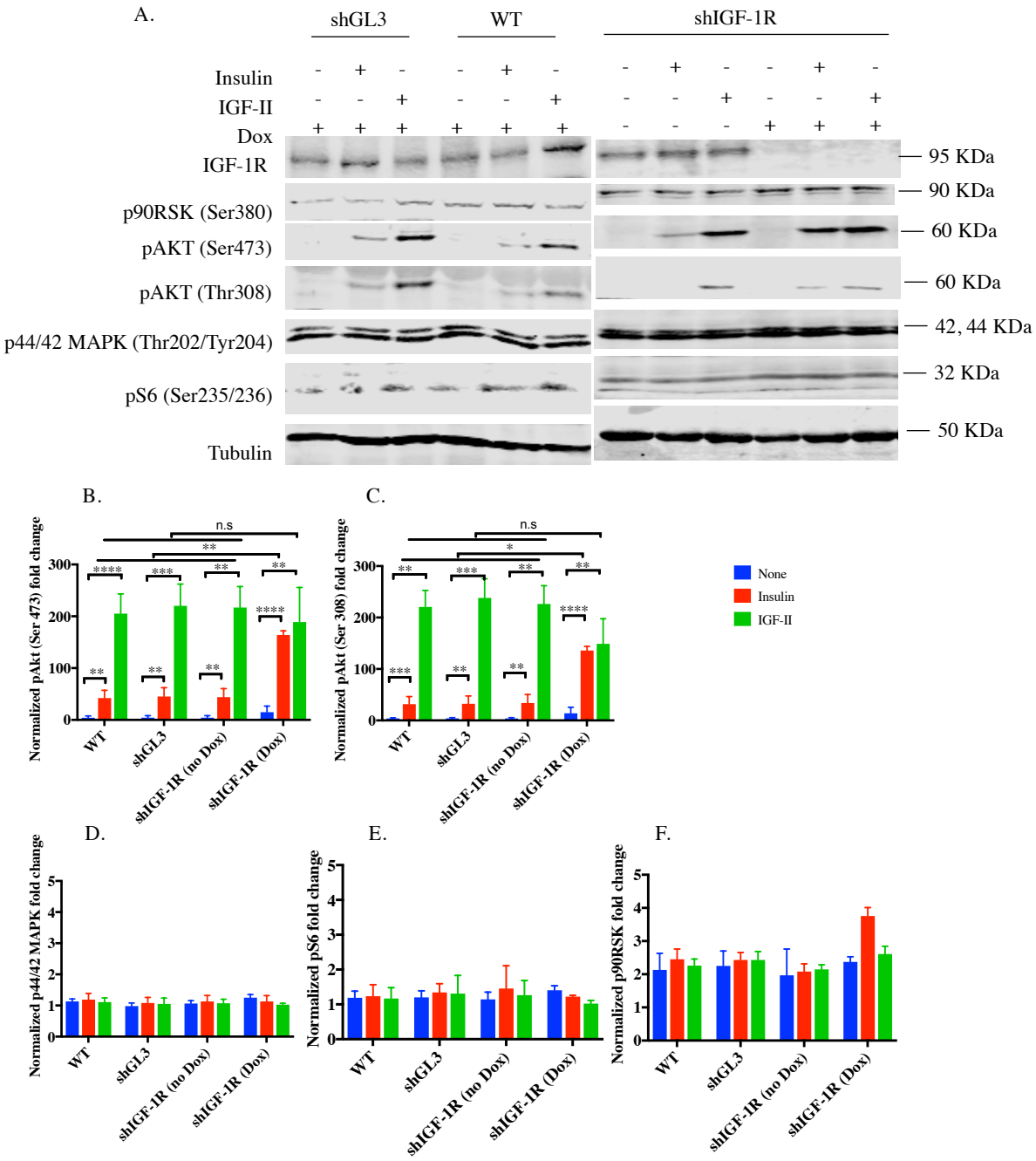

Figure 5.12: Phosphorylation of signalling proteins in Akt and MAPK signalling pathways in response to insulin or IGF-II. MDA-MB-231 cells were cultured with/without Dox for 3 days and starved in serum-free medium with 1% BSA overnight. Cells were then treated with 10nM insulin or 100 nM IGF-II for 10 min. (A) Whole-cell lysates were immunoblotted for IGF-1R, tubulin, phosphorylated pAkt (pS308) and PathScan® Multiplex Western Cocktail I (Cell signalling #5301). (B) Akt phosphorylation (pSer473), (C) Akt phosphorylation (pThr308), (D) 90RSK (pSer380), (E) 44/42 MAPK (pThr202/pTyr204), (F) S6

(pSer235/236). Figure shows the representative result of biological triplicates. The raw data of Figure 5.12-A is shown in Appendix 16.

5.2.10 Proliferation of MDA-MB-231 cell lines

Next, the ability of IGFs and insulin to stimulate proliferation through activation of the IR or IGF-1R expressed by the MDA-MB-231 cell lines was assessed (Figure 5.13). The control GL3, shIR4 and shIGF-1R2 of MDA-MB-231 cell lines (Table 5.1) were cultured in medium containing Dox for three days to induce the knock down of IR or IGF-1R. All cell lines (including wild type MDA-MB-231 cells) were then seeded into two 48 well plates (4,000 cells/well) and were grown at least 24 hours in medium containing 10% FBS. They were then starved in medium containing 2% charcoal treated FBS overnight to get rid of the endogenous ligands. One plate was stimulated with IGFs and insulin at 0 nM, 1 nM, 10 nM and 100 nM diluted in medium containing 2% charcoal treated FBS. The other plate was immediately stained with crystal violet to determine the cell number at t=0 as described in section 3.3.11. Four days later, crystal violet staining was used to estimate the number of stimulated cells.

The response of each cell line to increasing ligand doses was measured (Figure 5.13-A). The growth rates of each cell line stimulated with ligand were normalized to the growth rates of that cell line without ligand stimulation (0 nM ligand, 2% charcoal treated FBS). Despite activation of downstream Akt signalling (Figure 5.12) the MDA-MB-231 wild-type cells had no significant response to any ligand (insulin, IGF-I and IGF-II) stimulation, even with ligand concentrations as high as 100 nM (Figure 5.13-A). Similar results were also shown with other MDA-MB-231 cell lines-shGL3, IRKD and IGF-1RKD (Figure 5.13-A).

The data was then re-analysed to compare relative growth rates between the different MDA-MB-231 cell lines, this time normalizing to the growth rate of MDA-MB-231 wild-type under starvation conditions (0 nM, 2% charcoal treated FBS). Growth differences between cell lines in response to ligands (insulin, IGF-I and IGF-II) were compared (Figure 5.13-B). The growth rate of the shRNA negative control-GL3 cell line was not significantly different to the wild-type MDA-MB-231 cells, indicating the introduction of lentivirus and the integration of shGL3 doesn't change the characteristics of cells. Most strikingly, the IR knock down in

MDA-MB-231 cells (IRKD) significantly enhanced cell growth by 3-5 fold compared to wild type MDA-MB-231 cells (Figure 5.13-B). In contrast, the IGF-1R knock down in MDA-MB-231 cells (IGF-1RKD) significantly inhibited growth compared to wild type cells (Figure 5.13-B).

In summary, wild type MDA-MB-231 cells were unresponsive to all three ligands. Knock down of the IR and IGF-1R resulted in changes in growth rates independent of insulin, IGF-I or IGF-II, suggesting that these receptors are playing an important role in regulating cell proliferation driven by other growth factors within FCS. These cells were maintained in 2% FCS and were not viable in medium containing lower concentrations. In this medium their doubling time was ~ 2 days.

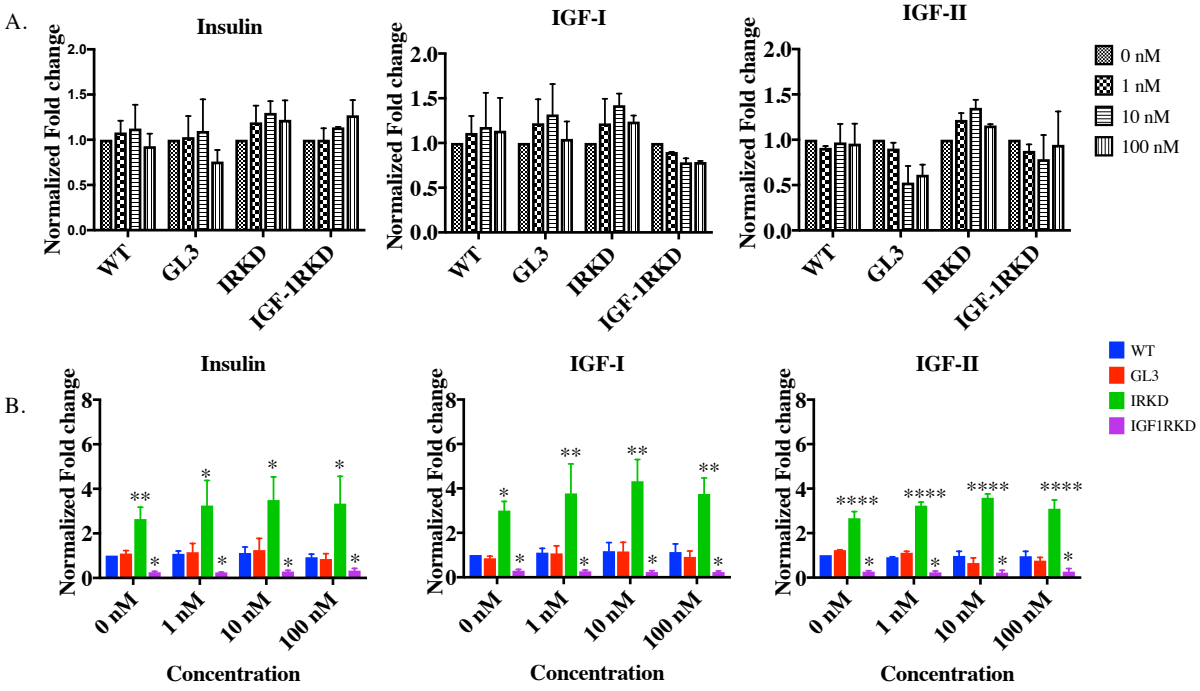

Figure 5.13: Growth of MDA-MB 231 cell lines in response to insulin and IGFs (0 nM, 1 nM, 10 nM and 100 nM). Crystal violet assay was conducted to assess the proliferation rate according to the method described in section 3.3.11. The dose response of each cell line was

measured (A). The growth rates in response to ligands (insulin, IGF-I and IGF-II) were normalized to the individual cell line growth rate in absence of ligand (0 nM, 2% charcoal treated FBS). The growth differences between cell lines were also compared (B). All growth rates were normalized to the MDA-MB-231 wild-type growth rate under starvation conditions (0 nM, 2% charcoal treated FBS). The bars show the S.E.M. of 3 biological replicates, each with technical triplicates. Statistical significance was determined by two-way ANOVA (ns, $P > 0.05$; *, $P \leq 0.05$; **, $P \leq 0.01$; ***, $P \leq 0.001$ ****, $P \leq 0.0001$).

5.2.11 Proliferation of MCF-7 cell lines

Proliferation assays were also used to assess the effect of IR or IGF-1R knock down on the proliferation of MCF-7 cells in response to IGF and insulin stimulation (Figure 5.14). As there was no difference in receptor expression in the shGL3 control MCF-7 cells (Figure 5.11) and the lentivirus infection and integration of shGL3 into the genome did not affect the cell characteristics in MDA-MB-231, this control cell line was not used in proliferation assays. The assay was conducted in the same way as the MDA-MB-231 cell proliferation assays described in section 5.3.8.

Firstly, the response of each MCF-7 cell line to increasing concentrations of each ligand was measured (Figure 5.14-A). Again, the growth rates of each cell line stimulated with ligand were normalized to the growth rates of that cell line without ligand stimulation (0 nM ligand, 2% charcoal treated FBS). The MCF-7 wild-type cells responded significantly to all the ligands (insulin, IGF-I and IGF-II) and the responses reached a maximum at 10 nM. Similar results were also shown with other cell lines- IRKD and IGF-1RKD.

The data was then re-analysed to compare relative growth rates between the different MCF-7 cell lines, this time normalizing to the growth rate of MCF-7 wild-type under starvation conditions (0 nM, 2% charcoal treated FBS). Growth differences between cell lines in response to ligands (insulin, IGF-I and IGF-II) were compared (Figure 5.14-B). The MCF-7 IR knock down cells (IRKD) responded to a similar extent to the wild-type MCF-7 cells to all the ligands (insulin, IGF-I and IGF-II), with the ligand stimulation concentration ranging from 0 nM to 100 nM (Figure 5.14-B). However, the growth of the MCF-7 IGF-1R knock down cells (IGF-1RKD) was significantly inhibited compared to wild type MCF-7 cells, while there was still an increasing response to all the ligands (Insulin, IGF-I and IGF-II), with the increasing ligand concentrations ranging from 0 nM to 100 nM (Figure 5.14-B).

In summary, MCF-7 cells grew in response to insulin, IGF-I and IGF-II. Higher growth rates were identified with increasing ligand concentrations. While the lack of the IR did not change

the growth rate of cells, the lack of IGF-1R significantly inhibited the cell growth. This indicates that the IGF-1R or hybrid receptors regulate the growth of MCF-7 cells rather than the IR.

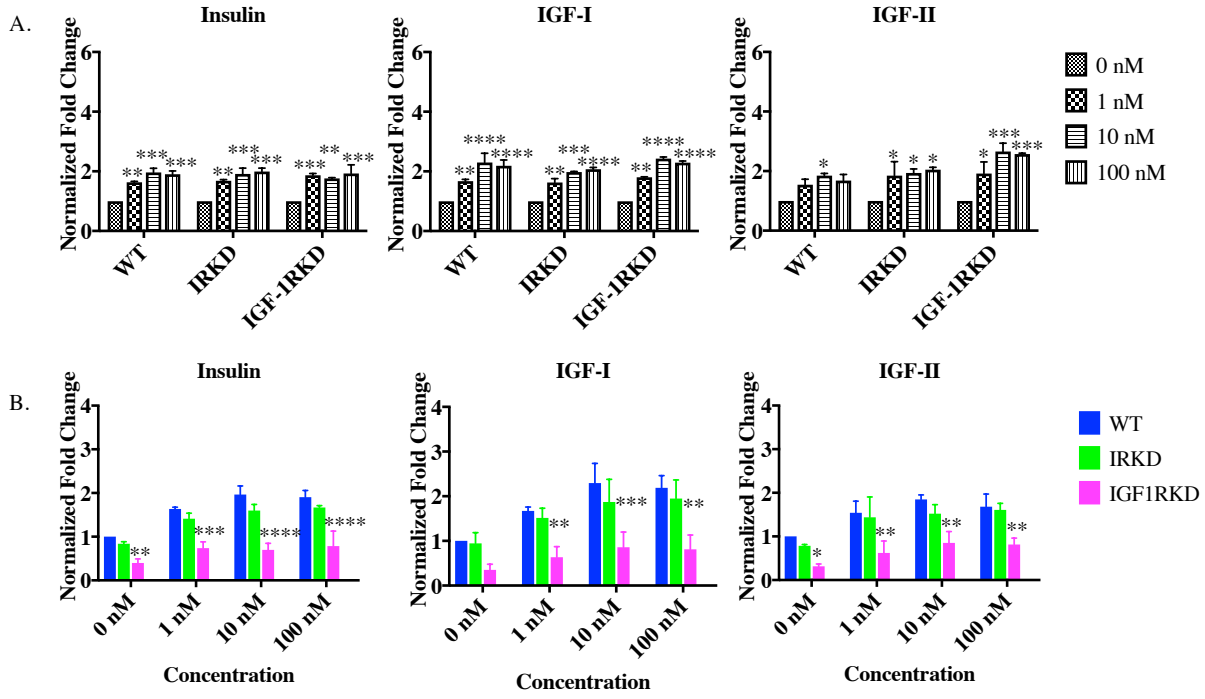

Figure 5.14: Growth of MCF-7 cell lines in response to insulin and IGFs (0 nM, 1 nM, 10 nM and 100 nM). Crystal violet assay was conducted to assess the proliferation rate according to the method described in section 3.3.11. The dose response of each cell line was measured (A). The growth rates were normalized to the individual cell line growth rate in starving conditions (0 nM, 2% charcoal treated FBS). The growth differences between cells in response to ligands (insulin, IGF-I and IGF-II) were also compared (B). All growth rates were normalized to the MCF-7 wild-type growth rate under starvation conditions (0 nM, 2% charcoal treated FBS). The bars show the S.E.M. of 3 biological replicates, each with technical triplicates. Statistical significance was determined by two-way ANOVA (ns, $P > 0.05$; *, $P \leq 0.05$; **, $P \leq 0.01$; ***, $P \leq 0.001$ ****, $P \leq 0.0001$).

5.2.12 IGF-1R knock down enhanced the migration rate of MDA-MB-231

Wound healing assays were used to assess the effect of IR or IGF-1R knock down on the migration of MDA-MB-231 cells (Figure 5.15). MDA-MB-231 cells were cultured in medium containing Dox (1 μg/ml) to induce the knock down of IR or IGF-1R. Then cells were seeded into 24-well plates to grow until confluent. Cells were starved in serum-free medium for 16 hours. A wound was made with a 200μl pipette tip and 10 nM of ligand (insulin, IGF-I or IGF-II) or 10% Fetal calf serum (FBS) were added to stimulate migration. Photographs were taken and the wound area was measured using CellProfiler software (Jones et al., 2008). Migration was monitored by comparing the wound area at t=0 at the time of making the wound and after 24 hours (No significant migration was found after 6 hours).

Firstly, the responses of MDA-MB-231with shRNA integration were compared to wild-type (Figure 5.15-A). With or without ligand stimulation the migration of MDA-MB-231 GL3 and IRKD cells was not significantly different to the wild type MDA-MB-231 cells. However, the IGF-1RKD enhanced the migration of MDA-MB-231 cells compared to wild type MDA-MB-231 cells (smaller wound area at 24 hours), even in the absence of ligand stimulation.

Secondly, the ligand effect of increasing ligand concentrations on migration of individual MDA-MB-231 cell lines was assessed (Figure 5.15-B). The extent of migration of MDA-MB-231 wild type cells was significantly greater in response to insulin, IGF-I and FBS compared to no treatment. The migration of the MDA-MB-231 GL3 cell line was similar to wild type MDA-MB-231 cells, although there was no significant response to insulin. In fact, all cells migrated to a greater extent in response to FCS compared to no treatment. While it appeared that IGF-II promoted increased migration in all of the MDA-MB-231 cell lines this effect was not statistically significant. All cell lines responded significantly to IGF-I except for the MDA-MB-231 IGF-1RKD cell line. Migration of the MDA-MB-231 IRKD cell line was slower than wild type cells and significant responses were only seen to insulin and FCS. The

migration of IGF-1RKD was only significantly enhanced in response to FBS, and not to any other ligand.

In summary, insulin, IGF-I and IGF-II were found to promote the migration of MDA-MB-231 cells. The MDA-MB-231 cells lacking the IGF-1R had enhanced migration with or without the ligand stimulation. This suggests that signalling via the IR-A when present as homodimers (rather than hybrids) promotes migration of MDA-MB-231 cells. At same time, the migration of MCF-7 cells was also measured with the same method. However, no migration was detected in any type of the MCF-7. Because MCF-7 is a well-known non-metastatic cell line, this result was not unexpected.

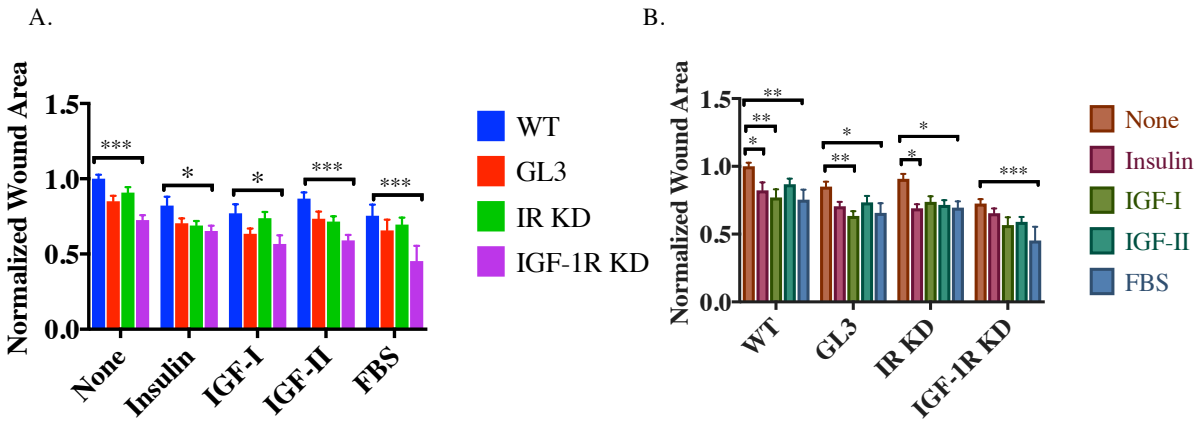

Figure 5.15: Migration of MDA-MB-231 cell lines in response to ligand stimulation (10nM) or FBS (10%). Wound healing assays were conducted to assess the migration rate according to the method described in section 3.3.9. The migration rates are expressed as the ratio of wound area after 24 hours compared to the starting wound area. Photographs were taken and the wound area was measured using CellProfiler software (Jones et al., 2008).

These data were either expressed as a comparison of response to each ligand between cells (A) or as a comparison of the responses to the ligands of each cell line (B). The unstimulated conditions ("None") were serum-free DMEM medium containing 1% BSA. Cells were stimulated with 10 nM of individual ligand diluted in serum-free DMEM medium containing 1% BSA. The bars show the S.E.M. of 3 biological replicates, each with technical triplicates. Statistical significance was determined by two-way ANOVA (ns, $P > 0.05$; *, $P \leq 0.05$; **, $P \leq 0.01$; ***, $P \leq 0.001$.)

5.2.13 The E-cadherin levels in MDA-MB-231 cell lines

An increased migration was seen with IGF-1RKD in MDA-MB-231 even in the absence of stimulating ligand. Since the epithelial mesenchymal transition (EMT) usually precedes migration and a feature of EMT is the decrease in expression of E-cadherin, we assume the expression level of E-cadherin will be lower in IGF-1RKD cells comparing the MDA-MB-231 wild-type. However, Taliaferro-Smith et al., reported that the level of E-cadherin was increased after knock down of the IGF-1R (Taliaferro-Smith et al., 2015). We thus decided to measure the E-cadherin level in all of the MDA-MB-231 cell lines and to see if there was a change in the IGF-1RKD cells that could account for the increased migration (Figure 5.16). Interestingly, contrary to the report by Taliaferro-Smith et al., E-cadherin was not detected in any of the MDA-MB-231 cell lines (wild-type, GL3, IRKD or IGF-1RKD). MCF-7 is a well known non-metastatic cell line and is known to express E-cadherin, so MCF-7 mRNA was used as a positive control in this PCR. High levels of E-cadherin mRNA level were detected in MCF-7 cells.

In summary, IGF-1RKD in MDA-MB-231 improved the migration ability compared to wild type.

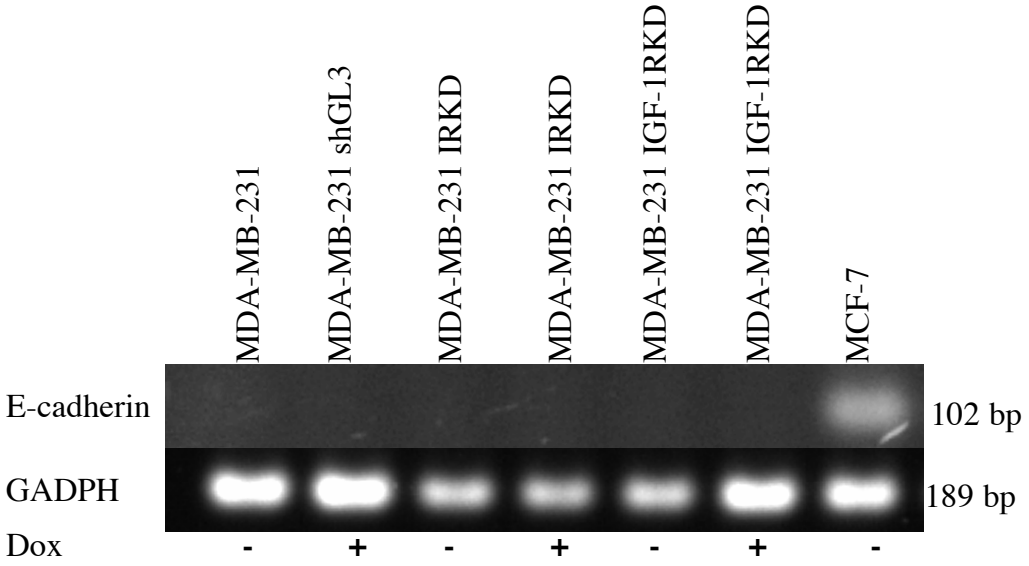

Figure 5.16: E-cadherin mRNA levels in MDA-MB-231 and MCF-7 cell lines. The cells were cultured in DMEM medium with/without Dox for 4 days. The mRNA was extracted and semi-quantitative PCR was conducted according to the method described in section 3.1.17.

5.3 Discussion

We aim to investigate the biological role of IGF-II/IR-A in breast cancer cells in this chapter. Because the IR and IGF-1R are co-expressed in the cells, we constructed a miR30 shRNA knock down system to inducibly knock down the IR or IGF-1R of breast cancer cell lines described in the first part of this chapter. The shRNAs that target the CDS and 3'UTR region were designed for each receptor. We have found that shRNA that targets the CDS region of mRNA always induced better knock down effects than shRNA targeting the 3'UTR region, although both CDS and 3' UTR region were identified as effective targeting region for siRNA and shRNA design (Lai et al., 2013). However, the effectiveness of the shRNA can be caused by other factors, such as the thermostability of the secondary structure of shRNA (Lai et al., 2013; Saito and Saetrom, 2010), which could account for the difference between the designed shRNAs.

The relative receptor levels of IGF-1R and two isoforms of IR (IR-A and IR-B) were measured in MCF-7 (ER^+, PR^+, HER^-) and MDA-MB -231 (ER^-, PR^-, HER^-) cells. MCF-7 was found to express high IGF-1R levels, while MDA-MB-231 expressed low IGF-1R levels. Both MCF-7 and MDA-MB-231 expressed similar IR level. However, MCF-7 expressed similar levels of IR-A and IR-B, while MDA-MB-231 mainly expressed IR-A. Our data is consistent with Zhang et al and Mancini et al ((Mancini et al., 2014; Zhang et al., 2007). However, this data is partially different to that reported by Davison et al, which showed by immunoblotting that the two cell lines express similar high levels of IGF-1R (Davison et al., 2011). The report by Davison et al is in doubt because no loading control was showed in their data.

The phosphorylation of signalling proteins in Akt and MAPK signalling pathways in response to insulin or IGF-II were also measured in MDA-MB-231 cells and MDA-MB-231 cells with IGF-1RKD. The wild-type cells had low insulin sensitivity, which was indicated by the activation of Akt. The IGF-1RKD increased its insulin sensitivity. A similar result was found

in other studies (Zhang et al., 2007). One possible explanation is that the IR/IGF-1R hybrid preferentially transduces the IGF signals, but is barely activated by insulin (Slaaby, 2015; Slaaby et al., 2006; Zhang et al., 2007). We also found that IGF-II was more potent in activating the Akt than insulin, which indicates that insulin and IGF-II might induce different signalling pathways.

These different receptor expression levels of the breast cancer cells could very likely affect their ligand responses. Both IGFs and insulin could promote MCF-7 proliferation, while MDA-MB-231 cells failed to proliferate in response to any ligand. The ligand responses of MCF-7 found in this study are consistent with other reports (Bartucci et al., 2001; Chappell et al., 2001; Lundby et al., 2015; ter Braak et al., 2014). Controversy still exists as to whether MDA-MB-231 cells proliferate in response to IGFs and insulin. Davison et al. reported that IGF-I stimulated MDA-MB-231proliferation (Davison et al., 2011), while many others reported that they did not respond to IGF-I (Bartucci et al., 2001; Belfiore et al., 1996; Costantino et al., 1993; Rose and Vona-Davis, 2012; Sasi et al., 2014). Other triple negative breast cancer cell lines have also been shown to not respond to IGF stimulation (Jackson and Yee, 1999; Sepplorenzino et al., 1994). IGF-1R expression level was originally thought to be the main reason for the lack of response. MDA-MB-157 cells that express approximately 5 times more IGF-1R than MDA-MB-231 were reported to have higher growth rate in response to IGFs and insulin stimulation than MDA-MB-231 (Sciacca et al., 1999). However, IGF-1R overexpression in MDA-MB-231 cells still failed to restore a response to insulin or IGFs (Bartucci et al., 2001).

With the successively selected breast cancer cell lines with IRKD or IGF-1RKD, the biological activities were assessed in order to investigate the roles of IR/IGF-1R in breast cancer cells. IR knock down inhibited the proliferation in a minor way, while IGF-1R knock down drastically inhibited the growth in MCF-7, whereby similar observations have been previously reported by others (Bartucci et al., 2001; Chappell et al., 2001). The down

regulation of IGF-1R expression on MCF-7 cells was also found to lead to a decrease in the ERα and GPER level, thus inducing multiple effects on the cells (De Marco et al., 2013; Mendoza et al., 2011). The IRKD in MDA-MB-231 cells increased cell proliferation, while the IGF-1RKD drastically inhibited the cell growth. Brierley et al. also reported that knock down of IR increased the viability of colon cancer cells (Brierley et al., 2010). The increased viability with IRKD cells could account for the increased cell proliferation. The reason for the increased proliferation rate of MDA-MB-231 with IRKD is most likely due to the disruption of IR/IGF-1R hybrid formation. The depletion of IR increased the IGF-1R homodimers. Here indicated the potency of IR/IGF-1R hybrid is lower than the IGF-1R homodimers.

Even though IGFs and insulin did not stimulate proliferation of MDA-MB-231 cells, they did promote their migration. The IGF-1RKD in MDA-MB-231 increased their migration rate. This is in contrast to the report of Chen et al. who found that the depletion of IGF-1R in MDA-MB-231 cells inhibited migration in a transwell migration assay (Chen et al., 2012). The different assay methods could account for these differences. Because the would healing assay is to examine the ability of cell monolayer to close the wound, while the transwell migration assay is to examine the ability of single cell to migrate towards specific stimulant. The wound healing assay is also affected by the epithelial-mesenchymal transition (EMT) process. Clinical studies supporting the idea that IGF-IR level negatively correlates with metastasis potential in tumours, which explains the enhanced metastasis potential of IGF-1RKD cells (Pezzino et al., 1996; Schnarr et al., 2000; Surmacz, 2000). However, there are also experiments indicating that the IGF-1R is positively correlated with the metastasis potential (Chen et al., 2012; Taliaferro-Smith et al., 2015). Further understanding is needed to elucidate the discrepancy in clinical study and lab experiment.

The mRNA level of E-cadherin was also measured because it is a marker of the EMT process. The mRNA level of E-cadherin was not detected in MDA-MB-231 with and without knock down of IR/IGF-1R. This indicates that the MDA-MB-231 still had high metastasis potential

with/without IRKD and IGF-1RKD. This was contradictory to the study by Taliaferro-Smith et al., which demonstrated that the level of E-cadherin was increased after knock down of the IGF-1R (Taliaferro-Smith et al., 2015). Other study supported our results, which found the IGF-1RKD induced more aggressive phenotypes in MMTV-Wnt1 tumor cells (Rota et al., 2014).

In R$^-$IR-A cells, both insulin and IGF-II were found to promote the proliferation (Frasca et al., 1999; Sacco et al., 2009), which was also observed in MCF-7 cells with IGF-1RKD. In addition, the migration rate of R$^-$IR-A was also increased with insulin and IGF-II stimulation (Denley et al., 2006; Denley et al., 2007). Furthermore, insulin and IGF-II had been verified to activate different signalling pathways and gene expression patterns in R$^-$IR-A (Frasca et al., 1999; Morcavallo et al., 2011; Pandini et al., 2003; Rajapaksha and Forbes, 2015; Sacco et al., 2009). In this study, even though we discovered that insulin and IGF-II activated the Akt at a different potency in MDA-MB-231 cells with IGF-1RKD, the further phosphoproteomics study would provide more detailed downstream signalling.

In conclusion, we investigated the role of IR/IGF-1R in different types of breast cancer cell lines. IGF-1R was more important for mediating proliferation signals in both MCF-7 and MDA-MB-231 cells. In fact, the disruption of IR increased the proliferation rate in MDA-MB-231 cells. However, the depletion of IGF-1R will increase the migration rate of MDA-MB-231 cells and didn't promote the mesenchymal to epithelial transition (MET), which was indicated by an increase of E-cadherin mRNA expression. The IGF-1RKD in MDA-MB-231 was found to increase the insulin sensitivity. However, insulin and IGF-II still had different potencies to activate the Akt signalling. Further studies would help to elucidate the differences between insulin and IGF-II signalling in cancer cells.

Chapter 6 Quantitative Phosphoproteomics comparison of Insulin/IR-A and IGF-II/IR-A signalling pathway

6.1 Introduction

The insulin receptor isoform A (IR-A) has attracted interest because of its ability to bind to insulin and IGF-II with high affinity (Frasca et al., 1999; Morcavallo et al., 2014a; Sciacca et al., 2002). The IR-A plays important roles in embryonic and foetal development (Belfiore et al., 2009). In adult life, IR-A is mainly expressed in tissues that are not related to glucose regulation by insulin, such as the brain and spleen (Frasca et al., 1999). In cancers of the breast, lung or colon, the insulin receptor isoform B (IR-B) mRNA expression decreases, thereby increasing the IR-A/IR-B ratio (Frasca et al., 1999; Huang et al., 2011). Total knockdown of the IR (both isoforms) inhibits prostate cancer proliferation, while IR-B specific knockdown has no effect (Heidegger et al., 2014; Heidegger et al., 2012) suggesting that IR-A signalling plays a role in cancer cell proliferation. In addition, deregulation of IGF-II is found in many types of cancer (including breast, colon and prostate), and the IGF-II/IR-A autocrine loop is found to promote mitogenic signaling in these cancers (Morcavallo et al., 2014a; Rota et al., 2014; Sciacca et al., 2002). Furthermore, the IGF-II/IR-A autocrine loop provides an alternative pathway that promotes cancer growth for cancer cells that are resistant to anti-IGF-1R drugs (Avnet et al., 2009; Rota et al., 2014; Sciacca et al., 2002).

Several studies have used R^-IR-A cells (IR-A overexpressing mouse fibroblast cells from IGF-1R knock out mice) as a model to investigate IR biological activities of the IR (Denley et al., 2006; Denley et al., 2007; Frasca et al., 1999; Morcavallo et al., 2012; Pandini et al., 2003). R^- IR-A cells proliferate in response to insulin and IGF-II (Frasca et al., 1999; Morcavallo et al., 2014b; Morcavallo et al., 2012; Morrione et al., 1997). Insulin and IGF-II were also able to promote survival and migration of R^-IR-A cells (Denley et al., 2006; Denley et al., 2007). Higher IGF-II and IR-A expression also enhanced the β-catenin stability, and thus promoting more aggressive phenotypes (Rota et al., 2014).

Binding of different ligands to the IR-A can lead to different biological outcomes. Insulin stimulation via the IR-A leads primarily to metabolic effects (measured by glucose uptake), while IGF-II leads primarily to mitogenic effects (measured by [^{3}H]thymidine DNA synthesis assays) (Frasca et al., 1999; Morrione et al., 1997). Notably, insulin can also promote mitogenic effects, an undesirable property for patients who rely on long-term insulin treatments. Thus, many studies have been dedicated to optimise insulin analogues in order to minimise the mitogenic effects (Zaykov et al., 2016). For example, S597, an optimised peptidomimetic, has a similar binding affinity to the IR and a similar potency to lower blood glucose *in vivo* compared to insulin, but barely stimulates proliferation (Jensen et al., 2007; Rajapaksha and Forbes, 2015).

These different biological activities were associated with selective changes in gene expression, differential recruitment and activation of intracellular substrates, receptor internalization and activation time (Jensen et al., 2008; Morcavallo et al., 2011; Morrione et al., 1997; Pandini et al., 2004; Pandini et al., 2003; Sciacca et al., 2002). Pandini et al (Pandini et al., 2003) found that insulin and IGF-II induced different gene expression patterns via IR-A. Among a total of 6,000 functionally characterized murine genes and 6,000 expressed sequence tags (ESTs) measured in this experiment, a majority of the regulated genes (214 out of 259) were similarly regulated by insulin and IGF-II. This demonstrated that there is a high similarity between insulin and IGF-II signaling. A total of 45 transcripts (27 genes and 18 ESTs) were differentially regulated: 12 transcripts (7 genes and 5 ESTs) were regulated only by insulin: 6 transcripts (3 genes and 3 ESTs) were regulated only by IGF-II and 27 transcripts (17 genes and 10 ESTs) were regulated by both ligands but IGF-II was more potent than insulin. This study provided one way of understanding the biological function of IR-A (Pandini et al., 2003). Similarly, S597 and insulin also promoted different gene expression patterns via IR-A. Almost half of the differentially expressed genes are involved in growth and proliferation (Jensen et al., 2008). The gene expression data verifies that different ligands (insulin, IGF-II

or S597) induce different outcomes through the activation of IR-A. However, this approach does not reveal which signalling pathways are involved in promoting these different gene expression profiles.

These different gene expression patterns most likely arise due to quantitative and temporal differences of docking protein activation (Denley et al., 2006; Denley et al., 2007). Here in the Forbes laboratory, we have shown that Akt (Protein kinase B) and mTOR (mechanistic target of rapamycin) activation kinetics are different in R^-IR-A cells in response to insulin, IGF-II or S597 stimulation (Figure 6.1). IGF-II also induces a higher p70S6K/Akt ratio than insulin (Sacco et al., 2009). This quantitative tyrosine phosphoproteomics approach revealed more details of insulin and IGF-II induced signaling pathways (Morcavallo et al., 2011) albeit the information is still limited. As such, a global phosphoproteomics approach would enable us to obtain a better understanding of the pathways involved.

In addition, comparison of IGF-II/IR-A signalling between R^- cells (mouse fibroblast cells from IGF-1R knock out mice) cells and cancer cells showed differences in signalling (Morcavallo et al., 2011). For example, Eph4B activation by insulin or IGF-II was not consistent between R^- and MCF-7 cells (Morcavallo et al., 2011). Differences in expression of adaptor or downstream protein groups in each cell type could explain this effect. This observation highlights the fact that it would be preferable to use a cancer cell line when seeking to understand IR-A signalling mechanisms in cancer.

Therefore, we hypothesised that insulin/IR-A and IGF-II/IR-A signalling pathways are different in cancer cells. To test this hypothesis, we choose the triple negative MDA-MB-231 breast cancer cell line as the study model. I aim to compare the insulin/IR-A and IGF-II/IR-A signalling pathways in the MDA-MB-231 breast cancer line (with IGF-1R depleted by shRNA) using a global quantitative phosphoproteomics approach.

Quantitative phosphoproteomics

Protein phosphorylation is an important process for signal transduction and regulation. However, the phosphorylation step can be transient and reversible. Thus, a fundamental understanding of the signalling processes requires the capture of low abundance phosphorylated peptides. Mass spectrometry provides a powerful tool to conduct a global analysis of the proteome. Recently, many methods were developed to enrich phosphopeptides for mass spectrometry detection. These methods include antibody-based pull down of phosphopeptides, metal ion-based affinity capture and ion exchange chromatography (von Stechow et al., 2015). Of these methods the titanium dioxide (TiO_2) method has been well developed and has robustly enabled detection of high numbers of phosphopeptides (Baker et al., 2011; Humphrey et al., 2015; Larsen et al., 2005; Thingholm et al., 2006).

Quantitative proteomics allows us to identify protein expression changes between two states eg. Disease and healthy. Stable isotope labelling of amino acids in cell culture (SILAC) is a metabolic labelling strategy that can incorporate stable isotope-labelled amino acids via a growth medium into the cellular proteome. It provides an easy and robust method for quantitative analysis (Geiger et al., 2011; Ong and Mann, 2006). Combining SILAC, phosphopeptide enrichment and mass spectrometry we can compare the phosphorylation network in different conditions quantitatively.

Methodology

Previously in our lab, Rajapaksha conducted a time course experiment to investigate Akt and MAPK phosphorylation using R$^-$IR-A cells in response to insulin and IGF-II stimulation (Rajapaksha and Forbes, 2015). Here, it was found that at approximately 10 min, both Akt and MAPK were phosphorylated at near maximal levels (Figure 6.1). At this time point, tyrosine phosphorylation of the initial mediators of the pathway (such as IRS-1, IRS-2 and Shc) lead to increased serine phosphorylation of later mediators, such as Akt or mTOR substrates (Monetti et al., 2011). Based on that study we chose to use the following conditions

for this phosphoproteomics study: cells were serum starved in DMEM medium (supplemented with 1% BSA) overnight and stimulated with 10 nM insulin or 100 nM IGF-II for 10 minutes according to the protocol described in section 3.3.8.

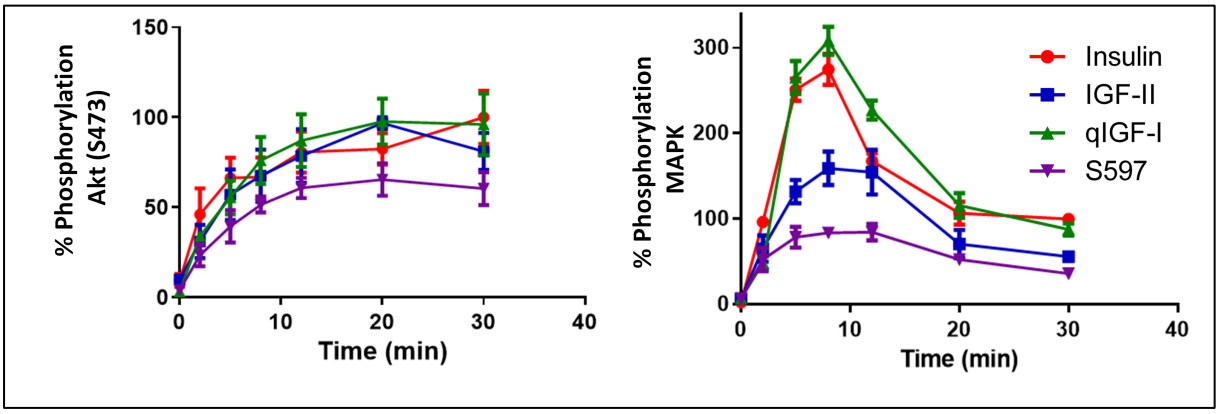

Figure 6.1: Phosphorylation of Akt (pS473) (left) and MAPK (right) time course. Serum-starved R$^-$IR-A cells were treated with 10 or 100 nM insulin, IGF-II, qIGF-I, or S597 for 10 min. Whole-cell lysates were immunoblotted for phosphorylated pAkt (pS473) (A) and pMAPK (B). Edited from Rajapaksha (Rajapaksha and Forbes, 2015).

The initial quantitative phosphoprotomics workflow used in this study is shown in Figure 6.2. First, the cells were labelled with different isotope labelled amino acids. SILAC labelling was achieved by culturing cells for at least 3 passages in light, medium, or heavy isotope labelled amino acid containing media according to the protocol described in section 3.4.1. The incorporation efficiency was determined according to the protocol described in section 3.4.2 and above 95% efficiency was achieved.

Cells were lysed and mixed with 1:1:1 ratio. The mixture was then Trypsin and Lys-C digested. The combination of Trypsin and Lys-C increased the digestion efficiency because the Lys-C complements the low efficiency of trypsin toward Lysine residues (Giansanti et al., 2016; Glatter et al., 2012). Phosphopeptides were enriched with TiO_2 and analysed by LC–MS/MS. Peptide identification and relative changes in the extent of phosphorylation were

determined using MaxQuant (Version 1.5.8.3). Statistical analysis to determine significant changes in phosphosites was performed using Perseus or Excel. Network analysis was performed with InnateDB database or NetworkAnalyst (Breuer et al., 2013; Xia et al., 2014; Xia et al., 2015).

The phosphopeptide enrichment steps were optimised in this study prior to the whole process.

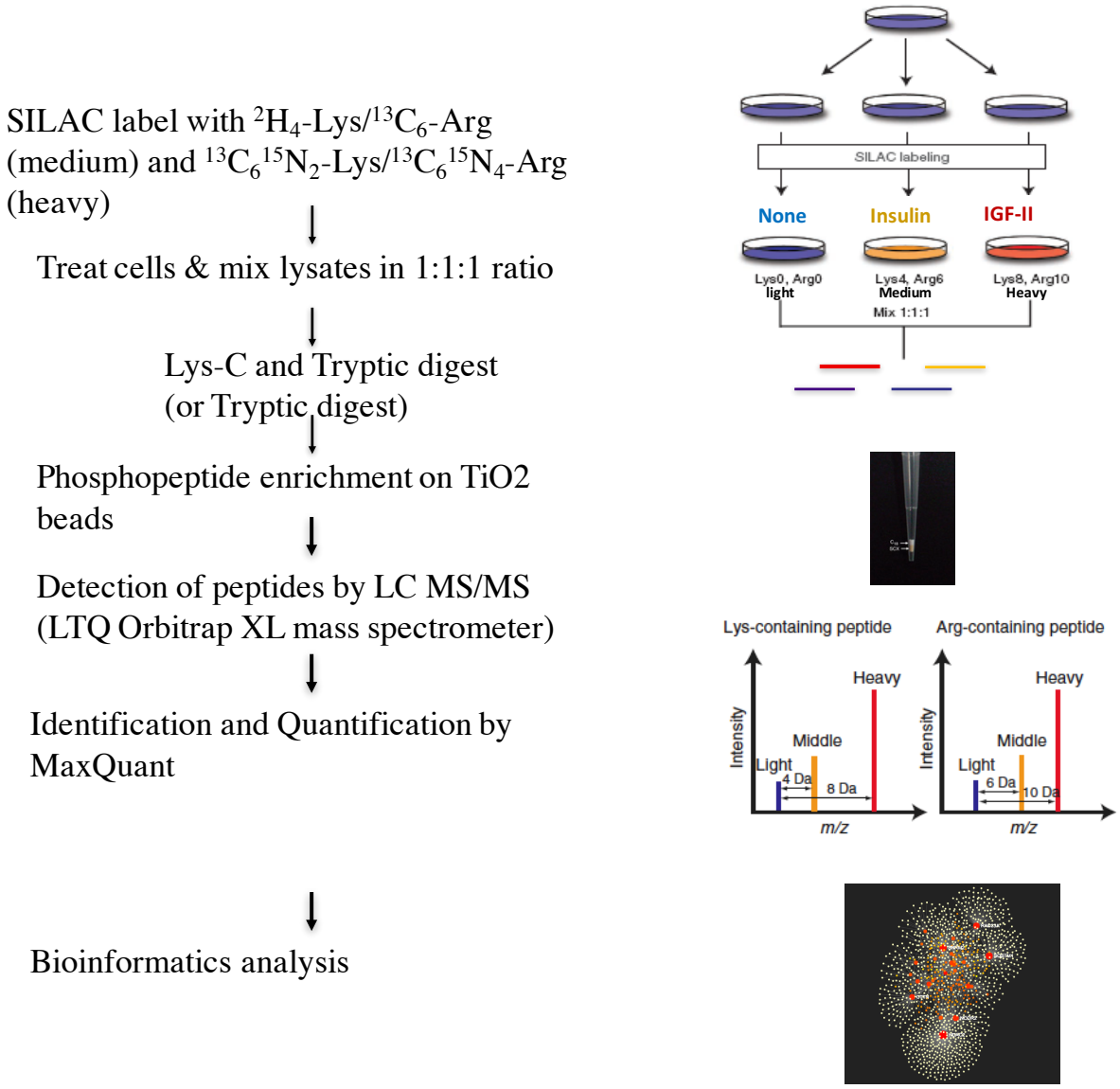

Figure 6.2: Workflow of quantitative phosphoproteomics. SILAC labeled cells were achieved by culturing cells for at least five doubling times in light, medium, or heavy isotope labeled amino acid containing media, serum starved in DMEM medium (supplemented with 1% BSA) overnight and stimulated with 10 nM insulin or 100 nM IGF-II for 10 minutes. Starved, insulin and IGF-II treated cells were lysed and mixed by ratio of 1:1:1. The mixture was then Trypsin and Lys-C digested. Phosphopeptides were enriched with TiO_2 and analysed by LC–MS/MS. Peptide identification and relative changes in the extent of phosphorylation were determined using MaxQuant (Version 1.5.8.3). Statistical analysis to determine significant changes in phosphosites was performed using Perseus or Excel. Network analysis was performed with InnateDB database or NetworkAnalyst.

6.2.1 Phosphopeptide enrichment optimisation

The first step in optimising the quantitative phosphoprotomics workflow was to optimise the phosphopeptide enrichment method. The steps of protein sample treatment for Trypsin and Lys-C digestion, TiO_2 phosphopeptide binding and elution, as well as phosphopeptide desalting were optimised using analysis on a MALDI-TOF mass spectrometer (Figure 6.3). At the same time, different matrices for phosphopeptide detection with MALDI-TOF mass spectrometry were also compared. Initial protocols were developed using β-casein, because β-casein is a phosphorylated protein with known sequence (thus predictable phosphopeptides with known m/z values) (Appendix 5). Once optimised, these conditions were applied to insulin or IGF-II stimulated MDA-MB-231 cell lysates spiked with β-casein with enrichment. These samples were then analysed using HPLC-MS/MS (nanoLC 3000 RSLC, LTQ Orbitrap XL ETD).

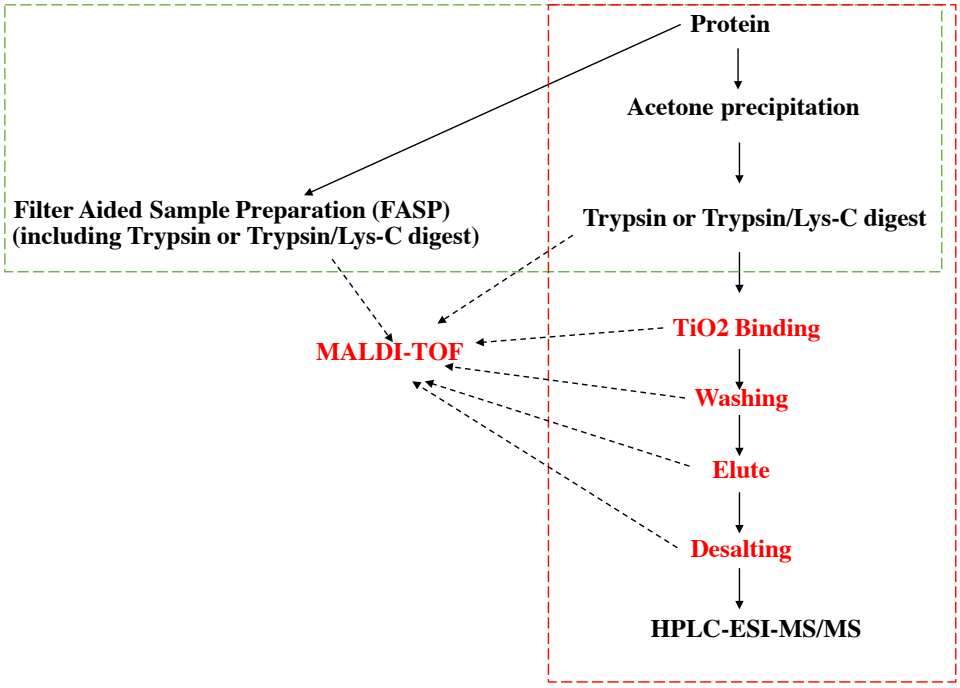

Figure 6.3: Phosphopeptide enrichment flow chart. Prior to the phosphopeptide enrichment optimisation, enzyme digests from Filter Aided Sample preparation and acetone precipitated protein were compared (Green box). The phosphopeptide enrichment involved TiO_2 binding, washing, elution and desalting (Red box) were also optimised. The steps optimised are marked in red. All the samples from each step were analysed by MALDI-TOF mass spectrometry. In the last step, HPLC-ESI-MS/MS was used for peptide quantification and identification.

6.2.1.1 Comparison of methods for concentration of protein and tryptic and Lys-C digestion: Acetone precipitation versus Filter-aided sample preparation (FASP)

Filter-aided sample preparation (FASP) provides a platform for combined sample trypsin or trypsin/Lys-C digestion and buffer exchange using a spin column with a 30KDa molecular weight cut off. This method has been used previously for in-depth analysis of phosphopeptides (Manza et al., 2005; Wisniewski et al., 2009). However, it gives approximately 50% yield of the applied protein sample because of the loss of proteins smaller than the cut-off size (normally 30K). Acetone precipitation is another common way to clean up protein samples before trypsin digestion for mass spectrometry (Crowell et al., 2013). It allows for large-scale protein clean up. However it has the problem of water-soluble protein loss (Crowell et al., 2013). Theoretically, protein samples will form different spectral patterns of peptides between these two cleaning methods. Here, MALDI-TOF spectra of peptides between the FASP treated and acetone precipitation treated MDA-MB-231 lysates were compared. Proteins in lysis buffer and after precipitation in TFE were initially analysed with SDS-PAGE gel in order to compare the overall proteins. Here, very similar patterns were found between the two samples (Figure 6.4-A). This meant that the sample complexity loss was at a very low percentage. The trypsin and Lys-C digested peptides after acetone precipitation were also run on an SDS-PAGE gel (Figure 6.4-A). No protein with a size greater than 37KD was found on the gel, which indicates that the digestion was successful. Next the sample cleaned by FASP (Figure 6.4-B) and the acetone precipitated samples (Figure 6.4-C) were trypsin and Lys-C digested and the peptide patterns were compared with MALDI-TOF MS. Equal amounts of samples (8ng calculated from the initial protein estimation of 20 µg total) were analysed with the MALDI-TOF MS and no obvious differences of peptide patterns (peaks above 700-800Da) were found between the acetone precipitated and in solution digested and FASP digested samples . As there is no

limit to the protein amount that can be acetone precipitated and the low cost of this method, I chose to use acetone precipitation for subsequent experiments.

A.

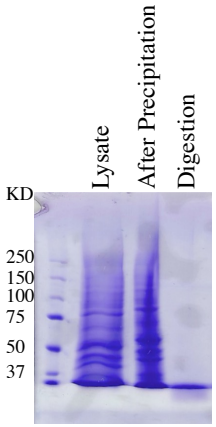
Lysate
After Precipitation
Digestion
KD
250
150
100
75
50
37

B.

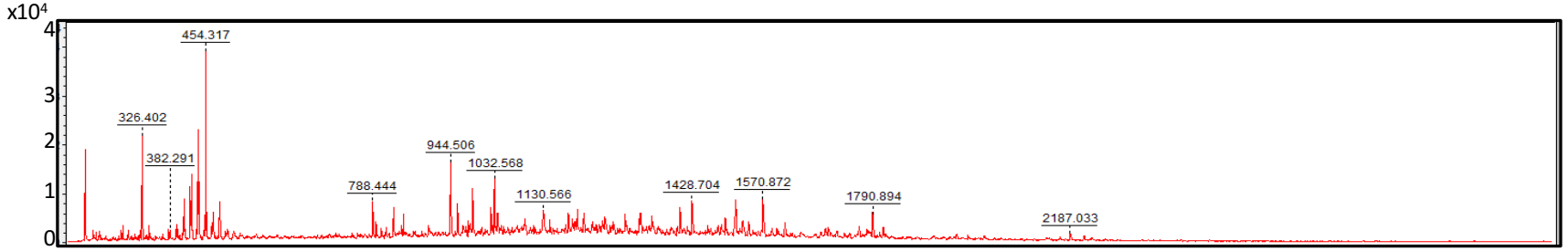
x10^4
4
3
2
1
0
454.317
326.402
382.291
944.506
1032.568
788.444
1130.566
1428.704
1570.872
1790.894
2187.033

C.

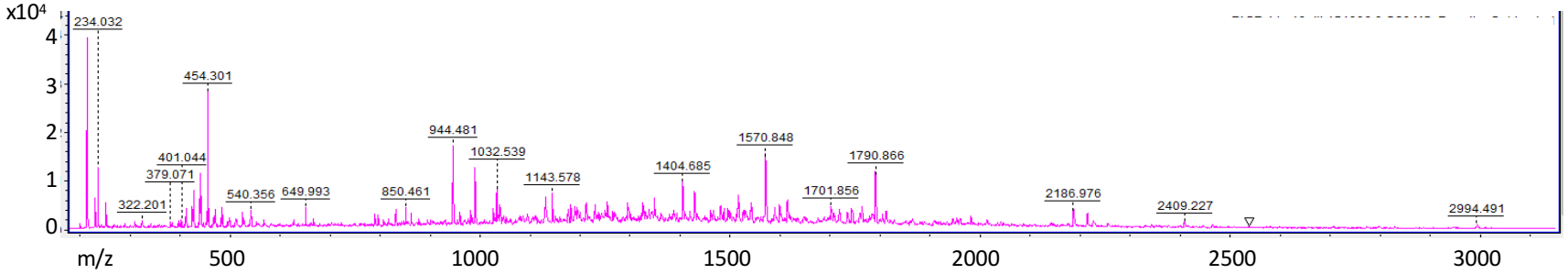
x10^4
4
3
2
1
0
234.032
454.301
944.481
1032.539
1570.848
401.044
379.071
1790.866
1404.685
1143.578
540.356
649.993
850.461
1701.856
322.201
2186.976
2409.227
2994.491
m/z
500
1000
1500
2000
2500
3000

Figure 6.4: Analysis of enzymatic digestion of MDA-MB-231 lysate by SDS-PAGE and mass spectrometry. A: 20 μg of each sample was subjected to SDS-PAGE. “Lysate” refers to the MDA-MB-231 lysate in GdmCl lysis buffer. “After precipitation” refers to the MDA-MB-231 lysate in TFE buffer after acetone precipitation. “Digestion” is acetone-precipitated sample that has been trypsin digested. B and C show the MALDI-TOF mass spectrometry analysis of MDA-MB-231 lysates *trypsin/Lys-C* digested by different methods. B: 8ng of MDA-MB-231 lysate digested with FASP method. C: 8ng of acetone precipitated MDA-MB-231 lysate after in-solution digestion.

6.2.1.2 Optimization of matrix used for MALDI-TOF spectrometry detection of phosphopeptides: HCCA versus DHB

A MALDI-TOF mass spectrometer is a convenient, accurate instrument to detect phosphopeptides. The running cost is much lower than the Q-TOF and Orbitrap mass spectrometers. It was used for analysis of the phosphopeptide enrichment optimisation protocols described in this chapter.

Matrix selection is one of the most important parameters influencing the detection of phosphopeptides with MALDI-TOF MS. Here, I tested the ability to detect trypsin digested β-casein peptides mixed with HCCA (alpha-Cyano-4-hydroxycinnamic Acid) and DHB (2,5-Dihydroxybenzoic acid) matrices (Condina et al., 2010). The expected m/z values from Trypsin and Lys-C digestion of β-casein are shown in Appendix 5. The complete digestion of β-casein by Trypsin and Lys-C yields two phosphopeptides: peptides with singly phosphorylated amino acid (m/z at 2061) and peptides with four phosphorylated amino acids (m/z at 3121.2). The peptides with four phosphorylated serines of β-casein (m/z at 3121.2) was identified with DHB matrix (Figure 6.5-B), but not with HCCA matrix (Figure 6.5-A). However, the singly phosphorylated phosphopeptide (m/z at 2061) was not seen with either of the matrices. It was concluded that DHB was a better matrix for phosphopeptide identification with MALDI-TOF.

A.

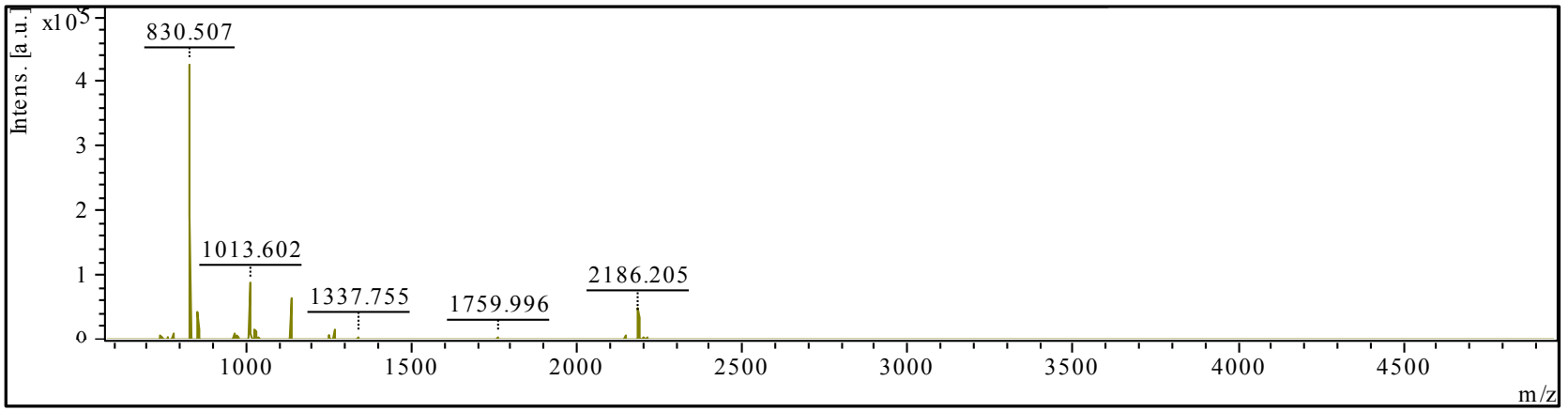

B.

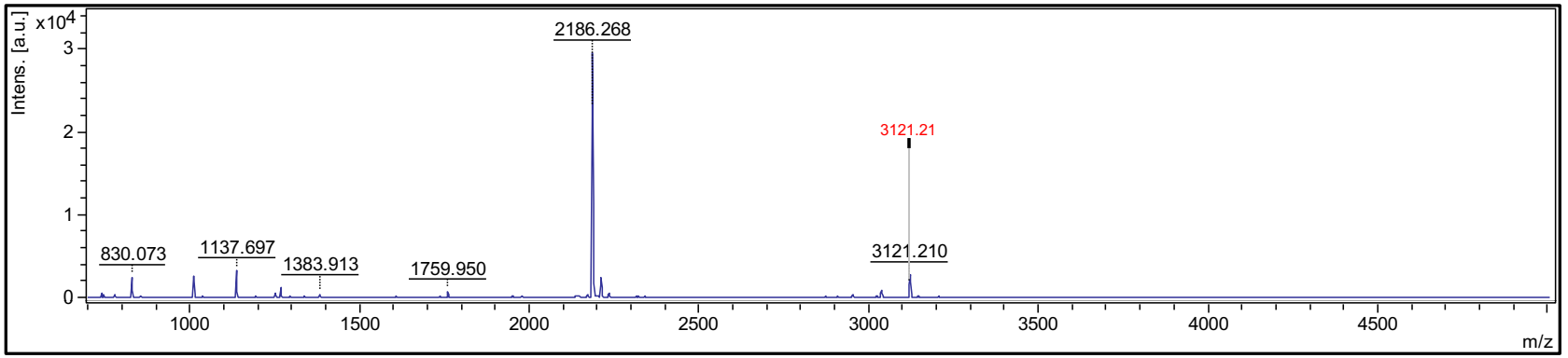

Figure 6.5: The peptide detection of trypsin digested β-casein with MALDI-TOF mass spectrometry with different matrix: HCCA matrix (A), DHB matrix (B).

6.2.1.3 Phosphopeptide enrichment

Phosphopeptide enrichment was conducted according to the method described in section 3.4.7 (but using the un-optimised binding buffer: 30mg/ml DHB in 2% TFA). The methodology is shown in Figure 6.3. Before enrichment, only one phosphopeptide (m/z=3122) was detected and had low abundance (Figure 6.6-A). After the enrichment, TiO_2 bead elutes were directly detected with MALDI-TOF mass spectrometry (Figure 6.6-D). The other phosphopeptide (m/z=2062) was also enriched in binding buffer (30mg/ml DHB in 2% TFA, Figure 6.6-D), even though there were still phosphopeptides found in the flow through with this binding condition (Figure 6.6-B). No phosphopeptides were washed off from the TiO_2 beads during washing step (Figure 6.6-C). This was good a start for the phosphopeptide enrichment step.

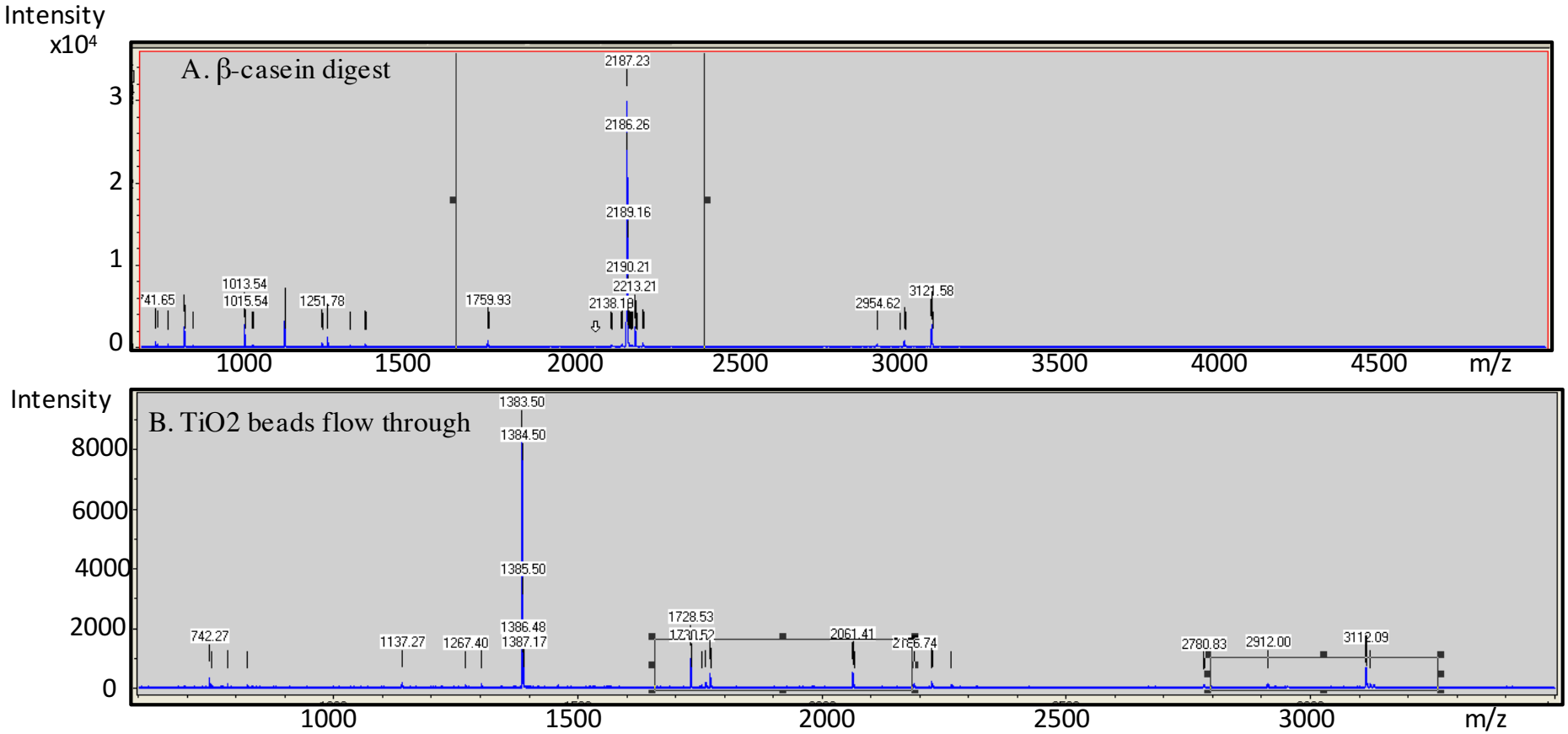
Intensity
x10⁴
A. β-casein digest
2187.23
2186.26
2189.16
2190.21
2213.21
1013.54
1015.54
1251.78
741.65
1759.93
2138.18
2954.62
3121.58
m/z
Intensity
B. TiO2 beads flow through
1383.50
1384.50
1385.50
1386.48
1387.17
742.27
1137.27
1267.40
1728.53
2061.41
2780.83
2912.00
3112.09
m/z

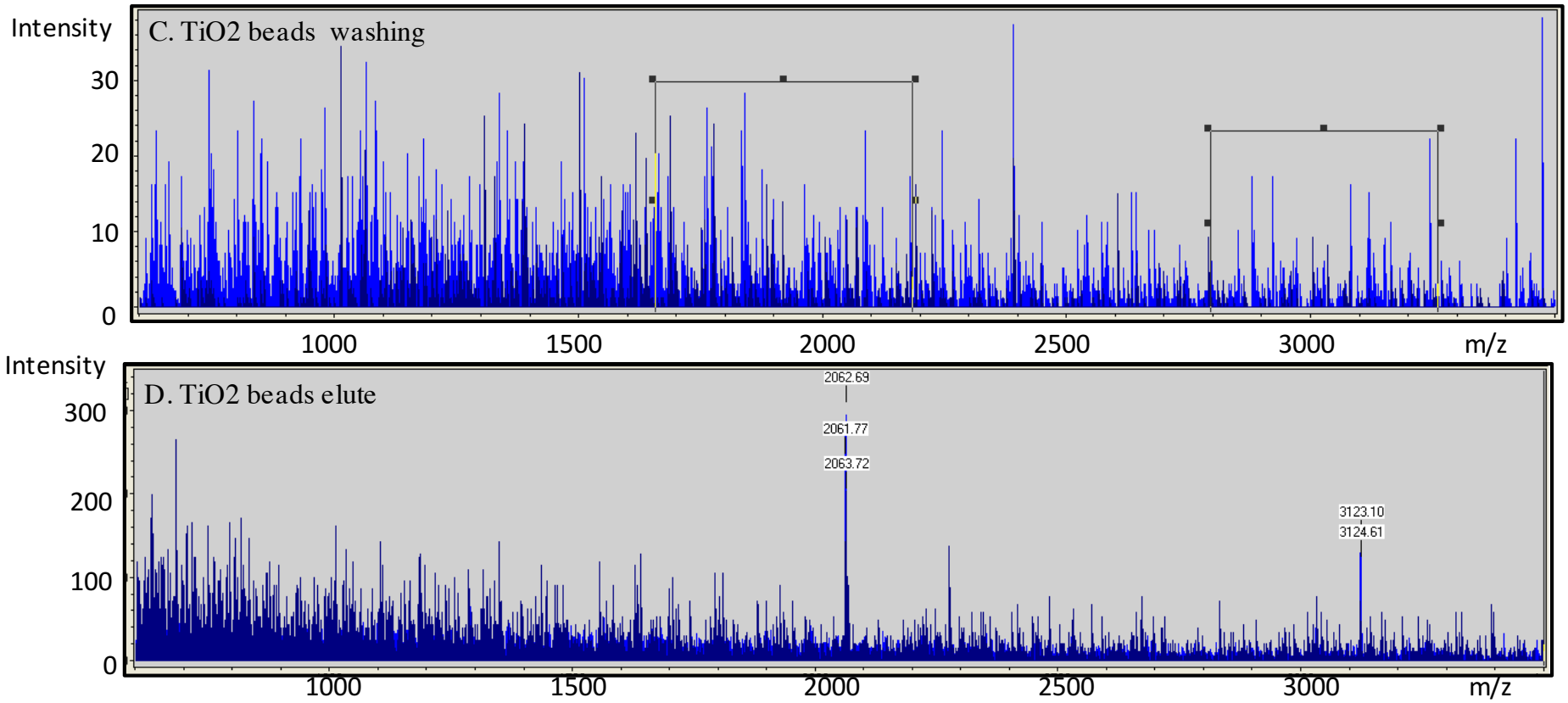

Figure 6.6: MALDI-TOF mass spectrometry of β-casein digestion (A), TiO_2 beads flow through (B) and wash buffer (C) and phosphopeptide eluate (D). The two expected phosphopeptides are m/z=2061 and m/z=3122.

6.2.1.4 Optimisation of phosphopeptide elution from TiO_2 beads: MALDI-TOF mass spectrometry of β-casein and HPLC-MS/MS of MDA-MB-231 eluted with 0.83% and 2.5 % NH_4OH

The binding of the phosphopeptides to the TiO_2 beads relies on their negative charge. The elution was conducted by increasing the pH of the elution solution. Here, NH_4OH diluted in water was used as the elution buffer. NH_4OH (0.83%) was used as the first elution step and then 2.5% NH_4OH was used as a second elution step, based on the hypothesis that peptides with increasing numbers of phosphorylated sites will be more negatively charged and therefore require higher pH to be effectively eluted from TiO_2 beads. We expected that sequential elution with increasing pH could be necessary if sample complexity was very high.

Phosphopeptide enrichment from 200µg of MDA-MB-231 lysate (complex sample including peptides with singly phosphorylated peptides and multiply phosphorylated peptides) was enriched according to section 3.4.7 (but using the un-optimised binding buffer: 30mg/ml DHB in 2% TFA). The sequentially eluted peptides were analysed with HPLC-ESI-MS/MS for peptide identification. In order to assign peptide identities to the spectra the raw data from the HPLC-ESI-MS/MS was analysed with Maxquant software against the human SwissProt database (downloaded on September 2015), with a false-discovery rate (FDR) < 0.01 at the level of proteins, peptides and modifications, according to the method described in section 3.4.11. Peptides phosphorylated at one, two or three sites are named 1p, 2p, 3p respectively. It is important to note that a single peptide might be phosphorylated at one, two or three sites. The proportion of multiply phosphorylated peptides was increased in elute 2 (for example, the proportion of 3p peptides was increased from 1.34% to 11.08%) (2.5% NH_4OH, right part of Figure 6.7-A)

compared to lower concentrations of NH_4OH (left part of Figure 6.7-A). However, fewer phosphopeptides were identified in the second elute as compared to elute 1. These data suggest that the use of sequential elution increased the number of peptides identified (Figure 6.7-B).

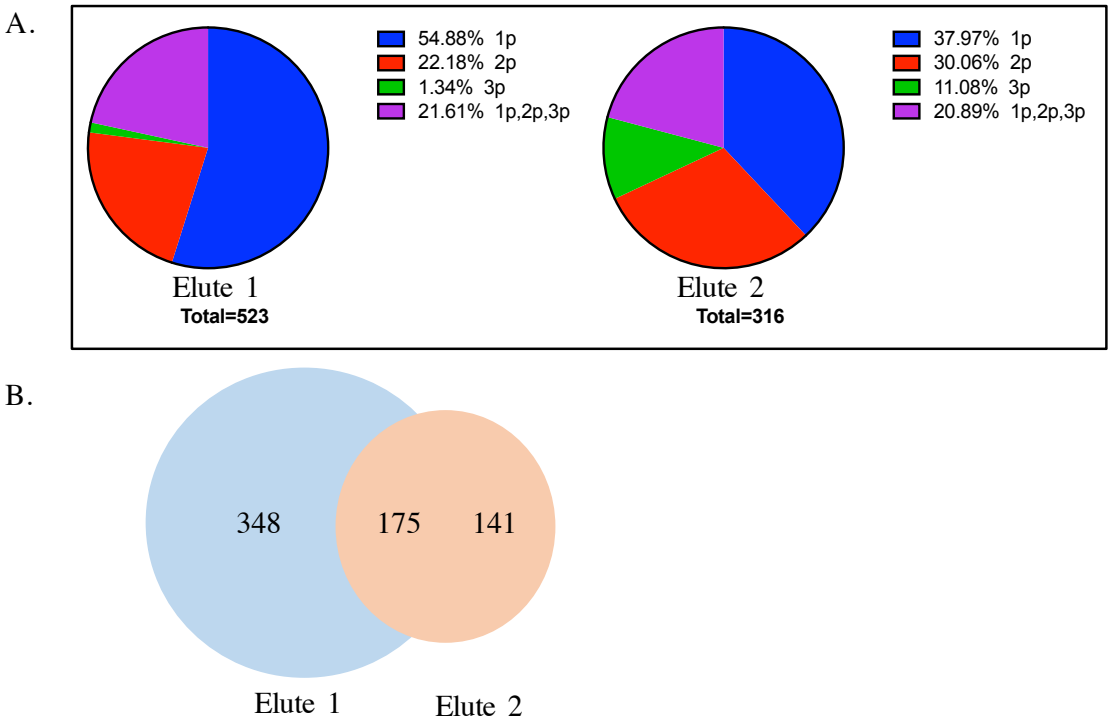

Figure 6.7: HPLC-ESI-MS/MS of MDA-MB-231 eluted with 0.83% (elute1) and 2.5% NH_4OH (elute2). A total of 200 µg of MDA-MB-231 lysate were used for enrichment, and phosphopeptides were eluted with 0.83% (elute1) followed by 2.5 % NH_4OH (elute2). One twentieth of each elute was desalted with a Ziptip and subjected to HPLC-ESI-MS/MS analysis. (A) The percentage of phosphopeptides containing different numbers of phosphate groups and a comparison between elute1 and elute 2. (B) The numbers of specific and shared phosphopeptides identified from different elutes. The singly and multiply phosphorylated peptides are named as 1p, 2p, or 3p (some peptides were both singly and multiply phosphorylated and occur in more than one category). One experiment was conducted. Raw spectra are shown in appendix 17.

6.2.1.5 DHB concentration optimization

In the experiment above, the binding buffer condition (30 mg/ml DHB in 2% TFA) had not been optimised. The phosphopeptides only accounted for about 62% of the total peptides identified (Figure 6.8), suggesting that there were non-specific peptides binding to the TiO_2 beads. Even though the phosphopeptide identification number increased dramatically from nearly no identification at all before enrichment, it still needed to be improved. A high percentage (~90%) of phosphopeptides was necessary to increase the number of phosphopeptides identified. In order to minimise the non-specific binding, two strategies were combined. Firstly, the TFA concentration in the binding buffer was increased from 2% to 6% in order to neutralise the negative charge of certain amino acids (i.e. aspartic acid and, glutamic acid). Secondly, the DHB concentration was increased from 30 mg/ml to 200 mg/ml. A higher concentration of DHB is crucial because DHB is very efficient in reducing the binding of non-phosphorylated peptides to TiO_2 while retaining its high binding affinity for phosphorylated peptides (Larsen et al., 2005). By introducing both of these strategies the proportion of phosphopeptides detected increased to 92% (Figure 6.8).

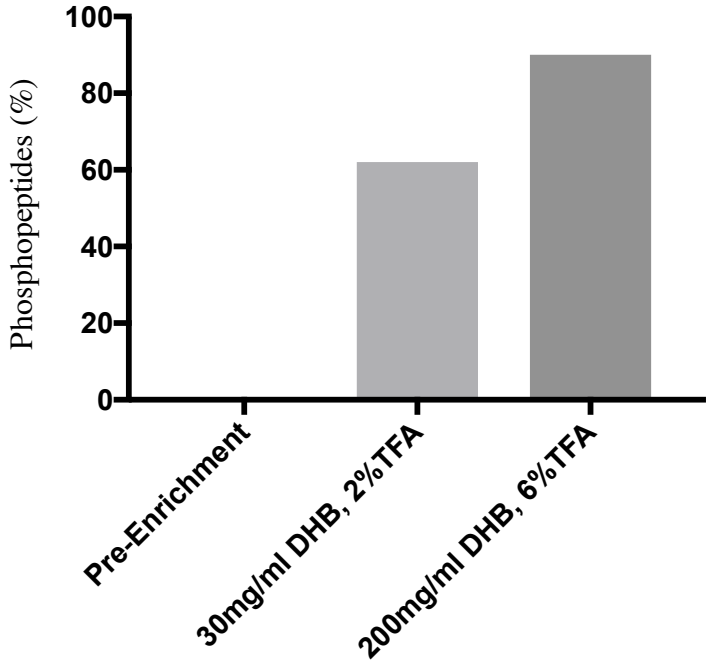

Figure 6.8: Proportion of phosphopeptides detected in Trypsin/Lys-C digested MDA-MB-231 lysates identified with HPLC-MS/MS before and after TiO_2 bead enrichment. Digested peptides were incubated with TiO_2 beads in different buffers: 30 mg/ml DHB in 2% TFA or 200 mg/ml DHB in 6% TFA. Peptides were desalted with a C18 ziptip before HPLC-MS/MS. A total of 729 unique phospeptides was identified after enrichment with the buffer condition of 30 mg/ml DHB in 2% TFA, while A total of 721 unique phospeptides was identified after enrichment with the buffer condition of 200 mg/ml DHB in 6% TFA. Due to the high cost of running HPLC-ESI-MS/MS only one experiment was conducted.

6.2.1.6 Optimization of desalting methods

Samples needed to be desalted before being loaded onto the HPLC for ESI-MS/MS. In addition, residual beads in the elutes have the potential to clog the HPLC column. Therefore, a cleaning procedure is necessary for the samples eluted from the TiO_2 beads.

Here, comparisons of different desalting methods were conducted (Figure 6.9). C18 and SRB-RPS (Styrenedivinylbenzene - Reversed Phase Sulfonate) stagetips were made by

pressing 2 layers of either C18 membrane or SDB-RPS membrane into a 200 µl pipette tip and these were compared to C18 ziptips (purchased from Sigma). SDB-RPS is a styrenedivinylbenzene resin that has been modified with sulfonic acid groups to make it hydrophilic. It can act in both reverse phase and cation exchange manners, and therefore was expected to have superior ability to bind phosphopeptides to either of the C18 tips. Phosphopeptides enriched from 200 µg of trypsin and Lys-c digested MDA-MB-231 lysates were desalted according to the method described in section 3.4.8. The final elute was diluted to 25µl and 10µl of the dilution was analysed using HPLC-MS/MS. The C18 Ziptip resulted in 92% phosphopeptides identification (Figure 6.8 and 6.9). However, the total number of phosphopeptides is low (Figure 6.9). SDB-RPS method had a similar result to the C18 Ziptip method. Phosphopeptides eluted from the C18 stagetip had the highest purity to 95%. C18 stagetip also resulted in the recovery of the highest number of phosphopeptides It was not a surprise that C18 Ziptip resulted in fewer phosphopeptides being recovered because the capacity of the Ziptip is smaller (Typically 5 µg) than the SDB-RPS (4-8 µg) and the C18 stagetip (4-8 µg). However, it was a surprise that SDB-RPS had no advantage of over the C18 ziptip. It can be speculated that larger amounts of phosphopeptides cannot bind to the SDB-RPS due to its higher selectivity than C18. It should be noted that only one experiment was conducted due to the high cost of running HPLC-MS/MS and the technical variability has not been assessed.

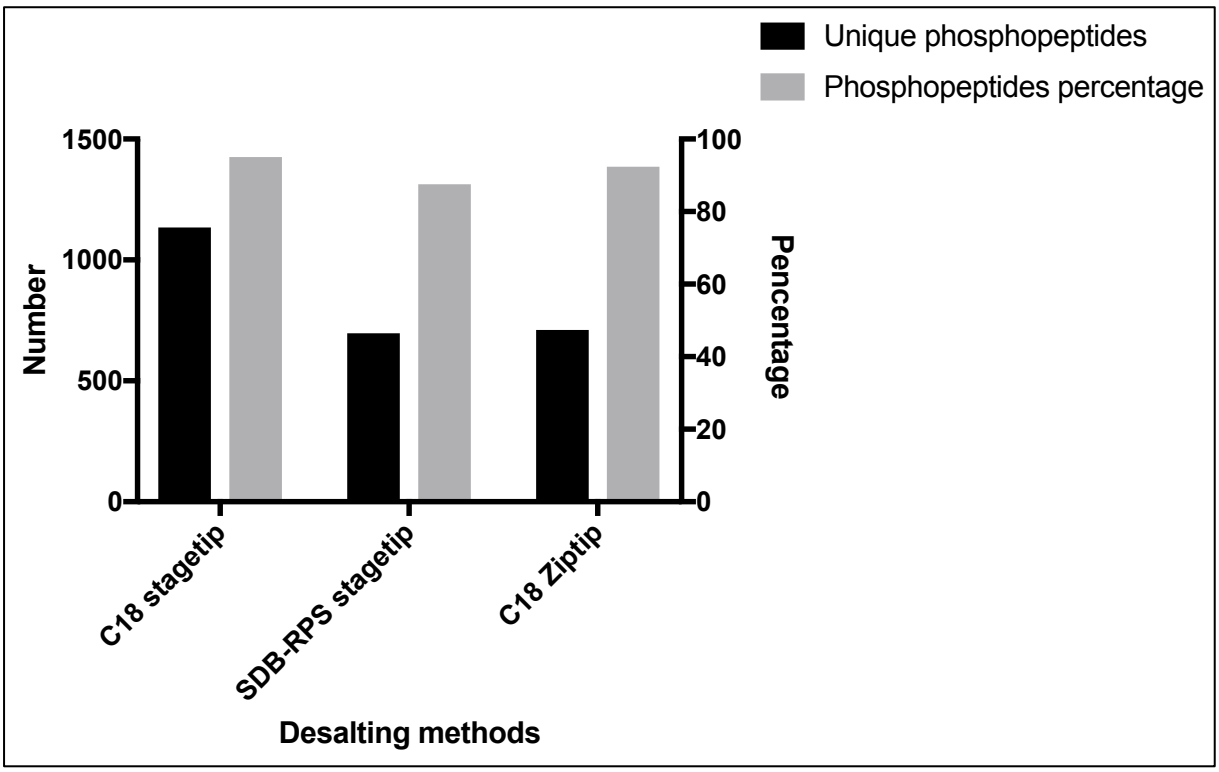

Figure 6.9: Total number of unique phosphopeptides and proportion of unique phosphopeptides identified by HPLC-MS/MS. Phosphopeptides eluted from TiO_2 beads were desalted with a C18 stagetip, SDB-RPS stagetip or C18 Ziptip according to the methods described in section 3.4.8. Only one experiment was conducted.

6.2.2 Quantitative phosphoproteomic analysis of the Insulin/IR-A and IGF-II/IR-A signalling pathways

The detailed phosphorylation of MDA-MB-231 IGF-1RKD cells in response to insulin or IGF-II stimulation was investigated in the last part of this chapter.

Three biological replicates (B1, B2, B3) were conducted to stimulate the MDA-MB-231 IGF-1RKD cells and collected the protein samples. For each biological replicate, the phosphopeptides were enriched on TiO_2 beads and gradually eluted twice with different concentrations of elution buffer (first elution or E1 with 0.85% NH_4OH, and second elution or E2 with 2.5% NH_4OH). In order to minimise the machine errors, each elute was analysed twice by HPLC-MS/MS, thus generates two technical replicates of MS/MS runs (R1, R2). A

total of 12 MS/MS runs were conducted with the above samples. Additionally, the sample of biological 1 was enriched in order to test the experimental conditions. Its first elute was analysed twice by HPLC-MS/MS, thus these two runs were named "B1_E1_R1_Old" and "B1_E1_R2_Old" separately. I also tried to test whether the flow through from the TiO_2 beads still contained phosphopeptides, thus the flow through from the TiO_2 beads of biological replicate 2 (B2) was reapplied to a second lot of fresh beads and eluted once (E1, 0.85% NH_4OH). This sample is named as "B2_2nd binding. Thus, a total of 15 MS/MS runs were conducted (Table 6.1) and all of the raw files were analysed together using Maxquant according to the protocols detailed in section 3.4.11.

File name	Sample name	Explanation
1	B1_E1_R1_Old	Biological 1_Elute1_Replicate 1_Old experiment
2	B1_E1_R2_Old	Biological 1_Elute1_Replicate 2_Old experiment
3	B1_E1_R1	Biological 1_Elute1_Replicate 1
4	B1_E1_R2	Biological 1_Elute1_Replicate 1
5	B1_E2_R1	Biological 1_Elute2_Replicate 1
6	B1_E2_R2	Biological 1_Elute2_Replicate 2
7	B2_2nd binding	Biological 2_Second binding
8	B2_E1_R1	Biological 2_Elute1_Replicate 1
9	B2_E1_R2	Biological 2_Elute1_Replicate 2
10	B2_E2_R1	Biological 2_Elute2_Replicate 1
11	B2_E2_R2	Biological 2_Elute2_Replicate 2
12	B3_E1_R1	Biological 3_Elute1_Replicate 1
13	B3_E1_R2	Biological 3_Elute1_Replicate 2
14	B3_E2_R1	Biological 3_Elute2_Replicate 1
15	B3_E2_R2	Biological 3_Elute2_Replicate 2

Table 6.1: Files in this project used for Maxquant Analysis.

6.2.2.1 Assessment of the Data Quality

6.2.2.1.1 MBR (Match Between Runs)

The use of the match between runs (MBR) alignments during a Maxquant search enables optimal peptide identification and verification from different MS/MS runs. However, an inappropriate time window could cause many false discoveries. To determine whether this was occurring during my Maxquant search, the Maxquant output was evaluated with the program PTXQC (Bielow et al., 2016) according to the protocol described in section 3.4.11.

MBR alignment is the first of two steps (1=align, 2=transfer) of the Match-between-runs. Following the PTXQC analysis, it was evident that the MaxQuant retention time (RT) shift window was small (most of the time less than 4 minutes) and the residual ΔRT (RT of identification in individual file compared to the reference Raw file) was small (most of the dots in the less than 0.7 minutes window) across all biological and technical replicates (Figure 6.10). Overall, this result indicated the MBR-alignment set up in the method described in section 3.4.11 was appropriate.

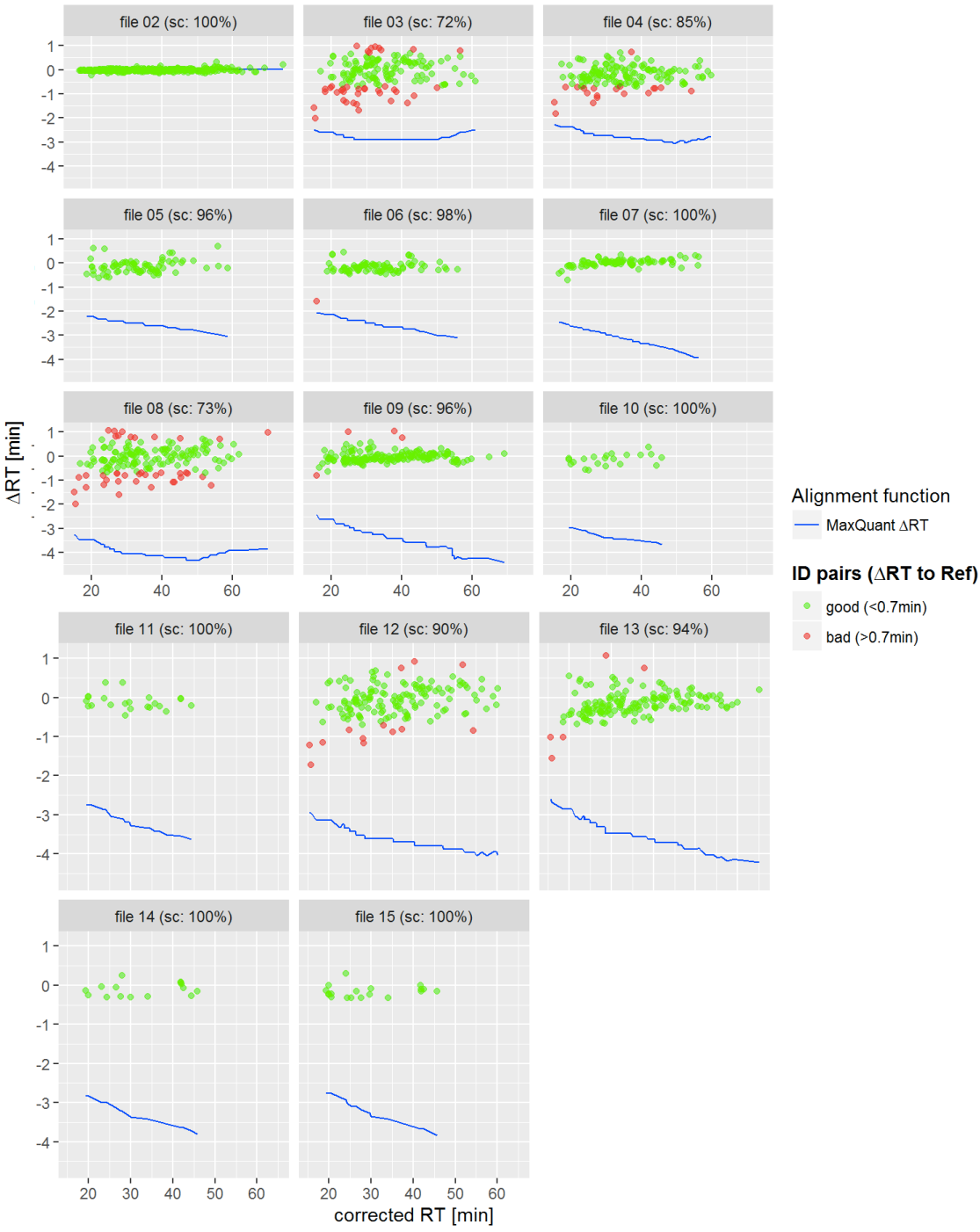

Figure 6.10: Match between run alignments. Here the first enrichment experiment of Biological 1_Elute1_Technical Replicate 1 (B1_E1_R1_Old) was used as a reference to assess the alignment between runs. The plots were based on real MS/MS identifications. Ideally, RTs of identical peptides should be equal (i.e. very small residual ΔRT) across Raw files after alignment. MaxQuant's RT correction was shown in blue – it should be well within the alignment search window (20 min by default) set during MaxQuant configuration. The

resulting residual Δ RT after RT alignment (compared to a reference Raw file) was shown as green/red dots, respectively. One dot represents one peptide identification pair that exists in both the individual file and reference file. Every dot (peptide) outside an allowed residual ΔRT (0.7min by default) was coloured red. All others were coloured green. SC represents the score of RT alignment within a 0.7 minute window (range from 0-100%). File numbers are the same as Table 6.1.

MBR Transfer is the second of the two steps (1=align, 2=transfer) during Match-between-runs. After retention times have been calibrated, MaxQuant transfers peptideIDs from one Raw file to any other Raw file, assigning a peptide ID to unlabelled three-dimensional (3D) peaks (the mass (x-axis) and intensity (y-axis) of the peptide peaks in a mass spectrometry (MS) spectrum are assembled into 3D peaks over the m/z retention time (z-axis) plane) thus increase the number of peptide identifications. However, a bad alignment of 3D peaks from the matched runs usually leads to a low identification value or large false positive identification value. Here, this quality control is to check the transfer of identifications across all the files. In our Maxquant search, almost all of the peptides (close to 100%) were identified once across all biological and technical replicates (Figure 6.11). This means that false positive identifications are highly unlikely.

Figure 6.11: MBR Transfer: Last of two steps (1=align, 2=transfer) during Match-between-runs. The first enrichment experiment of Biological 1_Elute1_Technical Replicate 1 (B1_E1_R1_Old) was used as the reference. The same peptide should not be annotated twice (or more) at vastly different points in RT. This plot shows three columns: - left: the 'genuine' situation (represent no peptide identification was assigned to the unknown peptide spectra); - middle: looking only at transferred IDs (represent peptide identification was assigned to unknown peptide spectra); - right: combined picture (a mixture of left + middle, represent the identified peptide and the assigned peptide identification). If the peptide peak was identified

only once-either genuine OR a transferred ID, it is true identification (good, green). If the peptide peak was identified more than once, but their retention times are very close. We assume these identifications are also trustful (in group, also good). However, if the retention times of the identified peptide peak have huge differences, we assume this is false identification (out-group, red). File numbers are the same as Table 6.1.

6.2.2.1.2 Biological and technical replicate correlation

In the raw data, all of the phosphopeptide identifications were found in the first elute. So the correlation analysis among the first elutes (Figure 6.12) and second elute (Figure 6.13) was conducted separately. The peptide intensities from "medium" isotope labelled samples (M = insulin treated, $^{13}C^{2}H$) were compared to the peptide intensity from "light" isotope labelled samples (L = untreated, $^{12}C^{14}N$) and a ratio of intensities (M/L) was derived. This ratio represents the fold change in abundance of a particular phosphopeptide in response to insulin stimulation. Similarly, the peptide intensities from "heavy" isotope labelled samples (H = IGF-II treated, $^{13}C^{15}N$) were compared to the peptide intensities from "light isotope labelled samples (L, untreated). The H/L ratio represents fold change in abundance of a particular phosphopeptide in response to IGF-II stimulation. The ratios of M/L and H/L from every individual peptide were studied. A mean correlation between measurements of 0.7-0.8 (Figure 6.12 and 6.13) was seen, where >0.7 indicates a strong positive correlation. We, therefore, conclude that our results are consistent and reproducible.

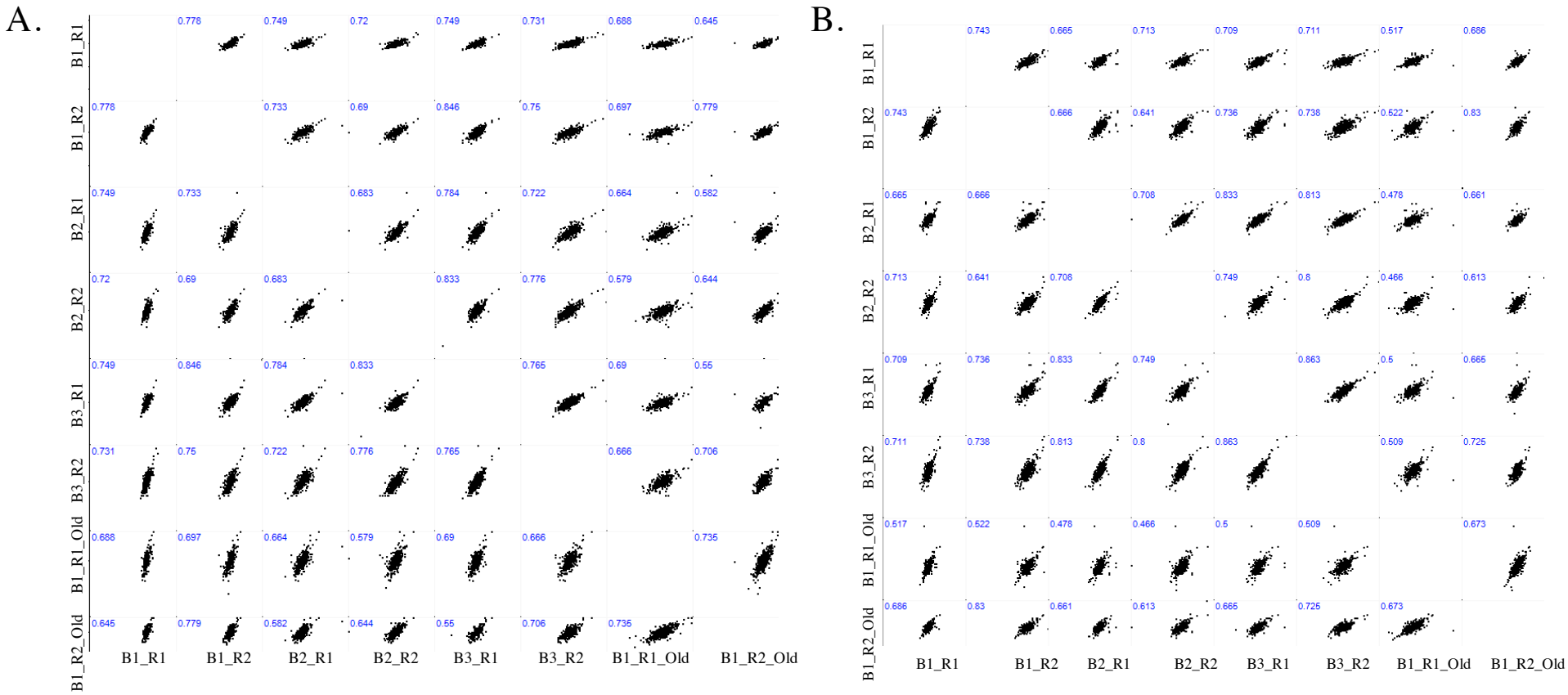

Figure 6.12: Multi-scatter plots represent pairwise comparisons of the normalized log $_2$ ratios (M/L and H/L, representing insulin/control and IGF-II/control, respectively) measured in each experiment of M/L (A) and H/L (B) from first elute. Biological replicate (B1 or B2), Technical replicate (R1 or R2).

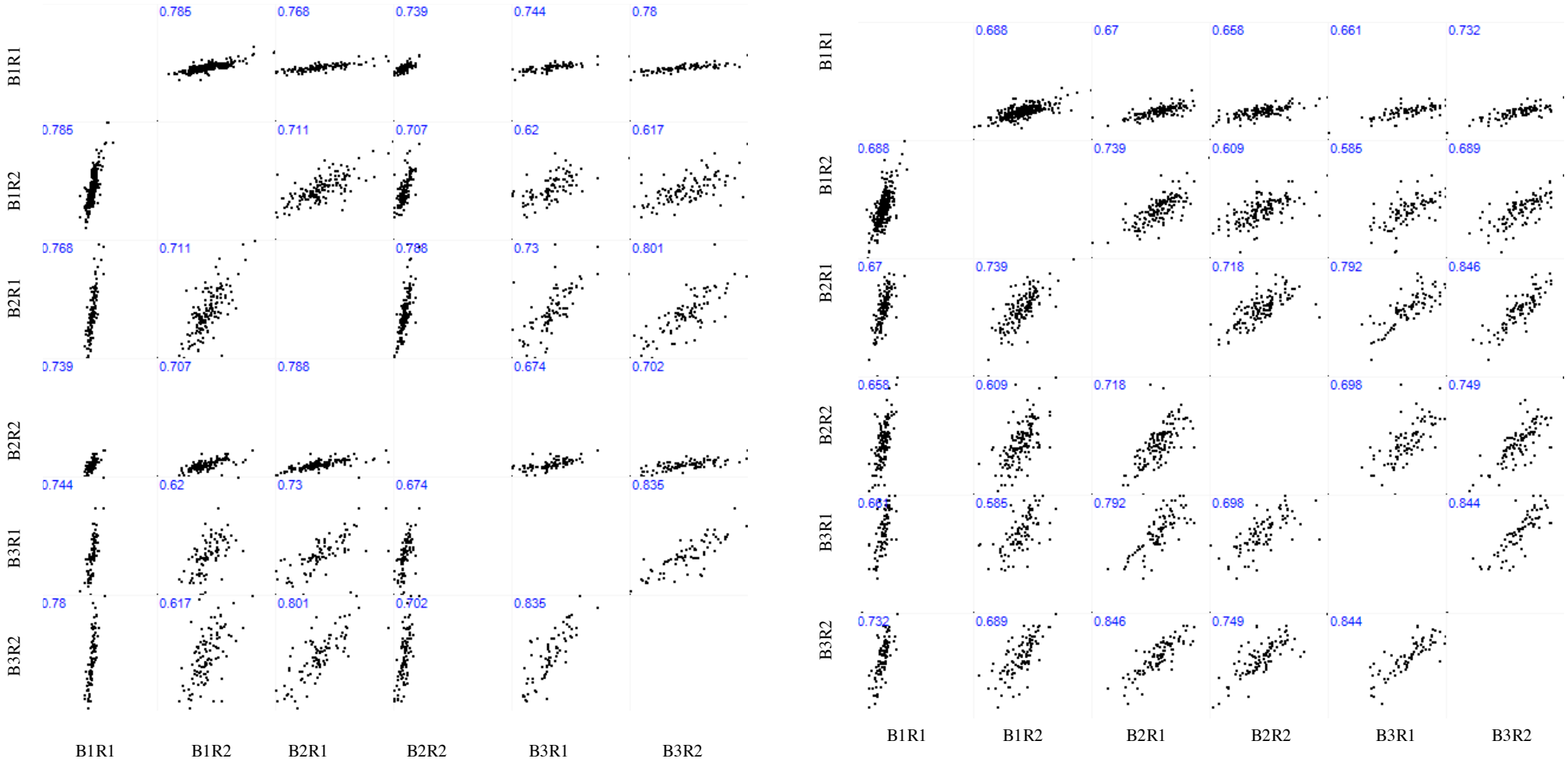

Figure 6.13: Multi-scatter plots represent pairwise comparisons of the normalized log $_2$ ratios (M/L and H/L, representing insulin/control and IGF-II/control, respectively) measured in each experiment of M/L (A) and H/L (B) from second elute. Biological replicate (B1 or B2), Technical replicate (R1 or R2).

6.2.2.1.3 Scatter plot

To ensure the data in each replicate experiment was normally distributed and properly normalized, the log2 transformed peptide ratios were viewed as histograms. The median value of each plot is close to zero (Figure 6.14), indicating very little variability between experiments. The small variances indicated equal mixing of light, medium and heavy isotope labelled cell samples and therefore that the proteome was not drastically changed in response to treatments.

A.

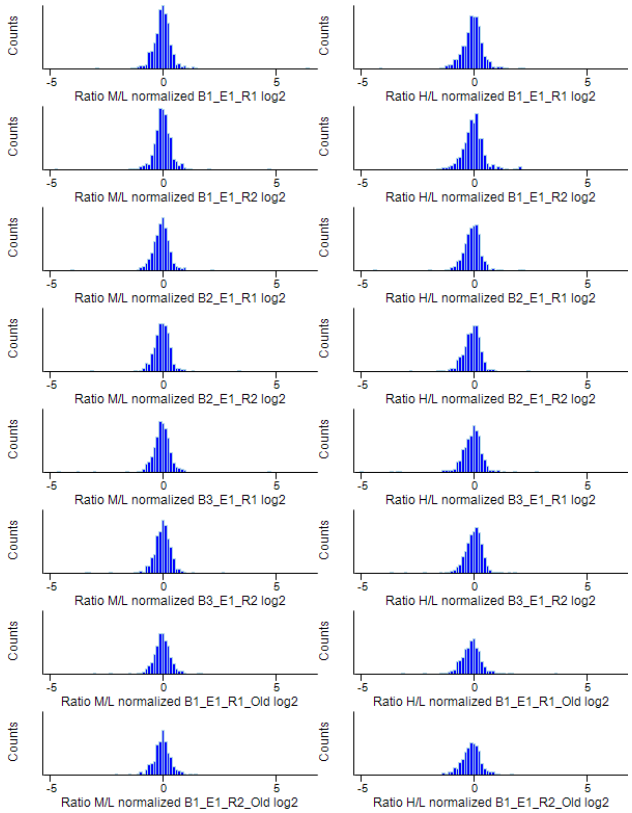

B.

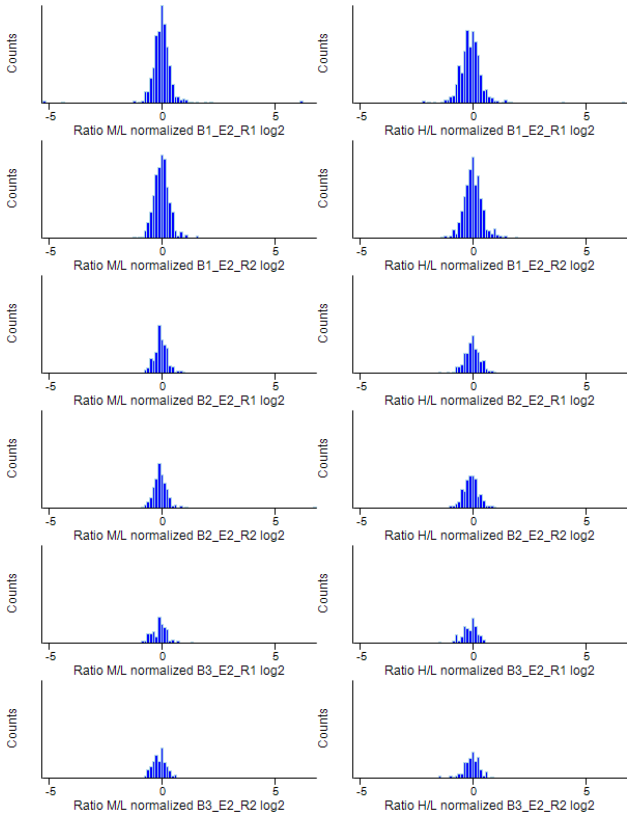

Figure 6.14: The distribution of normalized, log $_2$ transformed ratios of phosphopeptides enriched from insulin or IGF-II treated MDA-MB-231 cells compared to control cells (M/L or H/L) of the first elute (A) and seconde elute (B). The histograms of SILAC encoded peptide ratios measured in all replicate experiments exhibited a normal distribution.

6.2.2.2 Data analysis

6.2.2.2.1 Phosphoproteome profiling of insulin or IGF-II stimulated MDA-MB-231 IGF-1RKD cells

In the whole experiment, 3291 unique phosphosites were identified with a false discovery rate of less than 1%, including 2265 Class I phosphosites (the phosphorylation probability of this site is above 0.75). Approximately 1500 phosphosites were present in at least two different biological replicates (Appendix 6). A total of 307 sites (including 188 Class I phosphosites) have not previously been reported according to the largest phosphorylation site database, http://www.phosphosite.org (Figure 6.15).

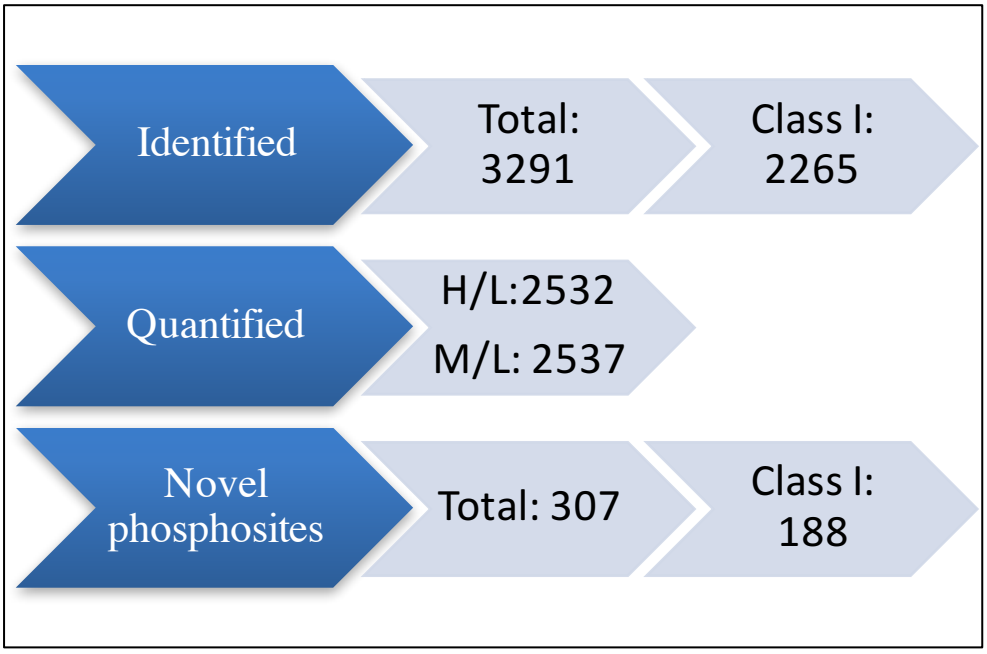

Figure 6.15: Summary of number of phosphosites identified and quantified in the dataset and those regulated in response to insulin (M/L) or IGF-II (H/L). Class I: Phosphorylation probability above 0.75 in MaxQuant search. Novel Phosphosites: not reported according to the phosphorylation site database, http://www.phosphosite.org analysed with Perseus (Tyanova et al., 2016).

A commonly used method for identifying differentially regulated proteins is to measure the fold change (FC) between two treatment groups. By this approach, proteins with an FC larger than a defined cut off (e.g. 1.5) are classified as differentially regulated. Since many of the phosphopeptides were only quantified in one biological experiment, we first extracted the phosphorylated peptides observed that exhibited more than 1.5 fold change ($log2>0.58$ or $log2<-0.58$) (Figure 6.16-A). Using this approach, a total of 118 sites were identified as only regulated with insulin stimulation (60 up regulated and 58 down regulated), while a total of 192 sites were regulated with only IGF-II stimulation (56 up regulated and 136 down regulated). A total of 233 sites (84 up regulated and 149 down regulated) were regulated by both insulin and IGF-II stimulation. Interestingly, six sites were regulated by both insulin and IGF-II, but in opposite directions.

As t-tests have been widely used to identify deviation from the mean, phosphosites with a minimum 1.5 fold change in at least two biological replicates combined with a $p < 0.05$ were considered significant for further analysis (Figure 6.16-B). A total of 38 sites were regulated only by insulin stimulation (18 up regulated and 20 down regulated), while a total of 64 sites were regulated by IGF-II stimulation (11 up regulated and 53 down regulated). A total of 80 sites (42 up regulated and 38 down regulated) were regulated by both insulin and IGF-II stimulation. The regulated sites are shown in Appendix 7-12. An example of a raw spectrum is shown in appendix 18.

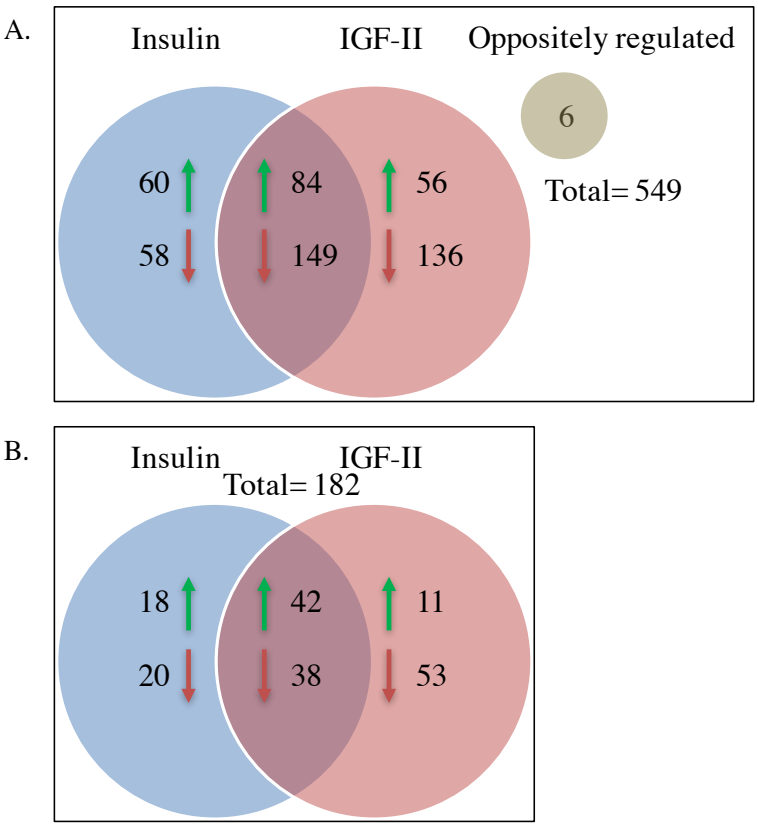

Figure 6.16: Venn diagram showing the number of phosphopeptides regulated by Insulin and/or IGF-II with above 1.5 fold change (log2>0.58 or log2<-0.58). (A) Phosphosites with a minimum of 1.5 fold change. (B) Phosphosites with a minimum 1.5 fold change in at least two biological replicates and with $p < 0.05$ were considered significant.

Using pathway analysis it was seen that the insulin receptor signalling pathway is enriched using the insulin regulated phosphosites list (Appendix 7, 8, 9, and 10). These analyses verified that MDA-MB-231 IGF-1RKD cells are responsive to insulin stimulation.

Several studies have investigated the IR signalling pathway in response to insulin stimulation using a range of cell types (Humphrey et al., 2015; Humphrey et al., 2013; Morcavallo et al., 2011; Parker et al., 2015). The fold changes of the phosphosites generated in this study were compared to these published data. It appears that the phosphosites regulated by insulin are highly conserved between human and mouse, as many were identified in this study and the study by Humphrey et al (Humphrey et al., 2015; Humphrey et al., 2013), which measured the phosphorylation states of a mouse adipocyte cell line and in mice in response to insulin stimulation (Humphrey et al., 2015; Humphrey et al., 2013). Commonly identified phosphosites include TBC1D4 (Akt substrate of 160 kDa, also known as AS160), which is activated (phosphorylation of site S591 increased) in response to insulin stimulation to promote glucose transport (Kramer et al., 2006; Peck et al., 2006), and PEA-15, which regulates the insulin-dependent Glut4 transportation (Condorelli et al., 1998).

6.2.2.2.2 Comparative analysis of insulin and IGF-II phosphoproteomes

The 38 insulin only regulated phosphosites are from a total of 30 unique proteins (Appendix 9 and 10) and the 64 IGF-II-only regulated phosphosites are from a total of 43 unique proteins (Appendix 11 and 12). However, insulin and IGF-II regulate different phosphosites on 5 common proteins (ARHGAP17, EGFR, DYNC1LI1, MAP1B, and SCRIB). Thus they were omitted for further analysis.

To determine the biological processes that emerged as being enriched in insulin or IGF-II regulated phosphoproteomes, I performed Gene Ontology Biological Process (GOBP) analysis (Figure 6.17) against the entire human database using InnateDB and NetworkAnalyst online with the 25 insulin only regulated proteins or 38 IGF-II only regulated proteins (Breuer

et al., 2013; Xia et al., 2014; Xia et al., 2015). Biological process annotations with a p-value less than 0.05 were retained in this analysis. The predicted annotations were first ranked by the p-value. Then from this list the top significantly enriched GOBP annotations were identified (the first 10 annotations ranked by p-value, red box). Following this a further list of GOBP annotations were identified that were associated with >3 protein entries (Figure 6.17, green box). Enriched pathways included the dUTP metabolic process and glucosamine biosynthetic process, indicating the metabolic function of insulin. The other enriched processes (such as cell division) indicated the mitogenic function of insulin. Not surprisingly, IGF-II regulated the mitogenic pathways, indicated by many enriched processes, such as gene expression, mRNA processing, translational initiation, and many others. In addition, cell-cell signalling involved in cell-cell junction organization, positive regulation of microtubule motor activity, microtubule-based movement, Notch signalling pathway and transforming growth factor beta receptor signalling pathways were among the enriched processes under IGF-II only stimulated condition. Moreover, the phosphorylation sites on proteins involved in these processes were identified (Table 6.2). For example, phosphorylation of S125 and S131 of tight junction protein ZO-1 (TJP1) were specifically inhibited by IGF-II. The annotated MS/Ms spectrum identifying the phosphorylation of S125 and S131 of tight junction protein ZO-1 (TJP1) is shown in appendix 18.

To characterize the specific signalling pathways that are modulated by insulin and IGF-II, a pathway enrichment analysis was conducted using the REACTOME database. The top significantly enriched pathways were determined (Figure 6.18). Similar to the GOBP result, the pathways related to mitogenic signalling were enriched when searching with proteins regulated by both insulin and IGF-II. Again, searching with proteins only regulated by IGF-II the Notch1 signalling pathway and TGF-β signalling pathways were enriched. These data indicated the IGF-II/IR-A signalling pathway might be involved in cell-cell connections and

communication. However, the functions of many of these phosphorylation sites are not understood yet (www.phosphosite.org).

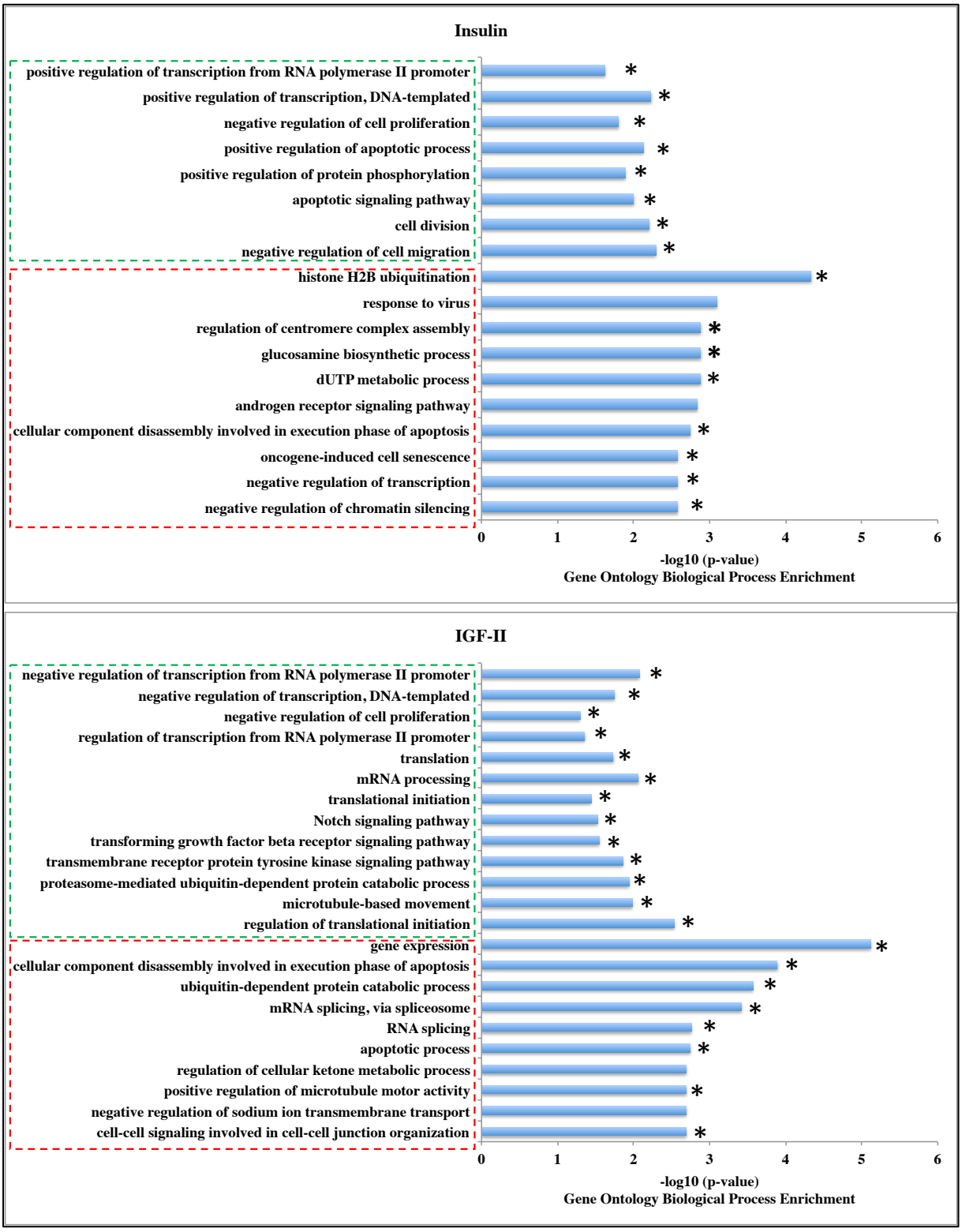

Figure 6.17: Gene Ontology Biological Process (GOBP) analysis of the insulin (above) and IGF-II (below) regulated proteins. The GOBP annotations with a p-value less than 0.05 are shown. Those GOBP terms with the smallest p-value shown in ascending order and

highlighted in red. The green area represents the GOBP terms identified as (not the first 10 annotations ranked by p-value) but have large number of gene entries. Red area represents the top (the first 10 annotations ranked by p-value) annotations. Star represents the annotations related to the insulin or IGF-II functions in breast cancer cells.

GOBP	Gene Name	Protein Name	Phossphorylation Site	Fold Change Insulin	Fold Change IGF-II	Pathway P-Value
cell-cell signaling involved in cell-cell junction organization	TJP1	Tight junction protein ZO-1	S125, S131	0.95	0.67	0.002
positive regulation of microtubule motor activity	MTCL1	Microtubule cross-linking factor 1	S263	0.81	0.54	0.002
microtubule-based movement	KIF23	Kinesin-like protein KIF23	S503	0.71	0.56	0.010
Notch signaling pathway	SNW1	SNW domain-containing protein 1	S234	0.71	0.61	0.030
	NCOR2	Nuclear receptor corepressor 2	T156	0.81	0.48	0.030
transforming growth factor beta receptor signaling pathway	NEDD4L	E3 ubiquitin-protein ligase NEDD4-like	S334	0.75	0.62	0.028

Table 6.2: Phosphorylation sites and their fold changes that are linked to selected GOBPs.

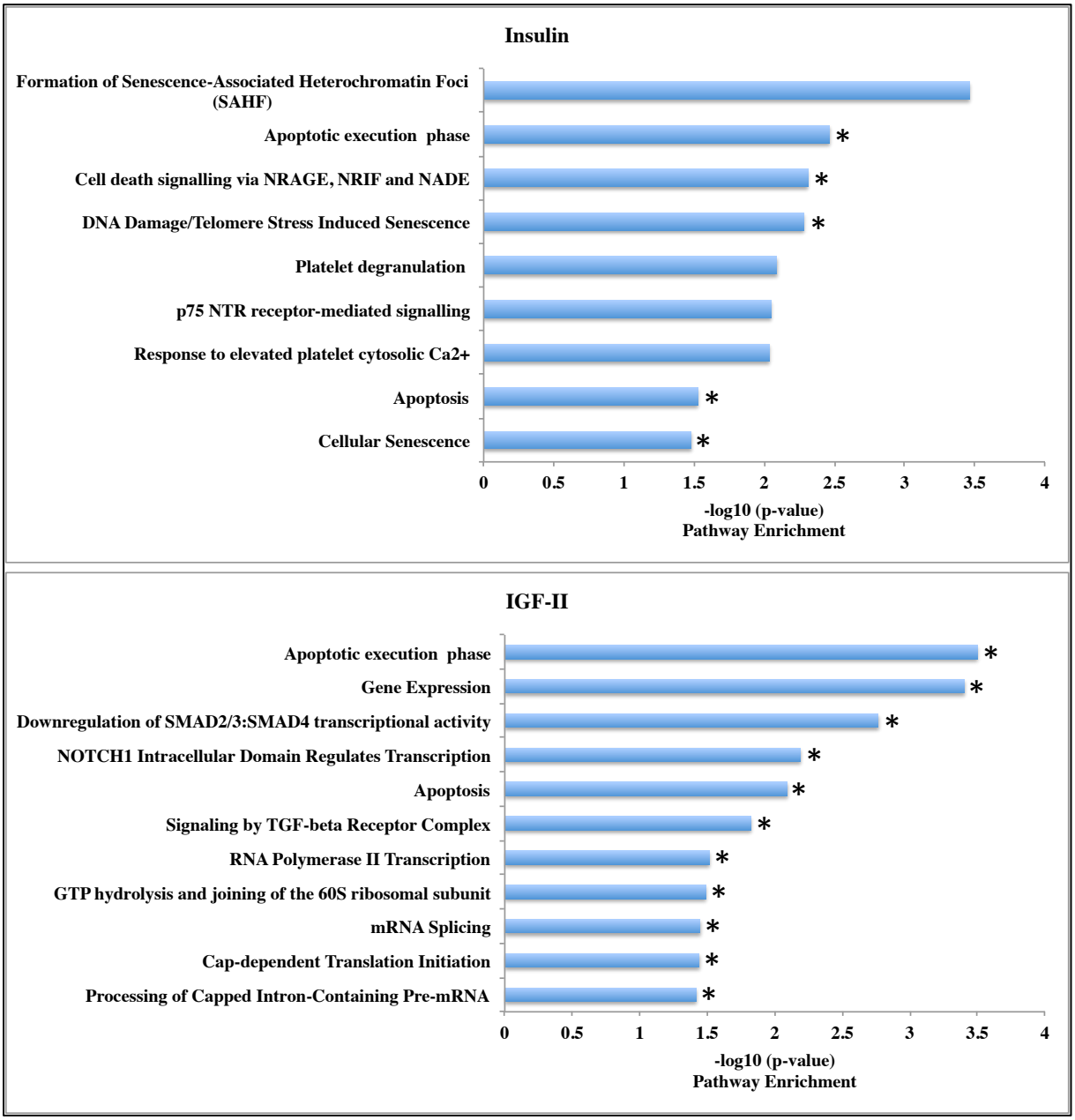

Figure 6.18: Pathway analysis of the insulin (top) and IGF-II (bottom) regulated proteins against the REACTOME database. The annotations with a p-value less than 0.05 were retained. Star represents the annotations related to the insulin or IGF-II that would be relevant to functions in breast cancer cells.

6.3 Conclusion

Insulin and IGF-II, through the IR-A, activate overlapping signals. However, many studies show that they also have unique signalling cascades, even though these cascades are not fully defined yet (Frasca et al., 1999; Morcavallo et al., 2011; Rajapaksha and Forbes, 2015; Sacco et al., 2009). I thus addressed this gap in this chapter.

In the first part of this chapter, MALDI-TOF MS and HPLC-MS/MS were used to optimise the phosphopeptide enrichment method. The DHB matrix was proved to be a better matrix for phosphopeptides detection with MDLDI-TOF MS. Higher concentrations of TFA and DHB used in TiO_2 binding buffer were found to inhibit non-specific peptide binding to the TiO_2 beads. Additionally, C18 stagetips was also found to be a good method to clean up the TiO_2 elutes before HPLC-MS/MS. This optimisation provided a good platform for future work.

In the second part of this chapter, the insulin/IR-A and IGF-II/IR-A signalling pathways were quantitatively compared by combining the optimised phosphopeptide enrichment method and SILAC labelling technology in MDA-MB-231 cells with IGF-1R depletion constructed in Chapter 5. Here, the MDA-MB-231 IGF-1RKD cells were SILAC labelled, stimulated with 10 nM insulin or 100 nM IGF-II for 10 minutes with no stimulation as the control in order to study the intermediate signalling cascades. This study is the first quantitative phosphoproteomics study comparing the insulin/IR-A and IGF-II/IR-A cascades in breast cancer cells. This is also by far the largest dataset to show the differences between the insulin/IR-A and IGF-II/IR-A signalling pathways. The quantitative phosphoproteomics technique and statistical analysis provide accurate identification, large-scale quantification and reliable information. Approximately 3300 phosphosites were identified to be related to IR-A signalling cascades. The differentially phosphorylated proteins by insulin stimulation identified in this study were found to be highly consistent with previous studies with other cell lines or mouse models (Humphrey et al., 2015; Humphrey et al., 2013). This indicated a high conservation of the insulin signalling pathway. For example, TBC1D4 (Akt substrate of

160 kDa, also known as AS160) is activated (phosphorylation of site S591 increased) in response to insulin stimulation, which promotes glucose transport (Kramer et al., 2006; Peck et al., 2006). The GOBP analysis verified the role of insulin in energy homeostasis, indicated by the enriched glucosamine biosynthetic and dUTP metabolic processes. Phosphorylation of S243 of GFPT1 (Glutamine--fructose-6-phosphate aminotransferase [isomerizing] 1) was only increased in response to insulin stimulation, and not in response to IGF-II. Its phosphorylation regulates the hexosamine biosynthesis and surprisingly promotes angiogenesis. It is an AMP-activated protein kinase (AMPK) substrate (Li et al., 2007; Zibrova et al., 2017). The GOBP and pathway analysis also confirmed the mitogenic function of both insulin and IGF-II, because many biological processes and pathway enriched, such as gene expression, mRNA processing and cell division, induce mitogenic outcome. For example, HMGA1 is already confirmed to be an insulin receptor signalling targeted nuclear factor, and its phosphorylation regulates the gene transcription (Chiefari et al., 2012). The phosphorylation of S44 of HMGA1 (High mobility group protein HMG-I/HMG-Y) was increased in response to insulin stimulation. Many unique proteins that are regulated only by IGF-II indicated its role in cell-cell interaction and migration, shown by the GOBP processes such as cell-cell signalling involved in cell-cell junction organization, positive regulation of microtubule motor activity. Phosphorylation of S168 of tight junction protein ZO-1 (TJP1) disrupts the cell- cell contact ion and promotes cell migration (Hamalisto et al., 2013). Here, the phosphorylation of S125 and S131 of TJP1 was decreased by the IGF-II stimulation. Further experiments are necessary to verify whether the phosphorylation of S125 and S131 has similar or different roles to phosphorylation of S168 in regulating TJP1 function. Microtubule cross-linking factor 1 (SOGA2, MTCL1) is also found to involve in microtubule dynamics regulation (Sato et al., 2014), however, the molecular mechanism and its relation to IGF-II signalling is unknown. Notably, the Notch and TGF-β (Transforming growth factor beta) signalling pathways were enriched with the IGF-II regulated phosphoproteins. These

two pathways play important roles in EMT process and are indicated to be the reasons of failure of anti-IGF-1R drugs in cancers (Li et al., 2017; Rota and Wood, 2015). Furthermore, the inhibition of IGF-1R is found to amplify the Notch signalling in triple negative breast cancer cells through increased IR-A signalling, thus induce the tumour development (Rota and Wood, 2015). The findings from this study will help us better understand IR-A signalling in a large picture. Hopefully, these identified proteins can be candidate drug targets for anti-IGF-1R drug resistant cancers in the future.

Chapter 7 Final discussion

The involvement of IR-A in insulin resistance and cancer has drawn much attention. IR-A is able to bind insulin and IGF-II with similar affinities and transduce their metabolic and mitogenic biological activities. Studies have shown that insulin and IGF-II induce different signalling pathways through IR-A (Frasca et al., 1999; Morcavallo et al., 2011; Sacco et al., 2009). More importantly, the IGF-II/IR-A signalling pathway provides an alternative pathway for anti-IGF-1R drug resistant cancer growth (Frasca et al., 1999; Sciacca et al., 2002). The main purpose of this thesis is to identify the signalling proteins involved in IGF-II/IR-A signalling in breast cancer cells. These may provide novel drug targets. Additionally, in the process of characterizing IR phosphorylation kinetics our lab discovered that Thr^{1148} phosphorylation was only detected on peptides *lacking* phosphorylation of neighbouring Tyr^{1146}, Tyr^{1150} and Tyr^{1151} residues (phosphorylation of these three Tyr are necessary for IR activation). We hypothesised that the Thr^{1148} phosphorylation affect the IR activation, thus a study was conducted to evaluate its function of Thr^{1148} phosphorylation in IR activation. The above information and present studies in this field were introduced in Chapter 1 and the materials and methods used in this thesis were elaborated in Chapter 2 and 3.

As described earlier, the phosphorylation of the activation loop is necessary for the IR activation (Cabail et al., 2015). The ligand binding induces the ectodomain structural change and thus induces intracellular domain structural change (Ward et al., 2013). The structure of the inactivated state and activated states of the tyrosine kinase domain have been extensively studied (Cabail et al., 2015; Hubbard, 1997; Hubbard et al., 1994). In the inactivated state, the activation loop inhibits the access of substrates to the catalytic site thus holding the IR in an inactivate state (Hubbard et al., 1994). After ligand binding, the Tyr^{1150} is phosphorylated first, followed by the phosphorylation of the other two tyrosines: Tyr^{1146}, and Tyr^{1151}. When these three Tyr are phosphorylated, they provide docking sites for the downstream signalling molecules and the structural change induces the phosphorylation of the other sites in the IR (Hubbard, 1997). It has only been recently recognised that Thr^{1148}, which lies in between the

three Tyr^{1146}, Tyr^{1150} and Tyr^{1151} on the activation loop, is phosphorylated. In chapter 4, the role of Thr^{1148} phosphorylation in IR-A was investigated. In this chapter, recombinant wild type and mutants with Thr^{1148} mutated to Ala or Asp were generated and overexpressed in R^- cells. The Thr^{1148}Ala and Thr^{1148}Asp mutants were introduced to either prevent phosphorylation or mimic a constitutively phosphorylated state at that residue, respectively. Both Thr^{1148}Ala and Thr^{1148}Asp were found to be significantly less responsive to insulin than the wild type IR-A. This data indicates that phosphorylation of Thr^{1148} is related to IR activation. At the same time, Petersen et al also investigated the role of Thr^{1160} in IR-B (which equals Thr^{1148} in IR-A) by mutate the Thr to Ala and Glu respectively (Petersen et al., 2016). Petersen et al also found that Thr^{1148}Glu inhibited the IR activation (Petersen et al., 2016). However, Petersen et al found that Thr^{1148}Ala increased the IR activation, which measured by the phosphorylated Tyr^{1162} (equals to Tyr^{1150} in IR-A) (Petersen et al., 2016). As I used the phosphorylated $Tyr^{1146, 1150, 1151}$ to measure the activated IR, I believe we measured the different stages of IR activation. As shown previously, the phosphorylation of $Tyr^{1146, 1150, 1151}$ are conducted sequentially (Hubbard, 1997). Petersen et al showed the Thr^{1148}Ala mutation did not affect the first step: phosphorylation of Tyr^{1150}, while my data showed the following step, phosphorylations of Tyr^{1146} and Tyr^{1151}, is inhibited.

Recent evidence has demonstrated mechanisms that regulate Thr^{1148} phosphorylation. I*n vitro* studies by Petersen et al and Marin et al provide *in vitro* evidence that phospholipase C epsilon (PKCε) and protein kinase CK2 can act as kinases at Thr^{1148} (Marin et al., 1996; Petersen et al., 2016). Also, when present on a synthetic peptide the phosphorylation of three tyrosine sites $Tyr^{1146,1150,1151}$, especially that of Tyr^{1151}, was found to be necessary for the phosphorylation of Thr^{1148} by CK2 (Marin et al., 1996). Whether this is the case on the intact receptor has not been investigated, but these experiments indicate that Thr^{1148} phosphorylation may be required for for IR inactivation.

Phosphatases (T-Cell Protein Tyrosine Phosphatase) and adaptor proteins (Growth factor receptor-bound protein 7,10,14) are known to dephosphorylate the phosphorylated Tyr^{1146}, Tyr^{1150}, Tyr^{1151} (Goenaga et al., 2009; Goldstein et al., 2000; Han et al., 2001; Stein et al., 2001; Walchli et al., 2000). The introduction of Ala and Asp by the Thr^{1148}Ala and Thr^{1148}Asp mutants may induce the conformational change in the activation loop and negative charged acidic side chain of Asp by Thr^{1148}Asp mutant might also induce the electrostatic repulsion.

To explain the differences between the data generated in this thesis, which suggests Thr^{1148} is sensitive to mutation and inhibits IR activation, and that of Petersen showing that mutation of Thr^{1148} to Ala promotes IR activation will require further investigation. A kinetic study using antibodies directed to both Tyr^{1146}, Tyr^{1150}, and Tyr^{1151} and to Tyr^{1146} alone would be the next step. With the wild-type IR and the mutants constructed in this study, an IR activation time course could be conducted in response to insulin. In addition, the antibodies that target the phosphorylated Tyr^{1150} alone, or Tyr^{1146}, Tyr^{1150}, and Tyr^{1151} will be used to measure the phosphorylation kinetics. We would expect that the Thr1148 phosphorylation might affect the Tyr^{1146}, Tyr^{1150}, and Tyr^{1151} phosphorlyation at a different rate than Tyr^{1146}phosphorylation. Another experiment would be to investigate the potential phosphatases from the immunoprecipitated IR with antibody that target the phosphorylated Thr^{1148}. Structural studies of the IR kinase domain with Cryo-electron microscopy are more promising to investigate the intermediate steps of IR activation and how the Thr^{1148} affect the IR phosphorylation. These experiments will provide us more understanding of IR activation.

In chapter 5, we assessed the roles of IR and IGF-1R in breast cancer cells. Firstly, I verified that insulin and IGF-II activates the Akt signalling pathway through IR in MDA-MB-231 cells. In wild type cells expressing equal levels of IGF-1R and IR the cells responded poorly to 10 min stimulation of 10 nM insulin. This indicated that IR/IGF-1R hybrids are barely able to transduce insulin signalling. The existence of IR/IGF-1R hybrids decreases the insulin sensitivity, while they have no effect on IGF-II sensitivity of MDA-MB-231 cells. This is

likely because the IGF-II can act via three kinds of receptors. A similar result was found in other studies (Zhang et al., 2007). One possible explanation is that the IR/IGF-1R hybrids preferentially transduce IGF signals, but are barely activated by insulin (Slaaby, 2015; Slaaby et al., 2006; Zhang et al., 2007). As the expression levels of IR and IGF-1R are similar in MDA-MB-231 cells, IR/IGF-1R probably is the main isoforms thus inhibit the insulin signalling. We can learn from this study that silencing the expression of one protein can increase signalling of other pathways, a fact that should be carefully considered if taking this approach to target signalling pathways for therapeutic purposes.

There is evidence to suggest that hybrid receptor formation is stochastic (Bailyes et al., 1997; Frattali et al., 1992a). However, in some cancer tissues, some unknown factors affect the hybrid formation and the proportion of IR in hybrids is not random (Pandini et al., 1999). In the future, a systematic study on the expression levels of receptor homodimers and heterodimers in different tissues, normal tissues and cancer tissues should be conducted. The biological significance of IR/IGF-1R and the reason that they are less sensitive to insulin is poorly understood. A study to measure the IR/IGF-1R level in insulin resistant patients should be measured, even though there are studies shown the IR-A is upregulated in cancers (Frasca et al., 1999; Vella et al., 2002); this will give us a new information in order to design more effective insulin analogues. From a structural perspective, the IR/IGF-1R does not affect the binding of IGF to the ectodomain, while the affinity for insulin is decreased. A structural study to compare the differences between insulin and IGF bound to a hybrid receptor, while technically extremely challenging, would be helpful for development of drugs that inhibit the IR/IGF-1R transduced signals in cancer cells.

I also found that MDA-MB-231 and MCF-7 have different biological responses to ligand stimulation in both cell lines, IGF-1R is necessary for cell proliferation. Both IGFs and insulin promoted MCF-7 proliferation. IR knock down had a minimal affect on proliferation, while IGF-1R knock down drastically inhibited growth. This is the same as other studies (Bartucci

et al., 2001; Chappell et al., 2001; Saxena et al., 2008). In contrast, MDA-MB-231 did not respond to either ligand in this study. However, the IRKD increased cell proliferation, while the IGF-1R knock down drastically inhibited MDA-MB-231 cell growth. Low expression level of IGF-1R was thought to be the main reason for the lack of response to IGF in MDA-MB-231 cells (Sciacca et al., 1999). However, MDA-MB-231 with IGF-1R overexpression still failed to respond to ligands (Bartucci et al., 2001). MCF-7 is a well known cancer cell with low metastatic potential. Neither IR KD nor IGF-1R KD changed its migration response to ligands and therefore its likely metastatic potential *in vivo*. In contrast, MDA-MB-231 cells have high metastatic potential, and the IGF-1RKD in MDA-MB-231 increased the MDA-MB-231 migration rate in this study. This result also indicates that silencing the expression of IGF-1R in cancer may not be wise without perhaps also targeting the IR at the same time.

Since the epithelial mesenchymal transition (EMT) usually precedes migration and a feature of EMT is the decrease in expression of E-cadherin, theoretically we could propose that the expression level of E-cadherin will be lower in IGF-1RKD cells compared to the MDA-MB-231 wild-type. Taliaferro-Smith et al., surprisingly reported that MDA-MB-231 cells express E-cadherin protein and this occurs after knock down of the IGF-1R (Taliaferro-Smith et al., 2015). Consistent with the metastatic phenotype of MDA-MB-231 cells I did not detect any E-cadherin in wild-type MDA-MB-231 or IRKD or IGF-1RKD using PCR method. This result also correlates with the migration results. Therefore, the molecular mechanisms responsible for the change in migration rate with IGF-1RKD remain unknown. For this reason I decided to perform a detailed signalling pathway analysis as outlined in Chapter 6.

In the first part of chapter 6, MALDI-TOF and HPLC-MS/MS were used to optimise the phosphopeptides enrichment method, which provides a good starting point for a later molecular mechanism study. In the second part of chapter 6, insulin/IR-A and IGF-II/IR-A signalling pathways were compared with phosphoproteomics in MDA-MB-231 breast cancer cell with IGF-1RKD. This study is the first quantitative phosphoproteomics study comparing

the insulin/IR-A and IGF-II/IR-A signalling cascades in cancer. The phosphosites with a minimum 1.5 fold change in at least two biological replicates combined with a $p<0.05$ were considered to be significantly regulated. I found 188 novel sites in IR downstream signalling that have not been reported on the largest phosphorylation site database (http://www.phosphosite.org). There were 38 insulin only regulated sites, 64 IGF-II only regulated sites, and 80 insulin and IGF-II regulated sites.

The proteins identified as being differentially regulated by insulin or IGF-II were subjected to Gene Ontology and KEGG pathway analysis, which further confirmed the insulin/IR-A and IGF-II/IR-A signalling pathways induce different biological outcomes. The IGF-II/IR-A stimulated signalling pathways related to cell migration, and included cell-cell signalling pathways involving cell-cell junction organisation, microtubule based movement and Notch signalling. This data supports the finding in chapter 5 that the IGF-1R KD increases the MDA-MB-231 migration ability.

A more detailed analysis of individual phosphosites revealed interesting sites regulated specifically by IGF-II. Notably, Ser185 of PCBP2 (hnRNP E2) is preferentially phosphorylated in response to IGF-II compared to insulin. PCBP2 is known to play a role in cancer cell growth. The phosphorylation of this site by ERK1/2 is necessary to maintain its stability in BCR/ABL-expressing myeloid precursors, and causes the arrest of differentiation- a feature of chronic myelogenous leukemia cells (Chang et al., 2007; Perrotti et al., 2002). Additionally, high levels of PCBP2 predicts poor overall and disease-free survival of gastric carcinoma and it promotes gastric carcinoma (Hu et al., 2014). Further experiments are needed to understand the relation of PCBP2 with IGF-II/IR-A signalling pathway. Several other phosphosites were preferentially phosphorylated or dephosphorylated in response to IGF-II including PGRMC1 (known to be overexpressed and regulated by phosphorylation (Neubauer et al., 2008; Neubauer et al., 2013) and CCAR1 (Cell division cycle and apoptosis regulator 1, regulates apoptosis (Muthu et al., 2014; Muthu et al., 2015). These and the

PCBP2 example listed above are primary candidates (selected as being significantly regulated by IGF-II, fold change >1.5 and $p<0.05$) among others that need now to be verified. Possible methods of verification of the MS/MS data include direct detection using antibodies that target the specific phosphorylated proteins. However, this method is limited by the lack of availability of specific antibodies. Alternatively, multiple reaction monitoring (MRM) mass spectrometry would be an ideal method to validate the data from this study. Following this knock down experiments would also allow an *in vivo* confirmation of the function of specific phosphosites in candidate signalling proteins. Ultimately inhibitors of these validated IGF-II/IR-A signalling specific targets could be developed and tested in animal models as potential breast cancer therapies.

At present, the IR/IGF-1R targeting strategies have not been successful for cancer treatment in clinical trials, especially phase III trials. Co-targeting several hallmarks of cancer is likely to be more effective. For example, NT157, which targets both IGF-1R and STAT3 (a protein in inflammation signalling pathway), has shown promising effect (Sanchez-Lopez et al., 2016). Due to its capabilities of decreasing insulin resistance, metformin has become a hot research topic again, inhibiting cancer growth and inducing longevity. Combination therapy using this drug and IR/IGF-1R signalling inhibitors could be a more effective approach than using IR/IGF-1R signalling inhibitors alone. Also, ultimately it would be good to conduct *in vivo* experiments to test the efficacy of targeting both the IGF-1R and the novel IGF-II/IR-A signalling inhibitors developed against targets identified in this study. Another possible reason for the failure of the IR/IGF-1R targeting strategies so far is that cancer patients in these trials might not be have had tumours dependent on IR/IGF-1R signalling. At the time of the clinical trials there were no specific, validated biomarkers. In general, an adequate biomarker should help to identify the tumours that are sensitive to a specific therapy. As such investigation should be continued to define specific IR/IGF-1R signalling biomarkers that would be invaluable in future clinical trials with mono and combined therapy approaches. Some of the

specific IGF-II/IR-A signalling pathway components identified in this study could be investigated as biomarkers in the future.

In summary, I have shown that Thr^{1148} mutation inhibits IR activation. I verified IGF-1R is necessary for proliferation in both MCF-7 and MDA-MB-231 cells. I found the silence of IGF-1R expression increases the insulin sensitivity of MDA-MB-231 cells and increases its migration ability. In the quantitative phosphoproteomics study comparing the insulin/IR-A and IGF-II/IR-A signalling pathways in MDA-MB-231 cells with IGF-1R silenced. Proteins related to migration are regulated by IGF-II stimulation. The findings in this thesis provide valuable information to cure the IGF-1R and IR promoted cancer.

References

Abe, H., Yamada, N., Kamata, K., Kuwaki, T., Shimada, M., Osuga, J., Shionoiri, F., Yahagi, N., Kadowaki, T., Tamemoto, H., *et al*. (1998). Hypertension, hypertriglyceridemia, and impaired endothelium-dependent vascular relaxation in mice lacking insulin receptor substrate-1. J Clin Invest *101*, 1784-1788.

Adams, T.E., Epa, V.C., Garrett, T.P., and Ward, C.W. (2000). Structure and function of the type 1 insulin-like growth factor receptor. Cell Mol Life Sci *57*, 1050-1093.

Ahmed, Z., Smith, B.J., Kotani, K., Wilden, P., and Pillay, T.S. (1999). APS, an adapter protein with a PH and SH2 domain, is a substrate for the insulin receptor kinase. Biochem J *341 (Pt 3)*, 665-668.

Alvino, C.L., McNeil, K.A., Ong, S.C., Delaine, C., Booker, G.W., Wallace, J.C., Whittaker, J., and Forbes, B.E. (2009). A novel approach to identify two distinct receptor binding surfaces of insulin-like growth factor II. The Journal of biological chemistry *284*, 7656-7664.

Avnet, S., Sciacca, L., Salerno, M., Gancitano, G., Cassarino, M.F., Longhi, A., Zakikhani, M., Carboni, J.M., Gottardis, M., Giunti, A., *et al*. (2009). Insulin receptor isoform A and insulin-like growth factor II as additional treatment targets in human osteosarcoma. Cancer research *69*, 2443-2452.

Bailyes, E.M., Nave, B.T., Soos, M.A., Orr, S.R., Hayward, A.C., and Siddle, K. (1997). Insulin receptor/IGF-I receptor hybrids are widely distributed in mammalian tissues: quantification of individual receptor species by selective immunoprecipitation and immunoblotting. Biochem J *327 (Pt 1)*, 209-215.

Baker, J., Liu, J.P., Robertson, E.J., and Efstratiadis, A. (1993). Role of insulin-like growth factors in embryonic and postnatal growth. Cell *75*, 73-82.

Baker, M.A., Smith, N.D., Hetherington, L., Pelzing, M., Condina, M.R., and Aitken, R.J. (2011). Use of titanium dioxide to find phosphopeptide and total protein changes during epididymal sperm maturation. Journal of proteome research *10*, 1004-1017.

Bartucci, M., Morelli, C., Mauro, L., Ando, S., and Surmacz, E. (2001). Differential insulin-like growth factor I receptor signaling and function in estrogen receptor (ER)-positive MCF-7 and ER-negative MDA-MB-231 breast cancer cells. Cancer research *61*, 6747-6754.

Baserga, R. (2013). The decline and fall of the IGF-I receptor. J Cell Physiol *228*, 675-679.

Beardsall, K., Diderholm, B.M., and Dunger, D.B. (2008). Insulin and carbohydrate metabolism. Best practice & research Clinical endocrinology & metabolism *22*, 41-55.

Beckwith, H., and Yee, D. (2015). Minireview: Were the IGF Signaling Inhibitors All Bad? Molecular endocrinology *29*, 1549-1557.

Belfiore, A., Costantino, A., Frasca, F., Pandini, G., Mineo, R., Vigneri, P., Maddux, B., Goldfine, I.D., and Vigneri, R. (1996). Overexpression of membrane glycoprotein PC-1 in MDA-MB231 breast cancer cells is associated with inhibition of insulin receptor tyrosine kinase activity. Molecular endocrinology *10*, 1318-1326.

Belfiore, A., Frasca, F., Pandini, G., Sciacca, L., and Vigneri, R. (2009). Insulin receptor isoforms and insulin receptor/insulin-like growth factor receptor hybrids in physiology and disease. Endocr Rev *30*, 586-623.

Belfiore, A., and Malaguarnera, R. (2011). Insulin receptor and cancer. Endocrine-related cancer *18*, R125-147.

Bendell, J.C., Jones, S.F., Hart, L., Spigel, D.R., Lane, C.M., Earwood, C., Infante, J.R., Barton, J., and Burris, H.A. (2015). A phase Ib study of linsitinib (OSI-906), a dual inhibitor

of IGF-1R and IR tyrosine kinase, in combination with everolimus as treatment for patients with refractory metastatic colorectal cancer. Invest New Drugs *33*, 187-193.

Benyoucef, S., Surinya, K.H., Hadaschik, D., and Siddle, K. (2007). Characterization of insulin/IGF hybrid receptors: contributions of the insulin receptor L2 and Fn1 domains and the alternatively spliced exon 11 sequence to ligand binding and receptor activation. Biochem J *403*, 603-613.

Bersten, D.C., Sullivan, A.E., Li, D., Bhakti, V., Bent, S.J., and Whitelaw, M.L. (2015). Inducible and reversible lentiviral and Recombination Mediated Cassette Exchange (RMCE) systems for controlling gene expression. PLoS One *10*, e0116373.

Bielow, C., Mastrobuoni, G., and Kempa, S. (2016). Proteomics Quality Control: Quality Control Software for MaxQuant Results. Journal of proteome research *15*, 777-787.

Bodzin, A.S., Wei, Z., Hurtt, R., Gu, T., and Doria, C. (2012). Gefitinib resistance in HCC mahlavu cells: upregulation of CD133 expression, activation of IGF-1R signaling pathway, and enhancement of IGF-1R nuclear translocation. J Cell Physiol *227*, 2947-2952.

Boes, M., Booth, B.A., Sandra, A., Dake, B.L., Bergold, A., and Bar, R.S. (1992). Insulin-like growth factor binding protein (IGFBP)4 accounts for the connective tissue distribution of endothelial cell IGFBPs perfused through the isolated heart. Endocrinology *131*, 327-330.

Braiman, L., Alt, A., Kuroki, T., Ohba, M., Bak, A., Tennenbaum, T., and Sampson, S.R. (2001). Insulin induces specific interaction between insulin receptor and protein kinase C delta in primary cultured skeletal muscle. Molecular endocrinology *15*, 565-574.

Breuer, K., Foroushani, A.K., Laird, M.R., Chen, C., Sribnaia, A., Lo, R., Winsor, G.L., Hancock, R.E., Brinkman, F.S., and Lynn, D.J. (2013). InnateDB: systems biology of innate immunity and beyond--recent updates and continuing curation. Nucleic Acids Res *41*, D1228-1233.

Brierley, G.V., Macaulay, S.L., Forbes, B.E., Wallace, J.C., Cosgrove, L.J., and Macaulay, V.M. (2010). Silencing of the insulin receptor isoform A favors formation of type 1 insulin-like growth factor receptor (IGF-IR) homodimers and enhances ligand-induced IGF-IR activation and viability of human colon carcinoma cells. Endocrinology *151*, 1418-1427.

Burnier, J.V., Wang, N., Michel, R.P., Hassanain, M., Li, S., Lu, Y., Metrakos, P., Antecka, E., Burnier, M.N., Ponton, A., *et al.* (2011). Type IV collagen-initiated signals provide survival and growth cues required for liver metastasis. Oncogene *30*, 3766-3783.

Cabail, M.Z., Li, S., Lemmon, E., Bowen, M.E., Hubbard, S.R., and Miller, W.T. (2015). The insulin and IGF1 receptor kinase domains are functional dimers in the activated state. Nat Commun *6*, 6406.

Chang, J.S., Santhanam, R., Trotta, R., Neviani, P., Eiring, A.M., Briercheck, E., Ronchetti, M., Roy, D.C., Calabretta, B., Caligiuri, M.A., *et al.* (2007). High levels of the BCR/ABL oncoprotein are required for the MAPK-hnRNP-E2 dependent suppression of C/EBPalpha-driven myeloid differentiation. Blood *110*, 994-1003.

Chao, W., and D'Amore, P.A. (2008). IGF2: epigenetic regulation and role in development and disease. Cytokine & growth factor reviews *19*, 111-120.

Chappell, J., Leitner, J.W., Solomon, S., Golovchenko, I., Goalstone, M.L., and Draznin, B. (2001). Effect of insulin on cell cycle progression in MCF-7 breast cancer cells - Direct and potentiating influence. Journal of Biological Chemistry *276*, 38023-38028.

Chen, Y., Zhu, C., Peng, Z., Dai, Y., and Gu, Y. (2012). Lentivirus-mediated short-hairpin RNA targeting IGF-1R inhibits growth and lymphangiogenesis in breast cancer. Oncol Rep *28*, 1778-1784.

Chernicky, C.L., Tan, H., Yi, L., Loret de Mola, J.R., and Ilan, J. (2002). Treatment of murine breast cancer cells with antisense RNA to the type I insulin-like growth factor receptor decreases the level of plasminogen activator transcripts, inhibits cell growth in vitro, and reduces tumorigenesis in vivo. Mol Pathol *55*, 102-109.

Cheung, L.W., Mak, A.S., Cheung, A.N., Ngan, H.Y., Leung, P.C., and Wong, A.S. (2011). P-cadherin cooperates with insulin-like growth factor-1 receptor to promote metastatic signaling of gonadotropin-releasing hormone in ovarian cancer via p120 catenin. Oncogene *30*, 2964-2974.

Chiefari, E., Nevolo, M.T., Arcidiacono, B., Maurizio, E., Nocera, A., Iiritano, S., Sgarra, R., Possidente, K., Palmieri, C., Paonessa, F., *et al.* (2012). HMGA1 is a novel downstream nuclear target of the insulin receptor signaling pathway. Scientific reports *2*, 251.

Condina, M.R., Gustafsson, J.O., Klingler-Hoffmann, M., Bagley, C.J., McColl, S.R., and Hoffmann, P. (2010). EZYprep LC-coupled MALDI-TOF/TOF MS: an improved matrix spray application for phosphopeptide characterisation. Proteomics *10*, 2516-2530.

Condorelli, G., Vigliotta, G., Iavarone, C., Caruso, M., Tocchetti, C.G., Andreozzi, F., Cafieri, A., Tecce, M.F., Formisano, P., Beguinot, L., *et al.* (1998). PED/PEA-15 gene controls glucose transport and is overexpressed in type 2 diabetes mellitus. The EMBO journal *17*, 3858-3866.

Constancia, M., Hemberger, M., Hughes, J., Dean, W., Ferguson-Smith, A., Fundele, R., Stewart, F., Kelsey, G., Fowden, A., Sibley, C., *et al.* (2002). Placental-specific IGF-II is a major modulator of placental and fetal growth. Nature *417*, 945-948.

Costantino, A., Milazzo, G., Giorgino, F., Russo, P., Goldfine, I.D., Vigneri, R., and Belfiore, A. (1993). Insulin-resistant MDA-MB231 human breast cancer cells contain a tyrosine kinase inhibiting activity. Molecular endocrinology *7*, 1667-1676.

Crowell, A.M., Wall, M.J., and Doucette, A.A. (2013). Maximizing recovery of water-soluble proteins through acetone precipitation. Analytica chimica acta *796*, 48-54.

Cullen, B.R. (2004). Transcription and processing of human microRNA precursors. Mol Cell *16*, 861-865.

Davison, Z., de Blacquiere, G.E., Westley, B.R., and May, F.E. (2011). Insulin-like growth factor-dependent proliferation and survival of triple-negative breast cancer cells: implications for therapy. Neoplasia *13*, 504-515.

Dawson, S.J., Rueda, O.M., Aparicio, S., and Caldas, C. (2013). A new genome-driven integrated classification of breast cancer and its implications. The EMBO journal *32*, 617-628.

De Marco, P., Bartella, V., Vivacqua, A., Lappano, R., Santolla, M.F., Morcavallo, A., Pezzi, V., Belfiore, A., and Maggiolini, M. (2013). Insulin-like growth factor-I regulates GPER expression and function in cancer cells. Oncogene *32*, 678-688.

De Meyts, P. (2004). Insulin and its receptor: structure, function and evolution. BioEssays : news and reviews in molecular, cellular and developmental biology *26*, 1351-1362.

De Meyts, P., and Whittaker, J. (2002). Structural biology of insulin and IGF1 receptors: implications for drug design. Nat Rev Drug Discov *1*, 769-783.

Denley, A., Bonython, E.R., Booker, G.W., Cosgrove, L.J., Forbes, B.E., Ward, C.W., and Wallace, J.C. (2004). Structural determinants for high-affinity binding of insulin-like growth factor II to insulin receptor (IR)-A, the exon 11 minus isoform of the IR. Molecular endocrinology *18*, 2502-2512.

Denley, A., Brierley, G.V., Carroll, J.M., Lindenberg, A., Booker, G.W., Cosgrove, L.J., Wallace, J.C., Forbes, B.E., and Roberts, C.T. (2006). Differential activation of insulin

receptor isoforms by insulin-like growth factors is determined by the C domain. Endocrinology *147*, 1029-1036.

Denley, A., Carroll, J.M., Brierley, G.V., Cosgrove, L., Wallace, J., Forbes, B., and Roberts, C.T., Jr. (2007). Differential activation of insulin receptor substrates 1 and 2 by insulin-like growth factor-activated insulin receptors. Mol Cell Biol *27*, 3569-3577.

Denley, A., Cosgrove, L.J., Booker, G.W., Wallace, J.C., and Forbes, B.E. (2005). Molecular interactions of the IGF system. Cytokine Growth Factor Rev *16*, 421-439.

Dickins, R.A., Hemann, M.T., Zilfou, J.T., Simpson, D.R., Ibarra, I., Hannon, G.J., and Lowe, S.W. (2005). Probing tumor phenotypes using stable and regulated synthetic microRNA precursors. Nat Genet *37*, 1289-1295.

Dool, C.J., Mashhedi, H., Zakikhani, M., David, S., Zhao, Y., Birman, E., Carboni, J.M., Gottardis, M., Blouin, M.J., and Pollak, M. (2011). IGF1/insulin receptor kinase inhibition by BMS-536924 is better tolerated than alloxan-induced hypoinsulinemia and more effective than metformin in the treatment of experimental insulin-responsive breast cancer. Endocrine-related cancer *18*, 699-709.

Dow, L.E., Premsrirut, P.K., Zuber, J., Fellmann, C., McJunkin, K., Miething, C., Park, Y., Dickins, R.A., Hannon, G.J., and Lowe, S.W. (2012). A pipeline for the generation of shRNA transgenic mice. Nature protocols *7*, 374-393.

Eliasz, S., Liang, S., Chen, Y., De Marco, M.A., Machek, O., Skucha, S., Miele, L., and Bocchetta, M. (2010). Notch-1 stimulates survival of lung adenocarcinoma cells during hypoxia by activating the IGF-1R pathway. Oncogene *29*, 2488-2498.

Emanuelli, B., Peraldi, P., Filloux, C., Sawka-Verhelle, D., Hilton, D., and Van Obberghen, E. (2000). SOCS-3 is an insulin-induced negative regulator of insulin signaling. J Biol Chem *275*, 15985-15991.

Fair, A.M., Dai, Q., Shu, X.O., Matthews, C.E., Yu, H., Jin, F., Gao, Y.T., and Zheng, W. (2007). Energy balance, insulin resistance biomarkers, and breast cancer risk. Cancer detection and prevention *31*, 214-219.

Farooq, A., Plotnikova, O., Zeng, L., and Zhou, M.M. (1999). Phosphotyrosine binding domains of Shc and insulin receptor substrate 1 recognize the NPXpY motif in a thermodynamically distinct manner. J Biol Chem *274*, 6114-6121.

Fassnacht, M., Berruti, A., Baudin, E., Demeure, M.J., Gilbert, J., Haak, H., Kroiss, M., Quinn, D.I., Hesseltine, E., Ronchi, C.L., *et al*. (2015). Linsitinib (OSI-906) versus placebo for patients with locally advanced or metastatic adrenocortical carcinoma: a double-blind, randomised, phase 3 study. Lancet Oncol *16*, 426-435.

Fellmann, C., Zuber, J., McJunkin, K., Chang, K., Malone, C.D., Dickins, R.A., Xu, Q.K., Hengartner, M.O., Elledge, S.J., Hannon, G.J., *et al*. (2011). Functional Identification of Optimized RNAi Triggers Using a Massively Parallel Sensor Assay. Molecular Cell *41*, 733-746.

Fierz, Y., Novosyadlyy, R., Vijayakumar, A., Yakar, S., and LeRoith, D. (2010). Insulin-sensitizing therapy attenuates type 2 diabetes-mediated mammary tumor progression. Diabetes *59*, 686-693.

Fiore, E., Campani, D., Muller, I., Belardi, V., Giustarini, E., Rossi, G., Pinchera, A., and Giani, C. (2010). IGF-II mRNA expression in breast cancer: predictive value and relationship to other prognostic factors. Int J Biol Markers *25*, 150-156.

Firth, S.M., and Baxter, R.C. (2002). Cellular actions of the insulin-like growth factor binding proteins. Endocrine reviews *23*, 824-854.

Fox, E.M., Miller, T.W., Balko, J.M., Kuba, M.G., Sanchez, V., Smith, R.A., Liu, S.Y., Gonzalez-Angulo, A.M., Mills, G.B., Ye, F., *et al*. (2011). A Kinome-Wide Screen Identifies the Insulin/IGF-I Receptor Pathway as a Mechanism of Escape from Hormone Dependence in Breast Cancer. Cancer research *71*, 6773-6784.

Frasca, F., Pandini, G., Scalia, P., Sciacca, L., Mineo, R., Costantino, A., Goldfine, I.D., Belfiore, A., and Vigneri, R. (1999). Insulin receptor isoform A, a newly recognized, high-affinity insulin-like growth factor II receptor in fetal and cancer cells. Mol Cell Biol *19*, 3278-3288.

Frattali, A.L., Treadway, J.L., and Pessin, J.E. (1992a). Insulin/IGF-1 hybrid receptors: implications for the dominant-negative phenotype in syndromes of insulin resistance. J Cell Biochem *48*, 43-50.

Frattali, A.L., Treadway, J.L., and Pessin, J.E. (1992b). Transmembrane signaling by the human insulin receptor kinase. Relationship between intramolecular beta subunit trans- and cis-autophosphorylation and substrate kinase activation. J Biol Chem *267*, 19521-19528.

Freier, S., Weiss, O., Eran, M., Flyvbjerg, A., Dahan, R., Nephesh, I., Safra, T., Shiloni, E., and Raz, I. (1999). Expression of the insulin-like growth factors and their receptors in adenocarcinoma of the colon. Gut *44*, 704-708.

Friedbichler, K., Hofmann, M.H., Kroez, M., Ostermann, E., Lamche, H.R., Koessl, C., Borges, E., Pollak, M.N., Adolf, G., and Adam, P.J. (2014). Pharmacodynamic and antineoplastic activity of BI 836845, a fully human IGF ligand-neutralizing antibody, and mechanistic rationale for combination with rapamycin. Molecular cancer therapeutics *13*, 399-409.

Gee, J.M., Robertson, J.F., Gutteridge, E., Ellis, I.O., Pinder, S.E., Rubini, M., and Nicholson, R.I. (2005). Epidermal growth factor receptor/HER2/insulin-like growth factor receptor signalling and oestrogen receptor activity in clinical breast cancer. Endocrine-related cancer *12 Suppl 1*, S99-S111.

Geiger, T., Wisniewski, J.R., Cox, J., Zanivan, S., Kruger, M., Ishihama, Y., and Mann, M. (2011). Use of stable isotope labeling by amino acids in cell culture as a spike-in standard in quantitative proteomics. Nature protocols *6*, 147-157.

Giansanti, P., Tsiatsiani, L., Low, T.Y., and Heck, A.J. (2016). Six alternative proteases for mass spectrometry-based proteomics beyond trypsin. Nature protocols *11*, 993-1006.

Glatter, T., Ludwig, C., Ahrne, E., Aebersold, R., Heck, A.J., and Schmidt, A. (2012). Large-scale quantitative assessment of different in-solution protein digestion protocols reveals superior cleavage efficiency of tandem Lys-C/trypsin proteolysis over trypsin digestion. Journal of proteome research *11*, 5145-5156.

Goenaga, D., Hampe, C., Carre, N., Cailliau, K., Browaeys-Poly, E., Perdereau, D., Holt, L.J., Daly, R.J., Girard, J., Broutin, I., *et al*. (2009). Molecular determinants of Grb14-mediated inhibition of insulin signaling. Molecular endocrinology *23*, 1043-1051.

Goldstein, B.J., Bittner-Kowalczyk, A., White, M.F., and Harbeck, M. (2000). Tyrosine dephosphorylation and deactivation of insulin receptor substrate-1 by protein-tyrosine phosphatase 1B. Possible facilitation by the formation of a ternary complex with the Grb2 adaptor protein. J Biol Chem *275*, 4283-4289.

Gu, T.L., Deng, X., Huang, F., Tucker, M., Crosby, K., Rimkunas, V., Wang, Y., Deng, G., Zhu, L., Tan, Z., *et al*. (2011). Survey of tyrosine kinase signaling reveals ROS kinase fusions in human cholangiocarcinoma. PLoS One *6*, e15640.

Gualberto, A., and Pollak, M. (2009). Emerging role of insulin-like growth factor receptor inhibitors in oncology: early clinical trial results and future directions. Oncogene *28*, 3009-3021.

Gupte, A., and Mora, S. (2006). Activation of the Cbl insulin signaling pathway in cardiac muscle; dysregulation in obesity and diabetes. Biochem Biophys Res Commun *342*, 751-757.

Haluska, P., Menefee, M., Plimack, E.R., Rosenberg, J., Northfelt, D., LaVallee, T., Shi, L., Yu, X.Q., Burke, P., Huang, J., *et al*. (2014). Phase I dose-escalation study of MEDI-573, a bispecific, antiligand monoclonal antibody against IGFI and IGFII, in patients with advanced solid tumors. Clin Cancer Res *20*, 4747-4757.

Haluska, P., Shaw, H.M., Batzel, G.N., Yin, D., Molina, J.R., Molife, L.R., Yap, T.A., Roberts, M.L., Sharma, A., Gualberto, A., *et al*. (2007). Phase I dose escalation study of the anti insulin-like growth factor-I receptor monoclonal antibody CP-751,871 in patients with refractory solid tumors. Clin Cancer Res *13*, 5834-5840.

Hamalisto, S., Pouwels, J., de Franceschi, N., Saari, M., Ivarsson, Y., Zimmermann, P., Brech, A., Stenmark, H., and Ivaska, J. (2013). A ZO-1/alpha5beta1-integrin complex regulates cytokinesis downstream of PKCepsilon in NCI-H460 cells plated on fibronectin. PLoS One *8*, e70696.

Han, D.C., Shen, T.L., and Guan, J.L. (2001). The Grb7 family proteins: structure, interactions with other signaling molecules and potential cellular functions. Oncogene *20*, 6315-6321.

Hanke, S., and Mann, M. (2009). The phosphotyrosine interactome of the insulin receptor family and its substrates IRS-1 and IRS-2. Molecular & cellular proteomics : MCP *8*, 519-534.

Heidegger, I., Kern, J., Ofer, P., Klocker, H., and Massoner, P. (2014). Oncogenic functions of IGF1R and INSR in prostate cancer include enhanced tumor growth, cell migration and angiogenesis. Oncotarget *5*, 2723-2735.

Heidegger, I., Ofer, P., Doppler, W., Rotter, V., Klocker, H., and Massoner, P. (2012). Diverse functions of IGF/insulin signaling in malignant and noncancerous prostate cells: proliferation in cancer cells and differentiation in noncancerous cells. Endocrinology *153*, 4633-4643.

Heldin, C.H., and Ostman, A. (1996). Ligand-induced dimerization of growth factor receptors: variations on the theme. Cytokine & growth factor reviews *7*, 3-10.

Herkert, B., Kauffmann, A., Molle, S., Schnell, C., Ferrat, T., Voshol, H., Juengert, J., Erasimus, H., Marszalek, G., Kazic-Legueux, M., *et al*. (2016). Maximizing the Efficacy of MAPK-Targeted Treatment in PTENLOF/BRAFMUT Melanoma through PI3K and IGF1R Inhibition. Cancer research *76*, 390-402.

Hills, C.E., and Brunskill, N.J. (2008). Intracellular signalling by C-peptide. Exp Diabetes Res *2008*, 635158.

Hribal, M.L., Federici, M., Porzio, O., Lauro, D., Borboni, P., Accili, D., Lauro, R., and Sesti, G. (2000). The Gly-->Arg972 amino acid polymorphism in insulin receptor substrate-1 affects glucose metabolism in skeletal muscle cells. The Journal of clinical endocrinology and metabolism *85*, 2004-2013.

Hu, C.E., Liu, Y.C., Zhang, H.D., and Huang, G.J. (2014). The RNA-binding protein PCBP2 facilitates gastric carcinoma growth by targeting miR-34a. Biochem Biophys Res Commun *448*, 437-442.

Huang, J., Morehouse, C., Streicher, K., Higgs, B.W., Gao, J., Czapiga, M., Boutrin, A., Zhu, W., Brohawn, P., Chang, Y., *et al*. (2011). Altered expression of insulin receptor isoforms in breast cancer. PLoS One *6*, e26177.

Hubbard, S.R. (1997). Crystal structure of the activated insulin receptor tyrosine kinase in complex with peptide substrate and ATP analog. The EMBO journal *16*, 5572-5581.

Hubbard, S.R. (2013). The insulin receptor: both a prototypical and atypical receptor tyrosine kinase. Cold Spring Harb Perspect Biol *5*, a008946.

Hubbard, S.R., and Till, J.H. (2000). Protein tyrosine kinase structure and function. Annual review of biochemistry *69*, 373-398.

Hubbard, S.R., Wei, L., Ellis, L., and Hendrickson, W.A. (1994). Crystal structure of the tyrosine kinase domain of the human insulin receptor. Nature *372*, 746-754.

Humbel, R.E. (1990). Insulin-like growth factors I and II. European journal of biochemistry / FEBS *190*, 445-462.

Humphrey, S.J., Azimifar, S.B., and Mann, M. (2015). High-throughput phosphoproteomics reveals in vivo insulin signaling dynamics. Nat Biotechnol *33*, 990-995.

Humphrey, S.J., Yang, G., Yang, P., Fazakerley, D.J., Stockli, J., Yang, J.Y., and James, D.E. (2013). Dynamic adipocyte phosphoproteome reveals that Akt directly regulates mTORC2. Cell Metab *17*, 1009-1020.

Hwa, V., Oh, Y., and Rosenfeld, R.G. (1999). The insulin-like growth factor-binding protein (IGFBP) superfamily. Endocrine reviews *20*, 761-787.

Inoue, H., Nojima, H., and Okayama, H. (1990). High efficiency transformation of Escherichia coli with plasmids. Gene *96*, 23-28.

Irie, H.Y., Pearline, R.V., Grueneberg, D., Hsia, M., Ravichandran, P., Kothari, N., Natesan, S., and Brugge, J.S. (2005). Distinct roles of Akt1 and Akt2 in regulating cell migration and epithelial-mesenchymal transition. J Cell Biol *171*, 1023-1034.

Jackson, J.G., and Yee, D. (1999). IRS-1 expression and activation are not sufficient to activate downstream pathways and enable IGF-I growth response in estrogen receptor negative breast cancer cells. Growth Hormone & Igf Research *9*, 280-289.

Jaquish, D.V., Yu, P.T., Shields, D.J., French, R.P., Maruyama, K.P., Niessen, S., Hoover, H., D, A.C., Cravatt, B., and Lowy, A.M. (2011). IGF1-R signals through the RON receptor to mediate pancreatic cancer cell migration. Carcinogenesis *32*, 1151-1156.

Jensen, M., Hansen, B., De Meyts, P., Schaffer, L., and Urso, B. (2007). Activation of the insulin receptor by insulin and a synthetic peptide leads to divergent metabolic and mitogenic signaling and responses. J Biol Chem *282*, 35179-35186.

Jensen, M., Palsgaard, J., Borup, R., de Meyts, P., and Schaffer, L. (2008). Activation of the insulin receptor (IR) by insulin and a synthetic peptide has different effects on gene expression in IR-transfected L6 myoblasts. Biochem J *412*, 435-445.

Jones, A.G., and Hattersley, A.T. (2013). The clinical utility of C-peptide measurement in the care of patients with diabetes. Diabet Med *30*, 803-817.

Jones, T.R., Kang, I.H., Wheeler, D.B., Lindquist, R.A., Papallo, A., Sabatini, D.M., Golland, P., and Carpenter, A.E. (2008). CellProfiler Analyst: data exploration and analysis software for complex image-based screens. BMC Bioinformatics *9*, 482.

Kasus-Jacobi, A., Bereziat, V., Perdereau, D., Girard, J., and Burnol, A.F. (2000). Evidence for an interaction between the insulin receptor and Grb7. A role for two of its binding domains, PIR and SH2. Oncogene *19*, 2052-2059.

Kishi, K., Mawatari, K., Sakai-Wakamatsu, K., Yuasa, T., Wang, M., Ogura-Sawa, M., Nakaya, Y., Hatakeyama, S., and Ebina, Y. (2007). APS-mediated ubiquitination of the insulin receptor enhances its internalization, but does not induce its degradation. Endocr J *54*, 77-88.

Kramer, H.F., Witczak, C.A., Taylor, E.B., Fujii, N., Hirshman, M.F., and Goodyear, L.J. (2006). AS160 regulates insulin- and contraction-stimulated glucose uptake in mouse skeletal muscle. J Biol Chem *281*, 31478-31485.

Lai, C.F., Chen, C.Y., and Au, L.C. (2013). Comparison between the repression potency of siRNA targeting the coding region and the 3'-untranslated region of mRNA. Biomed Res Int *2013*, 637850.

Lamhamedi-Cherradi, S.E., Menegaz, B.A., Ramamoorthy, V., Vishwamitra, D., Wang, Y., Maywald, R.L., Buford, A.S., Fokt, I., Skora, S., Wang, J., *et al*. (2016). IGF-1R and mTOR Blockade: Novel Resistance Mechanisms and Synergistic Drug Combinations for Ewing Sarcoma. J Natl Cancer Inst *108*.

Langer, C.J., Novello, S., Park, K., Krzakowski, M., Karp, D.D., Mok, T., Benner, R.J., Scranton, J.R., Olszanski, A.J., and Jassem, J. (2014). Randomized, phase III trial of first-line figitumumab in combination with paclitaxel and carboplatin versus paclitaxel and carboplatin alone in patients with advanced non-small-cell lung cancer. J Clin Oncol *32*, 2059-2066.

Larsen, M.R., Thingholm, T.E., Jensen, O.N., Roepstorff, P., and Jorgensen, T.J. (2005). Highly selective enrichment of phosphorylated peptides from peptide mixtures using titanium dioxide microcolumns. Molecular & cellular proteomics : MCP *4*, 873-886.

Lewis, R.E., Cao, L., Perregaux, D., and Czech, M.P. (1990a). Threonine 1336 of the Human Insulin-Receptor Is a Major Target for Phosphorylation by Protein Kinase-C. Biochemistry *29*, 1807-1813.

Lewis, R.E., Wu, G.P., MacDonald, R.G., and Czech, M.P. (1990b). Insulin-sensitive phosphorylation of serine 1293/1294 on the human insulin receptor by a tightly associated serine kinase. J Biol Chem *265*, 947-954.

Lewitt, M.S., Saunders, H., Phuyal, J.L., and Baxter, R.C. (1994). Complex formation by human insulin-like growth factor-binding protein-3 and human acid-labile subunit in growth hormone-deficient rats. Endocrinology *134*, 2404-2409.

Li, H., Batth, I.S., Qu, X., Xu, L., Song, N., Wang, R., and Liu, Y. (2017). IGF-IR signaling in epithelial to mesenchymal transition and targeting IGF-IR therapy: overview and new insights. Mol Cancer *16*, 6.

Li, S., Covino, N.D., Stein, E.G., Till, J.H., and Hubbard, S.R. (2003). Structural and biochemical evidence for an autoinhibitory role for tyrosine 984 in the juxtamembrane region of the insulin receptor. J Biol Chem *278*, 26007-26014.

Li, S., Wang, N., and Brodt, P. (2012). Metastatic cells can escape the proapoptotic effects of TNF-alpha through increased autocrine IL-6/STAT3 signaling. Cancer research *72*, 865-875.

Li, Y., Roux, C., Lazereg, S., LeCaer, J.P., Laprevote, O., Badet, B., and Badet-Denisot, M.A. (2007). Identification of a novel serine phosphorylation site in human glutamine:fructose-6-phosphate amidotransferase isoform 1. Biochemistry *46*, 13163-13169.

Liu, J.P., Baker, J., Perkins, A.S., Robertson, E.J., and Efstratiadis, A. (1993). Mice carrying null mutations of the genes encoding insulin-like growth factor I (Igf-1) and type 1 IGF receptor (Igf1r). Cell *75*, 59-72.

Lundby, A., Bolvig, P., Hegelund, A.C., Hansen, B.F., Worm, J., Lutzen, A., Billestrup, N., Bonnesen, C., and Oleksiewicz, M.B. (2015). Surface-expressed insulin receptors as well as IGF-I receptors both contribute to the mitogenic effects of human insulin and its analogues. Journal of applied toxicology : JAT *35*, 842-850.

Malaguarnera, R., and Belfiore, A. (2011). The insulin receptor: a new target for cancer therapy. Front Endocrinol (Lausanne) *2*, 93.

Mancini, M., Gariboldi, M.B., Taiana, E., Bonzi, M.C., Craparotta, I., Pagin, M., and Monti, E. (2014). Co-targeting the IGF system and HIF-1 inhibits migration and invasion by (triple-negative) breast cancer cells. British journal of cancer *110*, 2865-2873.

Manza, L.L., Stamer, S.L., Ham, A.J.L., Codreanu, S.G., and Liebler, D.C. (2005). Sample preparation and digestion for proteomic analyses using spin filters. Proteomics *5*, 1742-1745.

Marin, O., Meggio, F., Perich, J.W., and Pinna, L.A. (1996). Phosphotyrosine specifies the phosphorylation by protein kinase CK2 of a peptide reproducing the activation loop of the insulin receptor protein tyrosine kinase. Int J Biochem Cell Biol *28*, 999-1005.

Martinez-Quetglas, I., Pinyol, R., Dauch, D., Torrecilla, S., Tovar, V., Moeini, A., Alsinet, C., Portela, A., Rodriguez-Carunchio, L., Sole, M., *et al*. (2016). IGF2 is Upregulated by Epigenetic Mechanisms in Hepatocellular Carcinomas and is an Actionable Oncogene Product in Experimental Models. Gastroenterology.

McKern, N.M., Lawrence, M.C., Streltsov, V.A., Lou, M.Z., Adams, T.E., Lovrecz, G.O., Elleman, T.C., Richards, K.M., Bentley, J.D., Pilling, P.A., *et al*. (2006). Structure of the insulin receptor ectodomain reveals a folded-over conformation. Nature *443*, 218-221.

Mendoza, R.A., Enriquez, M.I., Mejia, S.M., Moody, E.E., and Thordarson, G. (2011). Interactions between IGF-I, estrogen receptor-alpha (ERalpha), and ERbeta in regulating growth/apoptosis of MCF-7 human breast cancer cells. The Journal of endocrinology *208*, 1-9.

Mireuta, M., Birman, E., Barmash, M., and Pollak, M. (2014). Quantification of binding of IGF-1 to BI 836845, a candidate therapeutic antibody against IGF-1 and IGF-2, and effects of this antibody on IGF-1:IGFBP-3 complexes in vitro and in male C57BL/6 mice. Endocrinology *155*, 703-715.

Mlinar, B., Marc, J., Janez, A., and Pfeifer, M. (2007). Molecular mechanisms of insulin resistance and associated diseases. Clinica chimica acta; international journal of clinical chemistry *375*, 20-35.

Moller, D.E., Yokota, A., Caro, J.F., and Flier, J.S. (1989). Tissue-specific expression of two alternatively spliced insulin receptor mRNAs in man. Molecular endocrinology *3*, 1263-1269.

Monetti, M., Nagaraj, N., Sharma, K., and Mann, M. (2011). Large-scale phosphosite quantification in tissues by a spike-in SILAC method. Nature methods *8*, 655-658.

Morali, O.G., Delmas, V., Moore, R., Jeanney, C., Thiery, J.P., and Larue, L. (2001). IGF-II induces rapid beta-catenin relocation to the nucleus during epithelium to mesenchyme transition. Oncogene *20*, 4942-4950.

Morcavallo, A., Buraschi, S., Xu, S.Q., Belfiore, A., Schaefer, L., Iozzo, R.V., and Morrione, A. (2014a). Decorin differentially modulates the activity of insulin receptor isoform A ligands. Matrix Biology *35*, 82-90.

Morcavallo, A., Buraschi, S., Xu, S.Q., Belfiore, A., Schaefer, L., Iozzo, R.V., and Morrione, A. (2014b). Decorin differentially modulates the activity of insulin receptor isoform A ligands. Matrix Biol *35*, 82-90.

Morcavallo, A., Gaspari, M., Pandini, G., Palummo, A., Cuda, G., Larsen, M.R., Vigneri, R., and Belfiore, A. (2011). Research resource: New and diverse substrates for the insulin receptor isoform A revealed by quantitative proteomics after stimulation with IGF-II or insulin. Mol Endocrinol *25*, 1456-1468.

Morcavallo, A., Genua, M., Palummo, A., Kletvikova, E., Jiracek, J., Brzozowski, A.M., Iozzo, R.V., Belfiore, A., and Morrione, A. (2012). Insulin and insulin-like growth factor II differentially regulate endocytic sorting and stability of insulin receptor isoform A. J Biol Chem *287*, 11422-11436.

Morrione, A., Valentinis, B., Xu, S.Q., Yumet, G., Louvi, A., Efstratiadis, A., and Baserga, R. (1997). Insulin-like growth factor II stimulates cell proliferation through the insulin receptor. Proceedings of the National Academy of Sciences of the United States of America *94*, 3777-3782.

Muthu, M., Cheriyan, V.T., Munie, S., Levi, E., Frank, J., Ashour, A.E., Singh, M., and Rishi, A.K. (2014). Mechanisms of neuroblastoma cell growth inhibition by CARP-1 functional mimetics. PLoS One *9*, e102567.

Muthu, M., Cheriyan, V.T., and Rishi, A.K. (2015). CARP-1/CCAR1: a biphasic regulator of cancer cell growth and apoptosis. Oncotarget *6*, 6499-6510.

Neubauer, H., Clare, S.E., Wozny, W., Schwall, G.P., Poznanovic, S., Stegmann, W., Vogel, U., Sotlar, K., Wallwiener, D., Kurek, R., *et al.* (2008). Breast cancer proteomics reveals correlation between estrogen receptor status and differential phosphorylation of PGRMC1. Breast Cancer Res *10*, R85.

Neubauer, H., Ma, Q., Zhou, J., Yu, Q., Ruan, X., Seeger, H., Fehm, T., and Mueck, A.O. (2013). Possible role of PGRMC1 in breast cancer development. Climacteric *16*, 509-513.

Ong, S.E., and Mann, M. (2006). A practical recipe for stable isotope labeling by amino acids in cell culture (SILAC). Nature protocols *1*, 2650-2660.

Orci, L. (1986). The insulin cell: its cellular environment and how it processes (pro)insulin. Diabetes Metab Rev *2*, 71-106.

Pandini, G., Conte, E., Medico, E., Sciacca, L., Vigneri, R., and Belfiore, A. (2004). IGF-II binding to insulin receptor isoform A induces a partially different gene expression profile from insulin binding. Ann N Y Acad Sci *1028*, 450-456.

Pandini, G., Frasca, F., Mineo, R., Sciacca, L., Vigneri, R., and Belfiore, A. (2002a). Insulin/insulin-like growth factor I hybrid receptors have different biological characteristics depending on the insulin receptor isoform involved. Journal of Biological Chemistry *277*, 39684-39695.

Pandini, G., Frasca, F., Mineo, R., Sciacca, L., Vigneri, R., and Belfiore, A. (2002b). Insulin/insulin-like growth factor I hybrid receptors have different biological characteristics depending on the insulin receptor isoform involved. J Biol Chem *277*, 39684-39695.

Pandini, G., Medico, E., Conte, E., Sciacca, L., Vigneri, R., and Belfiore, A. (2003). Differential gene expression induced by insulin and insulin-like growth factor-II through the insulin receptor isoform A. J Biol Chem *278*, 42178-42189.

Pandini, G., Vigneri, R., Costantino, A., Frasca, F., Ippolito, A., Fujita-Yamaguchi, Y., Siddle, K., Goldfine, I.D., and Belfiore, A. (1999). Insulin and insulin-like growth factor-I (IGF-I) receptor overexpression in breast cancers leads to insulin/IGF-I hybrid receptor overexpression: evidence for a second mechanism of IGF-I signaling. Clin Cancer Res *5*, 1935-1944.

Park, J.H., Choi, Y.J., Kim, S.Y., Lee, J.E., Sung, K.J., Park, S., Kim, W.S., Song, J.S., Choi, C.M., Sung, Y.H., *et al*. (2016a). Activation of the IGF1R pathway potentially mediates acquired resistance to mutant-selective 3rd-generation EGF receptor tyrosine kinase inhibitors in advanced non-small cell lung cancer. Oncotarget *7*, 22005-22015.

Park, J.Y., Lee, J.Y., Zhang, Y., Hoffman, R.M., and Bouvet, M. (2016b). Targeting the insulin growth factor-1 receptor with fluorescent antibodies enables high resolution imaging of human pancreatic cancer in orthotopic mouse models. Oncotarget.

Parker, B.L., Yang, G., Humphrey, S.J., Chaudhuri, R., Ma, X., Peterman, S., and James, D.E. (2015). Targeted phosphoproteomics of insulin signaling using data-independent acquisition mass spectrometry. Sci Signal *8*, rs6.

Pavelic, J., Matijevic, T., and Knezevic, J. (2007). Biological & physiological aspects of action of insulin-like growth factor peptide family. The Indian journal of medical research *125*, 511-522.

Pawson, T. (1995). Protein modules and signalling networks. Nature *373*, 573-580.

Peck, G.R., Ye, S., Pham, V., Fernando, R.N., Macaulay, S.L., Chai, S.Y., and Albiston, A.L. (2006). Interaction of the Akt substrate, AS160, with the glucose transporter 4 vesicle marker protein, insulin-regulated aminopeptidase. Molecular endocrinology *20*, 2576-2583.

Perrotti, D., Cesi, V., Trotta, R., Guerzoni, C., Santilli, G., Campbell, K., Iervolino, A., Condorelli, F., Gambacorti-Passerini, C., Caligiuri, M.A., *et al*. (2002). BCR-ABL suppresses C/EBPalpha expression through inhibitory action of hnRNP E2. Nat Genet *30*, 48-58.

Petersen, M.C., Madiraju, A.K., Gassaway, B.M., Marcel, M., Nasiri, A.R., Butrico, G., Marcucci, M.J., Zhang, D., Abulizi, A., Zhang, X.M., *et al*. (2016). Insulin receptor Thr(1160) phosphorylation mediates lipid-induced hepatic insulin resistance. Journal of Clinical Investigation *126*, 4361-4371.

Pezzino, V., Papa, V., Milazzo, G., Gliozzo, B., Russo, P., and Scalia, P.L. (1996). Insulin-like growth factor-I (IGF-I) receptors in breast cancer. Ann N Y Acad Sci *784*, 189-201.

Pierre-Eugene, C., Pagesy, P., Nguyen, T.T., Neuille, M., Tschank, G., Tennagels, N., Hampe, C., and Issad, T. (2012). Effect of insulin analogues on insulin/IGF1 hybrid receptors: increased activation by glargine but not by its metabolites M1 and M2. PLoS One *7*, e41992.

Pisani, P. (2008). Hyper-insulinaemia and cancer, meta-analyses of epidemiological studies. Archives of physiology and biochemistry *114*, 63-70.

Pivonello, C., Negri, M., De Martino, M.C., Napolitano, M., de Angelis, C., Provvisiero, D.P., Cuomo, G., Auriemma, R.S., Simeoli, C., Izzo, F., *et al*. (2016). The dual targeting of insulin and insulin-like growth factor 1 receptor enhances the mTOR inhibitor-mediated antitumor efficacy in hepatocellular carcinoma. Oncotarget.

Pollak, M. (2008). Insulin and insulin-like growth factor signalling in neoplasia. Nature reviews Cancer *8*, 915-928.

Pollak, M. (2012). The insulin and insulin-like growth factor receptor family in neoplasia: an update. Nature reviews Cancer *12*, 159-169.

Radhakrishnan, V.K., Hernandez, L.C., Anderson, K., Tan, Q., De Leon, M., and De Leon, D.D. (2015). Expression of Intratumoral IGF-II Is Regulated by the Gene Imprinting Status in Triple Negative Breast Cancer from Vietnamese Patients. Int J Endocrinol *2015*, 401851.

Rajapaksha, H., and Forbes, B.E. (2015). Ligand-Binding Affinity at the Insulin Receptor Isoform-A and Subsequent IR-A Tyrosine Phosphorylation Kinetics are Important Determinants of Mitogenic Biological Outcomes. Front Endocrinol (Lausanne) *6*, 107.

Rappsilber, J., Mann, M., and Ishihama, Y. (2007). Protocol for micro-purification, enrichment, pre-fractionation and storage of peptides for proteomics using StageTips. Nature protocols *2*, 1896-1906.

Reynolds, A., Leake, D., Boese, Q., Scaringe, S., Marshall, W.S., and Khvorova, A. (2004). Rational siRNA design for RNA interference. Nature Biotechnology *22*, 326-330.

Rinderknecht, E., and Humbel, R.E. (1976). Amino-terminal sequences of two polypeptides from human serum with nonsuppressible insulin-like and cell-growth-promoting activities: evidence for structural homology with insulin B chain. Proceedings of the National Academy of Sciences of the United States of America *73*, 4379-4381.

Rose, D.P., and Vona-Davis, L. (2012). The cellular and molecular mechanisms by which insulin influences breast cancer risk and progression. Endocrine-related cancer *19*, R225-241.

Rota, L.M., Albanito, L., Shin, M.E., Goyeneche, C.L., Shushanov, S., Gallagher, E.J., LeRoith, D., Lazzarino, D.A., and Wood, T.L. (2014). IGF1R inhibition in mammary epithelia promotes canonical Wnt signaling and Wnt1-driven tumors. Cancer research *74*, 5668-5679.

Rota, L.M., and Wood, T.L. (2015). Crosstalk of the Insulin-Like Growth Factor Receptor with the Wnt Signaling Pathway in Breast Cancer. Front Endocrinol (Lausanne) *6*, 92.

Sacco, A., Morcavallo, A., Pandini, G., Vigneri, R., and Belfiore, A. (2009). Differential signaling activation by insulin and insulin-like growth factors I and II upon binding to insulin receptor isoform A. Endocrinology *150*, 3594-3602.

Saito, T., and Saetrom, P. (2010). MicroRNAs--targeting and target prediction. N Biotechnol *27*, 243-249.

Saldana, S.M., Lee, H.H., Lowery, F.J., Khotskaya, Y.B., Xia, W., Zhang, C., Chang, S.S., Chou, C.K., Steeg, P.S., Yu, D., *et al*. (2013). Inhibition of type I insulin-like growth factor receptor signaling attenuates the development of breast cancer brain metastasis. PLoS One *8*, e73406.

Sanchez-Lopez, E., Flashner-Abramson, E., Shalapour, S., Zhong, Z., Taniguchi, K., Levitzki, A., and Karin, M. (2016). Targeting colorectal cancer via its microenvironment by inhibiting IGF-1 receptor-insulin receptor substrate and STAT3 signaling. Oncogene *35*, 2634-2644.

Sanderson, M.P., Apgar, J., Garin-Chesa, P., Hofmann, M.H., Kessler, D., Quant, J., Savchenko, A., Schaaf, O., Treu, M., Tye, H., *et al*. (2015). BI 885578, a novel IGF1R/INSR tyrosine kinase inhibitor with pharmacokinetic properties that dissociate anti-tumor efficacy and perturbation of glucose homeostasis. Molecular cancer therapeutics.

Sasi, W., Ye, L., Jiang, W.G., Mokbel, K., and Sharma, A. (2014). Observations on the effects of Suppressor of Cytokine Signaling 7 (SOCS7) knockdown in breast cancer cells: their in vitro response to Insulin Like Growth Factor I (IGF-I). Clin Transl Oncol *16*, 476-487.

Sato, Y., Hayashi, K., Amano, Y., Takahashi, M., Yonemura, S., Hayashi, I., Hirose, H., Ohno, S., and Suzuki, A. (2014). MTCL1 crosslinks and stabilizes non-centrosomal microtubules on the Golgi membrane. Nat Commun *5*, 5266.

Sawka-Verhelle, D., Tartare-Deckert, S., White, M.F., and Van Obberghen, E. (1996). Insulin receptor substrate-2 binds to the insulin receptor through its phosphotyrosine-binding domain and through a newly identified domain comprising amino acids 591-786. J Biol Chem *271*, 5980-5983.

Saxena, N.K., Taliaferro-Smith, L., Knight, B.B., Merlin, D., Anania, F.A., O'Regan, R.M., and Sharma, D. (2008). Bidirectional crosstalk between leptin and insulin-like growth factor-I

signaling promotes invasion and migration of breast cancer cells via transactivation of epidermal growth factor receptor. Cancer research *68*, 9712-9722.

Scagliotti, G.V., Bondarenko, I., Blackhall, F., Barlesi, F., Hsia, T.C., Jassem, J., Milanowski, J., Popat, S., Sanchez-Torres, J.M., Novello, S., *et al*. (2015). Randomized, phase III trial of figitumumab in combination with erlotinib versus erlotinib alone in patients with nonadenocarcinoma nonsmall-cell lung cancer. Ann Oncol *26*, 497-504.

Schillaci, R., Salatino, M., Cassataro, J., Proietti, C.J., Giambartolomei, G.H., Rivas, M.A., Carnevale, R.P., Charreau, E.H., and Elizalde, P.V. (2006). Immunization with murine breast cancer cells treated with antisense oligodeoxynucleotides to type I insulin-like growth factor receptor induced an antitumoral effect mediated by a CD8+ response involving Fas/Fas ligand cytotoxic pathway. J Immunol *176*, 3426-3437.

Schnarr, B., Strunz, K., Ohsam, J., Benner, A., Wacker, J., and Mayer, D. (2000). Down-regulation of insulin-like growth factor-I receptor and insulin receptor substrate-1 expression in advanced human breast cancer. Int J Cancer *89*, 506-513.

Sciacca, L., Costantino, A., Pandini, G., Mineo, R., Frasca, F., Scalia, P., Sbraccia, P., Goldfine, I.D., Vigneri, R., and Belfiore, A. (1999). Insulin receptor activation by IGF-II in breast cancers: evidence for a new autocrine/paracrine mechanism. Oncogene *18*, 2471-2479.

Sciacca, L., Mineo, R., Pandini, G., Murabito, A., Vigneri, R., and Belfiore, A. (2002). In IGF-I receptor-deficient leiomyosarcoma cells autocrine IGF-II induces cell invasion and protection from apoptosis via the insulin receptor isoform A. Oncogene *21*, 8240-8250.

Scotlandi, K., Maini, C., Manara, M.C., Benini, S., Serra, M., Cerisano, V., Strammiello, R., Baldini, N., Lollini, P.L., Nanni, P., *et al*. (2002). Effectiveness of insulin-like growth factor I receptor antisense strategy against Ewing's sarcoma cells. Cancer Gene Ther *9*, 296-307.

Sepplorenzino, L., Rosen, N., and Lebwohl, D.E. (1994). Insulin and Insulin-Like Growth-Factor Signaling Are Defective in the Mda Mb-468 Human Breast-Cancer Cell-Line. Cell Growth Differ *5*, 1077-1083.

Sesti, G. (2000). Insulin receptor substrate polymorphisms and type 2 diabetes mellitus. Pharmacogenomics *1*, 343-357.

Slaaby, R. (2015). Specific insulin/IGF1 hybrid receptor activation assay reveals IGF1 as a more potent ligand than insulin. Scientific reports *5*, 7911.

Slaaby, R., Schaffer, L., Lautrup-Larsen, I., Andersen, A.S., Shaw, A.C., Mathiasen, I.S., and Brandt, J. (2006). Hybrid receptors formed by insulin receptor (IR) and insulin-like growth factor I receptor (IGF-IR) have low insulin and high IGF-1 affinity irrespective of the IR splice variant. J Biol Chem *281*, 25869-25874.

Smith, B.J., Huang, K., Kong, G., Chan, S.J., Nakagawa, S., Menting, J.G., Hu, S.Q., Whittaker, J., Steiner, D.F., Katsoyannis, P.G., *et al*. (2010). Structural resolution of a tandem hormone-binding element in the insulin receptor and its implications for design of peptide agonists. Proceedings of the National Academy of Sciences of the United States of America *107*, 6771-6776.

Soh, C.L., McNeil, K., Owczarek, C.M., Hardy, M.P., Fabri, L.J., Pearse, M., Delaine, C.A., and Forbes, B.E. (2015). Exogenous administration of protease-resistant, non-matrix-binding IGFBP-2 inhibits tumour growth in a murine model of breast cancer. British journal of cancer *113*, 1640.

Soni, P., Lakkis, M., Poy, M.N., Fernstrom, M.A., and Najjar, S.M. (2000). The differential effects of pp120 (Ceacam 1) on the mitogenic action of insulin and insulin-like

growth factor 1 are regulated by the nonconserved tyrosine 1316 in the insulin receptor. Mol Cell Biol *20*, 3896-3905.

Stegmeier, F., Hu, G., Rickles, R.J., Hannon, G.J., and Elledge, S.J. (2005). A lentiviral microRNA-based system for single-copy polymerase II-regulated RNA interference in mammalian cells. Proceedings of the National Academy of Sciences of the United States of America *102*, 13212-13217.

Stein, E.G., Gustafson, T.A., and Hubbard, S.R. (2001). The BPS domain of Grb10 inhibits the catalytic activity of the insulin and IGF1 receptors. FEBS Lett *493*, 106-111.

Surmacz, E. (2000). Function of the IGF-I receptor in breast cancer. J Mammary Gland Biol Neoplasia *5*, 95-105.

Svensson, J., Kindblom, J., Shao, R., Moverare-Skrtic, S., Lagerquist, M.K., Andersson, N., Sjogren, K., Venken, K., Vanderschueren, D., Jansson, J.O., *et al*. (2008). Liver-derived IGF1 enhances the androgenic response in prostate. The Journal of endocrinology *199*, 489-497.

Taliaferro-Smith, L., Oberlick, E., Liu, T., McGlothen, T., Alcaide, T., Tobin, R., Donnelly, S., Commander, R., Kline, E., Nagaraju, G.P., *et al*. (2015). FAK activation is required for IGF1R-mediated regulation of EMT, migration, and invasion in mesenchymal triple negative breast cancer cells. Oncotarget *6*, 4757-4772.

Taniguchi, C.M., Emanuelli, B., and Kahn, C.R. (2006). Critical nodes in signalling pathways: insights into insulin action. Nature reviews Molecular cell biology *7*, 85-96.

Tennagels, N., Telting, D., Parvaresch, S., Maassen, J.A., and Klein, H.W. (2001). Identification of Ser(1275) and Ser(1309) as autophosphorylation sites of the human insulin receptor in intact cells. Biochem Biophys Res Commun *282*, 387-393.

Tennant, M.K., Thrasher, J.B., Twomey, P.A., Drivdahl, R.H., Birnbaum, R.S., and Plymate, S.R. (1996). Protein and messenger ribonucleic acid (mRNA) for the type 1 insulin-like growth factor (IGF) receptor is decreased and IGF-II mRNA is increased in human prostate carcinoma compared to benign prostate epithelium. The Journal of clinical endocrinology and metabolism *81*, 3774-3782.

ter Braak, B., Siezen, C.L.E., Kannegieter, N., Koedoot, E., van de Water, B., and van der Laan, J.W. (2014). Classifying the adverse mitogenic mode of action of insulin analogues using a novel mechanism-based genetically engineered human breast cancer cell panel. Arch Toxicol *88*, 953-966.

Thingholm, T.E., Jorgensen, T.J., Jensen, O.N., and Larsen, M.R. (2006). Highly selective enrichment of phosphorylated peptides using titanium dioxide. Nature protocols *1*, 1929-1935.

Tomari, Y., and Zamore, P.D. (2005). Perspective: machines for RNAi. Gene Dev *19*, 517-529.

Toretsky, J.A., and Helman, L.J. (1996). Involvement of IGF-II in human cancer. The Journal of endocrinology *149*, 367-372.

Tyanova, S., Temu, T., Sinitcyn, P., Carlson, A., Hein, M.Y., Geiger, T., Mann, M., and Cox, J. (2016). The Perseus computational platform for comprehensive analysis of (prote)omics data. Nature methods *13*, 731-740.

Uhles, S., Moede, T., Leibiger, B., Berggren, P.O., and Leibiger, I.B. (2003). Isoform-specific insulin receptor signaling involves different plasma membrane domains. J Cell Biol *163*, 1327-1337.

Ulanet, D.B., Ludwig, D.L., Kahn, C.R., and Hanahan, D. (2010). Insulin receptor functionally enhances multistage tumor progression and conveys intrinsic resistance to IGF-

1R targeted therapy. Proceedings of the National Academy of Sciences of the United States of America *107*, 10791-10798.

Vella, V., Pandini, G., Sciacca, L., Mineo, R., Vigneri, R., Pezzino, V., and Belfiore, A. (2002). A novel autocrine loop involving IGF-II and the insulin receptor isoform-A stimulates growth of thyroid cancer. The Journal of clinical endocrinology and metabolism *87*, 245-254.

von Stechow, L., Francavilla, C., and Olsen, J.V. (2015). Recent findings and technological advances in phosphoproteomics for cells and tissues. Expert Rev Proteomics *12*, 469-487.

Walchli, S., Curchod, M.L., Gobert, R.P., Arkinstall, S., and Hooft van Huijsduijnen, R. (2000). Identification of tyrosine phosphatases that dephosphorylate the insulin receptor. A brute force approach based on "substrate-trapping" mutants. J Biol Chem *275*, 9792-9796.

Ward, C.W., Menting, J.G., and Lawrence, M.C. (2013). The insulin receptor changes conformation in unforeseen ways on ligand binding: Sharpening the picture of insulin receptor activation. Bioessays *35*, 945-954.

Whittaker, L., Hao, C., Fu, W., and Whittaker, J. (2008). High-affinity insulin binding: insulin interacts with two receptor ligand binding sites. Biochemistry *47*, 12900-12909.

Wisniewski, J.R., Zougman, A., Nagaraj, N., and Mann, M. (2009). Universal sample preparation method for proteome analysis. Nature methods *6*, 359-362.

Wu, J., Tseng, Y.D., Xu, C.F., Neubert, T.A., White, M.F., and Hubbard, S.R. (2008). Structural and biochemical characterization of the KRLB region in insulin receptor substrate-2. Nat Struct Mol Biol *15*, 251-258.

Xia, J., Benner, M.J., and Hancock, R.E. (2014). NetworkAnalyst--integrative approaches for protein-protein interaction network analysis and visual exploration. Nucleic Acids Res *42*, W167-174.

Xia, J., Gill, E.E., and Hancock, R.E. (2015). NetworkAnalyst for statistical, visual and network-based meta-analysis of gene expression data. Nature protocols *10*, 823-844.

Xu, P., Jacobs, A.R., and Taylor, S.I. (1999). Interaction of insulin receptor substrate 3 with insulin receptor, insulin receptor-related receptor, insulin-like growth factor-1 receptor, and downstream signaling proteins. J Biol Chem *274*, 15262-15270.

Yamaguchi, Y., Flier, J.S., Benecke, H., Ransil, B.J., and Moller, D.E. (1993). Ligand-binding properties of the two isoforms of the human insulin receptor. Endocrinology *132*, 1132-1138.

Yoon, S., and Seger, R. (2006). The extracellular signal-regulated kinase: multiple substrates regulate diverse cellular functions. Growth factors *24*, 21-44.

Youngren, J.F. (2007). Regulation of insulin receptor function. Cell Mol Life Sci *64*, 873-891.

Yu, H., and Rohan, T. (2000). Role of the insulin-like growth factor family in cancer development and progression. J Natl Cancer Inst *92*, 1472-1489.

Zaykov, A.N., Mayer, J.P., and DiMarchi, R.D. (2016). Pursuit of a perfect insulin. Nat Rev Drug Discov *15*, 425-439.

Zeisberg, M., and Neilson, E.G. (2009). Biomarkers for epithelial-mesenchymal transitions. J Clin Invest *119*, 1429-1437.

Zeng, Y., Wagner, E.J., and Cullen, B.R. (2002). Both natural and designed micro RNAs can inhibit the expression of cognate mRNAs when expressed in human cells. Mol Cell *9*, 1327-1333.

Zhang, H., Fagan, D.H., Zeng, X., Freeman, K.T., Sachdev, D., and Yee, D. (2010). Inhibition of cancer cell proliferation and metastasis by insulin receptor downregulation. Oncogene *29*, 2517-2527.

Zhang, H., Pelzer, A.M., Kiang, D.T., and Yee, D. (2007). Down-regulation of type I insulin-like growth factor receptor increases sensitivity of breast cancer cells to insulin. Cancer research *67*, 391-397.

Zhao, H., Desai, V., Wang, J., Epstein, D.M., Miglarese, M., and Buck, E. (2012). Epithelial-mesenchymal transition predicts sensitivity to the dual IGF-1R/IR inhibitor OSI-906 in hepatocellular carcinoma cell lines. Molecular cancer therapeutics *11*, 503-513.

Zhong, H., Fazenbaker, C., Chen, C., Breen, S., Huang, J., Yao, X., Ren, P., Yao, Y., Herbst, R., and Hollingsworth, R.E. (2016). Overproduction of IGF-2 drives a subset of colorectal cancer cells, which specifically respond to an anti-IGF therapeutic antibody and combination therapies. Oncogene.

Zibrova, D., Vandermoere, F., Goransson, O., Peggie, M., Marino, K.V., Knierim, A., Spengler, K., Weigert, C., Viollet, B., Morrice, N.A., *et al*. (2017). GFAT1 phosphorylation by AMPK promotes VEGF-induced angiogenesis. Biochem J *474*, 983-1001.

Ziegler, A.N., Chidambaram, S., Forbes, B.E., Wood, T.L., and Levison, S.W. (2014). Insulin-like growth factor-II (IGF-II) and IGF-II analogs with enhanced insulin receptor-a binding affinity promote neural stem cell expansion. J Biol Chem *289*, 4626-4633.

Appendix

Appendix 1 pENTR1a-dsRed-miR30c

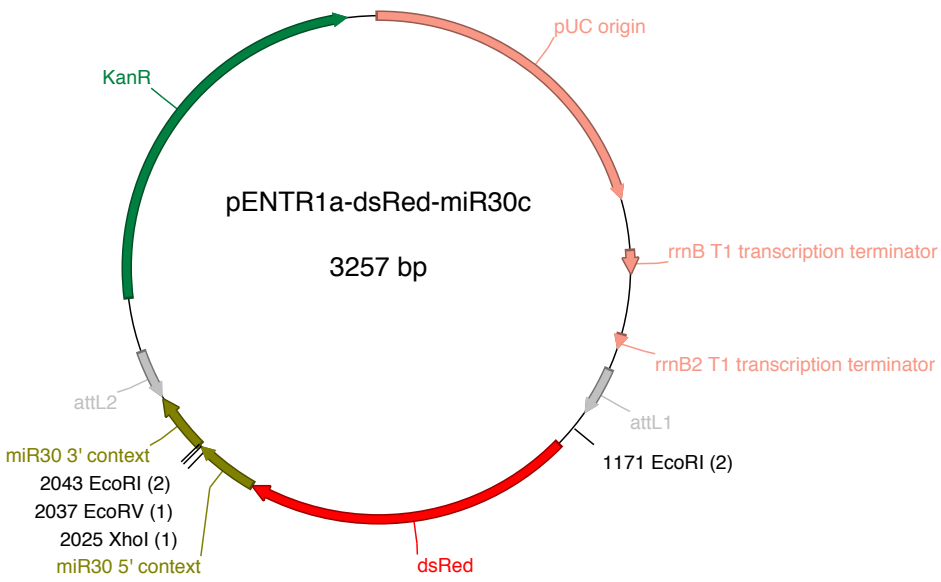

Appendix 1: Map of pENTR1a-dsRed-miR30c. KanR: Kanamycin resistance gene; pUC origin: origin of replication; dsRed: DsRed-expressed fluorescent protein gene. Restriction sites and their locations used for construction are also shown.

Appendix 2. pENTR1a-dsRed-miR30c-shRNA

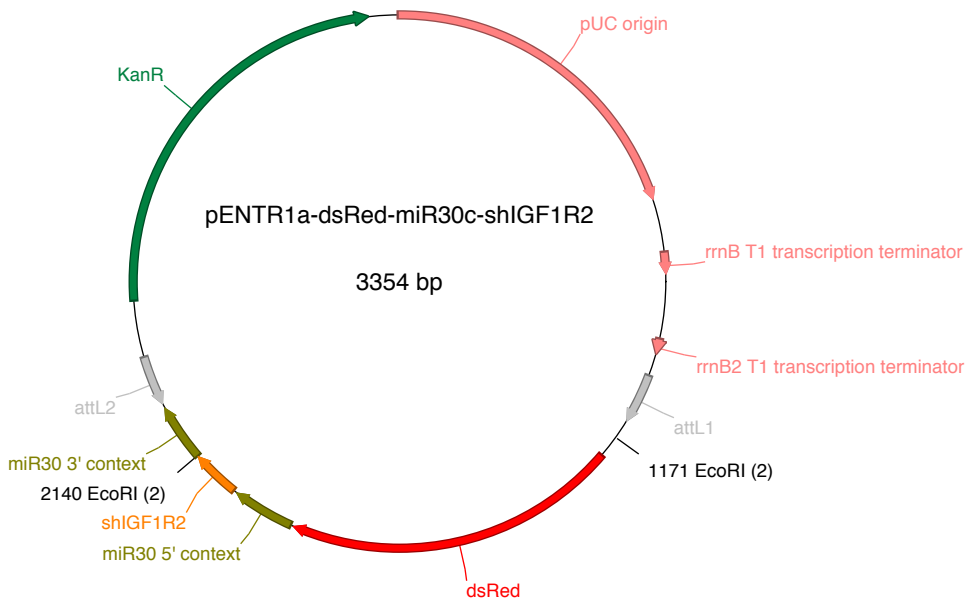

Appendix 2: Map of pENTR1a-dsRed-miR30c-shRNA. KanR: Kanamycin resistance gene; pUC origin: origin of replication; dsRed: DsRed-expressed fluorescent protein gene. shRNA (shIGF-1R2 used as example), Restriction sites and their locations used for construction are also shown.

Appendix3 pLVTPT

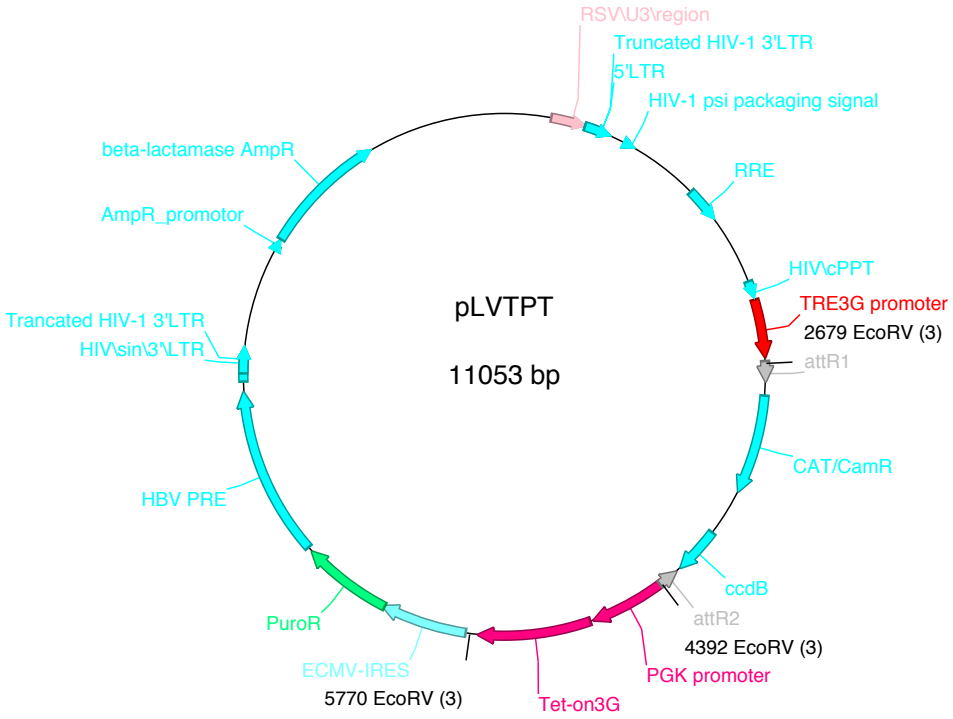

Appendix 3: Map of pLVTPT. Beta-lactamase AmpR: Ampicillin resistance gene; 5’ LTR: Acts as an RNA pol II promoter; 3’ LTR: Terminates transcription started by 5' LTR by the addition of a poly A tract just after the R sequence. RRE: Rev Response Element; TRE3G promoter: which provides the lowest basal expression of any tetracycline-inducible promoter in the absence of bound transactivator. attR1, attR2: recombination sites; ccdB: Toxin CcdB gene; PGK promoter: phosphoglycerate kinase promoter; Tet-on3G: Tet-On 3G transactivator, which binds to and activates expression from TRE promoters in the presence of doxycycline (Dox); PuroR: puromycin resistance gene; Restriction sites and their locations used for construction are also shown.

Appendix 4 pLVTPT shRNA

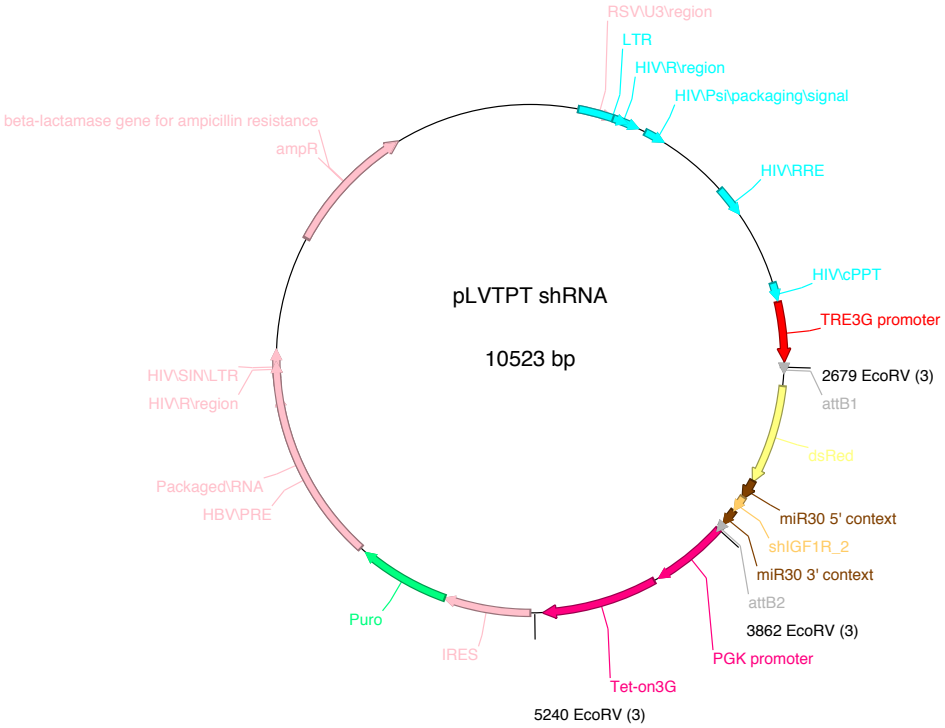

Appendix 4: Map of pLVTPT shRNA. Beta-lactamase AmpR: Ampicillin resistance gene; 5' LTR: Acts as an RNA pol II promoter; 3' LTR: Terminates transcription started by 5' LTR by the addition of a poly A tract just after the R sequence. RRE: Rev Response Element; TRE3G promoter: which provides the lowest basal expression of any tetracycline-inducible promoter in the absence of bound transactivator. attB1, attB2: recombination sites; ccdB: PGK promoter: phosphoglycerate kinase promoter; Tet-on3G: Tet-On 3G transactivator, which binds to and activates expression from TRE promoters in the presence of doxycycline (Dox); PuroR: puromycin resistance gene; shRNA (shIGF-1R2 as example) and its context, Restriction sites and their locations used for construction are also shown.

Appendix 5

No.	Range	Mono MH+	Partials	Sequence	Composition
2	[1- 28]	3477.488	1	RELEELNVPGEIVESLSSSEESITRINK(4*Phospho(ST))	C133H229N37O63P4
1	[1- 25]	3122.266	0	RELEELNVPGEIVESLSSSEESITR(4*Phospho(ST),)	C117H200N32O59P4
38	[177-202]	2997.602	1	AVPYPQRDMPIQAFLLYQEPVLGPVR	C140H217N35O36S1
41	[184-209]	2909.6	1	DMPIQAFLLYQEPVLGPVRGPFPIIV	C140H217N31O34S1
9	[29- 48]	2560.145	2	KIEKFQSEEQQQTEDELQDK(1*Phospho(ST))	C104H167N28O45P1
11	[30- 48]	2432.05	1	IEKFQSEEQQQTEDELQDK(1*Phospho(ST))	C98H155N26O44P1
40	[184-202]	2186.168	0	DMPIQAFLLYQEPVLGPVR	C102H160N24O27S1
13	[33- 48]	2061.828	0	FQSEEQQQTEDELQDK(1*Phospho(ST),)	C81H125N22O39P1
24	[100-113]	1640.829	2	EAMAPKHKEMPFPK	C74H117N19O19S2
35	[170-183]	1591.932	1	VLPVPQKAVPYPQR	C75H122N20O18
21	[98-107]	1138.64	2	VKEAMAPKHK	C50H87N15O13S1
26	[106-113]	1013.524	1	HKEMPFPK	C47H72N12O11S1
23	[100-107]	911.477	1	EAMAPKHK	C39H66N12O11S1
20	[98-105]	873.486	1	VKEAMAPK	C38H68N10O11S1
6	[26- 32]	872.556	2	INKKIEK	C39H73N11O11
37	[177-183]	830.452	0	AVPYPQR	C38H59N11O10
34	[170-176]	780.498	0	VLPVPQK	C37H65N9O9
28	[108-113]	748.37	0	EMPFPK	C35H53N7O9S1
42	[203-209]	742.45	0	GPFPIIV	C38H59N7O8

Appendix 5: Predicted trypsin digested β-casein peaks with MALDI-TOF detection.

Appendix 6

Phosphosites that were quantified and were present in at least two different biological replicates. Ratio normalized M/L (log2) = Insulin regulated phosphosites; Ratio normalized H/L (log2) = IGF-II regulated phosphosites; Known sites = Known phosphorylation sites in PhosPhoSitePlus Database (http://www.phosphosite.org); Localization Prob = phosphorylation probability; PEP = localization probability and occupancy error; Score = Andromeda score for the best associated MS/MS spectrum; Delta Score = Score difference to the second best identified peptide; Up arrow = number above 0.58 (1.5 fold upregulation), upregulated; Down arrow = number below -0.58 (1.5 fold downregualtion), downregulated; Right arrow = number between -0.58-0.58, no change.

Gene name	Amino acid_Positions	Known site	Ratio M/L normalized (log2)	Ratio H/L normalized (log2)	p<0.05 (M/L)	p<0.05 (H/L)	Localization prob	PEP	Score	Delta score
AAK1	S_623	+	-0.13	-0.04			0.83	0.0119111	55.097	16.082
AAK1	T_620	+	-0.09	-0.01			0.99	0.00779702	59.84	16.082
AAK1	S_624	+	-0.13	-0.06			0.81	0.00779702	59.84	56.46
AATF	S_316	+	0.21	0.13			1.00	7.60E-06	75.539	59.479
AATF	S_320	+	0.21	0.13			1.00	7.60E-06	75.539	59.479
AATF	S_321	+	0.21	0.13			1.00	7.60E-06	75.539	59.479
ABCF1	S_140	+	0.24	0.17	+	+	1.00	5.25E-26	124.82	124.82
ABCF1	S_105	+	-0.17	-0.22	+	+	1.00	6.86E-06	76.889	57.858
ABCF1	T_108	+	-0.06	-0.15		+	1.00	1.43E-38	147.1	74.896
ABCF1	S_109	+	0.20	-0.18		+	1.00	1.43E-38	147.1	74.896
ABLIM3	S_392	+	0.04	0.31		+	1.00	0.00241852	59.709	31.16
ABLIM3	S_393	+	0.04	0.31		+	1.00	0.00241852	59.709	31.16
ACACA	S_25	+	0.02	0.17			0.84	5.12E-10	94.955	94.955
ACACA	S_23	+	0.23	0.21	+		0.97	0.00010447	74.382	74.382
ACACA	S_29	+	0.22	0.11	+		1.00	1.03E-44	149.9	149.9
ACAP2	S_521	+	0.18	0.23	+	+	0.99	4.24E-05	92.952	63.875
ACIN1	S_240	+	0.21	0.09			0.76	3.30E-10	95.223	95.223
ACIN1	S_478	+	-0.09	-0.11	+		0.99	8.05E-24	114.66	99.599
ACIN1	S_482	+	-0.09	-0.11	+		0.75	8.05E-24	114.66	99.599
ACIN1	T_414	+	-0.04	-0.34			0.94	0.00071537	57.248	37.171
ACIN1	T_408	+	-0.44	-0.69		+	0.80	0.00057802	59.574	59.574
ACIN1	S_410	+	0.12	-0.01			0.90	1.48E-11	90.757	90.757
ACLY	S_481	+	-0.04	-0.05			1.00	0.00011263	87.99	87.99
ACSS2	S_30	+	-0.05	-0.18	+	+	1.00	4.71E-08	102.97	69.779
ACSS2	S_267	+	-0.15	-0.39	+	+	0.98	0.00050767	69.256	33.049
ACTA1;ACTA	S_197	+	0.26	0.03			0.98	1.97E-05	77.221	57.902
ADAM17	S_791	+	0.80	1.10	+	+	1.00	2.84E-05	97.223	59.566
ADD3	S_645	+	-0.01	0.10	+	+	0.99	1.22E-36	149.19	149.19
ADD3	S_641	+	-0.42	-0.25	+	+	1.00	1.22E-36	149.19	149.19
ADNP	S_953	+	0.12	0.11			1.00	0.00200153	49.924	49.924
ADNP	S_955	+	0.12	0.11			1.00	0.00200153	49.924	49.924
AFAP1	S_265	+	-0.72	-0.98	+	+	0.71	0.00669236	44.735	44.735
AFF4	S_703	+	0.14	-0.02			1.00	0.00298035	53.037	52.009
AFF4	S_706	+	0.14	-0.02			0.98	0.00298035	53.037	52.009
AHCTF1	S_1541	+	-0.25	0.07			1.00	0.00712214	72.433	28.84
AHNAK	S_5752	+	-0.02	-0.18			1.00	3.92E-51	155.47	155.47
AHNAK	S_210	+	-0.04	0.12			0.99	1.12E-64	163.49	163.49
AHNAK	S_177	+	-0.05	0.08	+		1.00	3.31E-75	176.18	113.45
AHNAK	S_135	+	0.23	0.34	+	+	1.00	2.35E-156	217.18	189.15
AHNAK	S_5731	+	-0.01	0.07			1.00	1.31E-77	180.76	140.28
AHNAK	S_4993	+	-0.11	-0.20	+		0.68	0.00040676	63.625	63.625
AHNAK	S_5110	+	-0.34	-0.24	+		1.00	4.09E-06	91.087	44.959
AHNAK	S_212	+	-0.12	-0.13	+	+	0.78	2.93E-16	118.15	118.15
AHNAK	S_511	+	0.05	0.03			1.00	2.33E-48	157.73	157.73
AHNAK	S_216	+	0.18	0.06			1.00	1.55E-51	181.54	105.2
AHNAK	S_5793	+	0.09	0.03			0.74	6.62E-06	76.804	76.804

AHNAK	S_5763	+	-0.10	-0.16	+	+	1.00	6.39E-181	228.99	228.99
AHNAK	S_5448	+	0.21	0.07	+		1.00	0.00463215	55.337	29.263
AHNAK	S_115	+	0.03	-0.05			1.00	6.83E-05	70.112	52.1
AHNAK	S_41	+	-0.04	-0.16			1.00	7.69E-96	182.77	182.77
AHNAK	S_5749	+	0.41	0.12	+		1.00	3.92E-51	155.47	155.47
AHNAK	S_5790	+	-0.12	-0.36		+	0.96	8.77E-09	85.518	85.518
AHNAK	T_5794	+	0.23	-0.17		+	0.55	3.22E-12	93.529	93.529
AKAP11	S_1240	+	-0.23	-0.01			0.78	0.00017979	75.743	50.789
AKAP11	T_1100	+	-0.37	-0.55	+	+	0.99	1.87E-09	99.092	72.544
AKAP2	S_375	+	-0.82	-0.59	+	+	0.99	0.00064809	53.278	33.564
AKAP2	S_152	+	-0.07	0.12			0.98	1.93E-33	130.05	130.05
AKAP2	S_393	+	-0.26	-0.14	+	+	1.00	7.37E-74	165	165
AKAP2	S_631	+	-0.21	-0.38	+	+	0.66	0.0188398	54.412	33.158
AKAP2	S_630	+	-0.21	-0.38	+	+	0.50	0.0188398	54.412	33.158
AKT1S1	S_212	+	-0.26	0.15			0.91	1.69E-05	79.455	29.233
AKT1S1	S_183	+	0.44	0.67	+	+	1.00	4.07E-18	119.17	119.17
AKT1S1	S_108	+	-0.95	-0.95	+	+	0.94	9.64E-10	84.674	84.674
AKT1S1	S_112	+	-0.84	-0.95		+	0.95	9.64E-10	84.674	84.674
ALKBH5	S_58	+	0.13	0.23		+	0.56	0.00015306	68.261	40.194
ALKBH5	S_53	+	0.11	0.23		+	0.93	0.00015306	68.261	40.194
ANKRD17	S_1808	+	-0.49	-0.29	+	+	1.00	9.27E-05	79.326	52.384
ANKS1A	S_666	+	0.09	0.33			1.00	5.74E-05	92.096	49.854
ANKS1A	S_663	+	0.06	0.24			0.98	2.04E-13	110.04	81.141
ANLN	S_524	+	0.03	0.29			0.76	0.00039993	98.188	52.648
ANLN	S_525	+	-0.14	-0.03			0.50	0.00039993	70.26	54.16
ANLN	S_182	+	-0.13	-0.39		+	0.93	0.00248265	47.68	47.68
ANXA1	S_5	+	0.96	1.12	+	+	1.00	0.0271567	55.064	22.744
AP2M1	T_154	+	0.35	0.29	+	+	1.00	1.26E-15	116.58	116.58
AP2M1	S_151	+	0.42	0.27	+	+	0.64	0.00247635	57.798	29.816
AP3D1	S_463	+	-0.13	-0.30	+		1.00	2.18E-05	63.701	63.701
AP3D1	S_465	+	-0.13	-0.30	+		1.00	2.18E-05	63.701	63.701
AP3D1	S_467	+	-0.13	-0.30	+		1.00	2.18E-05	63.701	63.701
ARAP1	S_229	+	-0.16	-0.48	+	+	1.00	7.98E-09	87.098	85.387
ARFGAP1	S_230	+	0.43	0.36	+	+	0.95	2.93E-10	99.409	70.085
ARFGEF2	S_227	+	-0.23	-0.16	+		1.00	1.48E-06	97.621	72.256
ARFGEF2	S_218	+	-0.18	-0.14			1.00	0.00628622	53.327	36.97
ARHGAP12	S_240	+	0.02	-0.12		+	1.00	8.21E-05	70.121	49.951
ARHGAP12	T_230	+	0.02	-0.12		+	0.50	8.21E-05	70.121	49.951
ARHGAP12	T_231	+	0.02	-0.12		+	0.50	8.21E-05	70.121	49.951
ARHGAP12	S_213	+	0.46	0.17	+		0.87	0.00129307	61.096	41.403
ARHGAP17	S_209	+	-0.62	-0.40	+		0.52	0.00023005	62.028	41.964
ARHGAP17	T_215	+	-0.62	-0.40	+		0.78	0.00063745	55.128	40.557
ARHGAP17	S_108	+	-0.47	-0.80	+	+	1.00	6.27E-10	77.907	77.907
ARHGAP17	S_207	+	-0.28	-0.74		+	0.78	0.00020105	63.158	25.632
ARHGAP18	S_24	+	0.54	0.75	+	+	0.98	0.00012869	63.674	44.327
ARHGAP18	S_21	+	0.49	0.71		+	0.82	0.00012869	63.674	44.327
ARHGAP29	S_176	+	0.94	1.11	+	+	0.77	3.41E-07	91.733	74.162
ARHGAP29	S_171	+	0.67	0.88	+	+	1.00	3.41E-07	91.733	74.162
ARHGAP29	S_1029	+	0.11	0.08			1.00	0.00506458	60.161	14.882
ARHGAP29	S_499	+	0.74	0.16			1.00	0.00142585	65.855	65.855
ARHGAP32	T_565		0.73	1.30	+	+	1.00	0.00230818	52.162	21.894

ARHGAP35	S_1176	+	0.27	0.14			0.96	8.56E-13	109.28	75.111
ARHGAP35	S_1179	+	0.52	0.34	+	+	1.00	8.56E-13	109.28	75.111
ARHGAP5	S_1218	+	0.15	0.05	+		0.74	0.00412126	94.325	49.934
ARHGAP5	T_1217	+	0.15	0.05	+		0.50	0.00530656	74.742	28.041
ARHGEF1	S_830	+	-0.04	-0.03			1.00	8.07E-05	80.541	17.45
ARHGEF18	S_1124	+	-0.64	-0.55	+	+	0.89	0.00134796	51.966	31.36
ARHGEF2	S_147	+	0.20	0.32	+	+	0.95	0.00052366	83.856	53.944
ARHGEF2	S_124	+	0.13	0.30			0.77	0.00110748	69.422	45.787
ARHGEF2	S_928	+	-0.57	-0.42	+	+	0.55	0.00675209	40.086	16.173
ARHGEF2	S_932	+	-0.57	-0.42	+	+	0.74	0.00675209	40.086	16.173
ARHGEF2	S_858	+	0.17	0.04	+		1.00	2.24E-25	123.87	123.87
ARHGEF2	S_668	+	0.06	-0.34			0.94	3.33E-17	99.641	72.291
ARHGEF6;AR	S_334	+	0.12	0.19	+		1.00	0.00284999	72.289	72.289
ARID1A	S_313	+	-0.33	-0.45	+	+	1.00	3.05E-15	112.34	112.34
ARID4B	T_474	+	0.31	0.38	+		0.99	1.39E-30	138.96	101.84
ARID4B	S_471	+	0.15	0.16	+		1.00	8.72E-64	166.38	144.18
ARID4B	Y_476	+	0.31	0.16	+		0.99	8.72E-64	166.38	144.18
ARL6IP4	S_137	+	0.28	0.19	+		1.00	4.73E-114	194.1	135.94
ASAP1	S_717	+	0.17	0.22	+		1.00	0.00461444	44.045	44.045
ATN1	S_101	+	0.02	-0.33			0.87	0.0086285	41.988	27.195
ATN1	S_107	+	0.02	-0.33			0.96	0.0086285	41.988	27.195
ATP2B1	T_1129	+	-0.14	-0.27	+		1.00	4.05E-08	84.371	66.018
ATP2B1	S_1119	+	-0.12	-0.38		+	1.00	1.23E-31	129.02	129.02
ATRX	S_392	+	-0.15	0.13			0.75	0.0118226	46.89	29.826
ATRX	S_473	+	0.11	0.02			0.97	2.82E-05	77.554	52.57
ATXN2L	S_111	+	-0.18	-0.14	+	+	1.00	5.42E-21	120.32	120.32
ATXN2L	S_594	+	-0.06	-0.14			1.00	1.92E-64	161.59	138.06
ATXN2L	S_559	+	0.10	-0.33			0.92	1.43E-15	115.91	115.91
ATXN2L	T_632	+	-0.64	-0.97	+	+	0.62	1.13E-15	95.746	65.571
ATXN2L	S_634	+	-0.76	-1.36	+	+	0.93	1.13E-15	95.746	65.571
BAG3	S_173	+	0.02	-0.04			0.79	1.62E-23	111.38	104.97
BAG3	T_285	+	-0.43	-0.55	+	+	0.81	2.92E-07	100.4	61.509
BAG3	S_289	+	-0.52	-0.55	+	+	0.98	2.92E-07	100.4	61.509
BAG3	S_291	+	-0.27	-0.42	+	+	0.79	0.0001821	87.99	53.03
BAG3	S_171	+	0.10	-0.20		+	0.72	4.84E-17	104.97	104.97
BAG3	S_381	+	-0.62	-0.84			0.67	0.0171806	42.639	18.361
BAG3	S_386	+	-0.89	-1.05	+	+	0.89	2.07E-48	141.82	141.82
BAG3	S_385	+	-0.85	-1.18	+	+	0.57	2.07E-18	166.62	135
BAG3	S_377	+	-1.02	-1.56	+	+	1.00	2.07E-48	166.62	135
BAG6	S_1003	+	0.09	-0.19		+	1.00	2.38E-06	85.397	85.397
BAP18	S_62	+	-0.20	-0.14			1.00	2.39E-08	96.464	96.464
BAZ1B	S_1464	+	0.19	-0.01	+		1.00	1.71E-39	145.73	127.71
BCL9L	S_970	+	-0.07	0.02			1.00	0.0019293	65.231	65.231
BCL9L	S_944	+	-0.19	-0.11			0.90	0.00088334	72.21	46.623
BCL9L	S_929	+	-0.17	-0.09	+		0.99	0.00066039	90.872	50.258
BCLAF1	S_510	+	-0.06	0.06			1.00	6.89E-36	147.73	117.62
BCLAF1	S_395	+	0.15	0.18	+	+	1.00	1.06E-115	238.49	209.85
BCLAF1	S_485	+	0.14	0.11	+	+	1.00	4.59E-13	111.52	53.251
BCLAF1	Y_282	+	-0.20	-0.14	+	+	0.77	0.00853315	44.662	35.164
BCLAF1	S_283	+	-0.16	-0.15	+		0.78	0.0155124	50.178	38.277
BCLAF1	S_285	+	-0.16	-0.15	+	+	0.81	0.0138447	50.178	38.277

BCLAF1	S_288	+	-0.15	-0.11			0.75	0.0129369	47.088	47.088
BCLAF1	S_383	+	0.14	0.09	+		1.00	3.56E-51	157.38	138.56
BECN1	S_421		-0.11	-0.15			0.94	0.00051297	59.242	59.242
BECN1	T_406	+	-0.11	-0.15			0.69	0.00051297	59.242	59.242
BIN1	S_265	+	-0.21	-0.34		+	0.93	5.69E-06	81.639	47.244
BIN1	S_267	+	-0.16	-0.16		+	0.81	5.69E-06	84.249	44.518
BLOC1S3	S_65	+	0.13	-0.26			1.00	0.00583738	55.977	26.69
BLOC1S3	T_63	+	0.13	-0.26			1.00	0.00583738	55.977	26.69
BMP2K	S_947	+	0.33	0.09			0.50	1.41E-05	78.025	39.84
BMP2K	S_949	+	0.33	0.09			0.50	1.41E-05	78.025	39.84
BMS1	S_639	+	0.13	-0.02			0.87	8.03E-16	118.23	58.524
BOD1L1	S_2986	+	-0.06	0.24			1.00	0.00651428	52.464	33.112
BOD1L1	S_482	+	0.07	0.07	+	+	1.00	5.85E-48	156.08	123.77
BOD1L1	S_484	+	0.07	0.07	+	+	1.00	5.85E-48	156.08	123.77
BPTF	S_2339	+	-0.20	-0.35	+	+	1.00	1.58E-07	87.323	70.082
BRD2	S_178	+	-0.13	-0.69		+	1.00	1.43E-10	119.16	95.287
BRD2	S_181	+	-0.13	-0.69		+	0.99	1.43E-10	119.16	95.287
BRD3	S_263	+	-0.15	-0.34			0.98	0.00494479	55.196	55.196
BRD8	T_124	+	-0.37	-0.09	+	+	1.00	0.00116601	69.979	69.979
BRD8	S_128	+	-0.58	-0.54	+	+	1.00	0.00116601	69.979	69.979
BYSL	S_98	+	-0.13	-0.23	+	+	1.00	3.83E-22	123.65	92.259
C11orf84	S_251	+	-0.46	-0.53		+	0.61	0.00046341	65.207	48.913
C11orf84	S_308	+	-0.40	-0.52		+	0.99	0.0346018	47.217	27.463
C11orf84	S_248	+	-0.31	-0.49		+	0.89	0.00046341	65.207	48.913
C15orf52	S_133	+	0.02	0.12			1.00	0.00026887	77.899	77.899
C1orf52	S_158	+	0.08	0.05			1.00	5.43E-112	199.91	136.45
C2CD2L	S_662	+	0.20	0.29	+	+	0.80	0.0143094	42.123	21.523
C2CD5	S_260	+	-0.19	-0.18	+	+	0.80	0.0200834	41.838	26.397
C2orf49	S_185	+	-0.25	-0.09	+		1.00	0.0189399	72.187	15.66
C9orf142	S_148	+	-0.08	0.16			1.00	0.00047025	82.651	63.408
CAD	S_1859	+	0.13	0.19			1.00	0.00212881	55.98	38.839
CANX	S_475	+	0.26	0.26	+	+	1.00	2.89E-18	121.95	74.316
CAP1	S_309	+	-0.31	-0.44	+	+	1.00	6.54E-93	185.96	185.96
CAP1	S_307	+	0.04	-0.28		+	0.98	6.54E-93	185.96	185.96
CAP1	T_306	+	0.01	-0.27	+	+	0.86	4.06E-27	130.52	130.52
CARHSP1	S_41	+	-0.15	-0.13	+	+	1.00	9.23E-05	89.26	65.882
CAST	S_125	+	-0.05	-0.13		+	0.97	2.46E-39	131.69	104.28
CCAR1	S_360		4.76	1.95	+	+	1.00	0.00043531	72.489	32.33
CCAR1	T_348		4.76	1.95	+	+	0.99	0.00043531	72.489	32.33
CCAR1	Y_347		4.76	1.95	+	+	0.98	0.00043531	72.489	32.33
CCDC43	T_139	+	0.33	0.38	+	+	1.00	4.73E-25	126.45	126.45
CCDC6	S_240	+	-0.24	-0.09	+		1.00	1.22E-25	130.77	101.81
CCDC6	S_244	+	-0.05	0.10	+		1.00	1.22E-25	130.77	101.81
CCDC86	S_47	+	-0.22	-0.35	+	+	0.99	9.32E-24	110.44	110.44
CCDC86	S_18	+	-0.04	-0.14			0.65	0.00240013	53.008	53.008
CCDC86	S_80	+	-0.31	-0.48	+	+	1.00	4.06E-11	91.64	91.64
CCDC86	S_91	+	-0.22	-0.50	+	+	1.00	4.24E-89	175.26	156.71
CCDC94	S_211	+	-0.43	-0.47	+	+	1.00	0.00014177	67.645	33.497
CCDC94	S_213	+	-0.43	-0.47	+	+	1.00	0.00014177	67.645	33.497
CCNL1	S_352	+	0.00	0.02			1.00	0.00053016	80.916	45.298
CCNL1	S_341	+	-0.32	-0.34			0.57	7.39E-13	92.034	65.315

CCNL1	S_338	+	-0.29	-0.37	+		0.88	7.39E-13	92.034	65.315
CCNL1	S_335	+	-0.07	-0.07	+		0.99	7.39E-13	92.034	65.315
CCNL1	S_342	+	-0.27	-0.39	+		0.78	7.39E-13	92.034	65.315
CCNY	S_272	+	0.18	0.22	+	+	0.83	8.53E-05	81.789	23.195
CCNYL1	S_274	+	0.39	0.12	+		1.00	4.44E-48	160.03	131.64
CD2AP	S_458	+	0.95	1.09	+	+	1.00	5.17E-75	173.19	134.61
CD3EAP	S_136	+	0.20	-1.15		+	1.00	8.43E-05	65.801	45.195
CD44	S_304	+	-0.12	-0.01	+		1.00	1.76E-05	82.651	56.003
CDC23	S_470	+	0.12	0.12			0.71	0.00216651	54.004	28.304
CDC23	T_478	+	0.12	0.12			1.00	0.00177253	84.479	53.058
CDC26	S_42	+	0.45	-0.11	+		1.00	1.26E-07	78.3	78.3
CDC37	S_13	+	0.22	0.40		+	0.93	0.00020784	51.659	31.538
CDC42EP1	S_192	+	0.03	0.12			1.00	5.56E-15	109.72	61.877
CDC42EP1	S_121	+	-0.04	-0.13			1.00	0.00015837	70.994	70.994
CDC42EP1	S_195	+	0.04	0.12		+	1.00	5.56E-15	109.72	61.877
CDC42EP1	S_343	+	0.44	0.03			1.00	0.00996573	88.108	63.693
CDC42EP1	S_346	+	0.44	0.03			1.00	0.00996573	88.108	63.693
CDC42EP2	S_141	+	-0.33	-0.53			0.88	0.00401204	45.237	29.577
CDC42EP2	T_137	+	-0.33	-0.53			1.00	0.00401204	45.237	29.577
CDC42EP3	S_89	+	-0.41	-0.34	+		0.57	0.00266957	61.709	61.709
CDC42EP3	S_100	+	-0.19	-0.12		+	0.99	8.98E-08	89.029	55.482
CDK1;CDK2;(	Y_15	+	0.10	0.25		+	1.00	3.09E-25	132.06	68.899
CDK1;CDK2;(	T_14	+	-0.13	-0.01		+	1.00	9.17E-35	144.77	54.619
CDK11A;CDK	S_124	+	0.22	-0.24			1.00	7.98E-05	68.434	52.773
CDK11A;CDK	T_123	+	0.22	-0.24			1.00	7.98E-05	68.434	52.773
CDK11A;CDK	S_14	+	0.17	0.12			1.00	5.96E-37	146.28	146.28
CDK12	S_684	+	-0.35	-0.61	+	+	1.00	2.77E-26	110.6	110.6
CDK12	S_680	+	-0.39	-0.74	+	+	1.00	2.77E-26	110.6	110.6
CDK13	S_395	+	-0.07	0.15		+	1.00	6.74E-08	104.16	64.733
CDK13	S_397	+	-0.07	0.15		+	1.00	6.74E-08	104.16	64.733
CDK13	S_400	+	-0.07	0.15		+	0.98	6.74E-08	104.16	64.733
CDK13	S_437	+	0.12	0.02			0.95	0.0175624	45.452	45.452
CDYL	S_160	+	0.05	-0.29			0.64	3.28E-05	54.711	54.711
CEP170	S_356	+	-0.03	0.04			1.00	6.46E-18	120.59	83.99
CEP170	S_359	+	-0.03	0.04			1.00	6.46E-18	120.59	83.99
CEP55	S_428	+	-0.40	-0.26	+		0.96	1.82E-27	133.35	133.35
CFL1	S_3	+	0.05	0.25	+	+	1.00	2.78E-91	184.51	127.24
CFL2	S_3	+	0.14	0.29	+	+	1.00	6.55E-05	93.424	38.177
CHAMP1	S_217	+	-0.49	-0.45	+		0.74	5.02E-05	70.837	70.837
CHAMP1	S_282	+	-0.25	-0.37	+		1.00	0.00055854	90.453	52.153
CHAMP1	S_653	+	0.11	0.13			0.92	0.00061976	65.887	46.926
CHAMP1	S_204	+	-0.46	-0.51	+	+	1.00	3.83E-05	72.433	72.433
CHAMP1	S_214	+	-0.46	-0.51	+	+	0.90	3.83E-05	72.433	72.433
CHAMP1	S_459	+	-0.06	-0.11			0.87	0.00945577	64.104	20.334
CHAMP1	S_427	+	-0.37	-0.58	+	+	1.00	5.51E-06	76.133	76.133
CHAMP1	S_432	+	-0.37	-0.58	+	+	1.00	5.51E-06	76.133	76.133
CHAMP1	S_436	+	-0.37	-0.58	+	+	1.00	5.51E-06	76.133	76.133
CHAMP1	S_286	+	-0.33	-0.42			0.93	0.00056142	90.453	52.153
CHAMP1	S_627	+	0.26	0.12	+		0.93	0.00022566	71.263	46.309
CHAMP1	S_443	+	-0.08	0.00			0.92	0.00706419	46.89	33.991

CHAMP1	S_651	+	0.27	0.26	+		0.81	6.09E-05	75.718	58.294
CHAMP1	S_452	+	-0.08	0.00			0.99	0.00706419	46.89	33.991
CHAMP1	S_652	+	0.38	0.07			0.81	6.09E-05	75.718	58.294
CHD4	T_1553	+	-0.72	-0.95			0.97	0.0103178	43.501	17.039
CHD8	S_1141	+	0.12	0.16			1.00	1.18E-06	82.59	69.165
CHD8	S_1145	+	0.12	0.16			1.00	1.18E-06	82.59	69.165
CHTF18	S_453	+	-0.08	-0.02			1.00	1.60E-08	86.617	69.266
CIC	S_1373	+	-0.36	-0.70	+	+	0.91	5.46E-05	66.401	48.561
CIC	S_1382	+	-0.36	-0.70	+	+	0.57	5.46E-05	66.401	48.561
CIR1	S_202	+	0.51	0.20			1.00	0.00102108	57.145	38.823
CLASP2	S_596	+	0.09	0.03			0.86	0.0015513	81.854	51.115
CLASP2	S_525	+	-0.14	-0.01	+		0.80	0.00745797	53.861	53.861
CLASP2	S_529	+	-0.14	-0.01	+		1.00	0.00745797	53.861	53.861
CLIC6	S_293	+	0.33	0.00			0.96	5.81E-07	69.77	69.77
CLIP1	S_197	+	-0.09	0.50	+		0.62	0.00531593	66.777	29.281
CLIP1	S_204	+	0.05	0.27		+	1.00	3.73E-21	124.85	75.078
CLIP1	S_200	+	0.05	0.20		+	1.00	3.73E-21	124.85	75.078
CLNS1A	S_102	+	-0.05	-0.13		+	1.00	2.05E-89	179.33	179.33
CLSPN	S_225	+	0.00	0.07			1.00	2.09E-39	135.64	114.87
COIL	T_122	+	-0.11	-0.14			1.00	0.00054127	79.837	54.218
COPA	S_173	+	0.10	0.13	+		1.00	4.12E-05	93.106	93.106
COPB2	S_830	+	0.11	-0.01			0.92	0.0001357	63.128	63.128
COPB2	T_832	+	-0.08	-0.09			0.76	0.00139608	54.985	54.985
CPD	T_1123	+	0.04	0.02			0.96	0.00140006	48.567	39.527
CSNK2B	S_2	+	0.32	0.38			0.65	0.00226909	79.489	52.83
CSNK2B	S_3	+	0.32	0.38			0.69	0.00226909	79.489	52.83
CSNK2B	S_4	+	0.32	0.38			0.65	0.00793297	43.164	29.556
CTAGE5	S_456	+	0.68	0.61			1.00	7.96E-05	85.576	70.456
CTNNA1	S_271	+	0.15	-0.07	+		1.00	5.42E-181	229.68	202.52
CTNND1	S_248	+	-0.07	-0.10			1.00	0.00740127	51.466	26.999
CTNND1	S_251	+	-0.07	-0.10			1.00	0.00740127	51.466	26.999
CTNS	S_394		-3.12	-1.50			0.82	0.0293247	43.946	16.265
CTNS	S_397	+	-3.12	-1.50			0.76	0.0293247	43.946	16.265
CTNS	S_392		-3.43	-2.57			0.51	0.0293247	41.513	15.076
CTNS	S_396		-3.43	-2.57			0.81	0.0293247	43.946	16.265
CTPS1	S_344	+	-0.01	0.18			0.97	5.50E-14	118.55	118.55
CTPS1	S_342	+	0.11	0.06			0.84	0.00113256	69.379	44.924
CTPS1	S_343	+	0.21	0.12			0.98	0.00113256	69.379	44.924
CTR9	T_925	+	0.20	0.03	+		1.00	1.54E-13	101.62	78.189
CTTN	S_389	+	0.72	0.92	+	+	0.79	0.0249585	47.499	10.576
CTTN	S_380	+	0.04	0.03			0.67	1.80E-09	108.18	92.639
CTTN	S_381	+	0.40	0.18	+	+	1.00	4.71E-94	191.36	163.42
CTTN	T_362	+	-0.18	-0.45	+	+	0.89	2.55E-29	136.77	98.718
CTTN	S_368	+	-0.14	-0.49	+	+	1.00	2.52E-51	160.12	123.67
CTTN	T_364	+	0.27	-0.34		+	1.00	2.52E-51	160.12	123.67
CTTNBP2NL	S_481	+	0.21	-0.03			0.94	0.00015856	70.986	70.986
CXADR	S_291	+	-0.49	-0.11	+		0.88	0.00587273	54.09	14.36
DAP	S_51	+	0.08	-0.01			0.99	2.40E-08	83.395	69.53
DAXX	S_596	+	-0.48	-0.29		+	0.94	9.67E-05	69.986	69.986
DAXX	S_593	+	0.02	-0.51		+	0.97	9.67E-05	69.986	69.986

DBN1	S_339	+	-0.40	-0.38	+	+	0.75	3.20E-51	151.2	109.09
DBN1	T_335	+	-0.53	-0.58	+		0.82	2.13E-21	108.57	108.57
DBN1	S_337	+	-0.37	-0.47	+	+	0.84	1.04E-22	127.9	92.859
DCAF6	S_649	+	-0.07	-0.42			0.97	7.53E-05	73.865	73.865
DCAF6	S_657	+	0.12	-0.07			0.98	6.66E-05	73.865	73.865
DCAF6	T_654	+	0.08	-0.34			0.95	6.66E-05	67.153	44.613
DCAF8	S_99	+	0.45	0.45		+	1.00	0.00810893	54.875	29.617
DCP1A	S_281	+	-0.72	-0.49	+	+	0.89	3.18E-09	79.512	79.512
DCP1A	S_277	+	-0.72	-0.43	+	+	0.98	3.18E-09	79.512	79.512
DCP1A	T_283	+	-0.78	-0.51	+	+	0.88	9.16E-05	52.721	52.721
DDX21	S_121	+	-0.40	-0.30	+	+	1.00	2.49E-37	145.73	98.105
DDX41	S_21	+	0.14	0.59		+	0.80	0.00269044	43.696	33.257
DDX41	S_23	+	0.02	-0.05			1.00	0.00269044	51.688	35.048
DDX42	S_109	+	-0.04	-0.08			1.00	2.93E-06	87.496	63.139
DDX42	S_111	+	-0.04	-0.08			1.00	2.93E-06	87.496	63.139
DDX46	S_804	+	0.15	0.12	+		1.00	0.00041846	56.225	45.566
DDX54	T_70		-0.62	-0.89	+	+	0.62	2.50E-24	119.37	86.102
DDX55	S_151	+	0.23	0.11			1.00	1.31E-10	97.059	97.059
DEK	T_15	+	-0.09	-0.03			0.97	2.23E-09	85.496	85.496
DHX16	S_106	+	0.09	-0.04		+	1.00	1.62E-13	117.22	117.22
DHX16	S_103	+	0.08	0.16	+	+	1.00	1.62E-13	117.22	117.22
DHX16	S_107	+	0.07	0.05			1.00	5.70E-13	112.56	43.533
DHX29	S_200	+	-0.15	-0.37			1.00	1.27E-07	88.951	88.951
DIDO1	S_1040	+	-0.14	0.03	+		1.00	2.89E-05	91.355	91.355
DIDO1	S_805	+	-0.35	-0.46	+		1.00	0.00349625	54.12	48.852
DKC1	S_453	+	-0.55	-0.02	+		1.00	8.02E-07	99.078	51.476
DKC1	S_451	+	-0.52	0.11	+		1.00	8.02E-07	99.078	51.476
DKC1	S_455	+	-0.23	-0.02			0.99	8.02E-07	85.362	36.455
DNAJC1	S_480	+	-0.16	0.14			0.96	3.42E-08	88.385	88.385
DNAJC1	S_479	+	-0.10	0.16			0.96	3.42E-08	88.385	88.385
DNAJC1	S_484	+	0.01	0.11			0.95	0.00277675	63.681	14.089
DNAJC2	S_60	+	-0.03	0.16			1.00	0.00177956	78.484	47.095
DNAJC2	S_63	+	-0.03	0.16			1.00	0.00177956	78.484	47.095
DNAJC5	S_10	+	0.14	0.32	+	+	0.92	1.08E-08	97.49	97.49
DNM1L	S_413	+	-0.48	-0.40	+	+	1.00	1.70E-05	88.385	67.138
DNM2	S_758	+	-0.24	0.33			0.53	9.94E-08	60.194	60.194
DNMT1	S_378	+	-0.69	-0.60	+	+	1.00	1.09E-09	88.239	64.301
DOCK5	S_1789	+	-0.23	-0.70		+	1.00	3.41E-05	74.703	35.045
DOCK5	T_1794	+	-0.23	-0.70		+	1.00	3.41E-05	74.703	35.045
DOCK7	T_907	+	-0.02	-0.43			0.82	3.73E-14	98.747	64.675
DOCK7	S_900	+	-0.11	-0.53		+	0.99	3.79E-69	178.42	135.19
DOCK9	S_37	+	0.13	0.05			1.00	1.28E-15	110.1	110.1
DOK1	S_142	+	0.13	-0.53		+	1.00	0.00112461	56.453	21.979
DOK1	S_152	+	-0.02	-0.86		+	0.99	0.00061782	61.241	61.241
DSP	S_2008	+	-0.08	0.24			0.69	4.20E-08	83.082	65.32
DSP	S_2007	+	-0.08	0.24			0.67	4.20E-08	83.082	65.32
DSTN	S_3	+	0.35	0.35	+	+	1.00	2.54E-35	141.85	116.38
DTNBP1	S_235	+	0.61	0.53	+		0.94	0.00079661	49.503	34.704
DTNBP1	S_240	+	0.61	0.53	+		0.99	0.00079661	49.503	34.704
DUT	S_11	+	-0.92	-0.56	+	+	0.99	8.54E-27	135.57	104.5

DYNC1I2	S_104	+	0.23	0.19			0.61	0.00886435	42.029	13.636
DYNC1LI1	T_512	+	-0.60	-0.46	+	+	0.91	1.56E-42	143.52	143.52
DYNC1LI1	T_513	+	-0.49	-0.44	+	+	0.94	1.56E-42	143.52	143.52
DYNC1LI1	S_207	+	-0.14	-0.41	+	+	1.00	3.18E-31	146.67	95.596
DYNC1LI1	T_515	+	-0.32	-0.61	+	+	0.72	4.76E-18	110.91	110.91
DYNC1LI1	S_510	+	-0.10	-0.59	+	+	0.89	1.17E-06	82.449	82.449
DYNC1LI1	S_516	+	-0.31	-0.71	+	+	0.92	6.01E-26	127.58	127.58
DYNC1LI2	S_117	+	0.10	0.01	+		1.00	1.27E-15	110.13	73.534
EAF1	S_165	+	-0.26	-0.34	+		1.00	0.0197078	58.32	11.018
EBAG9	S_36	+	0.27	-0.44			1.00	0.00037769	62.203	62.203
EEF1B2	S_106	+	0.50	0.38	+	+	1.00	7.33E-11	156.02	126.84
EEF1B2	S_95	+	0.13	-0.04			1.00	4.17E-135	206.95	206.95
EEF1D	S_109	+	-0.19	-0.08	+	+	0.60	0.0382145	42.976	31.861
EEF1D	S_138	+	-0.12	-0.11			1.00	3.27E-68	158.89	158.89
EFHD2	S_74	+	-0.19	-0.20	+		0.99	2.44E-19	119.37	87.476
EGFR	S_1166	+	0.60	0.52	+	+	0.99	4.55E-05	88.637	51.862
EGFR	S_1162	+	0.48	0.60	+	+	0.65	3.81E-15	108.25	108.25
EGFR	T_693	+	-0.05	-0.39		+	1.00	1.87E-42	142.93	142.93
EHBP1	S_391	+	-0.04	0.36			0.73	2.47E-08	95.153	78.588
EHBP1	S_401	+	-0.04	0.14			1.00	5.37E-11	103.92	84.514
EHBP1	S_393	+	-0.08	0.06			0.86	5.37E-11	103.51	84.209
EHBP1	S_397	+	-0.31	-0.38	+	+	1.00	5.37E-11	103.92	84.514
EHD2	S_302	+	0.10	0.06			1.00	1.75E-08	104.38	74.342
EIF2A	S_292	+	-0.27	-0.42	+	+	1.00	7.84E-62	165.16	145.87
EIF2A	S_289	+	-0.16	-0.30			0.84	6.14E-07	85.166	85.166
EIF2S2	S_2	+	0.11	0.16			1.00	0.00073484	61.165	61.165
EIF3C;EIF3CL	S_39	+	0.00	0.04			1.00	1.79E-27	138.98	104.23
EIF3G	S_42	+	-0.42	-0.45	+	+	0.96	2.27E-51	150.23	150.23
EIF3G	T_38	+	-0.52	-1.02	+	+	0.71	1.20E-08	87.352	61.942
EIF3G	T_41	+	-0.36	-0.82	+	+	0.96	2.27E-51	150.23	150.23
EIF3J	S_11	+	0.25	0.32	+	+	1.00	6.68E-28	116.73	116.73
EIF3J	S_13	+	0.22	0.15	+	+	1.00	2.13E-56	144.33	127.06
EIF4B	S_93	+	-0.13	-0.31		+	1.00	4.78E-44	146.17	146.17
EIF4EBP1	Y_34	+	0.13	0.00			0.95	0.00016534	64.583	48.277
EIF4EBP1	T_50	+	0.05	-0.02			0.78	2.61E-15	94.841	72.85
EIF4EBP1	T_46	+	0.08	-0.05			0.84	8.88E-23	108.31	104.32
EIF4EBP1	T_37	+	0.08	0.00	+		0.95	8.88E-23	108.31	104.32
EIF4EBP2	T_46	+	0.34	0.28	+		0.96	1.36E-09	79.663	65.025
EIF4EBP2	T_37	+	0.34	-0.11	+		0.90	1.36E-09	79.663	65.025
EIF5B	S_107	+	-0.06	0.70	+	+	1.00	1.42E-93	187.04	144.4
EIF5B	S_113	+	0.16	0.16	+	+	1.00	1.42E-93	188.16	131.86
EIF5B	S_214	+	0.00	0.02			1.00	1.66E-100	189.07	189.07
ELMO3	S_51		-0.15	-0.07	+		0.72	0.0126158	46.324	16.514
EME1	S_84	+	0.36	0.15	+		1.00	0.00190249	66.772	38.445
EME1	S_85	+	0.36	0.15	+		1.00	0.00190249	66.772	38.445
EME1	S_87	+	0.36	0.15	+		1.00	0.00190249	66.772	38.445
EPB41L2	S_87	+	0.17	-0.01			0.86	0.0420283	43.297	11.079
EPHA2	S_899	+	-0.35	-0.10	+		0.98	1.58E-05	94.487	94.487
EPHA2	S_897	+	-0.06	0.07	+		0.98	2.51E-08	105.19	75.558
EPHA2	S_901	+	-0.17	-0.01	+		1.00	0.00112338	77.137	50.589

EPHA2	T_898	+	-0.11	0.07	+		0.87	4.27E-07	99.069	69.489
EPN1	T_444	+	-0.06	-0.27			0.99	1.53E-14	100.01	100.01
EPN1	S_447	+	0.44	-0.01			0.82	0.00010382	67.396	46.088
EPRS	S_880	+	-0.12	-0.33		+	0.65	0.00116539	64.705	58.864
EPRS	S_886	+	-0.28	-0.72	+	+	0.90	9.95E-19	109.5	78.819
EPRS	S_885	+	-0.10	-0.62		+	0.77	1.91E-25	124.7	71.67
EPS15	S_500	+	-0.16	-0.46	+	+	1.00	2.10E-13	113.73	113.73
ERCC5	S_384	+	0.06	0.09			1.00	5.23E-13	114.03	89.53
ERCC5	S_563	+	0.08	0.24			1.00	8.01E-08	103.67	60.692
ERCC5	S_562	+	0.08	0.16			1.00	8.01E-08	103.67	60.692
ERCC6	S_429	+	0.16	-0.13			0.97	1.85E-05	60.029	31.753
ERCC6	S_430	+	0.16	-0.13			0.97	1.85E-05	60.029	31.753
ESF1	S_657	+	0.00	-0.13			1.00	0.00017606	66.31	52.505
ESF1	S_663	+	0.00	-0.13			1.00	0.00017606	66.31	52.505
ESYT2	T_160	+	0.04	-0.30		+	0.98	3.14E-14	103.85	103.85
ESYT2	S_168	+	-0.02	-0.41		+	1.00	3.14E-14	103.85	103.85
ESYT2	S_165	+	0.03	-0.34		+	0.99	3.14E-14	103.85	103.85
ESYT2	S_162	+	-0.02	-0.52		+	0.97	1.29E-10	97.94	97.94
EVA1A	S_114	+	0.12	0.17	+		1.00	2.90E-26	136.6	98.887
EVI2B	T_267	+	0.41	0.14			0.97	0.00115967	68.123	50.916
EVI2B	S_268	+	0.26	0.24	+	+	0.99	1.17E-18	127.2	127.2
EVI2B	S_295		0.11	0.00	+		0.55	0.00027813	73.294	52.022
EVI2B	S_271	+	0.17	0.26	+	+	1.00	1.17E-18	127.2	127.2
EVI2B	S_294	+	0.23	0.01	+		0.90	1.31E-13	115.74	115.74
EXOC7	S_250	+	-0.11	-0.21		+	0.97	0.00260892	59.585	12.523
EXOSC9	S_222	+	-0.09	-0.16	+	+	0.98	1.75E-19	129.17	89.508
EXOSC9	T_221	+	-0.14	-0.09			0.50	0.00039442	92.039	92.039
FAM122A	S_143	+	-0.55	-0.24	+	+	1.00	0.00513729	73.675	33.033
FAM122A	S_147	+	-0.55	-0.24	+	+	0.99	0.00513729	73.675	33.033
FAM129A	S_602	+	0.70	0.53	+	+	0.96	3.82E-06	74.222	52.272
FAM129A	S_646	+	0.29	-0.06	+		0.59	0.00676944	44.743	44.743
FAM129B	S_628	+	-0.35	-0.20	+	+	1.00	1.01E-20	102.76	102.76
FAM129B	S_633	+	-0.26	-0.38	+	+	0.99	1.01E-20	102.76	102.76
FAM129B	S_683	+	-0.34	-0.61	+	+	1.00	2.33E-14	105.71	105.71
FAM129B	S_678	+	-0.35	-0.44	+	+	0.94	2.33E-14	105.71	105.71
FAM129B	S_679	+	-0.29	-1.13	+	+	0.92	7.05E-10	93.712	93.712
FAM134C	S_118	+	0.20	0.33	+		0.99	9.02E-08	84.166	65.143
FAM134C	S_125	+	0.25	0.01	+		0.89	9.02E-08	84.166	65.143
FAM178A	S_710	+	0.06	0.27		+	1.00	0.00122432	58.461	37.513
FAM178A	T_711	+	0.06	0.27		+	1.00	0.00122432	58.461	37.513
FAM195B	S_21	+	0.14	-0.11	+		0.97	0.00113368	62.099	40.856
FAM208A	S_1042	+	-0.25	-0.08	+		0.87	0.0125388	45.722	20.38
FAM219A	T_102	+	-0.27	-0.13	+	+	1.00	4.88E-21	126.96	126.96
FAM219A	S_104	+	-0.28	-0.13	+	+	1.00	4.88E-21	126.96	126.96
FAM21A	S_539	+	0.33	0.44	+	+	1.00	4.05E-55	153.93	153.93
FAM21A;FAM	S_443	+	0.12	0.37			1.00	0.0003355	70.02	43.089
FAM21A;FAM	S_595	+	0.34	0.39			0.99	0.00081248	59.912	59.912
FAM21A;FAM	S_596	+	0.34	0.39			0.99	0.00081248	59.912	59.912
FAM21A;FAM	S_278	+	0.29	0.25	+	+	0.95	0.0014773	72.615	33.942
FAM21C	S_484	+	0.44	0.37	+	+	1.00	8.78E-24	116.05	102.47

FASN	T_2204	+	-0.14	-0.10			1.00	3.67E-67	150.64	135.27
FCHO2	S_463	+	-0.19	-0.53			0.75	8.72E-07	76.351	60.364
FCHO2	S_455	+	-0.33	-0.54	+	+	1.00	8.72E-07	76.351	60.364
FCHO2	S_500	+	0.31	-0.28		+	0.78	9.58E-09	84.674	84.674
FERMT2	S_159	+	0.21	-0.16			1.00	4.75E-06	62.034	62.034
FGFR1OP	S_160	+	-0.38	-0.16	+		1.00	0.00103406	53.254	53.254
FGFR1OP	S_156	+	-0.33	-0.23	+		0.93	0.00103406	53.254	53.254
FKBP15	S_1154	+	0.20	0.21			1.00	5.88E-08	105	105
FKBP15	S_1152	+	0.20	0.22	+	+	0.58	5.88E-08	105	105
FKBP15	S_1151	+	0.31	0.24			0.89	0.00147277	99.813	59.536
FLII	S_801	+	-0.25	-0.17	+	+	1.00	4.69E-13	114.55	90.27
FLNA	S_2144	+	-0.04	0.15		+	1.00	1.44E-07	104.68	69.639
FLNB	S_1927	+	0.30	0.07	+		1.00	3.82E-39	144.4	111.96
FLNB	S_2301	+	0.50	0.25	+	+	0.97	7.77E-05	72.286	72.286
FLNC	S_2200	+	1.57	1.50	+	+	1.00	4.00E-13	112.5	83.436
FMNL1	S_184	+	0.18	0.33	+	+	1.00	2.90E-36	144.3	121.72
FNBP4	S_116	+	-0.14	-0.03			0.98	0.00118506	53.995	31.013
FNDC3B	S_208	+	0.06	0.03			1.00	0.00413432	62.162	25.634
FOSL1	S_74	+	-0.68	-0.41	+	+	1.00	1.80E-47	151.04	151.04
FOSL2	S_161	+	-0.23	0.14	+		1.00	0.00216242	73.219	29.922
FOXK1	S_213	+	-0.52	-0.51	+	+	1.00	2.30E-14	103.6	86.989
FOXK1	S_223	+	-0.52	-0.51	+	+	1.00	2.30E-14	103.6	86.989
FOXK1	S_253	+	-0.44	-0.57	+	+	0.53	0.0297469	42.639	15.263
FOXK1	S_257	+	-0.44	-0.57	+	+	0.83	0.0297469	42.639	15.263
FOXK2	S_30	+	-0.23	-0.22	+	+	0.97	1.92E-05	47.128	19.574
FRMD6	S_167	+	-0.16	0.31		+	1.00	3.28E-12	112.53	85.023
FRMD6	S_164	+	0.12	0.08			0.99	3.28E-12	112.53	85.023
FRMD6	S_186	+	0.17	0.10			1.00	6.31E-13	108.68	76.255
FTSJ3	S_336	+	0.22	0.40	+	+	0.99	1.82E-12	96.923	96.923
FTSJ3	S_335	+	0.25	0.41	+	+	0.99	1.82E-12	96.923	96.923
FXR2	S_601	+	0.25	0.28	+	+	0.99	1.14E-06	80.031	80.031
FXR2	S_603	+	0.20	0.28	+	+	1.00	3.68E-19	110.94	110.94
FXR2	T_598	+	0.29	0.28			0.75	3.68E-19	110.94	110.94
G3BP1	S_149	+	-0.20	0.05			1.00	8.99E-14	117.21	93.911
G3BP1	S_232	+	-0.13	-0.35		+	0.78	8.65E-22	121.45	114.78
GALT	T_2		0.12	0.42			0.83	0.0103817	60.55	9.2487
GALT	T_15		0.12	0.42			0.84	0.0103817	60.55	9.2487
GATAD2A	S_107	+	-0.34	-0.25	+	+	1.00	4.18E-05	74.029	74.029
GATAD2A	S_100	+	-0.10	-0.31	+	+	1.00	2.60E-14	99.371	99.371
GATAD2A	S_114	+	-0.10	-0.31	+	+	1.00	2.60E-14	99.371	99.371
GATAD2A	S_113	+	0.05	-0.41			0.81	0.0019131	71.709	42.398
GATAD2B	S_122	+	0.03	0.01			1.00	4.93E-15	99.549	80.596
GATAD2B	T_120	+	0.03	0.01			1.00	4.93E-15	99.549	80.596
GATAD2B	S_129	+	-0.06	0.06			1.00	4.93E-15	99.549	80.596
GATAD2B	S_135	+	-0.16	-0.03			1.00	4.93E-15	99.549	80.596
GBF1	S_1298	+	-0.13	-0.23		+	0.89	4.08E-05	68.211	68.211
GBF1	S_1300	+	-0.09	-0.35			0.69	0.00152862	55.012	55.012
GFPT1	T_244	+	0.55	0.45	+	+	0.65	8.07E-18	127.66	127.66
GFPT1	S_243	+	0.67	0.48	+	+	0.99	1.29E-36	147.7	147.7
GFPT2	S_244	+	0.42	0.58			0.97	0.00353174	67.415	35.12

GIGYF2	S_26	+	→	-0.15	→	-0.46	+		0.99	5.95E-44	149.64	110.92
GIGYF2	S_30	+	→	-0.15	→	-0.46	+		1.00	5.95E-44	149.64	110.92
GIGYF2	T_25	+	→	-0.11	↓	-0.59			0.64	2.48E-09	88.627	88.627
GIT2	S_337	+	↑	1.26	↑	0.87			0.99	0.000531	106.1	70.107
GOLGA4	S_71	+	→	0.29	→	0.13	+		1.00	0.00665995	65.232	28.85
GOLGA4	S_266	+	→	0.11	→	-0.15	+		1.00	2.85E-33	130.72	88.434
GPALPP1	S_105	+	→	-0.09	→	-0.38			1.00	0.00012345	64.89	40.861
GPATCH1	S_6	+	→	0.10	→	-0.22			1.00	1.61E-27	109.19	95.901
GPATCH1	S_8	+	→	0.10	→	-0.22			1.00	1.61E-27	109.19	95.901
GPATCH8	S_1029	+	→	0.00	→	0.17			1.00	1.09E-36	140.96	112.67
GPATCH8	S_662	+	→	-0.35	↓	-0.67	+	+	0.96	1.60E-06	84.581	84.581
GPR39	S_425		→	0.16	→	0.33			0.76	2.86E-07	92.792	87.808
GPR39	S_427	+	→	0.15	→	0.12	+		0.99	2.86E-07	92.792	87.808
GPR39	S_430	+	→	0.16	→	-0.08			1.00	1.78E-05	79.025	50.194
GRK5;GRK6	S_484	+	→	0.11	→	0.16			1.00	9.18E-47	154.81	106.6
GRK5;GRK6	T_485	+	→	0.11	→	0.16			1.00	9.18E-47	154.81	106.6
GSG2	S_93	+	→	-0.09	→	-0.19		+	0.94	0.0166938	64.265	11.783
GSK3A;GSK3I	Y_216	+	→	0.12	→	0.17		+	0.74	0.0004025	84.892	56.315
GTF2F1	T_389	+	↑	0.66	↑	0.87			0.99	4.87E-10	88.108	71.868
GTF2F1	S_385	+	→	-0.20	→	0.02	+		1.00	1.92E-33	132.37	82.664
GTF2F1	S_391	+	→	0.54	↑	0.68			0.79	1.92E-33	132.37	82.664
GTSE1	S_575	+	→	-0.15	→	-0.24		+	1.00	0.00090125	65.179	36.276
GTSE1	S_580	+	→	-0.15	→	-0.24		+	1.00	0.00090125	65.179	36.276
HACD3	S_114	+	→	0.28	→	0.05	+		1.00	1.85E-47	158.65	158.65
HCFC1	S_597	+	→	-0.21	→	-0.22	+		1.00	1.17E-06	86.258	66.838
HDAC2	S_364	+	→	-0.02	→	-0.30		+	1.00	0.0016135	46.404	34.319
HDGF	S_158	+	→	-0.06	→	0.03			1.00	0.00018443	84.507	55.551
HDLBP	S_31	+	→	0.25	→	0.27			1.00	2.06E-29	133.93	133.93
HEATR6	S_642	+	→	-0.09	→	-0.31		+	0.55	0.00043956	67.648	51.577
HIRIP3	S_227	+	→	-0.20	→	-0.40			1.00	4.18E-38	150.01	115.43
HIST1H1C	S_2	+	→	-0.12	→	-0.33	+	+	0.91	0.00058827	69.747	11.624
HIST1H1E	T_18	+	↓	-0.62	↓	-0.79	+	+	1.00	5.39E-56	157.12	110.25
HJURP	S_388	+	→	-0.16	→	-0.10	+		0.97	0.0210184	42.395	22.632
HMGA1	S_36	+	→	-0.13	→	-0.15	+	+	1.00	2.56E-10	98.421	72.31
HMGA1	S_44	+	↑	0.72	→	0.32	+		1.00	1.16E-07	92.034	92.034
HMHA1	S_23	+	→	-0.23	→	-0.28	+		1.00	0.00348382	94.639	39.629
HN1	S_41	+	→	0.22	→	0.26	+	+	1.00	3.10E-62	170.22	125.53
HNRNPA1	S_4	+	→	-0.33	→	-0.17	+		0.99	9.09E-27	132.74	103.53
HNRNPA1	S_6	+	→	0.00	→	-0.02	+		1.00	9.09E-27	132.74	103.53
HNRNPA3	S_333	+	→	0.12	→	0.05			0.65	0.00040884	61.429	44.188
HNRNPC	S_180	+	→	0.27	→	0.31	+	+	1.00	2.85E-16	121.1	102.75
HNRNPH1;HI	T_100	+	→	-0.08	→	0.06			0.60	0.00285258	59.75	59.75
HNRNPH1;HI	S_104	+	→	-0.13	→	-0.02	+		0.98	2.79E-21	121.77	86.149
HNRNPU	S_252	+	→	-0.04	→	-0.37			0.90	0.00047091	44.698	31.609
HNRNPUL1	S_151	+	→	-0.03	→	-0.27			1.00	2.52E-07	72.859	64.203
HNRNPUL2	S_161	+	→	0.07	→	-0.14			0.99	0.00014132	62.765	62.765
HSF1	S_303	+	→	-0.21	→	-0.25	+		1.00	0.0265852	46.844	27.185
HSF1	S_307	+	→	-0.21	→	-0.25	+		1.00	0.0265852	46.844	27.185
HSF1	S_314	+	→	-0.01	→	-0.10			0.97	0.00100104	51.46	51.46
HSF1	S_326	+	→	-0.01	→	-0.10			0.88	0.00100104	51.46	51.46

HSP90AA1	S_252	+	0.03	-0.05			0.99	0.00201916	45.913	45.913
HSP90AA1;H	S_263	+	0.08	0.10	+	+	1.00	6.06E-267	262.59	262.59
HSP90AB1;H	S_177	+	0.09	0.18	+	+	1.00	2.56E-27	136.43	136.43
HSP90AB1;H	S_205	+	0.03	0.15		+	1.00	0.00148509	73.951	53.212
HSP90B1	S_306	+	2.15	2.20	+	+	1.00	3.26E-134	204.51	183.23
HSPB1	S_82	+	0.82	1.22	+	+	1.00	8.74E-06	96.229	35.832
HSPH1	S_516	+	0.05	0.23			0.98	3.81E-21	101.39	83.091
HTATSF1	S_713	+	0.06	0.17		+	1.00	7.92E-19	128.85	128.85
HTATSF1	S_714	+	0.06	0.17		+	1.00	7.92E-19	128.85	128.85
HTATSF1	S_676	+	0.15	0.09	+	+	1.00	5.48E-12	108.5	85.061
HTT	S_432	+	0.67	0.12			0.84	0.00011115	90.388	55.596
HTT	S_419	+	0.94	0.24			0.82	0.00011115	90.388	55.596
HUWE1	T_3908	+	-0.51	0.99	+		0.98	0.00065372	55.208	55.208
HUWE1	S_3800	+	-0.11	-0.01			0.89	6.44E-07	66.884	51.708
HUWE1	S_1898	+	0.35	0.24	+	+	1.00	5.45E-27	132.5	90.676
HUWE1	S_3903	+	-0.41	-0.80	+		1.00	6.20E-06	73.603	51.363
IFI16	S_153	+	0.18	-0.08	+		0.99	4.16E-12	94.671	60.982
IGF2BP2	S_101	+	-0.16	-0.26			1.00	6.71E-06	82.635	45.638
IGF2BP2	S_105	+	-0.18	-0.53	+	+	0.94	1.14E-07	93.215	67.339
IGF2R	S_2409	+	0.19	0.12	+		1.00	1.69E-23	111.01	111.01
INF2	T_1148	+	-0.38	-0.05			0.68	1.04E-09	84.025	58.858
INF2	S_1147	+	0.17	0.17			0.77	4.79E-17	93.712	72.469
INPPL1	S_132	+	-0.19	-0.62	+	+	1.00	0.00026443	67.415	67.415
IRF2BP2	S_175	+	0.01	-0.30		+	1.00	0.00540084	47.227	47.227
IRF2BPL	S_547	+	-0.07	-0.20	+	+	1.00	8.61E-06	87.654	64.123
IRS1	S_348	+	-0.04	0.27			0.94	5.12E-09	105.01	86.806
IRS2	S_391	+	-0.31	-0.29			1.00	2.70E-62	169.06	136.8
IRS2	S_306	+	0.40	0.46		+	0.87	4.78E-05	79.467	31.179
IRS2	S_308	+	0.56	0.33	+		0.60	2.86E-11	103.71	103.71
IRS2	S_1203	+	-0.15	-0.44	+	+	0.90	9.10E-14	99.378	99.378
IRS2	S_388	+	-0.04	-0.05			1.00	1.60E-05	89.816	89.816
IRS2	S_915	+	-0.07	-0.11			1.00	1.96E-39	147.28	117.2
IRS2	T_1202	+	-0.10	-0.35		+	0.55	5.58E-14	102.97	102.97
ITGB4	S_1387	+	0.25	-0.38	+	+	0.97	0.00076687	63.662	51.346
ITGB4	T_1385	+	0.49	-0.37	+	+	0.89	0.00076687	63.662	51.346
ITGB4	S_1384	+	0.19	-0.50	+		0.94	0.00076687	63.662	51.346
IWS1	S_287	+	0.06	-0.02			1.00	4.54E-06	94.176	77.881
IWS1	S_289	+	0.06	-0.02			1.00	4.54E-06	94.176	77.881
KANK2	S_19	+	-0.37	-0.87		+	1.00	0.00113753	64.349	64.349
KANK2	T_14	+	-0.37	-0.87		+	1.00	0.00113753	64.349	64.349
KCTD12	S_185	+	-0.26	-0.44	+	+	0.84	1.26E-56	160.23	160.23
KCTD12	S_187	+	-0.25	-0.49	+	+	0.66	8.04E-44	143.36	118.65
KDM1A	S_166	+	-0.62	-0.83	+	+	1.00	4.92E-05	60.527	42
KHSRP	S_184	+	-0.22	0.14			0.98	0.00014286	85.576	85.576
KHSRP	S_181	+	0.17	0.29		+	0.98	1.78E-05	94.007	66.326
KIAA0930	S_255	+	0.03	0.03			0.92	0.0204684	50.534	29.474
KIAA1429	S_1578	+	0.08	0.09			0.94	3.54E-05	94.82	57.311
KIF23	S_499	+	-1.13	-1.00			0.78	1.33E-06	128.52	70.539
KIF23	S_501	+	-1.13	-1.00			0.84	1.33E-06	128.52	70.539
KIF23	S_503	+	-0.50	-0.83		+	0.97	5.91E-44	145.2	145.2

KLC1	S_521	+	-0.16	0.31		+	1.00	6.07E-12	112.91	62.04
KLC1	S_524	+	-0.16	0.31		+	1.00	6.07E-12	112.91	62.04
KLC1	S_547	+	0.19	0.13	+	+	0.96	4.65E-12	110.6	86.78
KLC2	S_505	+	0.12	0.22	+	+	1.00	1.12E-37	150.09	107.28
KMT2A	S_1799	+	-0.69	-0.84	+	+	0.92	0.00137458	56.081	26.499
KMT2A	T_1807	+	-0.68	-0.86	+	+	0.99	0.00137458	56.081	26.499
KPNA2	T_61	+	0.03	-0.11	+	+	0.95	3.45E-50	155.49	120.36
KPNA2	S_62	+	0.04	-0.32	+	+	0.96	1.50E-64	167.89	167.89
KPNA3	S_60	+	0.08	0.03	+		1.00	2.49E-96	182.48	142.55
KRI1	S_171	+	0.22	0.16	+	+	1.00	5.55E-49	170.51	120.28
L1CAM	S_1172	+	0.45	0.17	+		0.99	1.80E-12	111.11	98.007
LARP1	S_697	+	-0.70	-0.50			0.99	0.00023182	83.53	62.216
LARP1	S_471	+	0.22	0.35	+	+	0.70	0.00020384	70.15	38.45
LARP1	S_689	+	0.44	0.47	+	+	0.96	0.00167041	68.525	68.525
LARP1	S_90	+	-0.20	-0.38	+	+	1.00	1.25E-13	83.764	83.764
LARP4B	S_601	+	-0.33	-0.20	+	+	0.97	0.00262141	61.213	31.208
LARP6	S_447	+	0.19	-0.40			1.00	0.00500289	84.173	48.878
LARP6	S_451	+	0.19	-0.40			0.99	0.00500289	84.173	48.878
LARP7	S_337	+	0.29	0.35	+		1.00	0.00172874	74.537	53.703
LARP7	T_338	+	0.29	0.35	+		1.00	0.00172874	74.537	53.703
LARP7	S_258	+	0.31	0.23	+	+	0.97	2.76E-21	119.34	92.795
LARP7	S_261	+	0.49	0.37	+	+	1.00	2.76E-21	119.34	92.795
LARP7	T_257	+	0.14	0.15	+		0.81	1.07E-10	98.747	78.683
LEO1	S_197	+	0.19	-0.06	+		1.00	0.00080542	83.856	57.306
LEO1	T_188	+	0.19	-0.06	+		1.00	0.00080542	83.856	57.306
LEO1	S_598	+	0.74	0.23	+		1.00	0.00019447	92.611	64.379
LIG1	S_46	+	-0.40	-0.28	+	+	1.00	4.27E-134	204.38	204.38
LIG1	T_164	+	-0.26	-0.09	+		1.00	1.19E-113	198.98	154.29
LIG1	S_36	+	-0.26	-0.39	+	+	1.00	4.27E-134	204.38	204.38
LIMA1	S_188	+	-0.13	-0.04	+		1.00	9.81E-07	97.129	97.129
LIMA1	S_225	+	0.01	0.19		+	0.77	9.53E-05	62.582	49.17
LIMCH1	S_217	+	0.14	-0.06			0.99	0.00676797	47.223	25.126
LIMCH1	T_215	+	0.14	-0.06			0.68	0.00676797	47.223	25.126
LIMCH1	S_1103	+	0.18	-0.06	+		1.00	4.33E-38	149.52	149.52
LMNA	S_516	+	0.27	0.35	+	+	1.00	8.56E-40	148.01	148.01
LMNA	S_280	+	0.05	-0.01			0.99	6.85E-12	112.12	70.103
LMNA	S_346	+	0.24	0.38		+	1.00	1.02E-12	114.56	72.648
LMNA	S_283	+	-0.02	0.01			0.98	6.33E-26	134.38	85.553
LMNA	S_278	+	0.02	0.03			1.00	6.33E-26	134.38	85.553
LMNB1;LMN	S_393	+	-0.26	-0.18	+		0.91	0.00258179	66.784	47.513
LMNB1;LMN	S_391	+	-0.18	-0.10	+		1.00	0.00258179	66.784	47.513
LMO7	S_1176	+	0.73	0.69	+	+	1.00	0.00070243	77.027	77.027
LMO7	S_342	+	0.80	0.70	+	+	1.00	2.47E-29	132.74	132.74
LMO7	S_370	+	0.48	0.38	+	+	0.99	5.58E-27	134.4	87.506
LMO7	S_471	+	0.74	0.78	+	+	1.00	1.33E-26	138.28	138.28
LMO7	S_533	+	0.15	-0.07	+	+	0.97	6.44E-24	112.37	112.37
LMO7	S_657	+	0.15	-0.22	+	+	0.95	7.81E-101	190.99	190.99
LMO7	T_656	+	-0.06	-0.30		+	0.84	5.20E-25	120.8	120.8
LMO7	S_660	+	0.35	-0.18			0.73	4.45E-21	104.77	104.77
LMO7	S_654	+	0.14	-0.32	+	+	1.00	7.81E-101	190.99	190.99

LRCH1	S_536	+	→	-0.05	→	-0.19			0.98	8.04E-25	120.44	120.44
LRCH1	S_532	+	→	-0.13	→	-0.25			1.00	8.04E-25	120.44	120.44
LRRFIP1	T_114	+	→	-0.17	→	-0.10			0.90	0.0010829	69.771	37.418
LRRFIP1	S_677	+	→	-0.29	→	0.05			0.54	2.73E-05	72.916	54.548
LRRFIP2	S_168	+	↑	0.67	→	0.36			0.99	8.20E-05	93.342	57.616
LRWD1	S_243	+	→	-0.35	→	-0.53	+	+	0.92	1.85E-12	108.71	85.199
LSM14A	S_175	+	→	-0.19	→	-0.20	+	+	1.00	0.00194971	62.035	58.116
LSM14A	S_142		→	-0.16	→	-0.25	+	+	0.60	0.0101447	60.157	24.563
LSR	S_209	+	→	-0.03	→	0.17		+	0.81	1.26E-06	96.805	69.375
LSR	S_490	+	→	0.09	→	0.24	+	+	1.00	1.71E-13	118.9	118.9
LSR	S_374	+	→	0.24	→	0.12			0.98	0.00153487	56.719	35.881
LSR	S_487	+	→	0.27	→	0.18	+	+	1.00	1.71E-13	118.9	118.9
LSR	S_337	+	→	0.01	→	-0.10			1.00	6.98E-44	144.11	144.11
LSR	T_345	+	→	-0.02	→	-0.12			0.97	1.57E-14	107.49	107.49
LSR	S_308	+	→	-0.14	↓	-0.76		+	1.00	1.50E-06	81.128	64.549
LUZP1	S_659	+	→	0.27	→	0.27	+	+	1.00	5.27E-07	85.563	65.895
LYN	S_13	+	→	0.16	→	0.18	+	+	1.00	1.65E-12	116.9	57.675
MACF1	S_2398	+	→	0.31	→	0.16			1.00	0.00087689	77.185	41.662
MACF1	T_3506	+	→	0.43	→	0.18	+		0.68	5.04E-08	79.416	79.416
MAP1B	S_2209	+	↓	-0.70	→	0.07	+		1.00	0.00555103	65.511	47.554
MAP1B	S_2211	+	↓	-0.70	→	0.07	+		1.00	0.00555103	65.511	47.554
MAP1B	S_1779	+	→	0.03	→	0.34			1.00	7.33E-11	90.729	90.729
MAP1B	S_1016	+	→	0.17	→	0.35	+	+	1.00	9.29E-06	76.351	65.808
MAP1B	S_1618	+	→	-0.58	→	-0.38	+	+	1.00	0.00141968	48.244	48.244
MAP1B	S_1620	+	→	-0.58	→	-0.38	+	+	1.00	0.00141968	48.244	48.244
MAP1B	S_1625	+	→	-0.58	→	-0.38	+	+	1.00	0.00141968	48.244	48.244
MAP1B	S_831	+	→	-0.01	→	0.15		+	1.00	2.35E-74	172.57	123.38
MAP1B	S_832	+	→	-0.01	→	0.15		+	1.00	2.35E-74	172.57	123.38
MAP1B	T_1302	+	→	-0.16	→	-0.04	+	+	0.93	7.31E-05	65.197	43.849
MAP1B	T_1949	+	→	-0.13	→	0.11			1.00	2.01E-07	99.813	70.45
MAP1B	S_1262	+	→	-0.47	↓	-0.58	+	+	0.93	9.54E-27	134.08	91.099
MAP1B	T_1503	+	→	-0.10	→	-0.18			0.74	7.53E-11	100.69	100.69
MAP1B	S_1256	+	↓	-0.65	↓	-0.61	+	+	0.99	1.63E-60	162.92	95.983
MAP1B	S_936	+	→	-0.03	→	0.09			0.89	2.53E-08	153.36	124.48
MAP1B	S_1881	+	→	-0.06	→	0.12			1.00	5.50E-131	206.13	206.13
MAP1B	S_828	+	→	-0.17	→	-0.04			0.94	0.00762393	54.859	9.7751
MAP1B	S_1501	+	→	-0.10	→	-0.07	+		1.00	4.58E-12	107.88	107.88
MAP1B	S_1785	+	→	-0.16	→	-0.15	+		1.00	2.39E-08	99.941	99.941
MAP1B	T_1788	+	→	-0.16	→	-0.15	+		1.00	7.33E-11	99.941	99.941
MAP1B	S_992	+	→	0.28	→	0.20	+		1.00	0.00123009	51.619	47.499
MAP1B	S_1782	+	→	-0.34	→	-0.23	+	+	1.00	7.33E-11	90.729	90.729
MAP1B	S_1965	+	→	-0.41	→	-0.30	+		0.99	0.00011932	83.964	58.434
MAP1B	S_1915	+	→	-0.14	→	-0.08	+	+	0.99	1.47E-37	149.31	149.31
MAP1B	S_995	+	→	0.50	↑	0.63	+		1.00	0.00123009	51.619	47.499
MAP1B	S_1396	+	→	-0.16	→	-0.13	+	+	1.00	8.55E-56	142.32	142.32
MAP1B	T_2034	+	→	-0.14	→	-0.01			1.00	0.00020931	87.429	56.431
MAP1B	S_1265	+	→	-0.02	→	-0.02			1.00	1.63E-60	162.92	95.983
MAP1B	S_1793	+	→	-0.29	→	-0.32	+	+	0.57	5.66E-51	153.14	153.14
MAP1B	S_1298	+	→	-0.37	→	-0.44	+	+	0.98	7.31E-05	65.197	43.849
MAP1B	S_937	+	→	0.10	→	0.07			0.89	2.53E-08	153.36	124.48

MAP1B	S_1258	+	-0.60	-0.73	+	+	1.00	9.54E-27	134.08	91.099
MAP1B	S_1154	+	0.04	0.13			0.66	4.82E-05	66.041	43.155
MAP1B	S_1312	+	0.16	-0.04			0.92	8.74E-06	71.905	71.905
MAP1B	S_1378	+	-0.45	-0.61	+	+	0.87	4.62E-19	115.85	78.757
MAP1B	S_1376	+	-0.45	-0.61	+	+	0.79	4.62E-19	115.85	78.757
MAP1B	T_948	+	0.15	0.17			1.00	2.40E-23	108.79	94.685
MAP1B	S_1400	+	0.10	-0.05			1.00	8.55E-56	142.32	142.32
MAP1B	S_1387	+	-0.34	-0.36			0.70	7.65E-11	97.784	65.277
MAP1B	S_1389	+	-0.07	-0.59	+	+	0.99	3.67E-68	162.72	162.72
MAP1B	S_1797	+	0.09	-0.38	+	+	1.00	5.66E-51	153.14	153.14
MAP1B	S_1260	+	0.07	-0.38	+	+	1.00	1.63E-60	162.92	95.983
MAP1B	S_1322	+	0.35	-0.22		+	0.91	0.00016665	60.562	46.37
MAP1S	S_629	+	-0.38	0.08	+		0.99	0.00571366	64.104	31.809
MAP1S	S_631	+	0.13	0.08			1.00	0.00571366	64.104	31.809
MAP1S	S_733	+	-0.12	-0.25			0.81	3.47E-14	101.53	79.886
MAP2K1	T_360	+	0.09	-0.03			0.61	0.00156986	42.709	42.709
MAP2K1;MA	S_186	+	0.09	0.23			0.98	8.12E-11	88.574	88.574
MAP2K1;MA	S_192	+	-0.17	0.08	+		1.00	5.50E-08	80.236	52.312
MAP2K1;MA	S_196	+	0.20	0.15			1.00	1.15E-24	135.1	94.052
MAP2K2	S_293	+	-0.12	-0.03			0.78	0.032888	41.838	23.522
MAP3K7	S_412	+	-0.10	0.08			1.00	2.18E-07	135.55	93.502
MAP4	T_571	+	-0.08	0.15			1.00	2.97E-19	128.73	104.79
MAP4	S_1073	+	0.32	0.22		+	1.00	1.65E-06	85.518	85.518
MAP4	S_507	+	-0.05	0.08			1.00	1.15E-26	132.87	110.96
MAP4	S_552	+	-0.03	-0.20		+	0.94	4.36E-07	92.538	30.945
MAP4	T_521	+	-0.09	-0.15		+	1.00	2.72E-47	152.94	152.94
MAP4	S_510	+	-0.04	0.10			0.99	1.15E-26	132.87	110.96
MAP7D1	S_116	+	-0.31	0.21	+		0.54	0.00127296	54.764	40.46
MAPK1	T_185	+	0.00	-0.04			1.00	9.43E-12	98.077	98.077
MAPK1	Y_187	+	0.18	-0.03			1.00	9.43E-12	98.077	98.077
MAPK1IP1L	S_15	+	-0.20	-0.56	+	+	1.00	2.22E-64	168.3	136.51
MAPK3	Y_204	+	0.12	0.18			0.99	1.28E-06	77.576	77.576
MAPK3	T_202	+	0.08	0.03			0.99	1.28E-06	77.576	77.576
MARCKS	S_101	+	-0.20	-0.27	+	+	1.00	2.23E-51	154.08	154.08
MARCKS	S_29	+	-0.22	-0.12			0.88	5.79E-07	83.751	83.751
MARCKS	S_27	+	0.01	-0.10			0.79	4.44E-26	127.32	112.59
MARCKS	S_170	+	-0.12	-0.28		+	1.00	0.0206493	53.013	25.585
MARCKS	T_120	+	0.08	-0.17		+	0.89	1.89E-05	62.049	62.049
MARCKS	S_167	+	-0.02	-0.10			0.96	4.27E-05	90.561	51.528
MARCKS	S_163	+	-0.02	-0.10			1.00	4.27E-05	90.561	51.528
MARCKSL1	S_101	+	-0.77	-1.41	+	+	1.00	0.00066054	82.529	29.082
MARCKSL1	S_104	+	-0.77	-1.41	+	+	1.00	0.00066054	82.529	29.082
MATR3	S_478	+	0.23	0.12			1.00	9.02E-06	72.676	63.201
MCM2	S_139	+	-0.30	-0.23	+	+	1.00	2.74E-08	97.08	97.08
MCM2	S_108	+	0.02	-0.01			0.92	0.00098405	54.521	54.521
MCM2	S_13	+	-0.11	-0.09		+	0.98	3.75E-11	105.01	105.01
MCRS1	S_12		0.11	-0.03			0.64	0.00861778	47.155	11.114
MDC1	S_495	+	-0.18	-0.27			1.00	0.00725168	57.316	43.276
MDC1	S_498	+	-0.18	-0.27			1.00	0.00725168	57.316	43.276
MDC1	S_329	+	-0.04	0.01			1.00	1.42E-29	136.88	112.11

MDC1	T_331	+	-0.04	0.01			1.00	1.42E-29	136.88	112.11
MECP2	S_80	+	0.01	-0.40		+	0.79	2.04E-05	75.334	61.139
MED1	T_1051	+	-0.12	-0.18	+	+	0.94	0.00158367	78.401	40.798
MEF2D	S_205	+	-0.61	-0.65	+	+	0.98	0.0340063	41.542	41.542
MELK	S_162	+	0.31	0.36			0.93	0.0153705	45.138	17.085
MFAP1	S_52	+	0.12	0.03	+		1.00	7.31E-08	144.33	120.3
MFAP1	S_53	+	0.12	0.03	+		1.00	7.31E-08	144.33	120.3
MFAP1	S_116	+	0.18	0.07	+		1.00	3.67E-83	174.76	174.76
MFAP1	S_118	+	0.18	0.07	+		1.00	3.67E-83	174.76	174.76
MFAP1	T_267	+	0.56	0.29		+	0.99	0.00252613	48.771	26.337
MKI67	S_1984	+	-0.58	-0.35			1.00	0.0104714	48.391	25.61
MKI67	S_224	+	-0.64	-0.48	+	+	1.00	5.69E-05	86.497	68.176
MKI67	S_308	+	0.11	0.11			1.00	1.99E-05	74.873	74.873
MKI67	S_1015	+	-0.47	-0.49	+	+	0.82	4.35E-06	80.545	60.873
MPHOSPH8	S_136	+	-0.07	0.04			1.00	0.00016311	71.842	71.842
MPHOSPH8	S_138	+	-0.07	0.04			1.00	0.00016311	71.842	71.842
MPHOSPH8	S_51	+	0.26	0.23	+	+	1.00	3.34E-100	183.1	183.1
MPRIP	S_224	+	0.00	-0.15			0.98	3.90E-08	84.025	65.67
MPRIP	S_226	+	-0.08	-0.20		+	0.88	6.55E-05	69.649	35.432
MPRIP	S_220	+	-0.09	-0.39			0.99	3.90E-08	84.025	65.67
MPRIP	S_294	+	-0.20	-0.78		+	0.67	0.00051259	59.372	59.372
MPRIP	T_295	+	-0.20	-0.78		+	0.67	0.00051259	59.372	59.372
MRE11A	S_621	+	0.42	0.09			0.99	0.00204277	53.355	38.114
MSH6	S_227	+	-0.09	-0.12	+	+	1.00	8.96E-51	155.86	133.29
MTCL1	S_1448	+	-0.22	-0.12			0.84	0.00469122	43.955	32.054
MTCL1	S_1061	+	-0.13	-0.11			1.00	2.63E-18	122.01	96.587
MTCL1	T_1057	+	-0.13	-0.11			1.00	2.63E-18	122.01	96.587
MTCL1	S_258	+	-0.39	-0.51	+	+	0.97	5.76E-16	98.443	74.414
MTCL1	S_262	+	-0.16	-0.54	+	+	1.00	1.45E-23	111.93	111.93
MTCL1	T_261	+	-0.16	-0.66			1.00	1.45E-23	111.93	111.93
MTCL1	S_263	+	-0.31	-0.89	+	+	1.00	1.24E-12	115.39	76.396
MTDH	S_426	+	0.15	0.11	+	+	1.00	8.44E-184	233.54	181.02
MTOR	T_1162	+	0.72	1.09		+	0.68	0.00196082	77.662	12.438
MUC19	S_5279		0.02	0.07		+	0.83	0.0264493	45.707	15.144
MVB12A	S_170	+	0.81	0.99	+	+	1.00	5.51E-37	143.14	95.023
MYBBP1A	S_1163	+	-0.25	-0.08	+		0.58	0.0310477	41.383	24.971
MYBBP1A	S_11	+	-0.04	-0.24		+	1.00	3.55E-39	140.84	106.4
MYBBP1A	S_1267	+	-0.15	-0.26	+		0.91	4.69E-22	124.04	78.828
MYCBP2	S_3467	+	-0.17	-0.23			0.99	0.00511084	54.768	54.768
MYEF2	S_17	+	-0.37	-1.11	+	+	1.00	3.56E-12	96.562	69.782
MYH9	S_1365	+	0.55	0.15	+		1.00	4.29E-12	92.613	78.912
MYL12A;MYI	T_18	+	0.07	0.14	+	+	1.00	1.48E-114	200.04	200.04
MYL12A;MYI	S_19	+	0.37	0.41	+	+	1.00	1.48E-114	200.04	200.04
MYO18A	S_1568	+	0.23	0.20	+	+	1.00	1.61E-26	130.09	114.7
MYO18A	S_1570	+	0.23	0.20	+	+	1.00	1.61E-26	130.09	114.7
MYO18A	S_1639	+	0.35	0.25	+	+	1.00	4.46E-19	115.77	100.84
MYO18A	S_1643	+	0.35	0.25	+	+	1.00	4.46E-19	115.77	100.84
MYO18A	S_1067	+	0.14	-0.17			0.79	0.00055082	50.723	50.723
MYO9B	S_1290	+	-0.02	0.15			0.99	0.00508347	46.324	28.696
MYO9B	T_1271	+	-0.63	-0.60	+	+	1.00	0.00189458	99.881	51.349

MYO9B	S_1267	+	-0.02	-0.42		+	1.00	0.00189458	99.881	51.349
MYOF	S_132	+	0.38	0.31	+		0.70	5.94E-08	100.43	64.319
NACA	S_166	+	0.27	0.19		+	0.98	3.68E-08	75.035	50.714
NAF1	S_315	+	-0.10	-0.44	+	+	1.00	7.00E-16	117.53	92.293
NAP1L1	S_10	+	-0.03	0.19		+	1.00	4.01E-18	107.58	84.23
NAP1L4	S_12	+	-0.10	-0.22			0.98	4.47E-16	117.22	117.22
NASP	S_141	+	0.10	0.31			1.00	3.48E-06	86.987	60.985
NASP	T_138	+	-0.01	0.07			0.77	8.54E-05	68.291	39.233
NASP	S_164	+	0.25	0.20		+	1.00	1.91E-05	74.278	74.278
NBN	S_432	+	-0.03	0.04	+		0.92	0.00068703	75.89	39.598
NCAPD2	S_1330	+	-0.34	0.04			0.94	0.00041908	101.71	54.898
NCAPD2	S_1333	+	-0.63	-0.23	+		0.96	2.96E-33	130.38	110.1
NCAPD2	T_1331	+	-0.38	0.05			0.68	1.28E-13	98.973	85.387
NCAPG	S_674	+	-0.06	0.10		+	1.00	2.10E-31	139.55	139.55
NCOR1	S_2081	+	-0.17	0.11	+		1.00	8.19E-06	94.61	94.61
NCOR2	S_1001	+	-1.04	-0.66	+	+	0.79	2.90E-11	112.47	86.057
NCOR2	S_2252	+	-0.29	-0.20	+		1.00	0.00057014	67.234	67.234
NCOR2	S_149	+	-0.70	-1.25	+	+	1.00	6.62E-06	85.054	57.783
NCOR2	S_152	+	-0.74	-1.36	+	+	1.00	6.62E-06	85.054	57.783
NCOR2	T_156	+	-0.30	-1.07	+	+	0.83	0.0056392	44.238	18.828
NDRG1	S_249	+	1.47	1.82	+	+	0.90	4.83E-07	93.371	93.371
NEDD1	S_427	+	0.13	-0.09			0.72	5.46E-11	96.591	65.722
NEDD4L	S_182	+	-0.37	0.09	+		0.94	0.00256323	61.265	61.265
NEDD4L	S_307	+	-0.28	-0.04	+		0.75	6.23E-41	150.13	115.04
NEDD4L	S_305	+	-0.33	-0.03	+		0.81	7.81E-12	108.25	108.25
NEDD4L	S_334	+	-0.42	-0.68	+	+	0.84	0.0004607	66.041	43.075
NELFB	S_557	+	-0.44	-0.99	+	+	1.00	3.74E-13	120.23	89.363
NELFE	S_115	+	0.95	1.25	+	+	1.00	4.44E-08	102.5	70.828
NEMF	S_375	+	0.10	0.16			1.00	9.88E-26	120.72	99.035
NEMF	S_705	+	0.22	0.26		+	1.00	5.76E-06	81.017	61.321
NEMF	S_706	+	0.22	0.26		+	1.00	5.76E-06	81.017	61.321
NFATC2IP	S_204	+	-0.30	3.09			1.00	0.00287178	90.379	43.487
NFIC	S_306	+	-0.02	0.17			1.00	6.68E-36	144.25	86.538
NFIC	S_290	+	-0.10	-0.44			0.98	2.90E-19	120.74	81.735
NIFK	T_234	+	-0.40	-0.40			0.92	0.0006059	72.082	44.124
NIFK	T_238	+	-0.40	-0.40			0.99	0.0006059	72.082	44.124
NIPBL	S_2658	+	-0.06	0.09			1.00	0.0012272	72.523	72.523
NMD3	T_470	+	0.13	-0.10	+		1.00	2.88E-22	186.74	147.55
NMD3	S_468	+	0.01	-0.14	+	+	1.00	2.88E-22	186.74	147.55
NOL8	S_822	+	0.09	0.05			1.00	7.48E-79	176.88	161.07
NOL8	T_820	+	0.09	0.05			1.00	7.48E-79	176.88	161.07
NOLC1	S_698	+	0.16	0.26			1.00	2.75E-29	131.72	131.72
NOLC1	T_607	+	-0.43	-0.35	+	+	1.00	1.81E-18	119.39	97.73
NOLC1	T_610	+	-0.43	-0.35	+	+	1.00	1.81E-18	119.39	97.73
NOP2	S_728	+	-0.28	0.08	+		1.00	5.09E-19	121.51	97.631
NOP2	S_782	+	-0.35	-0.35	+	+	0.98	0.00165346	72.531	43.468
NOP56	S_570	+	-0.41	0.01	+		1.00	7.96E-05	85.576	62.459
NOP56	S_569	+	-0.30	0.09	+		1.00	0.00053667	72.772	50.871
NOP56	S_520	+	0.05	-0.11			1.00	2.06E-25	125.73	125.73
NOP56	S_519	+	-0.07	-0.27			1.00	2.64E-06	78.225	60.329

NOP58	S_514	+	-0.34	-0.40	+	+	1.00	1.96E-68	171.89	132.43
NOP58	S_502	+	0.10	-0.16		+	1.00	2.24E-83	193.64	152.92
NOTCH2	S_1778	+	-0.18	-0.18			1.00	2.47E-21	122.64	88.426
NPM1	S_125	+	0.22	0.08	+		1.00	6.96E-05	56.774	56.774
NPM1	S_70	+	-0.02	-0.14		+	1.00	2.68E-68	166.65	166.65
NRBP1	T_433	+	0.00	0.10			0.99	0.0057331	73.802	42.731
NRBP1	T_431	+	-0.14	-0.06			0.94	0.00823078	69.261	25.581
NRBP1	S_2	+	0.05	-0.10			1.00	1.16E-06	87.356	67.263
NRBP1	S_422	+	-0.09	-0.52		+	0.92	0.00787351	47.732	32.944
NRD1	S_94	+	-0.10	-0.13	+		0.99	0.00011173	80.746	50.742
NSFL1C	S_114	+	-0.07	0.12			1.00	1.40E-07	101.53	101.53
NSL1	S_4	+	-0.05	-0.33			1.00	2.66E-19	122.97	98.604
NSRP1	S_33	+	0.07	-0.08			1.00	6.44E-74	165.77	165.77
NUCKS1	S_113	+	0.04	0.24			1.00	5.96E-07	131.98	107.24
NUCKS1	S_19	+	0.27	0.28	+	+	1.00	3.24E-210	234.03	234.03
NUCKS1	S_164	+	-0.06	-0.12		+	1.00	1.35E-55	153.59	128.35
NUCKS1	S_174	+	-0.07	-0.19	+	+	1.00	1.35E-55	153.59	128.35
NUCKS1	T_162	+	-0.06	-0.09	+		1.00	1.35E-55	153.59	128.35
NUDC	S_139	+	-0.04	0.10			1.00	5.95E-15	101.38	99.409
NUFIP2	S_652	+	0.70	0.67	+	+	1.00	7.03E-36	145.52	114.37
NUFIP2	S_629	+	-0.02	-0.15		+	0.98	2.40E-48	140.63	114.8
NUMA1	S_169	+	-0.15	-0.56	+	+	0.99	1.02E-07	81.878	81.878
NUMA1	S_1743	+	0.03	-0.50		+	1.00	3.29E-68	163.6	107.62
NUMB	T_113	+	-0.04	0.04			0.72	3.56E-06	64.16	64.16
NUMB	S_107	+	-0.17	0.02			0.89	3.56E-06	64.16	64.16
NUP188	S_1598	+	-0.35	-0.26	+	+	0.71	0.00892418	45.916	26.247
NUP214	T_437	+	-0.17	-0.49	+	+	0.94	5.19E-06	84.68	59.207
NUP214	S_433	+	-0.18	-0.49	+	+	0.65	1.24E-05	79.942	59.205
NUP98	S_595	+	0.04	-0.04			1.00	5.05E-92	181.69	181.69
NUP98	S_871	+	0.13	0.00	+		1.00	9.35E-11	105.72	93.427
NUP98	S_917	+	-0.19	-0.52	+	+	0.98	1.20E-06	86.222	86.222
NUP98	S_606	+	0.12	-0.13	+		1.00	1.95E-64	166.93	141.9
OGFR	S_537	+	-0.60	-0.65	+	+	1.00	2.05E-08	103.11	68.727
OGFR	S_565	+	-1.02	-1.14	+	+	1.00	1.79E-05	68.401	43.994
OGFR	S_559		-0.59	-0.91	+	+	0.92	0.00025771	60.951	27.078
OGFR	S_539		-0.88	-0.84	+	+	0.77	0.00102931	58.848	58.848
OGFR	T_561	+	-0.95	-1.32	+	+	0.99	1.79E-05	68.401	43.994
OPTN	S_469	+	0.18	0.40	+	+	0.90	1.16E-47	154.46	93.799
OSBP	S_190	+	0.48	0.34	+	+	1.00	3.63E-139	212.72	172.4
OSBP	S_351	+	0.42	0.03	+		1.00	1.01E-27	118.98	118.98
OSBP	S_193	+	0.65	0.26	+	+	1.00	3.63E-139	212.72	172.4
OSBPL11	S_181	+	-0.10	-0.04			0.83	1.10E-05	87.647	47.769
OSBPL8	S_765	+	0.03	0.36			0.69	0.00706942	43.956	43.956
OSBPL8	S_766	+	0.03	0.36			0.69	0.00706942	43.956	43.956
OSBPL8	S_768	+	0.03	0.36			0.59	0.00706942	43.956	43.956
OTUD4	S_1023	+	0.19	0.26	+	+	1.00	1.89E-19	125.96	125.96
OTUD4	S_1024	+	0.19	0.27	+	+	1.00	1.89E-19	125.96	125.96
OXR1	S_133	+	0.25	0.56	+	+	0.99	1.54E-08	103.73	76.694
OXR1	S_136	+	0.23	0.46	+	+	0.90	1.54E-08	103.73	76.694
PA2G4	S_2	+	0.28	0.23	+	+	1.00	4.03E-20	118.85	91.286

PAFAH1B2	S_2	+	0.50	0.14			0.98	2.74E-11	92.258	92.258
PAG1	S_298	+	0.14	0.22			0.93	0.019494	58.04	42.034
PAG1	S_295	+	0.22	0.25			0.79	0.019494	58.04	42.034
PAICS	S_27	+	0.01	-0.04			1.00	0.00148507	85.163	35.055
PAK2	S_141	+	-0.09	0.18	+	+	1.00	1.53E-75	174.23	174.23
PAK2	S_2	+	-1.52	-1.48			1.00	0.0148047	45.436	45.436
PAK2	S_197	+	-0.04	-0.13		+	1.00	1.07E-14	105.65	105.65
PAK4	S_181	+	-0.26	-0.34	+	+	0.64	0.00622795	40.384	40.384
PAK4	S_309	+	0.11	-0.14		+	1.00	1.30E-64	169.49	169.49
PAM	S_839	+	0.53	0.47	+	+	0.81	0.00582771	49.036	27.641
PAM	T_836	+	0.53	0.47	+	+	0.68	0.00582771	49.036	27.641
PATL1	S_177	+	0.62	0.68	+	+	0.55	0.00573632	61.165	61.165
PATL1	S_184	+	0.51	0.54	+	+	1.00	0.00105483	61.165	61.165
PCBP1	S_173	+	0.07	0.05			1.00	6.09E-79	172.09	172.09
PCBP2	S_185	+	-0.15	4.36		+	0.95	1.10E-05	100.69	59.127
PCM1	S_65	+	0.26	0.13			1.00	9.93E-38	148.52	148.52
PCM1	S_69	+	0.04	0.01			0.97	3.68E-27	133.94	107.58
PCM1	S_1710	+	0.46	0.26			1.00	0.00116285	54.072	32.379
PCM1	S_1713	+	0.46	0.26			1.00	0.00116285	54.072	32.379
PCNP	S_119	+	-0.15	-0.32	+	+	1.00	0.00697532	61.304	40.898
PCYT1A	S_347	+	-0.21	-0.06	+	+	1.00	0.00106605	82.529	64.139
PCYT1A	S_343	+	-0.21	-0.05	+	+	0.89	0.00106605	82.529	64.139
PDCD4	S_83	+	0.37	0.16	+	+	0.50	0.00290478	77.662	41.238
PDCD4	T_82	+	0.37	0.16	+	+	0.50	0.00290478	77.662	41.238
PDIA6	S_425	+	1.12	1.04	+	+	1.00	1.82E-49	149.09	149.09
PDLIM5	S_251	+	-0.07	-0.21		+	0.96	0.00022617	67.644	67.644
PDPK1;PDPK	S_114	+	0.18	-0.01			1.00	4.04E-15	107.95	88.601
PDS5B	T_1370	+	-0.30	0.00			0.84	6.47E-06	114.05	79.785
PDS5B	S_1283	+	-0.36	-0.30	+	+	1.00	0.00743563	91.926	44.199
PDS5B	S_1358	+	-0.01	-0.10			1.00	4.31E-65	168.17	168.17
PDYN	S_101	+	0.31	-0.14	+		1.00	0.00734241	70.908	8.4441
PEA15	S_116	+	1.01	1.04	+	+	1.00	3.18E-06	97.502	67.43
PEBP1	S_54	+	0.45	-0.38			0.53	0.00096595	65.511	65.511
PFKP	S_378	+	0.43	0.45	+	+	1.00	0.00447807	61.423	17.981
PGM1	S_117	+	0.06	-0.30	+		0.98	9.27E-08	79.88	59.016
PGM1	T_115	+	0.21	-0.26	+		0.82	7.75E-09	87.196	64.214
PGM3	T_62	+	0.23	-0.05			0.85	0.00024247	63.691	63.691
PGRMC1	S_129	+	-0.12	-0.31			1.00	8.83E-77	176.44	138.27
PGRMC1	S_57	+	-0.35	-0.94	+	+	1.00	1.77E-55	157.73	157.73
PGRMC1	S_54	+	-0.41	-0.76	+	+	0.99	2.33E-25	120.27	119.69
PGRMC2	T_211	+	0.11	0.16	+		0.95	3.11E-08	93.495	93.495
PGRMC2	S_208	+	0.55	0.35	+		0.87	6.81E-64	159.1	159.1
PGRMC2	Y_210	+	0.35	0.09	+		0.54	0.00166763	50.392	50.392
PHC2	S_36	+	-0.09	-0.12			0.96	0.00092313	51.557	51.557
PHC3	T_590	+	-0.22	-0.30	+	+	1.00	0.0053438	88.565	62.203
PHC3	S_597	+	-0.19	-0.41	+	+	1.00	0.0053438	88.565	62.203
PHIP	S_1783	+	0.18	0.11			1.00	5.55E-77	180.31	180.31
PHLDB2	S_384	+	0.30	0.56	+	+	1.00	9.56E-40	146.65	126.62
PHLDB2	S_387	+	0.30	0.56	+	+	1.00	9.56E-40	146.65	126.62
PHRF1	T_916	+	0.00	0.08		+	0.83	2.05E-08	80.412	80.412

PHRF1	S_914	+	0.38	0.17	+		0.54	2.05E-08	80.412	80.412
PI4K2A	S_47	+	-0.10	-0.06	+		1.00	0.00033609	72.315	72.315
PI4K2A	S_51	+	-0.16	-0.26	+	+	1.00	0.00033609	72.315	72.315
PI4KB	S_413	+	0.22	0.15	+		1.00	0.00085831	65.954	65.954
PIP4K2B	S_326	+	0.21	0.19		+	0.86	6.34E-05	51.758	37.41
PIP4K2B	T_322	+	0.21	0.19		+	0.64	6.34E-05	51.758	37.41
PITPNC1	S_299	+	-0.33	0.26			1.00	0.0191152	44.312	24.869
PKN2	S_256	+	0.17	0.45	+	+	0.50	0.00019215	81.01	50.834
PKN2	S_257	+	0.29	0.40	+	+	0.95	4.10E-37	147.53	100.29
PKP2	S_155	+	0.31	0.23	+		1.00	0.00439374	101.28	46.767
PKP2	S_151	+	0.29	0.12	+		1.00	0.00439374	101.28	46.767
PLEC	T_4454	+	0.27	0.35			0.64	7.32E-08	94.49	66.35
PLEC	S_1563	+	0.94	0.72			1.00	0.00408592	55.912	55.912
PLEC	S_4239	+	0.10	0.07			0.67	1.91E-45	131.97	109.5
PLEC	S_4213	+	0.70	0.61	+	+	1.00	4.71E-12	93.812	65.196
PLEC	S_4447	+	-0.02	-0.04			0.97	2.72E-51	152.63	115.02
PLEC	S_4453	+	0.26	0.31			0.80	2.16E-08	96.052	87.05
PLEC	T_19	+	0.14	0.13			0.73	2.06E-47	158.91	158.91
PLEC	S_4457	+	0.08	0.07		+	0.95	1.58E-08	96.052	64.495
PLEC	S_4216	+	0.68	0.61	+	+	0.87	2.18E-156	215.43	215.43
PLEC	S_21	+	0.31	0.19	+	+	0.95	1.37E-36	147.53	144.51
PLEC	S_4217	+	0.88	0.77	+	+	0.86	3.46E-51	156.08	156.08
PLEC	S_4215	+	0.57	0.27	+	+	0.88	2.18E-156	215.43	215.43
PLEC	S_4444	+	-0.16	-0.50			1.00	0.00048268	94.49	66.35
PLEC	S_4220	+	0.60	0.46	+		0.99	2.18E-156	215.43	215.43
PLEC	S_4227	+	-0.04	-0.50	+	+	1.00	1.59E-22	128.4	86.213
PLEKHA5	S_1021	+	-0.02	-0.18		+	0.94	1.88E-10	102.72	77.037
PLEKHA6	S_848	+	-0.54	-0.31			0.63	0.0405586	44.391	26.495
PLEKHA6	S_777	+	-0.35	-0.06			0.84	3.41E-08	99.392	78.659
PLEKHA6	T_779	+	0.03	-0.07		+	0.88	0.0003992	102.03	63.8
PLEKHF1	S_227	+	0.16	-0.02	+		1.00	0.00023831	67.668	49.93
PLEKHG3	S_1040	+	-0.36	-0.32	+	+	1.00	2.52E-27	135.81	135.81
PLEKHG3	S_1037	+	-0.36	-0.37	+	+	1.00	2.52E-27	135.81	135.81
PLEKHM1	T_434	+	0.28	0.51		+	0.66	0.00412493	67.952	36.23
PLEKHM1	S_435	+	0.37	0.57	+	+	0.88	0.00412493	77.192	26.488
PML	S_470	+	-0.17	0.00	+		1.00	0.00209268	65.765	65.765
PML	S_479	+	-0.17	0.00	+		1.00	0.00209268	65.765	65.765
PNKP	T_118	+	-0.30	-0.63	+	+	1.00	1.40E-13	113.65	67.081
POLR2A	S_1913	+	-0.43	-0.24	+		0.99	7.76E-09	107.72	50.357
POLR2A	T_1919	+	-0.35	-0.61			0.67	2.09E-05	94.325	60.142
PPA2	S_151	+	-0.53	-0.28			1.00	5.25E-26	131.17	131.17
PPAN	S_359	+	0.02	0.12		+	1.00	5.45E-27	132.5	105.73
PPP1R12A	T_356	+	0.35	0.43			0.83	0.00205938	75.564	62.801
PPP1R12A	S_358	+	0.31	0.25	+	+	0.94	1.40E-36	140.89	117.5
PPP1R13L	T_308	+	-0.09	-0.04	+		0.95	0.00273414	78.324	56.952
PPP1R2;PPP1	S_121	+	0.38	0.39	+		1.00	1.30E-99	182.21	182.21
PPP1R2;PPP1	S_122	+	0.34	-0.03	+		1.00	1.30E-99	182.21	182.21
PPP6R3	S_537	+	0.15	0.05	+		1.00	2.45E-157	221.21	194.75
PRCC	T_261	+	0.09	-0.17		+	0.95	0.0001243	65.887	65.887
PRCC	S_267	+	0.17	-0.24		+	0.95	1.23E-16	99.603	99.603

PRKAR1A	S_83	+	-0.49	-0.15	+	+	1.00	6.91E-93	183.73	183.73
PRKAR2A	S_99	+	0.14	0.10	+	+	1.00	4.54E-44	143.33	95.426
PRKAR2A	S_78	+	0.12	0.00	+		1.00	7.95E-233	251.7	251.7
PRKAR2A	S_80	+	0.12	0.00	+		1.00	7.95E-233	251.7	251.7
PRKAR2B	S_114	+	0.20	-0.10	+		1.00	3.66E-07	80.382	67.107
PRKCA	S_226	+	0.46	0.42	+	+	1.00	7.77E-13	121.51	66.653
PRKCA	S_13		0.19	0.25			0.71	0.00347403	56.719	32.623
PRKCA;PRKC	T_401	+	-0.02	-0.31		+	1.00	1.83E-118	196.1	174.06
PRKCD	S_506	+	-0.27	-0.37		+	0.50	1.84E-68	164.46	164.46
PRKCD	T_507	+	-0.27	-0.37		+	0.50	1.84E-68	164.46	164.46
PRPF31	T_455	+	-0.01	0.05			1.00	0.00019398	64.508	47.818
PRPF4B	S_431	+	0.21	0.12	+	+	1.00	1.59E-05	96.745	47.296
PRPF4B	S_437	+	0.22	0.12	+	+	1.00	1.59E-05	96.745	47.296
PRPF4B	Y_849	+	-0.12	-0.26			0.96	2.02E-12	96.379	96.379
PRRC2A	S_1085	+	0.03	0.17			0.51	0.00019257	72.566	57.712
PRRC2A	S_1092	+	0.22	0.41		+	0.92	1.50E-05	76.909	57.887
PRRC2A	S_1089	+	0.21	0.42			0.95	1.50E-05	76.909	57.887
PRRC2C	S_1862	+	-0.15	-0.12			1.00	3.03E-20	129.37	129.37
PSEN1	S_332	+	0.00	-0.01			0.73	0.00124784	64.423	40.765
PSEN1	S_333	+	-0.01	-0.11			0.75	1.46E-18	112.74	83.29
PSEN1	S_334	+	-0.13	-0.35			0.79	1.46E-18	112.74	83.29
PSMD1	S_315	+	-0.16	-0.15	+	+	1.00	7.71E-08	88.627	88.627
PSMD1	T_311	+	-0.16	-0.15	+	+	1.00	7.71E-08	88.627	88.627
PSMD2	S_16	+	-0.63	-0.69	+	+	1.00	2.97E-14	103.35	96.133
PTK2	T_222	+	-0.14	-0.39	+		0.50	0.00101154	65.149	39.163
PTK2	S_218	+	-0.03	-0.47	+	+	0.96	0.00101154	65.149	39.163
PTMA	S_2	+	0.11	0.07		+	1.00	2.60E-09	108.25	108.25
PTPN12	T_468		-0.03	-0.14			0.78	0.00092212	58.635	35.298
PTPN12	S_543	+	0.00	-0.26			0.99	0.0128138	45.614	45.614
PTPN12	S_476	+	-0.05	-0.17			0.93	0.00092212	58.635	35.298
PTPN12	S_473	+	-0.05	-0.17			0.98	0.00737881	54.465	54.465
PTPN14	S_314	+	-0.14	-0.05	+		0.98	9.86E-20	128.82	71.97
PTPN14	S_312	+	-0.15	-0.20		+	0.86	0.00015574	85.28	59.285
PTPN14	S_593	+	-0.03	-0.37			0.99	1.41E-18	127.88	102.81
PTPN14	S_594	+	-0.10	-0.78			1.00	1.41E-18	127.88	102.81
PTPN2	S_304	+	-0.43	-0.36			0.99	0.00087187	66.738	35.063
PTRF	S_173	+	0.06	0.06	+		1.00	8.26E-31	119.43	119.43
PTRF	S_174	+	0.06	0.06	+		1.00	8.26E-31	119.43	119.43
PTRF	S_112	+	0.16	0.14	+		1.00	4.06E-31	115.08	115.08
PTRF	S_113	+	0.16	0.14	+		1.00	4.06E-31	115.08	115.08
PURB	S_101	+	-0.27	-0.06			0.91	8.24E-07	72.728	59.367
PWP1	S_50	+	0.20	-0.11			1.00	2.05E-24	117.62	93.967
PWWP2A	S_81	+	-0.43	0.08	+		1.00	1.93E-27	137.27	118.3
PXN	S_85	+	0.01	0.21			0.76	0.00075996	66.022	66.022
PXN	T_132	+	-0.40	-0.41		+	0.77	0.00049766	54.875	54.875
PXN	S_106	+	0.25	0.23	+		1.00	9.23E-51	181.51	108.61
PXN	S_126	+	-0.11	-0.29		+	0.97	0.00043371	64.767	49.221
PXN	S_130	+	0.01	-0.30			0.91	0.00043371	64.767	49.221
PXN	S_84	+	-0.12	-0.32			0.76	0.00293338	58.246	58.246
QSOX2	S_578	+	0.34	0.23			0.76	9.34E-31	125.37	125.37

RAB11FIP5	S_356		0.45	0.56	+	+	0.59	6.92E-10	91.883	66.473
RAB11FIP5	S_176	+	0.31	0.27			0.99	0.00017021	86.016	58.687
RAB12	S_21	+	0.29	0.03			1.00	0.00174106	54.985	36.572
RABL6	S_640	+	0.28	0.28	+	+	1.00	1.86E-05	71.969	55.045
RABL6	S_641	+	0.28	0.28	+	+	1.00	1.86E-05	71.969	55.045
RABL6	S_596	+	-0.24	-0.76	+	+	1.00	0.00021797	75.524	44.164
RABL6	T_599	+	-0.24	-0.76	+	+	1.00	0.00021797	75.524	44.164
RAD18	S_471	+	-0.20	0.07	+		1.00	0.00038141	84.892	59.443
RAD23A	S_205		-0.41	0.19			0.91	0.00212095	41.889	31.341
RAD23A	S_123	+	-0.16	-0.27		+	0.83	9.13E-06	65.766	65.766
RAD23B	T_162	+	-0.17	-0.06			0.54	0.00051722	60.561	47.958
RAD23B	S_160	+	-0.07	-0.25		+	1.00	0	274.34	245.71
RAD50	S_496	+	0.77	0.84	+	+	1.00	1.11E-29	136.67	107.09
RAF1	S_29	+	0.17	0.06			0.88	1.31E-48	145.04	145.04
RALY	S_119	+	-0.30	-0.35	+	+	1.00	0.00165449	68.277	44.206
RANBP2	S_1400	+	-0.01	-0.43			0.79	0.00097263	52.432	52.432
RANBP2	T_1396	+	-0.19	-0.29			0.87	0.00097263	52.432	52.432
RANBP2;RGP	S_1463	+	0.29	0.29	+	+	1.00	0.00965613	62.287	46.915
RANBP2;RGP	T_1459	+	0.29	0.29	+	+	1.00	0.00965613	62.287	46.915
RAVER1	S_14	+	-0.03	-0.11		+	0.99	0.00157399	61.561	35.013
RB1	S_807	+	-0.62	-0.50	+	+	1.00	3.00E-29	133.21	133.21
RB1	S_811	+	-0.62	-0.50	+	+	1.00	3.00E-29	133.21	133.21
RB1	T_826	+	-0.50	-0.49	+	+	1.00	3.83E-19	129.43	88.443
RB1	T_821	+	-0.50	-0.50	+	+	1.00	3.83E-19	129.43	88.443
RB1	T_373	+	-0.51	-0.46	+		1.00	0.00692652	50.077	50.077
RB1	T_823	+	-0.40	-0.58	+	+	0.95	0.0001787	87.654	44.836
RBBP6	S_1294	+	0.17	0.33	+	+	1.00	1.65E-12	116.9	116.9
RBM10	S_658	+	0.13	0.24	+	+	1.00	4.65E-22	147.26	103.5
RBM10	S_660	+	0.13	0.24	+	+	1.00	4.65E-22	147.26	103.5
RBM15	S_250	+	0.23	0.10	+		1.00	0.00112868	73.834	46.153
RBM39	S_114	+	-0.01	-0.10			1.00	8.18E-22	120.74	104
RBM5	S_624	+	0.14	0.28	+	+	1.00	9.01E-44	148.1	148.1
RCAN1;RCAN	S_108	+	0.28	-0.02			1.00	1.89E-05	88.282	65.955
RCAN1;RCAN	S_112	+	0.28	-0.02			1.00	1.89E-05	88.282	65.955
RCSD1	S_216	+	0.01	0.11			0.99	0.00138795	78.419	37.052
RCSD1	S_179	+	0.20	0.18	+	+	0.98	7.16E-08	103.87	78.31
REEP4	S_152	+	0.36	0.41	+	+	1.00	0.0152581	63.473	25.478
REPS1	S_170	+	-0.01	-0.09			0.98	0.00050085	51.577	51.577
REPS1	S_162	+	-0.18	-0.16			0.99	0.00050085	51.577	51.577
REPS1	S_166	+	-0.18	-0.16			0.99	0.00050085	51.577	51.577
REPS1	S_174	+	-0.18	-0.22			0.61	0.00050085	51.577	51.577
REPS1	T_173	+	-0.36	-0.40			0.77	0.00050085	51.577	51.577
RFC1	S_71	+	0.03	0.16		+	0.97	2.31E-50	155.08	117.44
RFC1	S_69	+	0.00	0.16			1.00	2.31E-50	155.08	117.44
RFC1	S_73	+	-0.02	-0.02			0.60	1.21E-38	141.93	141.93
RFFL	S_229	+	0.08	-0.36		+	0.98	4.39E-05	85.185	59.567
RFFL	S_226	+	0.12	-0.27		+	0.95	4.39E-05	85.185	59.567
RHBDF2	S_296	+	-0.19	-0.42	+	+	0.93	0.0080591	53.861	53.861
RHBDF2	S_299	+	-0.19	-0.42	+	+	1.00	0.0080591	53.861	53.861
RIC8A	S_430	+	0.32	0.14	+		0.91	2.31E-06	103.4	75.959

RIC8A	T_435	+	0.32	-0.08	+		0.96	2.31E-06	103.4	75.959
RIOK1	S_21	+	0.18	0.03			0.81	6.26E-05	75.877	51.455
RNF113A	S_85	+	0.25	0.15	+	+	0.96	1.53E-07	81.574	81.574
RNF113A	S_84	+	0.31	0.14	+	+	0.96	2.11E-08	83.064	64.818
RNF113A	Y_80	+	0.31	0.10			0.82	2.11E-08	83.064	64.818
RNF20	S_138	+	-0.68	-0.53	+	+	0.98	5.13E-09	112.57	61.137
RNF4	S_94	+	0.21	0.35			0.98	0.00158384	51.851	51.851
RNF4	S_95	+	0.21	0.35			0.89	0.00158384	51.851	51.851
ROCK1	S_1105	+	-0.22	-0.43			0.92	3.93E-05	71.426	71.426
ROCK1	S_1098	+	-0.22	-0.43			0.84	3.93E-05	71.426	71.426
RPL27A	S_68	+	0.74	0.68	+	+	1.00	2.69E-08	106.87	75.518
RPLP1;RPLP2	S_104	+	-0.06	-0.02			1.00	2.47E-39	152.88	121.74
RPRD1A	S_120	+	0.11	-0.20		+	0.92	0.00106716	57.347	57.347
RPRD1B	S_166	+	0.08	-0.13			0.73	4.53E-05	52.556	32.572
RPRD2	S_337	+	0.22	0.15	+		1.00	4.88E-21	119.66	80.645
RPS3	T_221	+	-0.17	-0.01	+		1.00	3.02E-200	235.93	175.39
RPTOR	T_707	+	0.24	-0.03			0.87	0.00026435	76.051	76.051
RPTOR	S_701	+	0.04	-0.24			0.83	0.0042124	58.324	58.324
RPTOR	S_705	+	0.34	0.18	+		0.98	9.28E-09	96.153	96.153
RRAGC	Y_16		1.14	1.06		+	0.60	0.00630979	54.097	37.507
RRAGC	S_2	+	1.30	1.12	+	+	0.99	0.00023253	59.888	47.662
RRAS2	S_109	+	-0.41	-0.53	+	+	1.00	2.25E-61	164.69	116.17
RRAS2	T_113	+	-0.39	-0.89			0.87	1.38E-152	220.64	171.57
RRM2	S_20	+	-0.87	-1.30	+	+	1.00	4.85E-12	107.83	107.83
RRP12	S_1019	+	0.25	0.24	+	+	1.00	8.68E-17	103.88	103.88
RSF1	S_1093	+	-0.03	0.02			1.00	3.08E-76	174.87	174.87
RSF1	T_1053	+	0.25	0.11			1.00	0.00197262	52.898	40.518
RSL1D1	S_141	+	-0.24	-0.43	+	+	0.99	4.16E-22	127.5	127.5
RSRC2	S_168	+	-0.23	-0.16			1.00	0.00167056	50.884	27.416
RSRC2	S_170	+	-0.23	-0.16			1.00	0.00167056	50.884	27.416
RSRC2	S_174	+	-0.23	-0.16			1.00	0.00167056	50.884	27.416
RSRC2	T_172	+	-0.23	-0.16			1.00	0.00167056	50.884	27.416
RTN4	S_182	+	0.41	0.82	+	+	0.82	1.19E-17	106.89	77.291
RTN4	S_7	+	-0.27	-0.06	+		1.00	7.68E-09	84.113	84.113
RTN4	S_181	+	0.22	0.34	+	+	0.88	1.19E-17	106.89	77.291
RTN4	T_188	+	0.27	0.49	+	+	0.93	1.19E-17	106.89	77.291
RTN4	S_15	+	-0.01	-0.04			1.00	8.65E-50	146.18	146.18
RTN4	S_13	+	0.05	0.07	+		0.53	7.92E-06	72.09	72.09
RTN4	S_184	+	0.31	0.31	+	+	0.95	1.19E-17	106.89	77.291
RTN4	S_107	+	0.05	-0.04			0.87	0.0077606	41.69	41.69
SAP30	S_131	+	-0.60	0.71			0.99	0.0013845	51.321	27.431
SAP30BP	S_18	+	0.06	-0.09			0.54	0.00035317	42.709	42.709
SAP30BP	S_22	+	0.06	-0.09			0.79	0.00035317	42.709	42.709
SART3	S_10	+	-0.11	-0.35			0.86	0.0157908	47.217	47.217
SCAF1	S_734	+	0.18	0.16	+	+	1.00	2.43E-13	118.02	118.02
SCAF1	S_738	+	0.18	0.16	+	+	1.00	2.43E-13	118.02	118.02
SCAF1	T_1001	+	-0.27	-0.17			0.99	0.00135445	69.581	69.581
SCAF11	S_481	+	-0.17	-0.10			0.97	0.00561904	61.495	40.487
SCAF11	S_487	+	-0.17	-0.10			0.97	0.00561904	61.495	40.487
SCFD1	S_206	+	0.22	-0.23			0.62	3.53E-10	91.932	35.953

SCRIB	S_1267	+	-0.55	-0.50	+	+	0.91	1.58E-11	81.345	51.49
SCRIB	S_1272	+	-0.78	-0.73			0.79	0.00091358	43.34	43.34
SCRIB	T_1261	+	-0.62	-0.51	+	+	0.99	0.00033878	46.412	32.173
SCRIB	S_1367	+	0.04	-0.19			0.99	0.00037921	69.024	69.024
SCRIB	S_1139	+	0.29	0.17	+	+	1.00	0.00176376	84.895	54.89
SCRIB	S_423	+	-0.03	-0.25		+	0.94	5.20E-27	128.66	128.66
SCRIB	S_1485	+	-0.20	-0.69		+	0.99	6.80E-08	57.563	43.645
SCRIB	S_1466	+	0.15	-0.58			0.63	6.80E-08	57.563	43.645
SDAD1	S_488	+	0.09	0.21		+	1.00	7.57E-12	109.07	87.402
SDE2	S_183	+	-0.09	-0.37		+	0.50	0.00886033	42.705	42.705
SDE2	T_179	+	-0.09	-0.37		+	0.50	0.00886033	42.705	42.705
SDPR	S_287	+	0.24	0.09	+		0.50	0.00946064	52.463	40.405
SDPR	S_293	+	0.24	-0.06	+		0.99	1.26E-05	95.954	95.954
SDPR	S_288	+	0.20	-0.06	+		0.61	1.26E-05	95.954	95.954
SEC22B	S_137	+	0.66	0.82	+	+	1.00	8.78E-13	112.14	77.011
SEC31A	S_522	+	0.50	0.18	+	+	0.95	0.00455425	45.878	45.878
SEMA4B	S_788	+	0.10	0.12			1.00	0.00814835	68.123	22.054
SEPT9	S_218	+	0.08	0.02	+		1.00	1.32E-63	161.1	124.53
SEPT9	S_11		0.76	0.47	+	+	1.00	3.92E-79	175.77	175.77
SERBP1	S_231	+	-0.09	-0.01			0.85	7.83E-21	107.88	85.222
SF1	S_207	+	-0.10	-0.08			1.00	3.86E-13	118.31	92.19
SF1	S_205	+	-0.31	-0.41	+	+	1.00	3.86E-13	118.31	92.19
SF1	S_214	+	-0.35	-0.56	+	+	0.80	0.00074357	55.128	49.555
SF3A1	S_264	+	0.31	0.12			1.00	6.75E-08	135.64	83.27
SF3B2	S_309	+	0.20	0.36	+	+	1.00	6.44E-68	164.48	124.16
SF3B2	S_302	+	0.40	0.41	+	+	0.84	6.44E-68	164.48	124.16
SF3B2	S_307	+	0.20	0.38	+	+	0.97	5.36E-43	144.43	124.9
SF3B2	S_303	+	0.38	0.22			0.86	0.015239	44.474	19.743
SGPP1	S_112	+	0.32	0.30	+	+	0.99	3.44E-06	96.82	65.472
SGPP1	T_114	+	0.50	0.11	+		0.96	0.00058729	70.54	42.258
SH3BP4	S_296	+	-0.15	0.05			0.95	0.00061223	59.561	59.561
SH3BP4	S_246	+	0.36	0.34	+		0.98	3.89E-25	145.82	112.89
SIPA1	S_884	+	-0.08	-0.35		+	0.87	1.13E-05	69.272	55.649
SIRT1	S_14	+	0.19	0.21			0.97	1.45E-07	82.859	82.859
SKA3	S_155	+	0.07	0.14		+	1.00	1.85E-07	99.238	54.356
SLC26A6	S_692	+	0.03	0.10			1.00	0.00017486	86.411	43.369
SLC26A6	S_695	+	0.03	-0.08			0.99	0.00017486	86.411	43.369
SLC9A1	S_703	+	0.06	0.03			1.00	0.00039423	84.753	67.731
SLC9A3R1	S_135	+	0.51	0.06	+		0.90	2.19E-96	183.63	183.63
SLTM	S_122	+	-0.07	-0.13			1.00	0.00406431	58.817	37.563
SMAP	S_17	+	0.10	0.19	+	+	0.85	8.54E-125	199.3	199.3
SMAP	S_15	+	0.22	0.14	+	+	0.50	8.54E-125	199.3	199.3
SMARCA4	S_1419	+	-0.46	-0.24	+	+	1.00	0.00646561	57.149	38.48
SMC4	S_41	+	-0.06	-0.03		+	0.98	7.32E-52	158.53	158.53
SMC4	S_22	+	-0.35	-0.46	+	+	1.00	1.23E-06	103.9	61.587
SMC4	S_27	+	-0.75	-1.28	+	+	0.71	2.84E-06	94.588	58.225
SMC4	S_28	+	-0.71	-1.28	+	+	0.90	2.84E-06	94.588	58.225
SMCO3	S_138		-0.21	0.00	+		1.00	0.00134861	74.89	39.363
SMCO3	T_141		-0.21	0.00	+		0.56	0.00134861	74.89	39.363
SMN1	S_31	+	0.11	0.24	+	+	1.00	9.30E-115	198.32	133.13

SMN1	S_28	+	0.32	0.22	+	+	1.00	9.30E-115	198.32	133.13
SMN1	T_25	+	0.47	0.28	+	+	0.88	5.79E-07	87.748	87.748
SNAP23	S_110	+	0.27	0.24	+		1.00	6.18E-08	106.47	80.737
SNRNP200	S_225	+	0.22	0.19	+	+	1.00	6.06E-96	187.75	187.75
SNTB1	S_87	+	-0.05	-0.37		+	1.00	0.00382297	46.514	29.899
SNTB2	S_393	+	0.10	0.26	+		0.96	7.49E-05	87.138	64.021
SNTB2	S_95	+	-0.26	-0.17	+		1.00	0.00116233	78.615	43.812
SNTB2	S_233	+	0.12	-0.31			0.72	1.24E-06	72.228	72.228
SNW1	S_232	+	-0.40	-0.33	+	+	0.99	0.00020957	81.904	39.429
SNW1	S_224	+	-0.42	-0.41	+	+	1.00	0.00020957	81.904	39.429
SNW1	S_234	+	-0.50	-0.72	+	+	0.96	0.00271411	62.617	62.617
SON	S_1690	+	0.20	0.01			1.00	0.0047066	61.815	40.13
SON	S_1378	+	0.10	0.10		+	1.00	8.10E-19	124.04	89.19
SON	S_1692	+	0.38	0.33			1.00	0.0047066	62.633	38.168
SON	S_1694	+	0.38	0.33			1.00	0.0047066	62.633	38.168
SORBS3	S_188	+	-0.21	0.00	+		0.95	4.52E-08	135.23	91.64
SORBS3	T_187	+	-0.05	0.06			0.85	8.14E-18	120.63	120.63
SP100	S_372	+	0.41	0.54		+	1.00	0.00012228	64.27	64.27
SP100	S_374	+	0.41	0.54		+	1.00	0.00012228	64.27	64.27
SP100	S_375	+	0.41	0.54		+	1.00	0.00012228	64.27	64.27
SP100	S_327	+	0.26	0.00	+		1.00	2.81E-65	170.5	170.5
SPANXB1	S_13	+	0.03	-0.16		+	1.00	3.60E-15	111.11	77.939
SPANXB1	T_34		-0.44	-0.72			0.93	1.43E-05	81.526	49.767
SPRY4	S_125	+	-0.31	-0.41	+	+	1.00	0.00048131	69.331	55.389
SPTAN1	S_1197	+	0.25	0.18	+		1.00	0.0220953	46.796	10.112
SPTBN1	S_2169	+	-0.07	0.00	+		1.00	1.72E-27	139.76	93.1
SPTBN1	S_2165	+	-0.07	-0.02	+		1.00	1.72E-27	139.76	93.1
SPTBN1	S_14	+	0.60	0.58	+	+	0.98	1.38E-12	92.798	77.748
SPTBN1	S_2125	+	-0.08	-0.17		+	1.00	7.61E-115	200.04	170.31
SPTBN1	S_2164	+	-0.06	-0.15		+	0.79	0.0018127	62.338	50.484
SPTBN1	T_2328	+	0.29	-0.08	+		1.00	0.00107526	69.084	69.084
SPTBN1	S_2340	+	0.17	0.05			0.54	1.22E-07	86.997	72.901
SPTBN1	S_2332	+	0.36	0.12	+		0.69	0.00022113	67.01	67.01
SPTBN1	S_2341	+	-0.16	-0.51	+	+	1.00	9.57E-34	136.81	105.72
SQSTM1	S_193	+	-0.61	-0.09			0.82	0.0033757	83.964	46.487
SQSTM1	S_191	+	-0.55	0.02	+		0.77	2.38E-13	118.05	73.808
SQSTM1	S_188	+	-0.57	-0.18	+	+	1.00	3.24E-39	141.79	111.66
SQSTM1	T_185	+	-0.52	-0.08	+	+	1.00	3.24E-39	141.79	111.66
SQSTM1	S_24	+	-0.92	-0.57	+	+	0.91	0.00068517	53.589	34.48
SQSTM1	T_194	+	-0.55	-0.26	+		0.68	3.78E-27	137.73	104.45
SQSTM1	S_248	+	-0.07	0.09		+	1.00	1.17E-10	86.449	73.423
SQSTM1	S_282	+	-0.38	-0.09			0.63	1.08E-15	96.123	73.135
SQSTM1	S_192	+	-0.37	-0.13	+		0.82	1.00E-26	133.78	133.78
SRC	S_17	+	-0.23	-0.56	+		1.00	0.00312242	49.497	31.995
SRRM1	S_775	+	-0.74	-0.74	+	+	0.67	0.00034586	60.635	40.326
SRRM1	T_220	+	-0.20	-0.23	+	+	1.00	1.39E-07	105.95	77.742
SRRM1	S_771	+	-0.48	-0.45			0.99	0.00158771	49.076	49.076
SRRM1	S_872	+	0.15	0.14	+	+	1.00	2.87E-134	203.59	158.35
SRRM1	T_870	+	0.35	0.54	+	+	1.00	1.17E-114	197.07	185.58
SRRM1	S_773	+	-0.42	-0.45	+	+	0.92	1.96E-06	76.693	76.693

SRRM1	S_767	+	-0.42	-0.56	+	+	1.00	1.96E-06	76.693	76.693
SRRM1	S_388	+	0.00	-0.14	+	+	1.00	5.49E-05	81.643	81.643
SRRM1	S_402	+	-0.41	-0.40	+	+	1.00	0.0128581	58.98	25.139
SRRM1	S_392	+	0.05	-0.14	+	+	1.00	5.49E-05	81.643	81.643
SRRM1	S_779	+	-0.55	-0.91	+	+	0.92	2.25E-05	68.634	68.634
SRRM1	S_390	+	0.07	-0.11	+	+	1.00	5.49E-05	81.643	81.643
SRRM2	S_424	+	-0.62	0.16	+		1.00	0.00063018	108.94	71.604
SRRM2	S_398	+	-1.15	-1.49	+	+	0.81	5.27E-19	101.58	101.58
SRRM2	S_875	+	0.03	0.11		+	1.00	4.88E-18	123.92	123.92
SRRM2	S_2272	+	0.21	0.21	+		1.00	6.40E-08	98.902	93.228
SRRM2	S_1320	+	0.01	0.13		+	1.00	0.00055966	63.46	44.957
SRRM2	S_2031	+	-0.11	-0.17	+	+	1.00	7.97E-15	106.3	53.266
SRRM2	S_1329	+	0.00	0.02			1.00	1.97E-07	98.654	98.654
SRRM2	S_876	+	-0.04	-0.03			1.00	1.46E-91	185.32	185.32
SRRM2	S_2274	+	0.12	0.15	+	+	1.00	6.40E-08	98.902	36.01
SRRM2	S_2276	+	0.12	0.15	+	+	1.00	6.40E-08	98.902	36.01
SRRM2	S_1103	+	0.49	0.41	+	+	0.99	2.72E-12	113.37	92.476
SRRM2	S_1102	+	0.12	0.21	+	+	0.86	9.61E-12	113.37	59.509
SRRM2	S_2032	+	0.04	0.01			1.00	2.10E-11	101.39	38.86
SRRM2	T_2034	+	0.04	0.01			1.00	2.10E-11	101.39	38.86
SRRM2	S_215	+	0.00	0.00			0.88	0.00017173	61.963	44.923
SRRM2	S_1179	+	-0.04	-0.14	+	+	1.00	1.11E-05	88.781	88.781
SRRM2	S_2398	+	0.10	0.00	+		0.79	0.00074384	78.113	44.024
SRRM2	S_1124	+	0.18	0.17			1.00	0.0029808	66.393	39.981
SRRM2	S_2067	+	0.05	0.00			1.00	3.09E-08	102.15	102.15
SRRM2	S_2071	+	0.05	0.00			1.00	3.09E-08	102.15	102.15
SRRM2	T_2069	+	0.05	0.00			1.00	3.09E-08	102.15	102.15
SRRM2	S_1099	+	0.19	0.20	+	+	1.00	2.72E-12	112.41	92.476
SRRM2	S_1326	+	-0.04	-0.21			1.00	0.00056859	84.046	50.781
SRRM2	S_1101	+	0.16	0.07	+	+	1.00	2.72E-12	112.41	92.476
SRRM2	S_377	+	-0.29	-0.50	+	+	0.99	5.27E-19	101.58	101.58
SRRM2	S_857	+	0.07	-0.12			0.92	0.00073415	66.925	49.683
SRRM2	S_1318	+	0.52	0.21		+	1.00	0.00055966	63.46	43.796
SRRM2	T_1231	+	0.34	0.21	+	+	0.70	0.00089276	59.585	32.074
SRRM2	T_866	+	0.00	-0.32	+		0.98	0.00073415	68.291	48.199
SRRM2	S_255	+	-0.25	-0.43			0.78	0.0005891	45.14	26.277
SRRM2	S_257	+	-0.25	-0.43			0.74	0.0005891	45.14	26.277
SRRM2	S_261	+	-0.25	-0.43			0.77	0.0005891	45.14	26.277
SRSF10	S_131	+	0.18	0.24	+	+	1.00	0.00883553	65.038	65.038
SRSF10	S_133	+	0.18	0.24	+	+	1.00	0.00883553	65.038	65.038
SRSF2	S_200	+	-0.18	-0.08			1.00	2.63E-15	109.56	109.56
SRSF2	S_194	+	-0.15	-0.17			1.00	2.63E-15	109.56	109.56
SRSF2	S_196	+	-0.15	-0.17			1.00	2.63E-15	109.56	109.56
SRSF6	S_303	+	-0.22	-0.19	+	+	1.00	2.32E-18	125.33	125.33
SRSF9	S_216	+	-0.17	-0.12	+	+	1.00	0.00012646	87.669	87.669
SRSF9	S_211	+	0.10	0.09			1.00	0.00012646	87.669	87.669
SSFA2	S_584	+	0.59	0.59	+	+	1.00	3.01E-18	120.4	89.455
SSFA2	S_586	+	0.59	0.59	+	+	1.00	3.01E-18	120.4	89.455
ST13;ST13P4	S_75	+	-0.30	-0.27			1.00	6.04E-177	223.93	223.93
ST13;ST13P4	S_71	+	0.00	0.22			0.98	0.00177677	66.152	44.545

ST13;ST13P4	S_72	+	→	0.05	→	0.06			1.00	6.04E-177	223.93	223.93
STEAP3	S_20	+	→	0.10	→	0.30		+	0.74	2.72E-07	93.062	75.167
STEAP3	S_17	+	→	0.13	→	0.27			1.00	2.72E-07	93.062	75.167
STK10	S_438	+	→	0.09	→	0.02			1.00	2.10E-19	120.79	120.79
STK10	T_952	+	→	-0.14	→	-0.21	+	+	1.00	4.25E-154	222.93	176.05
STK24	S_4	+	→	-0.01	→	-0.26			1.00	0.0050225	64.5	20.064
STMN1	S_25	+	→	0.04	→	0.29	+	+	1.00	3.55E-110	195.87	169.16
STMN1	S_38	+	→	-0.23	→	-0.09	+	+	1.00	2.89E-06	112.02	65.293
STMN1	S_16	+	↑	0.77	→	0.45	+	+	1.00	2.58E-19	125.08	99.492
STMN1;STMI	S_46	+	↑	0.59	↑	0.74			1.00	0.0061168	66.023	18.031
STRIP1	S_63	+	→	0.06	→	0.39		+	0.59	0.00044007	58.796	41.171
STRIP1	S_240	+	→	-0.04	→	-0.08		+	1.00	4.97E-11	105.96	74.916
STRN	S_233	+	→	0.28	→	0.17	+	+	1.00	6.48E-102	191.53	163.49
SUDS3	S_236	+	→	-0.13	→	-0.18			0.75	0.0016175	48.354	48.354
SUDS3	S_234	+	→	-0.21	→	-0.22	+	+	0.98	3.73E-05	67.396	67.396
SUDS3	S_237	+	→	-0.28	→	-0.34			0.85	3.73E-05	67.396	67.396
SUMO1	S_2	+	→	-0.16	→	0.00	+		1.00	9.55E-05	81.016	81.016
SVIL	S_270	+	→	0.02	→	-0.17		+	1.00	5.89E-05	87.729	60.701
SVIL	S_261	+	→	0.03	→	-0.22		+	0.95	5.89E-05	87.729	60.701
SVIL	T_426	+	→	-0.04	→	-0.15			1.00	5.23E-30	138.54	115.69
SYMPK	S_1173	+	→	-0.30	→	-0.49			0.81	0.00050468	56.553	38.657
TACC2	S_21	+	→	-0.11	→	-0.14	+		1.00	3.95E-08	84.166	70.565
TACC2	S_2321	+	→	-0.11	→	-0.14	+		1.00	3.95E-08	84.166	70.565
TANC2	S_1530	+	→	-0.23	→	-0.10	+		1.00	0.0205049	50.102	32.871
TANC2	S_1534	+	→	-0.23	→	-0.10	+		1.00	0.0205049	50.102	32.871
TANC2	S_1442	+	→	-0.09	→	-0.54		+	1.00	0.0150497	49.076	49.076
TANC2	S_1445		→	0.04	↓	-0.70		+	0.94	0.0150497	49.076	49.076
TBC1D10B	S_658	+	→	-0.22	→	-0.39	+	+	0.78	0.00048046	69.704	41.155
TBC1D10B	S_661	+	→	-0.18	→	-0.29	+	+	1.00	0.00048046	69.704	41.155
TBC1D15	S_658	+	→	-0.05	→	0.36		+	1.00	7.89E-05	80.733	22.945
TBC1D22A	S_113	+	→	-0.48	→	-0.41			0.98	0.00341702	51.524	51.524
TBC1D4	S_588	+	↑	0.67	↑	0.61	+	+	1.00	6.38E-06	93.237	45.386
TBC1D4	S_591	+	↑	0.73	↑	0.61	+	+	1.00	6.38E-06	93.237	44.753
TCEAL3	S_65	+	↑	1.00	↑	1.82	+	+	1.00	0.00208755	64.522	42.47
TCOF1	S_1151	+	→	-0.30	→	-0.11	+	+	0.88	8.05E-06	94.673	94.673
TCOF1	S_1301	+	→	-0.49	→	-0.48	+	+	0.98	0.0004477	69.07	46.741
TERF2IP	S_203	+	→	0.08	→	-0.06			0.88	8.26E-13	111.11	86.853
TFDP1	S_23	+	→	-0.33	→	-0.54		+	1.00	0.00290201	62.68	44.722
TFPT	S_180	+	↓	-0.91	↓	-0.86			1.00	0.00014086	66.152	66.152
THRAP3	T_685	+	→	0.07	→	0.16			0.66	2.42E-35	143.04	64.267
THRAP3	S_682	+	→	-0.01	→	0.18			1.00	1.17E-26	132.17	79.781
THRAP3	S_320	+	→	-0.17	→	0.00	+		0.99	6.96E-07	81.357	81.357
THRAP3	S_253	+	→	0.00	→	0.02			1.00	5.19E-13	110.53	58.427
THRAP3	S_315	+	→	-0.15	→	0.00	+		1.00	6.96E-07	81.357	81.357
THRAP3	S_939	+	→	0.23	→	0.17	+	+	0.99	1.07E-51	157.53	127.17
THRAP3	S_379	+	↑	0.67	→	0.54	+	+	0.82	0.00163463	67.102	52.592
THUMPD1	S_86	+	→	-0.03	→	-0.02			1.00	5.56E-100	187.75	156.83
THUMPD1	S_88	+	→	-0.03	→	-0.02			1.00	5.56E-100	187.75	156.83
TJAP1	S_470	+	→	0.46	→	0.43	+	+	1.00	3.35E-62	167.9	128.15
TJAP1	S_225	+	→	0.07	→	0.07			1.00	5.65E-19	120.63	95.173

TJP1	S_125	+	-0.08	-0.58		+	1.00	5.75E-09	81.763	66.081
TJP1	S_131	+	-0.08	-0.58		+	0.55	5.75E-09	81.763	66.081
TJP2	T_902	+	0.20	0.45	+	+	0.94	3.73E-10	82.126	82.126
TJP2	T_910	+	0.20	0.45	+	+	0.95	3.73E-10	82.126	82.126
TJP2	S_371	+	0.10	0.09			0.55	0.00071018	57.21	57.21
TJP2	S_375	+	0.10	0.09			0.55	0.00071018	57.21	57.21
TJP2	S_377	+	0.10	0.09			0.87	0.00071018	57.21	57.21
TJP2	S_1012	+	0.20	0.25	+		1.00	3.11E-76	179.9	170.47
TJP2	S_679	+	0.66	0.54	+		0.50	0.00565282	47.774	47.774
TJP2	T_684	+	0.66	0.54	+		0.50	0.00565282	47.774	47.774
TJP2	S_107	+	-0.09	-0.18		+	1.00	2.93E-11	107.07	107.07
TJP2	S_1017	+	-0.41	-0.50	+	+	1.00	5.85E-06	93.181	76.047
TJP2	S_1009	+	0.03	-0.03			0.89	0.00529713	40.92	26.502
TK1	S_13	+	-0.52	-0.43	+	+	0.99	3.01E-19	122.12	122.12
TK1	S_15	+	-0.56	-0.55	+	+	0.85	0.00019041	77.42	77.42
TLE3	S_196	+	-0.06	0.46			0.90	2.43E-06	95.429	60.531
TLN1	S_425	+	-0.03	0.07			0.76	0.00062361	48.616	48.616
TMEM230	S_24	+	0.17	0.62			0.66	0.00039795	73.296	46.025
TMF1	S_344	+	0.37	0.55	+	+	1.00	1.25E-19	127.53	96.053
TMOD3	S_25	+	-0.02	-0.06			0.99	5.24E-06	79.942	48.265
TMPO	T_74	+	-0.21	-0.32	+	+	1.00	9.32E-09	84.948	84.948
TMPO	S_168	+	-0.31	-0.23		+	0.65	1.89E-05	78.419	58.145
TMPO	T_160	+	0.04	-0.23			0.73	4.17E-15	113.73	113.73
TMPO	S_158	+	-0.06	-0.11			0.68	7.01E-64	162.42	112.14
TMPO	S_306	+	-0.32	-0.40			1.00	0.00068248	68.168	68.168
TMPO	S_159	+	-0.03	-0.12			0.71	7.01E-64	162.42	112.14
TMPO	S_67	+	-0.11	-0.30	+	+	1.00	2.10E-67	152.63	152.63
TMPO	S_66	+	0.06	-0.21	+	+	1.00	2.10E-67	152.63	152.63
TMSB4X	S_31	+	0.93	0.35	+	+	0.99	1.10E-12	114.06	114.06
TMSB4X	T_34	+	0.80	0.26	+	+	1.00	0.00266155	63.091	50.251
TMX1	S_247	+	0.16	0.22	+	+	1.00	2.92E-119	194.59	194.59
TNKS1BP1	S_287	+	0.92	0.94	+	+	1.00	3.18E-05	94.281	74.984
TNKS1BP1	S_1620	+	0.08	0.09	+		1.00	3.29E-27	134.58	104.77
TNKS1BP1	S_344	+	0.10	0.52	+	+	0.79	0.00020295	63.869	47.254
TNKS1BP1	S_498	+	-0.05	-0.05			0.95	7.02E-37	129.08	113.79
TNKS1BP1	S_494	+	-0.05	-0.05			0.99	7.02E-37	129.08	113.79
TNKS1BP1	S_1621	+	0.25	0.06	+		1.00	3.29E-27	134.58	104.77
TNRC6B	S_879	+	-0.02	-0.45			1.00	2.52E-06	84.166	66.184
TNS1	S_1177	+	0.23	-0.03	+		0.99	0.00642082	52.451	52.451
TNS1	S_1271	+	0.17	-0.25			0.95	0.01879	55.258	36.158
TNS3	S_536	+	0.31	0.46	+		1.00	9.18E-20	117.96	87.716
TNS3	S_420	+	-0.43	-0.43	+	+	0.97	0.00028001	71.354	71.354
TOE1	S_5	+	-0.22	0.05			1.00	6.80E-11	96.181	65.092
TOM1L1	S_246	+	-0.04	-0.79		+	0.99	0.00148346	55.406	55.406
TOMM22	S_15	+	0.25	0.00	+		1.00	8.31E-34	134.29	134.29
TOP1	S_10	+	0.27	0.30	+	+	1.00	0.0019017	53.037	53.037
TOP2A	S_1247	+	-0.19	0.25	+		1.00	5.79E-20	163.61	115.88
TOP2A	S_1377	+	0.15	0.43	+	+	1.00	2.97E-12	113.65	85.973
TOP2A	S_1374	+	0.89	1.15	+	+	1.00	6.88E-08	106.6	69.653
TOP2B	S_1521	+	-0.03	0.10			1.00	1.98E-50	152.4	152.4

TOP2B	S_1461	+	-0.08	0.01			1.00	1.01E-25	126.96	100.8
TOP2B	S_1466	+	0.00	-0.34			0.54	0.00077198	65.105	65.105
TOP2B	S_1519	+	-0.02	-0.01			1.00	2.84E-29	133.51	133.51
TOP2B	S_1517	+	0.00	-0.04			1.00	1.98E-50	152.4	152.4
TOP2B	S_1576	+	-0.44	-0.53		+	0.64	2.79E-08	84.689	84.689
TOPORS	S_33	+	-1.47	-1.19	+	+	0.80	0.00898579	50.158	31.768
TOR1AIP1	S_156	+	0.16	0.13	+		1.00	1.35E-05	74.561	64.997
TOR1AIP1	S_154	+	0.15	0.13	+		1.00	1.35E-05	74.561	64.997
TOR1AIP1	S_157	+	0.64	0.16	+		1.00	1.35E-05	74.561	64.997
TOR1AIP1	T_147	+	-0.27	-0.69			0.81	0.00026326	64.454	48.142
TOR1AIP1	S_143	+	-0.15	-0.98			0.82	0.00919251	56.424	35.413
TP53	S_6	+	-0.34	-1.14			0.98	0.00906027	59.339	27.113
TP53BP1	S_1114	+	0.40	0.46			0.86	3.60E-39	136.61	113.48
TP53BP1	S_500	+	0.18	0.21	+	+	1.00	1.21E-51	160.05	160.05
TP53BP1	S_1067	+	0.29	0.22			0.50	0.00733981	76.301	41.975
TP53BP1	S_1068	+	0.29	0.22			0.50	0.00733981	76.301	41.975
TP53BP1	S_1113	+	0.23	0.19			0.99	1.14E-11	96.848	57.852
TP53BP1	S_294	+	0.16	-0.12	+	+	1.00	6.97E-19	112.37	112.37
TP53BP1	S_1426	+	0.01	-0.29		+	1.00	1.87E-11	95.141	95.141
TP53BP1	S_1430	+	0.01	-0.29		+	1.00	1.87E-11	95.141	95.141
TP53BP1	S_1759	+	0.32	-0.13	+		0.61	0.00046028	57.366	43.151
TP53BP1	S_1758	+	0.30	-0.17			0.61	0.00046028	57.366	43.151
TP53BP1	T_1756	+	0.30	-0.17			0.99	0.00046028	57.366	43.151
TPD52L2	S_12	+	0.00	-0.04			1.00	7.63E-37	142.23	119.6
TPI1	S_21	+	0.11	0.22	+	+	1.00	2.29E-93	182.77	182.77
TPR	S_2155	+	-0.03	0.02			1.00	0.00028001	71.354	71.354
TPX2	S_738	+	-0.30	-0.28	+	+	1.00	0.0006972	70.438	36.547
TRA2A	S_2	+	-0.01	0.15			1.00	0.00412934	66.059	48.043
TRA2A	S_14	+	0.18	0.09			1.00	0.018849	57.248	57.248
TRAF2	T_7	+	-0.17	0.52			1.00	0.00066549	77.221	42.132
TRAF2	S_11	+	-0.15	0.35			1.00	0.00066549	77.221	42.132
TRAFD1	S_415	+	0.19	-0.04	+		0.98	2.07E-76	177.04	146.93
TRIM28	S_50	+	-0.26	-0.15	+		0.84	3.83E-10	76.208	63.317
TRIM28	S_19	+	-0.11	-0.25	+	+	0.98	3.18E-21	107.09	107.09
TRIM56	S_469	+	0.00	0.04	+		1.00	0.00017904	64.377	53.625
TRIM56	S_475	+	-0.06	-0.19			1.00	7.13E-06	75.608	58.005
TRIM56	S_471	+	-0.29	-0.35			1.00	7.13E-06	75.608	58.005
TRIO	S_2400	+	-0.21	-0.33		+	0.71	3.35E-05	76.557	76.557
TRIO	S_2396	+	-0.23	-0.42		+	0.87	3.35E-05	76.557	76.557
TRIP10	S_299	+	-0.01	0.03			0.98	3.53E-06	81.594	62.77
TRIP10	S_296	+	-0.05	-0.23			1.00	2.06E-06	81.594	62.77
TRIP12	S_312	+	0.00	0.19		+	0.99	0.00802692	51.235	15.558
TSC22D4	S_279	+	-0.14	0.33			1.00	5.80E-60	160.84	124.16
TTC1	S_83	+	0.00	0.05			1.00	5.37E-19	110.89	84.757
TUBA1A;TUB	T_16	+	-0.14	-0.18			0.62	0.00409681	62.028	27.88
TUBA1A;TUB	S_13	+	-0.11	-0.18			0.86	6.60E-07	84.159	58.901
TUBA1B;TUB	S_224	+	-0.12	-0.05			1.00	2.34E-05	92.671	71.611
UBAP2L	S_468	+	-0.27	-0.49		+	0.63	0.00084405	50.858	50.858
UBAP2L	S_460	+	-0.22	-0.36	+	+	0.89	9.09E-08	77.51	77.51
UBAP2L	S_447	+	-0.69	-1.26	+	+	0.93	1.77E-19	113.05	113.05

UNC13D	S_150	+	→	-0.08	→	-0.18	+	+	0.99	8.30E-81	163.6	163.6
UNC13D	S_153	+	→	-0.02	→	-0.19			0.63	0.00046925	55.751	55.751
USP10	S_576	+	→	-0.04	→	0.14			1.00	0.0001637	65.854	53.931
USP15	S_229	+	→	-0.40	→	-0.09	+		1.00	0.0008364	77.726	55.814
USP24	S_2561	+	→	-0.02	↓	-0.74			0.87	0.00200874	56.972	56.972
UTP14A	S_29	+	→	0.41	→	0.24	+		1.00	8.39E-14	118.85	79.065
UTP14A	S_31	+	→	0.41	→	0.24	+		1.00	8.39E-14	118.85	79.065
UTP3	S_365	+	→	0.13	→	0.18			1.00	7.37E-42	191.13	119.45
UTP3	S_368	+	→	0.13	→	0.18			1.00	7.37E-42	191.13	119.45
VAMP4	S_30	+	→	0.11	→	0.09	+		1.00	7.23E-40	149.18	149.18
VAT1	S_18	+	→	0.12	→	-0.01			0.86	0.00446691	80.508	51.293
VCL	S_288	+	→	0.29	→	0.05			0.70	0.00277365	60.093	26.332
VCL	S_290	+	→	0.32	→	0.17	+		1.00	2.37E-27	131.37	98.224
VCL	S_721	+	↑	0.62	→	0.44	+	+	1.00	0.00066658	77.633	49.523
VDAC1	S_104	+	→	-0.12	→	-0.14	+	+	1.00	6.39E-20	129.05	96.895
VIM	S_420	+	→	0.26	↑	0.62	+	+	0.79	1.64E-61	166.45	166.45
VIM	S_51	+	→	-0.23	→	0.19			0.99	6.68E-37	145.79	145.79
VIM	S_419	+	→	0.42	↑	0.60	+	+	0.90	4.79E-77	180.48	180.48
VIM	S_430	+	→	0.39	↑	0.70	+	+	1.00	5.95E-05	82.709	42.064
VIM	S_56	+	→	-0.19	→	0.02			0.99	2.69E-61	163.44	163.44
VIM	S_55	+	→	-0.11	→	-0.01	+		0.95	2.21E-61	164.82	164.82
VIM	S_39	+	↑	1.10	↑	0.99	+	+	0.99	0.00026966	79.23	50.167
VIM	S_27	+	→	0.09	→	0.32		+	0.75	0.0167382	44.925	18.634
VIPR1	S_237	+	→	0.40	→	0.50	+	+	0.89	0.00918891	51.286	22.33
VIPR1	S_238	+	→	0.40	→	0.50	+	+	0.56	0.00918891	58.172	24.855
VIPR1	S_239	+	→	0.19	→	0.58	+	+	0.56	0.00918891	58.172	24.855
WAPAL	S_226	+	→	-0.31	→	-0.13	+	+	1.00	2.16E-36	148.97	86.279
WAPAL	S_221	+	→	-0.31	→	-0.15	+	+	1.00	2.16E-36	148.97	86.279
WAPAL	S_223	+	→	-0.34	→	-0.26	+	+	0.98	0.00043024	82.663	82.663
WAPAL	S_120	+	→	0.01	→	-0.25		+	0.99	1.88E-05	72.316	72.316
WDFY3	S_1011		↓	-4.17	↓	-2.61			0.98	0.0146208	46.847	7.6586
WDFY3	S_1015		↓	-4.17	↓	-2.61			0.99	0.0146208	46.847	7.6586
WDHD1	S_745	+	→	-0.01	→	0.16			1.00	0.0032171	48.025	33.669
WDR62	S_1228	+	→	-0.08	→	0.00			0.88	1.74E-25	122.6	122.6
WRAP53	S_90	+	→	-0.31	→	-0.24			0.94	7.51E-06	81.133	55.622
WRAP53	S_85	+	→	-0.21	→	-0.44			0.97	7.51E-06	81.133	55.622
WRAP53	T_489	+	→	-0.03	→	-0.43			0.80	8.46E-05	66.536	62.617
YAP1	T_63	+	→	0.08	→	0.19			0.72	1.35E-08	122.53	74.797
YAP1	S_61	+	→	-0.09	→	0.11			0.90	1.05E-64	163.96	163.96
YBX1;YBX2;Y	S_102	+	→	-0.04	→	0.12			1.00	3.45E-15	111.45	85.483
YTHDC1	S_308	+	→	0.09	→	0.23			1.00	0.0003172	77.674	38.37
ZBTB7A	S_525	+	→	-0.11	→	-0.49		+	0.79	0.00028823	64.589	46.273
ZC3H13	S_370	+	→	-0.08	→	-0.24			0.58	0.00112127	59.857	45.751
ZC3H13	S_381	+	→	-0.08	→	-0.24			0.97	0.00112127	59.857	45.751
ZC3H13	Y_374	+	→	-0.08	→	-0.24			0.60	0.00112127	59.857	45.751
ZC3H13	S_207	+	→	-0.17	→	0.00	+		1.00	3.70E-05	91.592	50.609
ZC3H13	S_209	+	→	-0.17	→	0.00	+		0.94	3.70E-05	91.592	50.609
ZC3H13	S_265	+	→	-0.40	↓	-0.71	+		1.00	4.75E-79	178.57	178.57
ZC3H13	T_263	+	→	-0.40	↓	-0.71	+		1.00	4.75E-79	178.57	178.57
ZC3H18	S_502	+	→	0.45	→	0.14			1.00	5.17E-06	89.189	48.109

ZC3H18	S_500	+	→	-0.01	→	-0.03			1.00	0.0108202	68.168	36.009
ZC3HC1	S_314	+	→	-0.25	→	-0.24			0.61	1.29E-08	99.409	99.409
ZDHHC5	S_568	+	→	-0.26	→	-0.21		+	1.00	2.29E-07	88.486	68.132
ZDHHC5	S_641	+	→	-0.27	→	-0.39	+	+	0.54	0.0101594	43.326	43.326
ZDHHC5	S_379	+	→	0.24	→	0.21	+	+	1.00	3.78E-156	217.73	170.81
ZDHHC5	S_327	+	→	0.27	→	0.17	+		0.66	0.0100876	42.947	16.004
ZEB1	S_612	+	→	-0.39	↓	-0.59	+	+	0.99	0.00262116	51.39	51.39
ZFYVE19	S_179	+	→	0.28	→	0.12	+	+	1.00	2.22E-156	219.96	190.49
ZMYM4	T_118	+	→	-0.07	→	0.05			0.50	9.18E-05	75.316	75.316
ZMYM4	S_122	+	→	-0.06	→	0.27			0.78	9.18E-05	75.316	75.316
ZNF185	S_64	+	↑	1.98	↑	1.79	+	+	0.78	0.00238864	70.47	53.799
ZNF185	S_103	+	→	0.24	→	0.23		+	0.98	0.00032205	70.072	43.06
ZNF185	T_210	+	→	-0.14	↓	-0.67	+	+	0.99	4.20E-43	144.43	107.52
ZNF579	T_482		→	-0.48	↓	-0.65	+		0.58	0.00026371	67.655	46.347
ZNF579	S_483	+	↓	-0.69	↓	-1.21	+	+	0.79	4.23E-06	83.666	61.999
ZRANB2	S_310	+	→	-0.27	→	0.00			0.67	0.00996677	46.282	31.009
ZRANB2	S_305	+	→	-0.08	→	0.13	+	+	1.00	1.33E-12	109.23	109.23
ZRANB2	S_307	+	→	-0.08	→	0.13	+	+	1.00	1.33E-12	109.23	109.23
ZRANB2	S_153	+	→	0.08	→	0.27		+	1.00	4.45E-55	153.06	153.06
ZRANB2	S_188	+	→	-0.01	→	0.10		+	1.00	2.15E-61	169.6	138.45
ZRANB2	S_181	+	→	-0.26	→	-0.14			1.00	6.38E-05	86.214	69.991
ZRANB2	S_120	+	→	0.18	→	0.00	+		1.00	7.28E-05	89.136	76.344
ZYX	S_142	+	→	0.12	→	0.25		+	0.50	5.14E-19	111.24	111.24
ZYX	S_143	+	→	0.12	→	0.25		+	0.50	5.14E-19	111.24	111.24
ZYX	S_187	+	→	-0.20	→	-0.14	+	+	1.00	2.03E-07	98.337	95.183

Appendix 7

Gene	Protein	Site	M/L(log2)	H/L(log2)
CCAR1	Cell division cycle and apoptosis regulator protein 1	S_360	4.76	1.95
CCAR1	Cell division cycle and apoptosis regulator protein 1	T_348	4.76	1.95
CCAR1	Cell division cycle and apoptosis regulator protein 1	Y_347	4.76	1.95
ZNF185	Zinc finger protein 185	S_64	1.98	1.79
RRAGC	Ras-related GTP-binding protein C	S_2	1.30	1.12
TBC1D4	TBC1 domain family member 4	S_591	0.73	0.61
PLEC	Plectin	S_4217	0.88	0.77
VIM	Vimentin	S_39	1.10	0.99
LMO7	LIM domain only protein 7	S_342	0.80	0.70
PLEC	Plectin	S_4213	0.70	0.61
RRAGC	Ras-related GTP-binding protein C	Y_16	1.14	1.06
PDIA6	Protein disulfide-isomerase A6	S_425	1.12	1.04
PLEC	Plectin	S_4216	0.68	0.61
FLNC	Filamin-C	S_2200	1.57	1.50
TBC1D4	TBC1 domain family member 4	S_588	0.67	0.61
RPL27A	60S ribosomal protein L27a	S_68	0.74	0.68
LMO7	LIM domain only protein 7	S_1176	0.73	0.69
NUFIP2	Nuclear fragile X mental retardation-interacting protein 2	S_652	0.70	0.67
SPTBN1	Spectrin beta chain, non-erythrocytic 1	S_14	0.60	0.58
SSFA2	Sperm-specific antigen 2	S_584	0.59	0.59
SSFA2	Sperm-specific antigen 2	S_586	0.59	0.59
TNKS1BP1	182 kDa tankyrase-1-binding protein	S_287	0.92	0.94
PEA15	Astrocytic phosphoprotein PEA-15	S_116	1.01	1.04
LMO7	LIM domain only protein 7	S_471	0.74	0.78

Gene	Protein	Site	M/L(log2)	H/L(log2)
HSP90B1	Endoplasmin	S_306	2.15	2.20
PATL1	Protein PAT1 homolog 1	S_177	0.62	0.68
RAD50	DNA repair protein RAD50	S_496	0.77	0.84
CD2AP	CD2-associated protein	S_458	0.95	1.09
SEC22B	Vesicle-trafficking protein SEC22b	S_137	0.66	0.82
ANXA1	Annexin A1	S_5	0.96	1.12
ARHGAP29	Rho GTPase-activating protein 29	S_176	0.94	1.11
MVB12A	Multivesicular body subunit 12A	S_170	0.81	0.99
CTTN	Src substrate cortactin	S_389	0.72	0.92
ARHGAP29	Rho GTPase-activating protein 29	S_171	0.67	0.88
TOP2A	DNA topoisomerase 2-alpha	S_1374	0.89	1.15
NELFE	Negative elongation factor E	S_115	0.95	1.25
ADAM17	Disintegrin and metalloproteinase domain-containing protein 17	S_791	0.80	1.10
NDRG1	Protein NDRG1	S_249	1.47	1.82
MTOR	Serine/threonine-protein kinase mTOR	T_1162	0.72	1.09
HSPB1	Heat shock protein beta-1	S_82	0.82	1.22
ARHGAP32	Rho GTPase-activating protein 32	T_565	0.73	1.30
TCEAL3	Transcription elongation factor A protein-like 3	S_65	1.00	1.82

Appendix 7: The significant phosphorylation changes **up-regulated** by **both insulin (M/L) and IGF-II (H/L)** with respect to the untreated samples are shown ($\log2 > 0.58$, $P < 0.05$).

Appendix 8

Gene	Protein	sites	M/L(log2)	H/L(log2)
NCOR2	Nuclear receptor corepressor 2	S_1001	-1.04	-0.66
TOPORS	E3 ubiquitin-protein ligase Topors	S_33	-1.47	-1.19
AKAP2	A-kinase anchor protein 2	S_375	-0.82	-0.59
DNMT1	DNA (cytosine-5)-methyltransferase 1	S_378	-0.69	-0.60
MAP1B	Microtubule-associated protein 1B	S_1256	-0.65	-0.61
OGFR	Opioid growth factor receptor	S_539	-0.88	-0.84
MYO9B	Unconventional myosin-IXb	T_1271	-0.63	-0.60
AKT1S1	Proline-rich AKT1 substrate 1	S_108	-0.95	-0.95
SRRM1	Serine/arginine repetitive matrix protein 1	S_775	-0.74	-0.74
MEF2D	Myocyte-specific enhancer factor 2D	S_205	-0.61	-0.65
OGFR	Opioid growth factor receptor	S_537	-0.60	-0.65
PSMD2	26S proteasome non-ATPase regulatory subunit 2	S_16	-0.63	-0.69
AKT1S1	Proline-rich AKT1 substrate 1	S_112	-0.84	-0.95
OGFR	Opioid growth factor receptor	S_565	-1.02	-1.14
MAP1B	Microtubule-associated protein 1B	S_1258	-0.60	-0.73
KMT2A	Histone-lysine N-methyltransferase 2A	S_1799	-0.69	-0.84
BAG3	BAG family molecular chaperone regulator 3	S_386	-0.89	-1.05
HIST1H1E	Histone H1.4	T_18	-0.62	-0.79
KMT2A	Histone-lysine N-methyltransferase 2A	T_1807	-0.68	-0.86
KDM1A	Lysine-specific histone demethylase 1A	S_166	-0.62	-0.83
AFAP1	Actin filament-associated protein 1	S_265	-0.72	-0.98
DDX54	ATP-dependent RNA helicase DDX54	T_70	-0.62	-0.89
OGFR	Opioid growth factor receptor	S_559	-0.59	-0.91

Gene	Protein	sites	M/L(log2)	H/L(log2)
ATXN2L	Ataxin-2-like protein	T_632	-0.64	-0.97
BAG3	BAG family molecular chaperone regulator 3	S_385	-0.85	-1.18
SRRM2	Serine/arginine repetitive matrix protein 2	S_398	-1.15	-1.49
OGFR	Opioid growth factor receptor	T_561	-0.95	-1.32
RRM2	Ribonucleoside-diphosphate reductase subunit M2	S_20	-0.87	-1.30
ZNF579	Zinc finger protein 579	S_483	-0.69	-1.21
SMC4	Structural maintece of chromosomes protein 4	S_27	-0.75	-1.28
BAG3	BAG family molecular chaperone regulator 3	S_377	-1.02	-1.56
NCOR2	Nuclear receptor corepressor 2	S_149	-0.70	-1.25
SMC4	Structural maintece of chromosomes protein 4	S_28	-0.71	-1.28
UBAP2L	Ubiquitin-associated protein 2-like	S_447	-0.69	-1.26
ATXN2L	Ataxin-2-like protein	S_634	-0.76	-1.36
NCOR2	Nuclear receptor corepressor 2	S_152	-0.74	-1.36
MARCKSL1	MARCKS-related protein	S_101	-0.77	-1.41
MARCKSL1	MARCKS-related protein	S_104	-0.77	-1.41

Appendix 8: The significant phosphorylation changes **down-regulated** by **both insulin (M/L) and IGF-II (H/L)** with respect to the untreated samples are shown ($log2 < -0.58$, $P < 0.05$).

Appendix 9

Gene	Protein	sites	M/L(log2)
EGFR	Epidermal growth factor receptor	S_1166	0.60
DTNBP1	Dysbindin	S_235	0.61
DTNBP1	Dysbindin	S_240	0.61
TJP2	Tight junction protein ZO-2	S_679	0.66
TJP2	Tight junction protein ZO-2	T_684	0.66
THRAP3	Thyroid hormone receptor-associated protein 3	S_379	0.67
PLEC	Plectin	S_4220	0.60
FAM129A	Protein Niban	S_602	0.70
VCL	Vinculin	S_721	0.62
GFPT1	Glutamine--fructose-6-phosphate aminotransferase [isomerizing] 1	S_243	0.67
SEPT9	Septin-9	S_11	0.76
STMN1	Stathmin	S_16	0.77
OSBP	Oxysterol-binding protein 1	S_193	0.65
HMGA1	High mobility group protein HMG-I/HMG-Y	S_44	0.72
TOR1AIP1	Torsin-1A-interacting protein 1	S_157	0.64
LEO1	RNA polymerase-associated protein LEO1	S_598	0.74
TMSB4X	Thymosin beta-4	T_34	0.80
TMSB4X	Thymosin beta-4	S_31	0.93

Appendix 9: The significant phosphorylation changes **up regulated** by **insulin (M/L) only** with respect to the untreated samples are shown ($\log2 > 0.58$, $P < 0.05$). The changes by IGF-II were not significant.

Appendix 10

Gene	Protein	sites	M/L(log2)
SRRM2	Serine/arginine repetitive matrix protein 2	S_424	-0.62
MAP1B	Microtubule-associated protein 1B	S_2209	-0.70
MAP1B	Microtubule-associated protein 1B	S_2211	-0.70
NCAPD2	Condensin complex subunit 1	S_1333	-0.63
DUT	Deoxyuridine 5'-triphosphate nucleotidohydrolase, mitochondrial	S_11	-0.92
SQSTM1	Sequestosome-1	S_24	-0.92
DCP1A	mRNA-decapping enzyme 1A	S_277	-0.72
DCP1A	mRNA-decapping enzyme 1A	T_283	-0.78
FOSL1	Fos-related antigen 1	S_74	-0.68
DCP1A	mRNA-decapping enzyme 1A	S_281	-0.72
ARHGAP17	Rho GTPase-activating protein 17	S_209	-0.62
ARHGAP17	Rho GTPase-activating protein 17	T_215	-0.62
MKI67	Antigen KI-67	S_224	-0.64
RNF20	E3 ubiquitin-protein ligase BRE1A	S_138	-0.68
DYNC1LI1	Cytoplasmic dynein 1 light intermediate chain 1	T_512	-0.60
RB1	Retinoblastoma-associated protein	S_807	-0.62
RB1	Retinoblastoma-associated protein	S_811	-0.62
SCRIB	Protein scribble homolog	T_1261	-0.62
ARHGEF18	Rho guanine nucleotide exchange factor 18	S_1124	-0.64
BRD8	Bromodomain-containing protein 8	S_128	-0.58

Appendix 10: The significant phosphorylation changes **down regulated** by **insulin (M/L) only** with respect to the untreated samples are shown ($\log2 < -0.58$, $P < 0.05$). The changes by IGF-II were not significant.

Appendix 11

Gene	Protein	sites	H/L(log2)
PCBP2	Poly(rC)-binding protein 2	S_185	4.36
EIF5B	Eukaryotic translation initiation factor 5B	S_107	0.70
DDX41	Probable ATP-dependent RNA helicase DDX41	S_21	0.59
RTN4	Reticulon-4	S_182	0.82
VIM	Vimentin	S_420	0.62
VIM	Vimentin	S_430	0.70
AKT1S1	Proline-rich AKT1 substrate 1	S_183	0.67
ARHGAP18	Rho GTPase-activating protein 18	S_21	0.71
ARHGAP18	Rho GTPase-activating protein 18	S_24	0.75
VIM	Vimentin	S_419	0.60
EGFR	Epidermal growth factor receptor	S_1162	0.60

Appendix 11: The significant phosphorylation changes **up-regulated** by **IGF-II (H/L) only** with respect to the untreated samples are shown ($\log2 > 0.58$, $P < 0.05$). The changes by insulin were not significant.

Appendix 12

Gene	Protein	sites	H/L(log2)
MAP1B	Microtubule-associated protein 1B	S_1262	-0.58
MAP1B	Microtubule-associated protein 1B	S_1378	-0.61
MAP1B	Microtubule-associated protein 1B	S_1376	-0.61
ZEB1	Zinc finger E-box-binding homeobox 1	S_612	-0.59
SNW1	SNW domain-containing protein 1	S_234	-0.72
ACIN1	Apoptotic chromatin condensation inducer in the nucleus	T_408	-0.69
NEDD4L	E3 ubiquitin-protein ligase NEDD4-like	S_334	-0.68
CDK12	Cyclin-dependent kinase 12	S_684	-0.61
FAM129B	Niban-like protein 1	S_683	-0.61
DYNC1LI1	Cytoplasmic dynein 1 light intermediate chain 1	T_515	-0.61
GPATCH8	G patch domain-containing protein 8	S_662	-0.67
ARHGAP17	Rho GTPase-activating protein 17	S_108	-0.80
PNKP	Bifunctional polynucleotide phosphatase/kinase	T_118	-0.63
KIF23	Kinesin-like protein KIF23	S_503	-0.83
CDK12	Cyclin-dependent kinase 12	S_680	-0.74
CIC	Protein capicua homolog	S_1373	-0.70
CIC	Protein capicua homolog	S_1382	-0.70
PGRMC1	Membrane-associated progesterone receptor component 1	S_54	-0.76
SRRM1	Serine/arginine repetitive matrix protein 1	S_779	-0.91
DYNC1LI1	Cytoplasmic dynein 1 light intermediate chain 1	S_516	-0.71
INPPL1	Phosphatidylinositol 3,4,5-trisphosphate 5-phosphatase 2	S_132	-0.62

Gene	Protein	sites	H/L(log2)
EPRS	Bifunctional glutamate/proline--tRNA ligase	S_886	-0.72
ARHGAP17	Rho GTPase-activating protein 17	S_207	-0.74
EIF3G	Eukaryotic translation initiation factor 3 subunit G	T_41	-0.82
DOCK5	Dedicator of cytokinesis protein 5	S_1789	-0.70
DOCK5	Dedicator of cytokinesis protein 5	T_1794	-0.70
SCRIB	Protein scribble homolog	S_1485	-0.69
DYNC1LI1	Cytoplasmic dynein 1 light intermediate chain 1	S_510	-0.59
EIF3G	Eukaryotic translation initiation factor 3 subunit G	T_38	-1.02
KANK2	KN motif and ankyrin repeat domain-containing protein 2	S_19	-0.87
KANK2	KN motif and ankyrin repeat domain-containing protein 2	T_14	-0.87
TJP1	Tight junction protein ZO-1	S_125	-0.58
TJP1	Tight junction protein ZO-1	S_131	-0.58
RABL6	Rab-like protein 6	S_596	-0.76
RABL6	Rab-like protein 6	T_599	-0.76
MAP1B	Microtubule-associated protein 1B	S_1389	-0.59
EPRS	Bifunctional glutamate/proline--tRNA ligase	S_885	-0.62
ZNF185	Zinc finger protein 185	T_210	-0.67
NELFB	Negative elongation factor B	S_557	-0.99
BRD2	Bromodomain-containing protein 2	S_178	-0.69
BRD2	Bromodomain-containing protein 2	S_181	-0.69
MPRIP	Myosin phosphatase Rho-interacting protein	S_294	-0.78
MPRIP	Myosin phosphatase Rho-interacting protein	T_295	-0.78
MTCL1	Microtubule cross-linking factor 1	S_263	-0.89
PGRMC1	Membrane-associated	S_57	-0.94

Gene	Protein	sites	H/L(log2)
	progesterone receptor component 1		
LSR	Lipolysis-stimulated lipoprotein receptor	S_308	-0.76
MYEF2	Myelin expression factor 2	S_17	-1.11
TANC2	Protein TANC2	S_1445	-0.70
TOM1L1	TOM1-like protein 1	S_246	-0.79
NCOR2	Nuclear receptor corepressor 2	T_156	-1.07
DOK1	Docking protein 1	S_152	-0.86
FAM129B	Niban-like protein 1	S_679	-1.13
CD3EAP	DNA-directed RNA polymerase I subunit RPA34	S_136	-1.15

Appendix 12: The significant phosphorylation changes **down regulated** by **IGF-II (H/L) only** with respect to the untreated samples are shown ($\log2 < -0.58$, $P < 0.05$). The changes by insulin were not significant.

Appendix 13

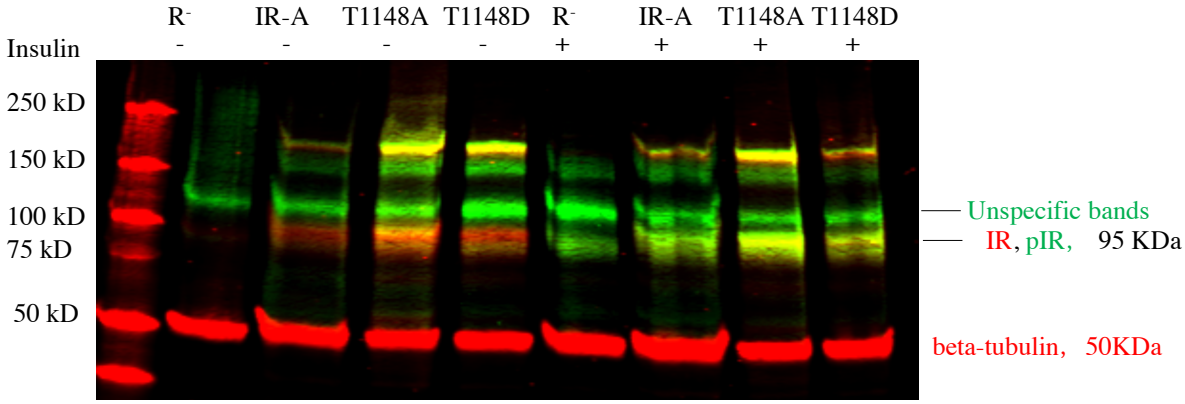

Appendix 13: Raw data of Figure 4.5-A. IR and Tubulin band are red and phosphor-IR band is green.

Appendix 14

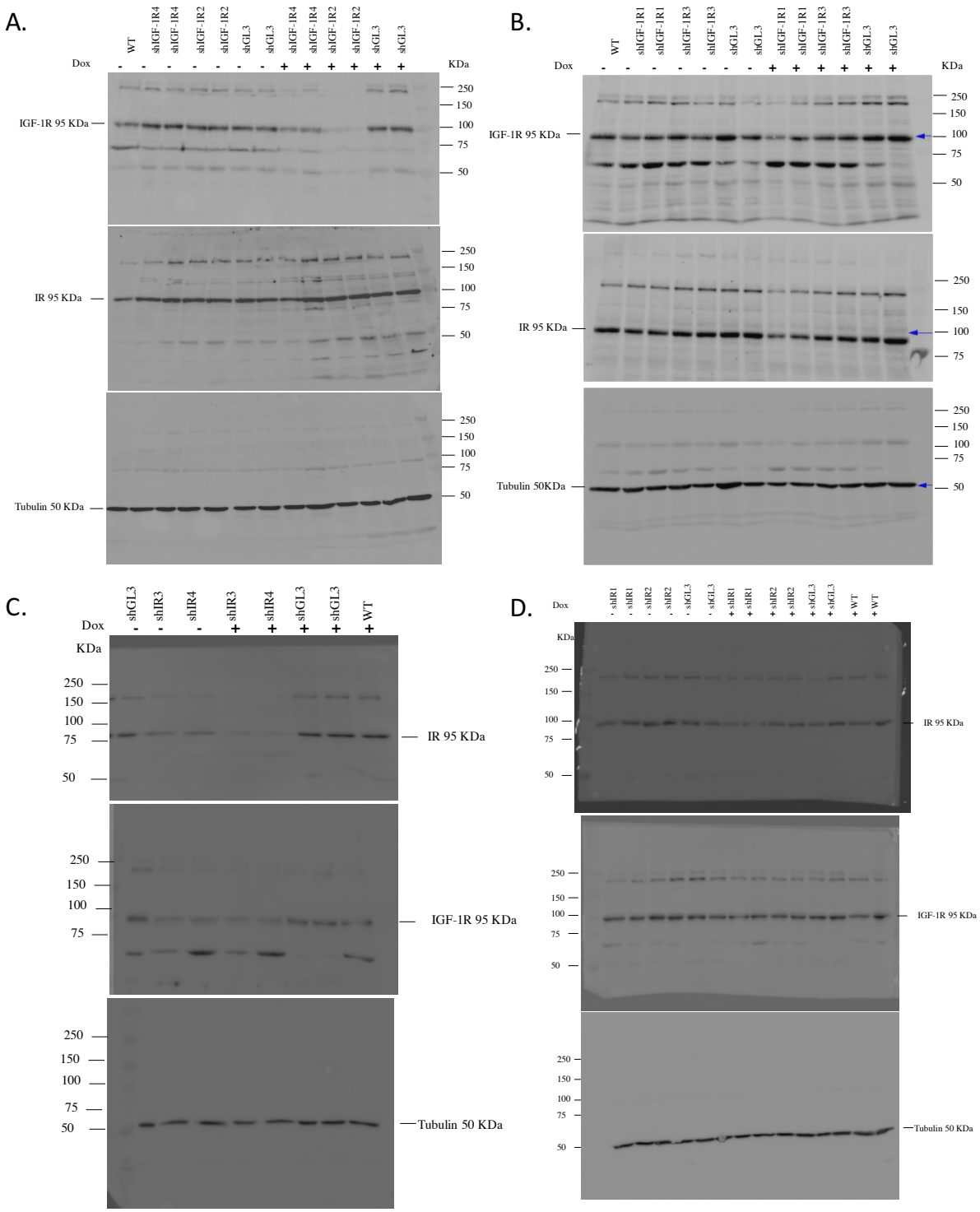

Appendix 14: Raw data of Figure 5.10. In this diagram non specific bands are present as a long exposure time was used in order to show the molecular weight markers. However, the intensities of these bands are much lower than the highlighted bands of interest.

Appendix 15

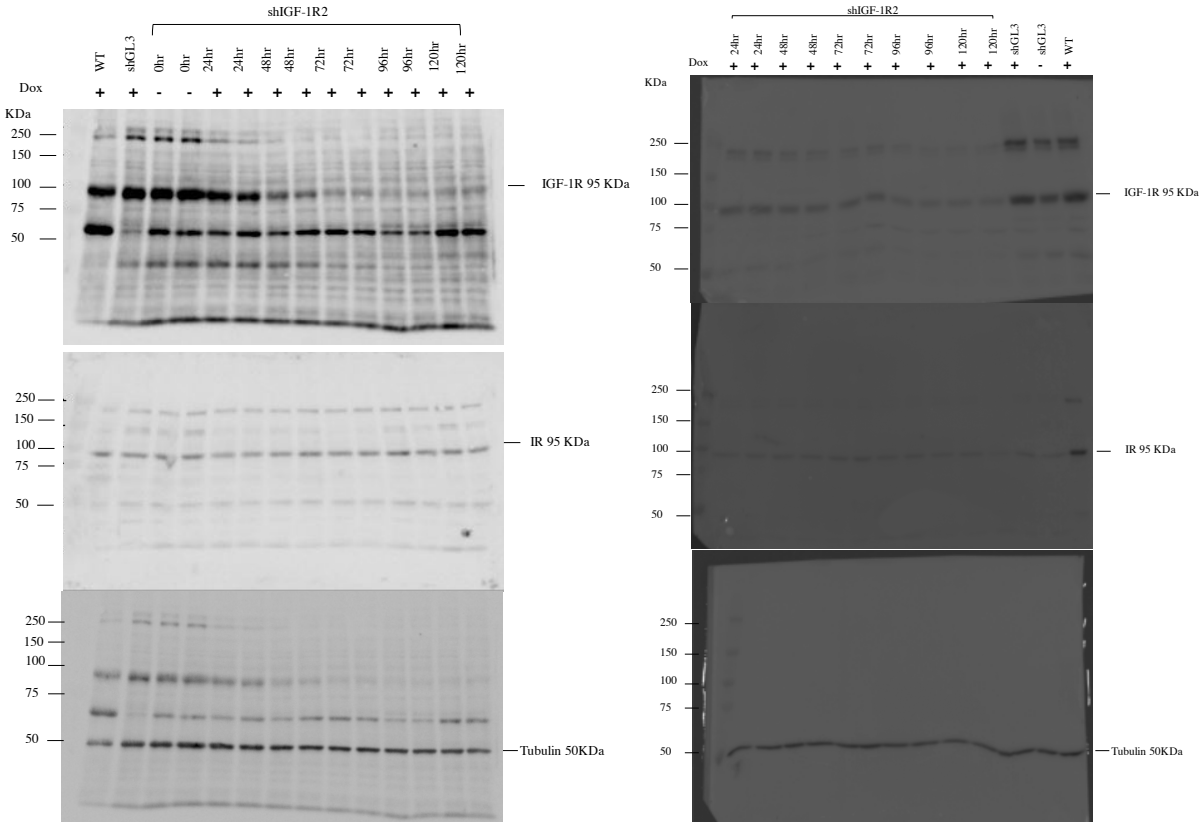

Appendix 15: Raw data of Figure 5.11.

Appendix 16

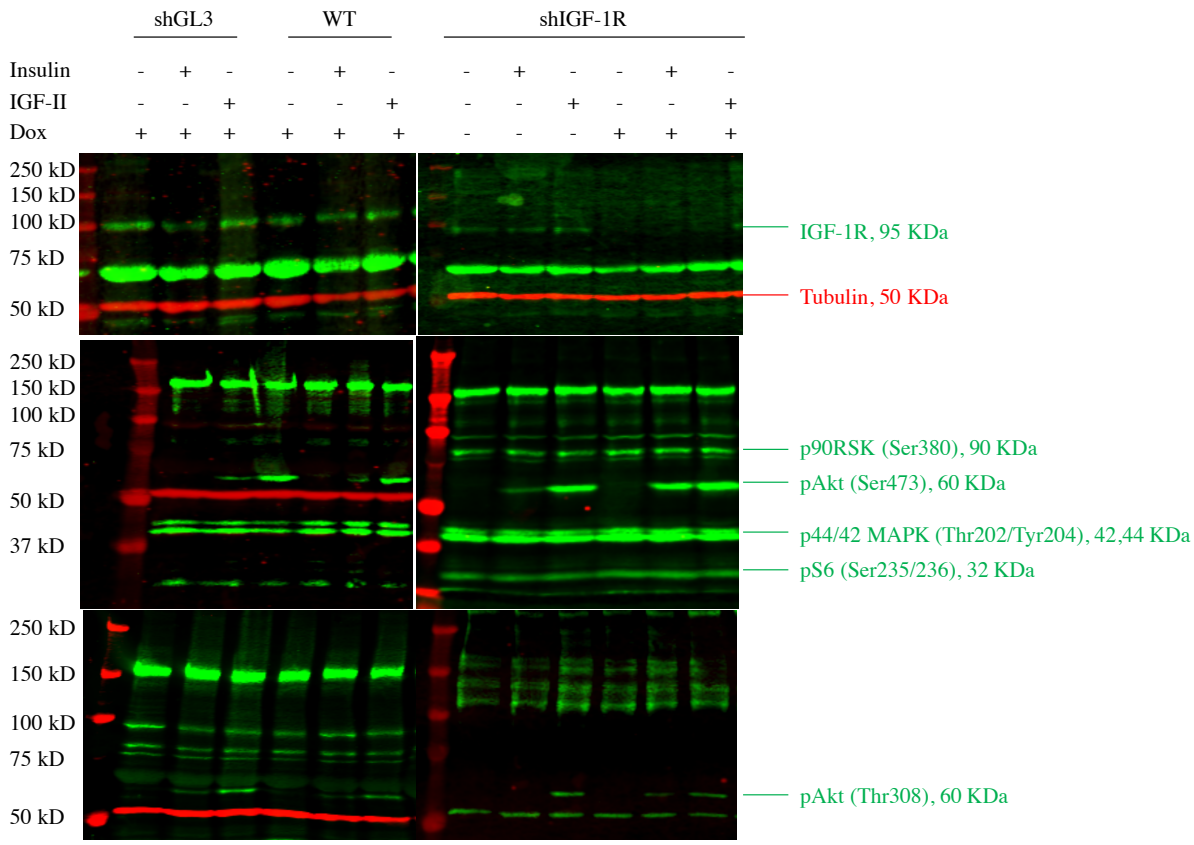

Appendix 16. Raw data of Figure 5.12-A.

Appendix 17

A.

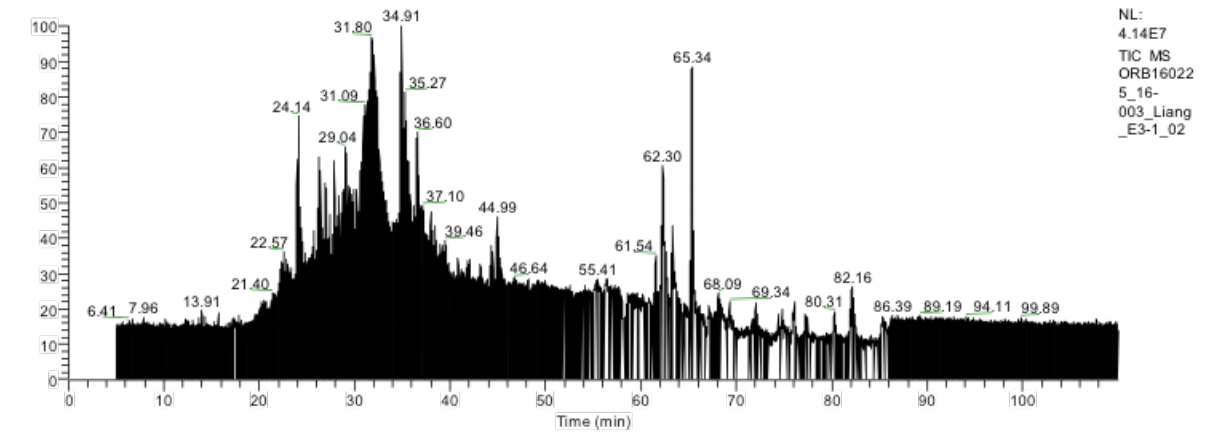

B.

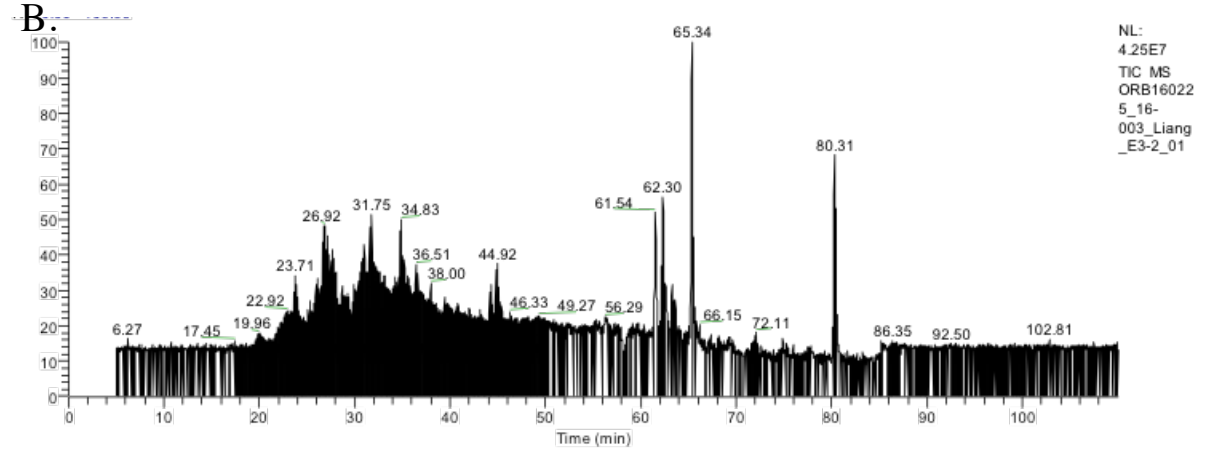

Appendix 17. Raw HPLC spectra of mass spectrometry runs used to generate Figure 6.7. (A) Elute with 0.83% (elute1) and (B) 2.5% NH_4OH (elute2).

Appendix 18

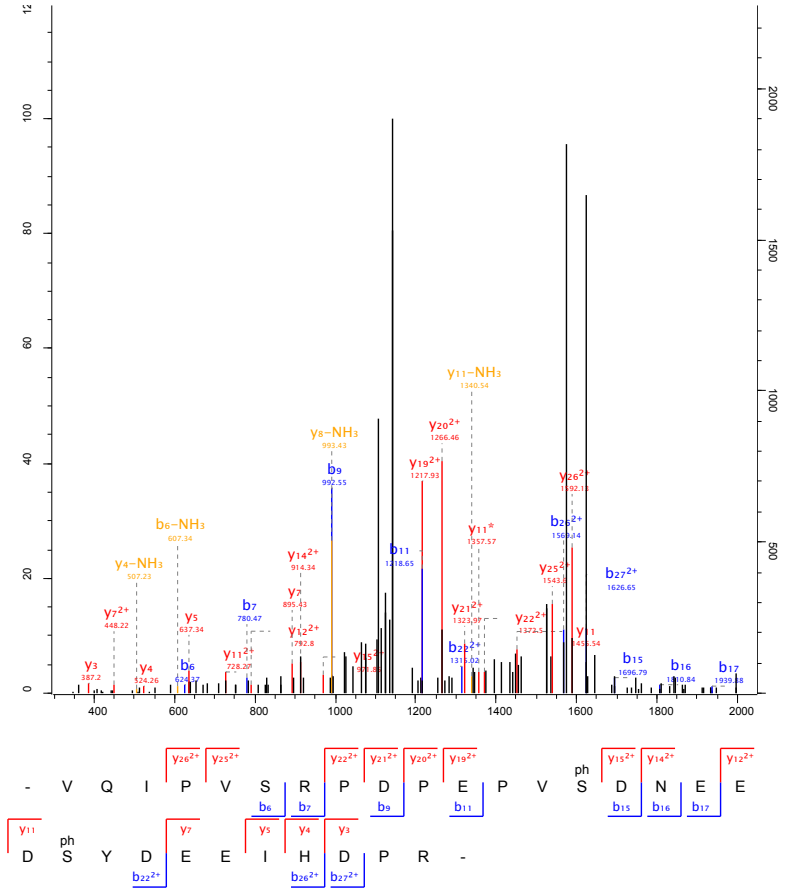

Appendix 18. Raw spectrum for the phosphorylation of s125 and s131 of TJP1.